Using a new generation of remote sensing to monitor Peru's mountain glaciers

Liam Steven Taylor

Submitted in accordance with the requirements for

the degree of Doctor of Philosophy

The University of Leeds

School of Geography

July 2022

Publication Statement

The candidate confirms that the work submitted is their own, except where work which has formed part of jointly authored publications has been included. The contribution of the candidate and the other authors to this work has been explicitly indicated below. The candidate confirms that appropriate credit has been given within the thesis where reference has been made to the work of others.

The work in Chapter 2 of this thesis has appeared in publication as follows, with additions for the format of the thesis:

Taylor, L.S., Quincey, D.J., Smith, M.W., Baumhoer, C.A., McMillan, M. and Mansell, D.T. (2021) Remote sensing of the mountain cryosphere: Current capabilities and future opportunities for research. *Progress in Physical Geography*. **45**(6). pp.931-964.

In this work, LST conceived the paper, performed all data analysis, and wrote the manuscript. DJQ, MWS, MM, and DTM supervised LST and edited the manuscript. CAB contributed text on artificial intelligence and machine learning.

The work in Chapter 3 of this thesis has appeared in publication as follows, with additions for the format of the thesis:

Taylor, L.S., Quincey, D.J., Smith, M.W., Potter, E.R., Castro, J. and Fyffe, C.L. (2022) Multi-decadal glacier area and mass balance change in the Southern Peruvian Andes. *Frontiers in Earth Sciences*. **10**. pp.1-14.

In this work, LST co-designed the study, conducted data analysis, and wrote the manuscript. DJQ and MWS co-designed the study and supervised data analysis. ERP conducted climate data analysis. JC and CLF contributed expertise on Peruvian glacier dynamics for data analysis. All authors edited the manuscript.

The work in Chapter 5 of this thesis has been submitted for publication as follows, with additions for the format of the thesis:

Taylor, L.S., Quincey, D.J., Smith, M.W. (2022) Evaluation of low-cost Raspberry Pi sensors for photogrammetry of glacier calving fronts. *Natural Hazards and Earth System Sciences*. (In Review).

In this work, LST co-designed the study, conducted data analysis, and wrote the manuscript. DJQ and MWS co-designed the study, supervised data analysis, and edited the manuscript.

Rationale for submitting the thesis in alternative format

This thesis begins by critically evaluating the current capabilities of remote sensing, before assessing three separate novel remote sensing techniques for their usability in monitoring mountain glaciers. Each technique forms its own distinct chapter with literature review, methods, results, and discussion. As such, the core four chapters of the thesis (overall literature review, followed by three data-based chapters for each technique) can be seen as independent pieces of work and have been, or are being, published as such. This thesis binds these works together by evaluating the potential application of each technique to monitoring Peruvian glaciers. While each chapter has been rewritten for inclusion in this thesis, in order to maintain the independence of each piece of work, there is inevitably some minor overlap between chapters.

The structure of the thesis is an introduction to the topic (Chapter 1), a critical evaluation on the current capabilities of remote sensing (Chapter 2), assessment of the performance of three novel techniques over mountain glaciers (Chapters 3-5), a discussion on their applicability to monitoring Peruvian glaciers (Chapter 6), and conclusion (Chapter 7).

Acknowledgements

Firstly, and most importantly, thank-you to my superb supervisory team – Duncan Quincey, Mark Smith, and Mal McMillan. Your creativity and wisdom have been genuinely inspiring, as was the trust you placed in me from the very beginning. You have given me experiences that I will never forget (in the case of some, no matter how hard I try) and have been a consistent source of insight, reassurance, and humour (sort of) over the last four years. Thank you.

It has been a privilege to work alongside talented colleagues in the School of Geography, particularly the RBPM cluster, for the past five years. Thanks particularly to Jonathan Carrivick, for joining my meetings out of sheer enthusiasm; Joe Mallalieu, for sparking my interest in SfM and allowing me to follow in your footsteps; Josh Chambers, for walking me and keeping me going for four years, across two continents; Max Fancourt, for entertaining my need to talk about remote sensing at any time of day; and Robert Vanderbeck, for rescuing us in the darkest hour of my PhD (a trip to Manchester Airport).

A special thanks goes to Josh Wolstenholme, Michael Grimes, and Hannah Barnett for also joining my overseas endeavours and providing me chocolate. To my Peruvian colleagues, who have helped me with everything from negotiating logistics to finding an excellent Pisco Sour, I will never forget the kindness you have shown me: Gracias to Fredy Monge, Nilton Montoya, and Carolina Garcia Pye. A special thank-you to the team at TodoVertical Cusco for keeping us alive in the field, despite the best efforts of a puma.

I'm very grateful to the wonderful co-authors of my publications who have all been a joy to work alongside: Celia Baumhoer, Joshua Castro, Catriona Fyffe, Damien Mansell, and Emily Potter. Thank-you to the reviewers and editors of my publications, with a particular thanks to Fabian Drenkhan who has reviewed half this thesis already. I'm also grateful to the organisations that have financially supported my endeavours; the Royal Geographical Society, Mount Everest Foundation, Gilchrist Educational Trust, water@leeds, Priestley Climate Centre, and Peplink.

Lastly, throughout my PhD, I have been enormously lucky to have had a loving and supportive personal network behind me. Firstly, thank-you to Daisy Curtis and Vicky Naylor. It has been a joy to exchange 227,931 messages with you during my PhD. There's no question, I couldn't have done it without you, your constant deliveries of cake and houseplants, and your relentless positivity and enthusiasm. Second, to my family, who allow me to raid the fridge on every visit and have generously given their time to practice fieldwork in Devon. Mum, I still owe you a clutch. Lastly, to my wonderful partner, Patrick. Thank you for always helping me see the bigger picture of my work, for celebrating every moment throughout my PhD journey, and pushing me to keep going right to the end. I look forward to repaying this favour with your own thesis!

Thank you.

Abstract

Remote sensing technologies are integral to monitoring mountain glaciers in a warming world. Tropical glaciers, of which around 70% are located in Peru, are particularly at risk as a result of climate warming. Satellite missions and field-based platforms have transformed understanding of the processes driving mountain glacier dynamics and the associated emergence of hazards (e.g. avalanches, floods, landslides), yet are seldom specialised to overcome the unique challenges of acquiring data in mountainous environments. A 'new generation' of remote sensing, marked by open access to powerful cloud computing and large datasets, high resolution satellite missions, and low-cost science-grade field sensors, looks to revolutionise the way we monitor the mountain cryosphere. In this thesis, three novel remote sensing techniques and their applicability towards monitoring the glaciers of the Peruvian Cordillera Vilcanota are examined. Using novel processing chains and image archives generated by the ASTER satellite, the first mass balance estimate of the Cordillera Vilcanota is calculated (-0.48 ± 0.07 m w.e. yr^{-1}) and ELA change of up to 32.8 m per decade in the neighbouring Cordillera Vilcabamba is quantified. The performance of new satellite altimetry missions, Sentinel-3 and ICESat-2, are assessed, with the tracking mode of Sentinel-3 being a key limitation of the potential for its use over mountain environments. Although currently limited in its ability to extract widespread mass balance measurements over mountain glaciers, other applications for ICESat-2 in long-term monitoring of mountain glaciers include quantifying surface elevation change, identifying large accumulation events, and monitoring lake bathymetry. Finally, a novel low-cost method of performing timelapse photogrammetry using Raspberry Pi camera sensors is created and compared to 3D models generated by a UAV. Mean difference between the Raspberry Pi and UAV sensors is 0.31 ± 0.74 m, giving promise to the use of these sensors for long-term monitoring of recession and short-term warning of hazards at glacier calving fronts. Together, this 'new generation' of remote sensing looks to provide new glaciological insights and opportunities for regular monitoring of data-scarce mountainous regions. The techniques discussed in this thesis could benefit communities and societal programmes in rapidly deglaciating environments, including across the Cordillera Vilcanota.

Table of Contents

List of Figures

List of Tables

Abbreviations

AI	Artificial intelligence
ASTER	Advanced Spaceborne Thermal Emission and Reflection Radiometer
DEM	Digital elevation model
DL	Deep learning
ELA	Equilibrium line altitude
EO	Earth observation
GLOF	Glacial lake outburst flood
GSD	Ground sampling distance
ML	Machine learning
NDSI	Normalised difference snow index
NDWI	Normalised difference water index
OLTC	Open-loop tracking command
RGI	Randolph glacier inventory
RMSE	Root mean squared error
SAR	Synthetic aperture radar
SfM	Structure-from-motion
SRAL	SAR altimeter (Sentinel-3)
SRTM	Shuttle radar topography mission
UAV	Unoccupied aerial vehicle

Chapter 1
Introduction

Climate change as a result of anthropogenic activity, is leading to glaciers across the world losing mass (Zemp et al., 2019; Fox-Kemper et al., 2021). Mass loss from mountain glaciers contributes to sea-level rise, water scarcity in mountain communities, and geomorphic hazards (Keiler et al., 2010; Baraer et al., 2012; Church et al., 2013). Projections indicate that as Earth's climate warms during the next century, mass loss from glaciers will increase (Zemp et al., 2019; Rounce et al., 2020). Over 1 billion people worldwide rely on fresh water originating from glaciers, primarily in the Himalaya (Immerzeel et al., 2019), Alps (Beniston, 2012) and Andes (Buytaert et al., 2017). Accurate predictions of how mountain glaciers are responding to warming, to provide insight into how they may respond to future warming, are essential to short-term hazard planning and long-term water resource management, yet there exists significant uncertainty in current estimates.

In the Andes, ongoing glacial recession poses increasing threats in the form of natural hazards, such as glacial lake outburst floods (GLOFs). As glaciers retreat, the number and size of glacial lakes increases (Hegglin and Huggel, 2008; Colonia et al., 2017; Shugar et al., 2020), which exacerbates the risk of GLOFs across the region (Vilímek et al., 2005; Schneider et al., 2014). As glaciers provide an essential water resource, populations frequently inhabit the lowlands, leaving them particularly vulnerable to outburst events (Baraer et al., 2012). GLOFs have killed thousands of people since the 1940s in the Peruvian Cordillera Blanca alone (Carey, 2005). At the same time, future glacial lake expansion also poses potential opportunities through increased tourism and hydroelectric power potential (Haeberli et al., 2016). Glacial meltwater to run hydropower, which can reach a capacity of 732 MW in Peru during drought (Buytaert et al., 2017), represents an important contribution for Andean countries aiming to reduce their reliance on fossil fuels in the wake of the UN Paris Agreement.

1.1. Mountain Glaciers of the Peruvian Andes

Around 70% of all tropical glaciers are located in Peru (Figure 1.1). These glaciers are found at high (~4,200+ meters above sea level; m a.s.l.) elevations in distinct mountain ranges of the Andes, known as Cordilleras. Glaciers across Peru

are rapidly receding in response to climate warming. A country-wide assessment shows a recession in glacier area from 2,042 km^2 in 1970 to 1,058 km^2 in 2019 (ANA, 2021). Some regions, such as the Cordillera Chila, have become almost entirely deglacierised as a result of this recession (Janský et al., 2011).

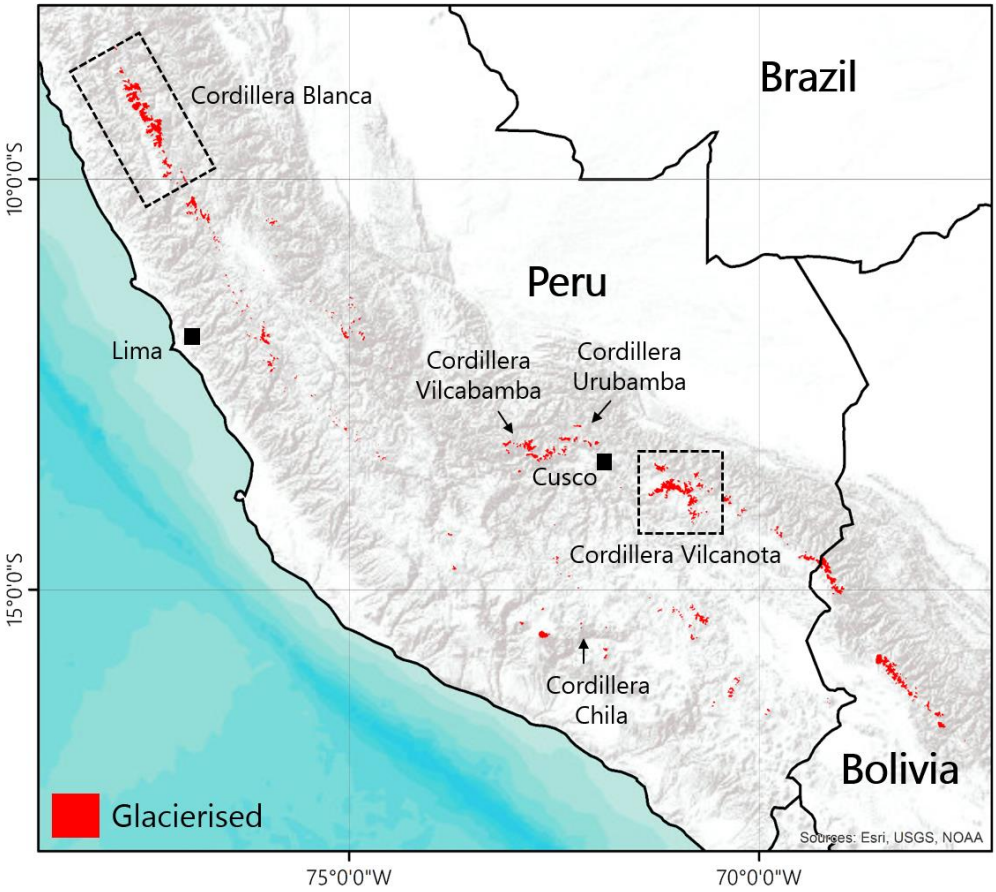

Figure 1.1 - Glacierised regions of Peru (red) from the Randolph Glacier Inventory (RGI Consortium, 2017).

The largest glacierised area of Peru is the Cordillera Blanca (431 km^2 as of 2019 (ANA, 2021), ranging in elevation from ~4,200 m to 6,768 m at Huascarán), where meltwater is important for contributing up to 30% of river discharge during the dry seasons (May to September) and ensuring consistent supply to key rivers such as the Río Santa (Mark and Seltzer, 2003; Baraer et al., 2012). Owing to its size, accessibility, and proximity to large towns and cities, glaciers of the Cordillera Blanca have received extensive scholarly attention with regards to its past (Georges, 2004; Burns and Nolin, 2014), present (Motschmann et al., 2020), and future (Schauwecker

et al., 2017). The second largest glacierised area is the Cordillera Vilcanota (246 km^2 as of 2017 (ANA, 2021), ranging in elevation from ~4,600 m to 6,384 m at Ausangate), located in the south-east of Peru, around ~200 km from the Bolivian border. Water from the Cordillera Vilcanota supplies the city of Cusco (population 470,000), acting as an important buffer during dry seasons and drought. For many indigenous communities and smaller settlements living closer to the ice, meltwater from the Cordillera Vilcanota is their primary source of freshwater (Figure 1.2).

Figure 1.2 – Meltwater is channeled from glaciers of the Cordillera Vilcanota (A) to provide a primary water resource for rural farms in the foothills (B).

To the south of the central range of the Cordillera is Laguna Sibinacocha: a glacial fed water reservoir (~20 km^2 in size) which occupies the former glacier extent at the last glacial maximum, and is now dammed at its southern end for hydropower (Figure 1.3). The dam has been in place since the 1990s and regulates water supply into a small river which feeds the Vilcanota-Urubamba basin. The east of the Cordillera Vilcanota is dominated by the Quelccaya ice cap: the second largest tropical ice cap, of ~40 km^2 glacierised area in 2020. Quelccaya has receded and thinned rapidly in recent decades owing to the expansion of lakes, particularly along its western margin, driving melt (Yarleque et al., 2018). Glaciers of the Cordillera Vilcanota represent a source of heritage, culture, and spirituality for communities living in close proximity to the ice. Centuries-old cultural practices have ceased due to glacier recession, such as the carving ice from Ausangate (the highest peak of the Vilcanota) during the annual El Señorde Qoyllur Rit'i catholic pilgrimage (Allison, 2015). Continued recession is leading to water anxiety, local tension, and the challenge of distrust of foreign interventions (Vuille et al., 2018).

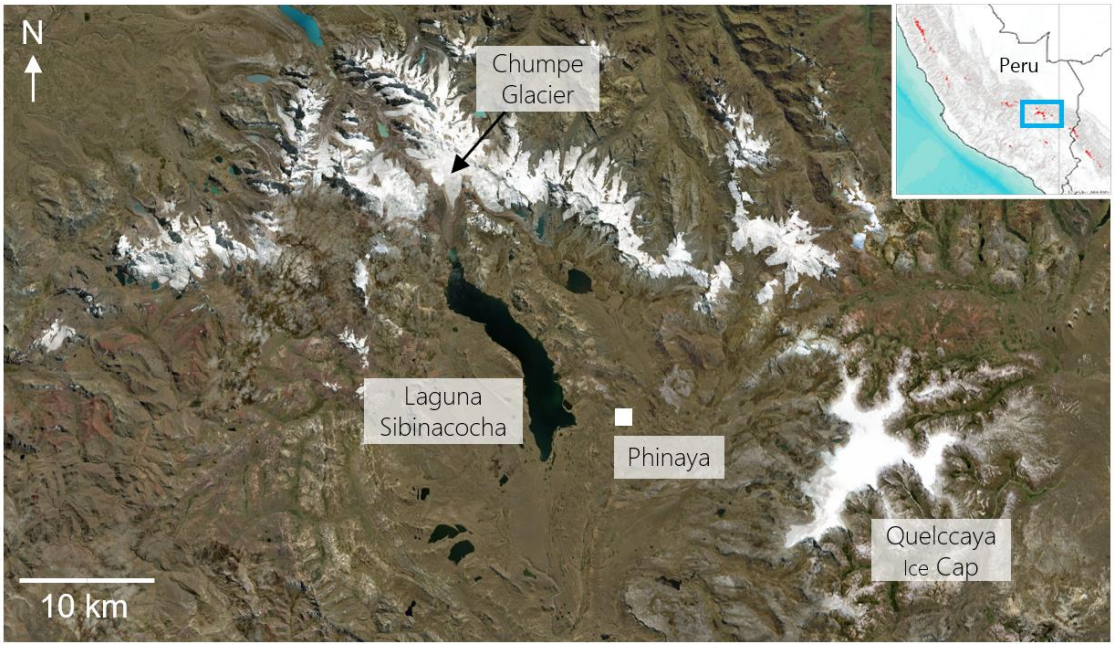

Figure 1.3 – Key locations within the Cordillera Vilcanota.

Nearby to the Cordillera Vilcanota (~100 km to the West) are the smaller Cordilleras Vilcabamba and Urubamba (glacierised area of 96 and 18 km^2 respectively (ANA, 2021), ranging in elevation from ~4,600 m to peaks of 6,271 m at Salcantay in the Vilcabamba and 5,893 m at Veronica in the Urubamba). Glaciers in these Cordilleras are generally smaller, steeper, and lower-lying than in the Cordillera Vilcanota (Guardamino and Drenkhan, 2016). Glaciers here also represent a significant point of heritage and tourism, with the UNESCO World Heritage site of Machu Picchu situated within the Cordillera Vilcabamba and the Willka Qhichwa (Sacred Valley of the Incas) within the Urubamba. This area has been farmed for over one thousand years, with irrigation systems channeling glacial meltwater from the mountains into the Urubamba valley for farming (Covey, 2006). This prevalence of glacial meltwater in irrigating agriculture in the rural headlands is of particular concern as climate change impacts this supply (Drenkhan et al., 2019). The concern over agriculture is particularly important for indigenous women, who make up a large portion of this sector (Del Aguila, 2015). The intersectionality of issues facing this population, from access to water to high poverty rates, means there is overall a lower capacity to adapt to dwindling water supplies.

1.2. A New Generation of Remote Sensing

To track the changes of glacierised regions, improve confidence in future climate projections, and protect communities from associated hazards, requires detailed and systematic monitoring programmes. Mountain glaciers present unique challenges for remote sensing, which has limited the applicability of traditional techniques in glaciology to mountainous regions. Steep topography creates issues such as layover and shadowing, often hiding small glaciers between peaks. Nevertheless, remote sensing is important in monitoring these highly dynamic, yet remote and inaccessible, environments. Optical data form much of our current observation of mountain glaciers and medium (<30 m) spatial resolution optical data, including ASTER, Sentinel-2, and Landsat, are frequently used in assessing and monitoring glacier hazards (Quincey et al., 2005; Shugar et al., 2021) and long-term change (Bolch et al., 2010; Veettil, 2018; Racoviteanu et al., 2019). Synthetic Aperture Radar (SAR) data, and derived products such as glacier velocity maps, can also be used in conjunction with optical and elevation data for assessing long-term change in glacier dynamics (Kääb, 2005; Quincey et al., 2007; Robson et al., 2015). Yet, there remains an array of remote sensing techniques and satellites that have seldom been applied to mountain glacier environments, despite having made significant advances in monitoring the changing ice sheets.

A new generation of high-resolution remote sensing techniques is increasing the potential for routine mountain glacier observation. First, stereoscopic images, whereby two or more optical images are used to generate a 3D digital elevation model (DEM), are powerful archives for monitoring glacier thinning and recession (Dussaillant et al., 2018), but mountain glaciers are vulnerable to issues such as layover and shadowing, and large data gaps can persist when cloud and snow conditions are heavy. In addition, harnessing the potential of archives of stereo data requires handling large volumes of data and creating new processing chains. In recent years, the accessibility of cloud computing (through, for example, Google Earth Engine) and open-source processing chains has borne global estimates of glacier volume change (Hugonnet et al., 2021), yet issues unique to mountain glaciers create challenges that result in high levels of uncertainty when applying these global datasets to understanding the dynamics of small mountain glaciers. On a local scale, stereo data archives can provide a robust estimate of mass balance change over mountain glaciers (Pieczonka et al., 2013; Watson et al., 2020), but this technique has yet to be applied to the Peruvian Andes. Indeed, no such current estimate of region-wide mass balance exists over the Cordilleras Vilcanota, Vilcabamba and

Urubamba, with field-based techniques providing valuable insights, but limited to specific glaciers.

Secondly, satellite altimetry, using the time taken for a radar or laser pulse to travel from a satellite to the ground beneath and return, has typically performed well over large, flat ice sheets (Shepherd et al., 2018; Slater et al., 2021). However, the high relief of mountainous areas has severely limited this technique (Harding et al., 1994), with manual corrections needed over smaller glaciers (Treichler and Kääb, 2016). The recent launch of the Sentinel-3 (ESA; 2016) and ICESat-2 (NASA; 2018) missions offer promise to the ability of using satellite altimetry to monitor mountain glaciers. Both satellites capture data at a finer spatial and temporal resolution than predecessor altimeters, with novel onboard processing techniques to acquire data even in challenging conditions. Early insights into both satellites indicate their strong potential over ice sheets (McMillan et al., 2019; Brunt et al., 2019), yet no assessment has been performed of their potential over mountain glaciers. The possible insights that satellite altimetry could offer are large: from seasonal monitoring of snowfall depth, to highly precise estimates of glacier mass balance.

Lastly, field-based remote sensing often offers the most accurate measurements of glacier dynamics, but is fraught with difficulties from the challenging logistical conditions of working at high altitude, rural sites. Glacier calving fronts are highly dynamic systems which can be monitored to track glacier velocity, mass loss, or, in the case of large calving events, GLOFs. Sensors to monitor glacier fronts *in-situ* can cost many thousands of pounds in order to operate over long time periods in sub-zero conditions (Kienholz et al., 2019), while data are often analysed months or years after acquisition as a site revisit is required to retrieve imagery (Mallalieu et al., 2017). The potential for structure-from-motion (SfM) timelapse arrays to monitor individual calving events for hazard management has been proven (Ryan et al., 2015; Mallalieu et al., 2017), yet must decrease in cost and include data transmission to be viable for inclusion in a hazard warning system. Microprocessors (small, low-powered computers) are carving out a new niche in other geoscience disciplines (Ferdoush and Li, 2014; Chan et al., 2020) by offering high spatial resolution monitoring at a low cost. However, their full potential has yet to be assessed in a glacierised environment, where they could provide regular updates on calving front dynamics.

Together, this new generation of remote sensing techniques can help better understand the responses of glaciers to changes in climate, and provide a monitoring system for the subsequent effects on water resources and natural hazards.

1.3. Research Objectives

The overall aim of this thesis is to develop, and test, the three 'new generation' remote sensing techniques outlined above, with a focus on quantifying glacier mass loss, monitoring potential changes in water availability, and protecting against natural hazards originating from Peruvian glaciers. Each of these techniques has been successfully applied in other glacierised settings or geoscience disciplines, presenting this thesis with a clear aim of assessing their potential over mountain glacier environments. Four objectives will help fulfil this aim and structure the thesis:

1. Explore the current state of remote sensing over the mountain cryosphere, and identify remote sensing techniques and sensors currently in development, or used in other geoscience disciplines, that can be applied to the mountain cryosphere (Chapter 2);
2. Quantify the mass balance and area change of glaciers in the Southern Peruvian Andes, concurrently examining the applicability of stereo archives to provide long-term monitoring over small mountain glaciers (Chapter 3);
3. Explore the applicability for using new satellite altimetry missions (Sentinel-3 and ICESat-2) over small mountain glaciers, concurrently identifying opportunities for integrating altimetry data into glacier monitoring schemes (Chapter 4);
4. Create a novel SfM-based system that generates science-grade 3D models of glacier calving fronts at a low-cost, concurrently providing a proof-of-concept for real-time, autonomous SfM for a GLOF hazard warning system (Chapter 5).

1.4. Thesis Structure

The thesis is broadly structured around the application of three remote sensing techniques (stereo optical imagery, satellite altimetry, and low-cost SfM; Chapters 3, 4, and 5) to monitoring mountain glaciers. Each of these data-driven chapters are written in the format of journal articles and are designed to be independent assessments of each technique. Other chapters provide the context behind selecting these techniques as the 'new generation of remote sensing' (Chapter 2) and a discussion on their use and potential deployment within management schemes (Chapter 6). To this end, the chapters of the thesis are structured as follows:

1. Thesis introduction
2. Remote sensing of the mountain cryosphere: Current capabilities and future opportunities for research
3. Multi-decadal glacier area and mass balance change in the Southern Peruvian Andes
4. Investigating the performance of novel satellite altimetry missions over mountain glaciers
5. Evaluation of low-cost Raspberry Pi sensors for near real-time photogrammetry of glaciers
6. Discussion and recommendations on the applicability of these techniques to monitoring Peruvian mountain glaciers
7. Conclusions

Chapter 2

Remote sensing of the mountain cryosphere: Current capabilities and future opportunities for research

2.1. Introduction

The mountain cryosphere, which we define as areas within mountainous environments that are frozen during part or all of the year, including glaciers, snow, permafrost, and lake ice, represents a source of fresh water for over one billion people worldwide (Immerzeel et al., 2019). Yet, mountain areas are increasingly threatened by climate warming, posing a threat to future water security (Hock and Rasul, 2019; Shugar et al., 2021). For communities living in mountain environments, such climate warming also poses an increased threat of natural hazards from the cryosphere, such as glacial lake outburst floods (GLOFs) (Carrivick and Tweed, 2016; Harrison et al., 2018), avalanches (Fischer et al., 2012; Ballesteros-Cánovas et al., 2018), slope failures (Huggel et al., 2012), debris flows (Perov et al., 2017), or a combination of one or more hazards in a cascading chain (Kirschbaum et al., 2019). Given the significance of the mountain cryosphere in water resource and hazard management, it is therefore imperative to be able to track its rapid change, with the goal of being able to develop predictive capacity. Earth Observation (EO) and field-based techniques are increasingly viewed as being able to play a key role in securing the sustainable development of mountain communities (e.g. Murthy et al., 2014; Veettil and Kamp, 2019). However, there often remains a disconnect between monitoring from afar and local co-operation (Nussbaumer et al., 2017).

Remote sensing has advanced rapidly in recent years, both in the physical hardware of the sensors and in the software used to subsequently process these data. However, the challenges associated with imaging areas of high relief are great, and the success of techniques that are now routinely applied over ice sheets (e.g. altimetry, gravimetry) has been limited (Kääb et al., 2005; Berthier et al., 2006; Racoviteanu et al., 2008a; Prinz et al., 2018). Optical satellite sensors are particularly hampered by persistent cloud, frequent and extensive snow cover, and accessibility of output data. Radar sensors can penetrate cloud, and quantify centimetric deformation rates (Joughin et al., 2010), but are often affected by radar shadow and layover from steep topography, and signal decorrelation due to the highly dynamic environment, which reorganises matching features. Field-based remote sensing techniques overcome such problems, and can offer very high spatiotemporal

resolution and bespoke data, but only from individual sites and with more challenging logistical obstacles, and many areas remain inaccessible for safety or geopolitical reasons.

Recent innovations in sensor technology and processing techniques can be applied to remote observations of the mountain cryosphere. Upcoming satellite missions, in particular satellite constellations, will increase acquisition rates over mountain glaciers, at an ever improving spatial, spectral, and radiometric resolution. Private-public partnerships are becoming increasingly common, which has seen an associated rise in commercial data being incorporated into research publications (Figure 2.1). Field-based techniques are also changing rapidly, as bespoke Unoccupied Aerial Vehicles (UAVs) and low-cost micro-sensors increasingly become part of a glaciologist's toolkit (Bhardwaj et al., 2016). Artificial Intelligence (AI) and cloud computing, with the vast increase in availability of free and open access data, are beginning to improve the processing of these new data.

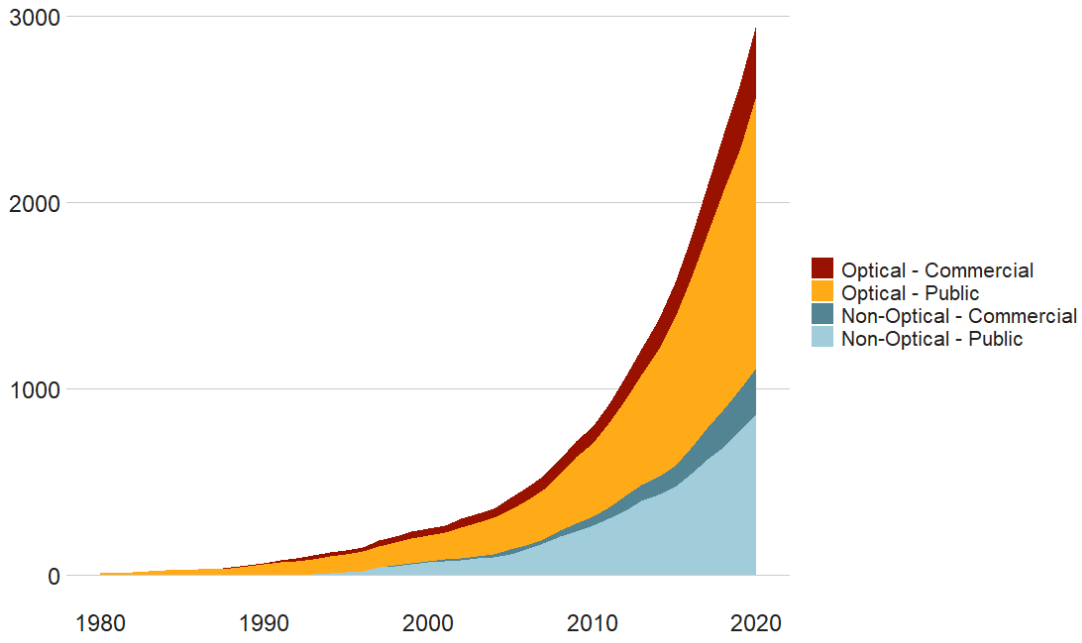

Figure 2.1 – Cumulative number of publications for the use of EO satellites in mountain glacier studies from Scopus. These data were generated from a systematic review of available literature from missions described in this chapter and then subsequently merged into commercial or public missions.

We are therefore in a period of rapid remote sensing, and consequently modelling, of the mountain cryosphere, presenting a timely opportunity to review the accomplishments to date and explore the future direction for this discipline. The aim of this chapter is to critically evaluate the performance of current remote sensing methods, identify limitations and gaps in current delivery, and discuss what emerging technologies could offer this research area in the future. This chapter will also further examine the background and future opportunities of harnessing stereoscopic image archives, new satellite altimetry missions, and low-cost microprocessors and their applications to monitoring Peruvian glaciers.

2.2. Current monitoring of the mountain cryosphere

There are a number of measurable parameters that can be used to chart the response of glacierised environments to climatic changes. Some parameters indicate changes in process rates (e.g. accumulation, ablation, ice deformation and sliding, sediment dynamics), while others are more pertinent to identifying features that may threaten downstream communities (e.g. glacial lakes, oversteepened and thawing slopes). In this section, we review the methods currently available for monitoring the mountain cryosphere, reflect on the key sensors available to researchers, and consider selected services available to local authorities.

2.2.1. Surface Mass Balance

Surface mass balance, the net sum of accumulation and ablation over a period, often one year, is perhaps the clearest indicator of how a glacier is responding to a warming climate (Dyurgerov and Meier, 2000). The overwhelming majority of remote sensing studies now calculate glacier-specific and region-wide mass balances using the geodetic approach.

The geodetic approach describes the process of differencing time-separated digital elevation models (DEMs) and summing the glacier-wide elevation changes, before converting the resulting volume to mass (Bamber and Rivera, 2007; Huss, 2013). It emerged during the late 1990s as an efficient means of deriving surface elevation measurements across broad areas within a single analysis (e.g. Wingham, 1998). Both the Shuttle Radar Topography Mission (SRTM; 2000), and ASTER Global Digital Elevation Model (GDEM; 2009) are typically used as ‘baseline’ datasets to establish the first elevation epoch (Zhou et al., 2017; Wu et al., 2018). The second

epoch is usually then established by constructing a DEM from stereo imagery (e.g. SPOT, ASTER) acquired some years later (Rabatel et al., 2016; Braun et al., 2019). Many data sources appropriate for such analysis remain restricted in access, however. In particular, the SPOT family of satellites provides one of the longest and highest resolution archives for constructing glacier mass balance, but as a commercial mission the imagery is costly for the majority of researchers without a data grant; ALOS PRISM (2.5 m spatial resolution) and TerraSAR-X/TanDEM-X data (3 m StripMap mode and 12 m respectively; Rizzoli et al., 2017) are similarly only available to classified users under license. ASTER imagery provides stereo DEMs at no cost, but at medium spatial resolution (15 m; GDEM 30 m) and often with errors that exceed the magnitude of the change being detected (Bolch et al., 2008). Protocols for automating DEM production (such as fitting a regression through an ASTER DEM chain to robustly separate signal from noise) represent a major step forward, by providing data redundancy in the form of multiple datasets (Brun et al., 2017; Hugonnet et al., 2021).

Longer records of glacier mass change have exploited archives of aerial imagery or declassified stereo imagery from US reconnaissance missions (e.g. HEXAGON and Corona), to produce baseline DEMs, giving rise to 50+ year estimations of glacier mass balance in mountainous regions (Surazakov et al., 2007; Bolch et al., 2008; Pieczonka et al., 2013; Kjeldsen et al., 2015; Falaschi et al., 2019). Coupled with contemporary assessments of glacier evolution these historical records can provide valuable information on rates of change (Maurer et al., 2019; King et al., 2019). After initial processing challenges brought about by non-conventional frame characteristics and missing location data, these declassified images are now also routinely fed into automated processing pipelines to derive elevation snapshots at multiple epochs (Maurer and Rupper, 2015) (Figure 2.2).

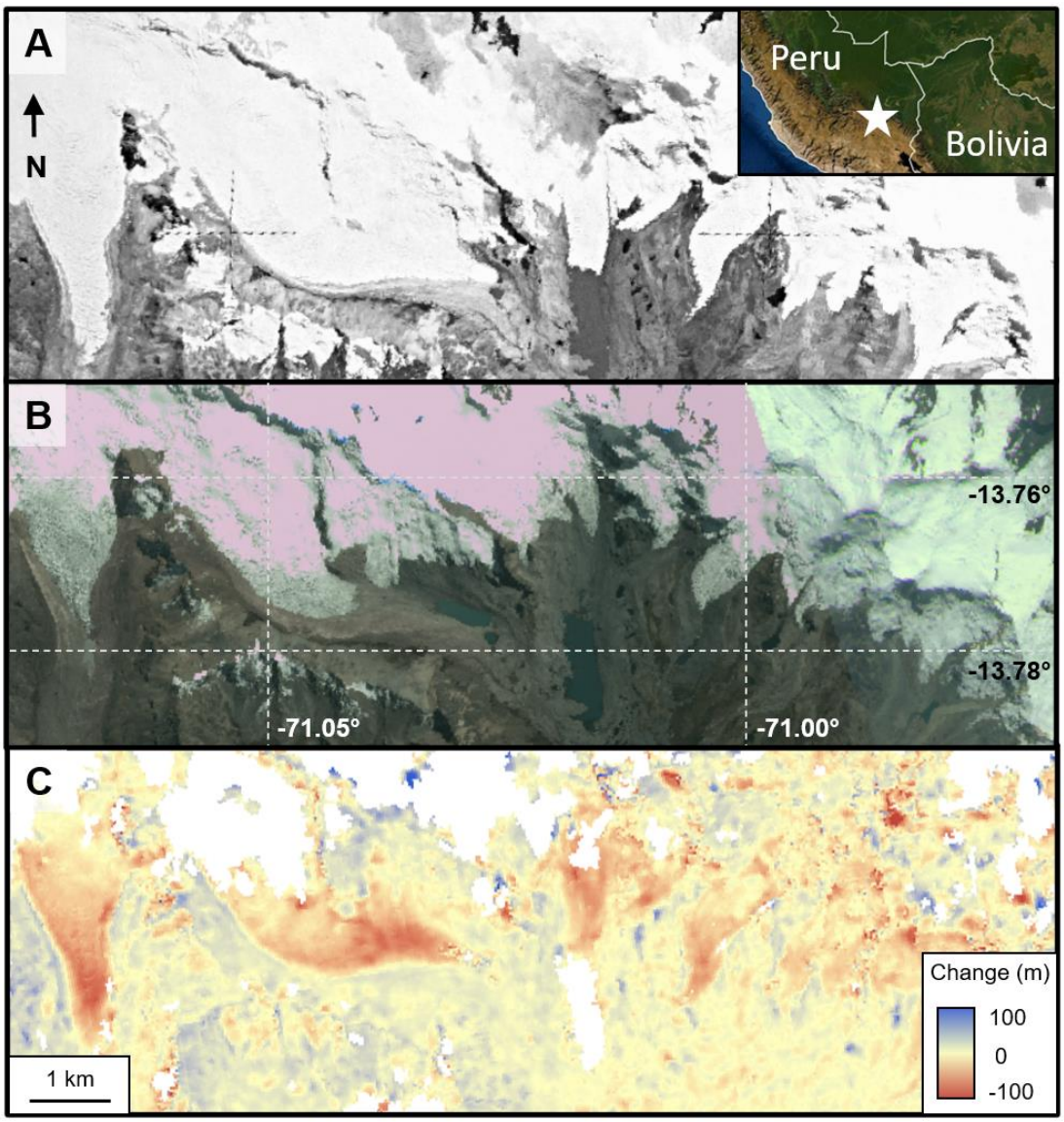

Figure 2.2 - Historic and contemporary images can be used to quantify mass change across the Cordillera Vilcanota, Peru (-13.76°N, -71.03°E). (A) KH-9 HEXAGON image from 3rd August 1980, georeferenced and overlain on a DEM generated using HEXIMAP (Maurer and Rupper, 2015). (B) Planet Imagery from May 2020 as a visual reference for glacier position today. (C) DEM differencing the KH-9 HEXAGON elevation model against a TanDEM-X DEM from July 2015. Positive values surrounding the glacier are likely due to georeferencing error of the HEXAGON image on very steep slopes.

Regional estimates of mass balance are often more robust indicators of glacier response to climate change than those focussing on a small subset. The

Gravity Recovery and Climate Experiment (GRACE) satellites (2002-2017), and their successor (GRACE-FO; launched in 2018), offer the possibility to calculate regional estimations of net mass change and the subsequent contributions to sea level rise (Chen et al., 2013). However, their coarse spatial resolution (~300 km), and inability to disaggregate individual contributions of change, means that signals of ice loss could not be separated from signals from groundwater storage depletion or surface lake drainage (Yi and Sun, 2014; Song et al., 2015). Satellite altimetry from ICESat (2003-2010) and CryoSat-2 (2010-) has also been used to produce estimates of glacier mass loss, but only over the largest glaciers where observations were regularly repeated (Kääb, 2008; Neckel et al., 2014; Ke et al., 2015; Trantow and Herzfeld, 2016). Altimeters are frequently used as a comparison for the accuracy of other DEMs (e.g. Liu et al., 2019), or as ground control points for stereo DEMs; yet, there remains a gap in the current satellite delivery for highly precise elevation measurements over mountain glaciers from altimeters, that may yet be fulfilled by ICESat-2 (2018-) as it builds an archive of repeat observations, albeit over a limited number of glaciers (Bisschop, 2021).

At a smaller scale, UAVs are important in the creation of cm-scale elevation models for monitoring surface mass balance through SfM photogrammetry. Repeat surveys can be used to monitor short-term surface melt through differencing point clouds (Dall'Asta et al., 2017; Bash et al., 2018). This is particularly important where melting dynamics are drastically different across the year (Rossini et al., 2018; Che et al., 2020). The cm-scale DEMs can also be used to measure the microtopography of glacier surfaces – an important component in the surface energy balance of glaciers (Chambers et al., 2019; Bash and Moorman, 2020; Bonekamp et al., 2020).

2.2.2. Ice Velocity

Glacier velocity products are important for determining the long-term response of a glacier or a region to climate warming (Dehecq et al., 2019), as well as for assessing likely locations for emerging hazards and those developing in the future (Quincey et al., 2007). Generating distributed velocity fields for mountain glaciers usually requires one of two approaches: feature tracking or Interferometric Synthetic Aperture Radar (InSAR). Feature tracking requires two images separated in time, captured within an optimal time window such that the features have moved sufficient distance to be detectable, but not such that they deform beyond recognition. Most algorithms employ normalised cross-correlation for matching features (e.g. Berthier

et al., 2005; Copland et al., 2009), but frequency-based approaches can also yield robust results (Leprince et al., 2007; Scherler et al., 2008); see Heid and Kääb (2012) for a comprehensive review. InSAR requires much shorter temporal baselines, such that the coherence of the radar signals between the two successive images is maintained (Rabus and Fatland, 2000), dependent therefore on periods of calm weather and geomorphic stability, neither of which are common in mountain environments. Where InSAR is successful, it can detect centimetre-scale displacements, at high precision, as well as performing well over relatively featureless (clean-ice or snow-covered) areas where feature tracking fails (Luckman et al., 2007).

Traditionally, radar imaging sensors have been used for velocity tracking, as a) radar speckle results in an image rich in texture over optically-featureless surface, and b) their ability to penetrate clouds allows for images to be captured regardless of weather conditions. Today, the European Space Agency's Sentinel-1 provides such imagery on a 6-day repeat cycle for deriving glacier velocity, building upon its predecessors ERS-1/2 (1991 and 1995) (Quincey et al., 2007; Luckman et al., 2007) and Envisat (2002) (Quincey et al., 2009). Images collected by commercial satellites, such as RADARSAT and TerraSAR-X, are also used to derive glacier velocity fields at high temporal frequency and spatial resolution (Abdel Jaber et al., 2012; Waechter et al., 2015), though these data are generally only available through licensing agreements or at great financial cost.

Where successive cloud-free images can be acquired, velocity products can also be derived from optical imagery. Medium resolution imagery (10 – 30 m) such as ASTER provides broad coverage for regional assessments (Redpath et al., 2013; Guillet et al., 2022), while the long Landsat archive offers a window into past glacier dynamics and their current response to changes in climate (Dehecq et al., 2019). The Operational Land Imager on-board Landsat-8 is particularly well-suited to this task, offering improved radiometric resolution and geometric fidelity compared to its predecessors, making it possible to produce glacier velocity products that are comparable in terms of accuracy to InSAR (Roy et al., 2014; Fahnestock et al., 2016). Applications such as Cosi-CORR (Leprince et al., 2007), IMCORR (Scambos et al., 1992), and auto-RIFT (Gardner et al., 2020) are used routinely to produce glacier velocity products from radar and optical data. However, given the cloudy and steep conditions of mountain glaciers, outputs from a range of correlation applications and sensors are often required for robust and complete coverage (Heid and Kääb, 2012).

2.2.3. Glacial Lakes

The growth of lakes as glaciers recede is one of the most visible reminders of climate warming impacting the mountain cryosphere (Shugar et al., 2020). Lakes present opportunities in hydropower and tourism, but also additional risk from the threat of larger and more frequent outburst floods to downstream populations (Bajracharya and Mool, 2009; Carrivick and Tweed, 2016; Haeberli et al., 2016; Drenkhan et al., 2019). Existing glacial lakes can be located using a Normalised Difference Water Index (NDWI) from medium-resolution optical imagery such as Sentinel-2 or the Landsat archive (Drenkhan et al., 2018; Watson et al., 2018). DEMs can also be used to identify glacial lakes from stereo optical imagery (Ukita et al., 2011) or higher-resolution SAR (Strozzi et al., 2012).

Establishing lake volume requires bathymetry measurements to capture the bed, and therefore an *in situ* component (Fujita et al., 2009). In the absence of these data, empirical scaling lake area with mean depth (from bathymetric maps and published data to avoid auto-correlation) can be used to provide a first-order assessment, though high uncertainty may suggest a mixed-model approach is most appropriate for datasets containing varying lake sizes (Cook and Quincey, 2015; Shugar et al., 2020). Estimates of glacial lake volume can also be determined from a depth-reflectance (Fitzpatrick et al., 2014) or depth-area relationship, but in the case of the latter approach, significant variability exists between sites depending on their style of formation (Cook and Quincey, 2015; Drenkhan et al., 2018). The recently launched ICESat-2 (2018) altimeter can obtain photon returns from both the lake surface and bed (accounting for refraction) to depths of around 40 m (Parrish et al., 2019), including from supraglacial lakes (Fair et al., 2020), though this is as yet untested in mountainous environments (see Chapter 4). Monitoring the changing lake surface height is theoretically possible from satellite altimeters or a continuous series of stereo DEMs. However, the archive for such measurements, at an appropriate accuracy to detect change through time, is not long. With extensive processing, data have been extracted from the Envisat era (2002-2012), with notable additions from ICESat (Neckel et al., 2014) and CryoSat-2 (Crétaux et al., 2016).

Remote sensing of glacier lakes now begins long before their formation, with bed topography data and modelling able to indicate their future extent and volume (Drenkhan et al., 2019) to provide an early indication that mitigation of an emerging hazard may be necessary. New lakes will likely form in the overdeepenings carved from the erosive force of glaciers, and so can be located with high confidence using

contemporary DEMs and the perfect plasticity approach to estimating ice thickness (Linsbauer et al., 2012; Rounce et al., 2017; Kapitsa et al., 2017; Viani et al., 2020). However, the timing of their evolution still requires numerical modelling of future rates of ice melt.

2.2.4. Supraglacial Ponds and Ice Cliffs

Glaciers have highly complex and dynamic surfaces, and features such as ponds and cliffs contribute to the surface energy balance and overall hydrological regime of mountain glaciers (Miles et al., 2016; Brun et al., 2016; Miles et al., 2018a; Brun et al., 2018). Medium-resolution (10–30 m) optical satellite data can classify supraglacial lakes (with Sentinel-2 outperforming Landsat-8 in spectral contrast between debris and water; Watson et al., 2018) on a regional scale (Veettil, 2018) and repeat imagery can be used to follow drainage events to identify associated changes in velocity and surface elevation (Miles et al., 2018b). However, sub-metre resolution data are essential to accurately assess the dynamics, and classify features, of complex glacier surfaces. Sub-metre resolution imagery and DEMs are paramount to being able to delineate features such as ice cliffs, which can contribute to increased rates of ablation (Buri et al., 2016). In lieu of satellite sensors being able to resolve such small-scale features, field-based remote sensing is frequently deployed. Airborne sensors (LiDAR, photogrammetry) have conducted such surveys (e.g. Baltsavias et al., 2001; Arnold et al., 2006; Janke, 2013; Reid and Brock, 2014), but are sparsely used given the financial cost of mounting such a campaign.

UAVs have rapidly become the most appropriate tool for very high resolution mapping of glacier surfaces. They are relatively low cost, yet rival the precision of traditional field-based surveying methods (e.g. ground mapping with GPS) (Gaffey and Bhardwaj, 2020), over an entire glacier surface in a fraction of the time (Figure 2.3). Repeat UAV surveys have shown that the development of ponds and cliffs can accelerate ice velocity (Immerzeel et al., 2014) and imagery has been used to produce quantitative measurements of cliff geometry to better understand their formation and evolution (Buri et al., 2016; Kraaijenbrink et al., 2016). A particular advantage of UAVs is their flexibility to observe rapidly changing vertical features, such as underhanging cliffs, that are obscured from space and may not be accessible for fixed time-lapse cameras (Scaioni et al., 2019). The vast quantity of data that are gathered from UAV surveys opens the opportunity for intelligent learning algorithms to speed up data processing as well as acquisition. AI has primarily been used in

remote sensing to classify surface features (Kraaijenbrink et al., 2016), but embedding AI within UAV systems has streamlined data processing elsewhere in other disciplines (Vasuki et al., 2014; Gonzalez et al., 2016; Ramirez-Atencia et al., 2017; Xu et al., 2018).

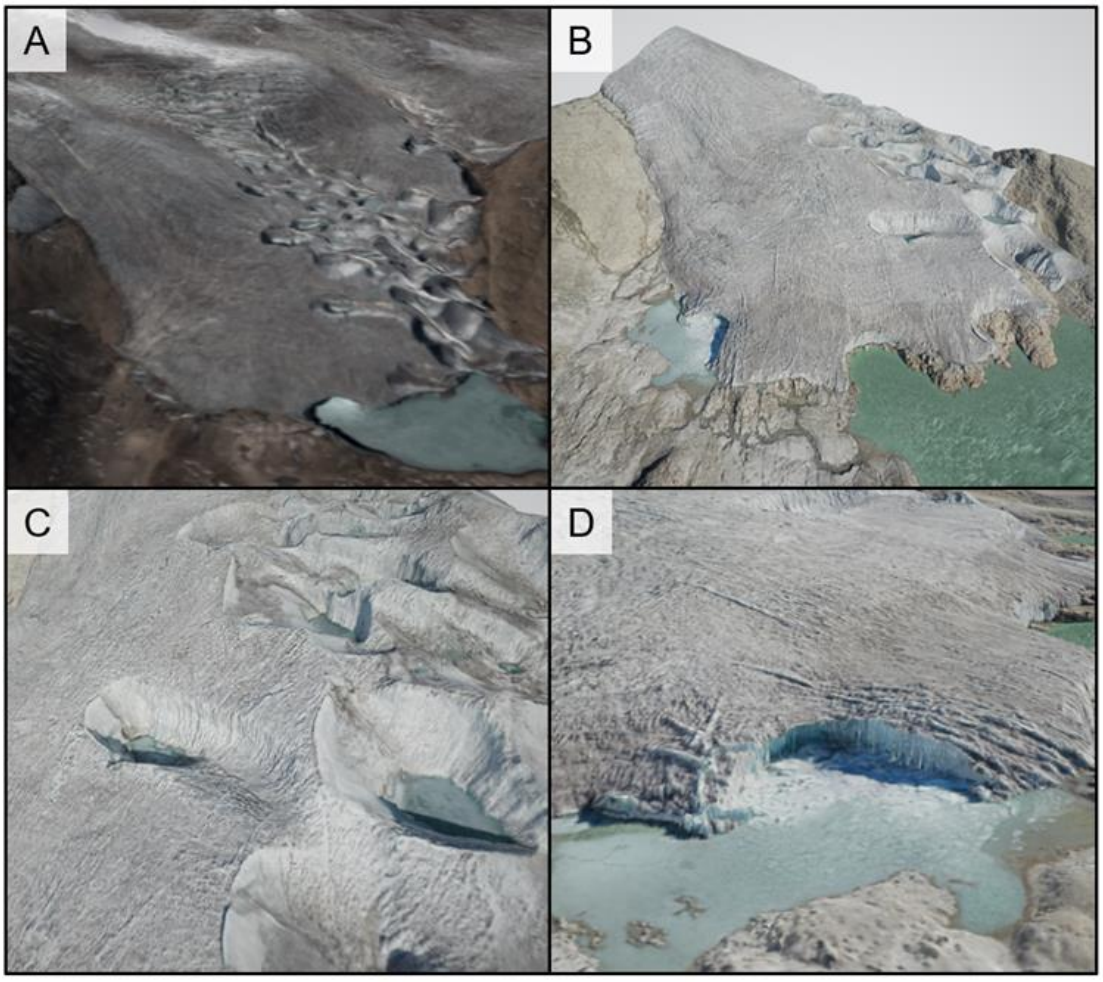

Figure 2.3 - UAVs offer a much sharper view of mountain glaciers compared to 3D alternatives from satellites, allowing a more accurate view of the ice surface, presented here from the western margin of the Quelccaya Ice Cap, Peru. (A) Pléiades multispectral image layered over a 3D reconstruction from tri-stereo images acquired in August 2016. (B) SfM reconstruction from 528 images of a UAV flight over the same glacier in September 2019. (C) and (D) show closer views of the UAV-derived SfM model to highlight the primary advantages of using UAVs for 3D reconstruction of mountain glaciers.

2.2.5. Snow

Snow cover in mountainous regions is important for hydropower, tourism, irrigation, water resource management and can represent a natural hazard for surrounding communities (Xiao et al., 2015; Hock and Rasul, 2019). Detecting snow with optical satellites is long established using band ratioing (Lopez et al., 2008; Rastner et al., 2014) and the Normalised Difference Snow Index (NDSI) (Salomonson and Appel, 2004; Gascoin et al., 2019). With these data in cloud computing platforms, global-scale snow cover maps are now being produced regularly at a medium spatial resolution (Dietz et al., 2015; Mityók et al., 2018; Gascoin et al., 2019). Snow cover on glaciers can be indicative of equilibrium line altitude (Rabatel et al., 2012). With the addition of a DEM, optical imagery can be autonomously processed to detect the snow-line altitude to an 80% accuracy, though clouds, shadows, and significant fresh snow remain key limitations (Rastner et al., 2019). Daily PlanetScope imagery could be used to detect snow-line altitude at much higher temporal resolution (Racoviteanu et al., 2019).

Accurate quantification of snow depth is important for water resource management, to enable planning on short to medium timescales. Typically these data come from *in situ* snow gauges (Egli and Jonas, 2009) or terrestrial laser scanners (Prokop, 2008). Digital photogrammetry can measure snow depth to avoid potentially dangerous field excursions to gather data using UAVs (Bühler et al., 2016) and even high resolution stereo satellite imagery by comparison to snow-free images (Marti et al., 2016) – a method which can offer sub-metre root mean squared error when compared to airborne lidar measurements (Deschamps-Berger et al., 2020). Passive microwave satellites can quantify snow water equivalent and indicate melting of snow large glaciers (Smith and Bookhagen, 2018) but wide sensor footprints (tens of km^2) can limit this over smaller glaciers (Clifford, 2010). SAR sensors have commonly been used for monitoring snow in the mountain cryosphere to identify wet snow (and thus indicate melt), from SeaSat (Rott, 1984) to Sentinel-1 (Tsai et al., 2019a). A comprehensive review of the role of SAR sensors in monitoring snow is available from Tsai et al. (2019b).

2.3. Upcoming innovations in sensor technology

Current trends and future forecasts both point towards a rapid rise in the launch of EO satellites, particularly from the commercial sector, over the next decade. Innovations will also positively impact field-based remote sensing, as UAVs become

increasingly accessible and interdisciplinary research leads to searching for solutions from outside of the mountain cryosphere. In this section, we review some of the upcoming planned missions that could address research gaps in observing the mountain cryosphere, and identify where gaps still remain.

2.3.1. Optical sensors

Established civilian programmes (Landsat, Copernicus) are facing increased competition in a world where innovation is being rapidly driven by the commercial sector. Landsat-9 (launched 2021) is designed with virtually identical sensors to its predecessor as a data continuity mission (Markham et al., 2016). Landsat-9 is acquiring imagery at 14-bit depth resolution, which allows for a quadrupled radiometric sensitivity (and thus better feature depiction) over bright targets such as snow and ice when compared to 12-bit sensors on-board Landsat-8, Sentinel-2, and Planet Labs' Dove satellites. This unbroken series of 50+ years from Landsat is particularly vital to the mountain cryosphere, where year-to-year changes in ice extent, surface albedo, or lake growth can be observed. Looking to the future, Landsat NeXt (the successor to Landsat-9, launching in the late 2020s) will include greater spectral range, narrower bands, and higher spatial resolution to retain relevance (beyond its long record) as competition grows from constellations and SmallSats (spacecraft with a mass less than 180 kg) (Wulder et al., 2019; Wu et al., 2019; NASA, 2021).

Satellite constellations designed for near real-time imaging (data distribution within hours of acquisition) are becoming more popular and promise to shape the coming decade of EO (Table 2.1). Having multiple satellites working together clearly offers numerous advantages over single satellite missions, but the trade-off may be in terms of uneven instrument degradation. Although Planet Doves are radiometrically calibrated against Landsat-8, RapidEye, and monthly lunar acquisitions, image quality and signal-to-noise ratio still varies between sensors (Leach et al., 2019). Noise within optical data usually arises from atmospheric interference (Jorge et al., 2017), which is typically corrected with shortwave infrared (SWIR) bands that SmallSats are lacking (Vanhellemont and Ruddick, 2018). These missing SWIR bands are also critical in distinguishing between the spectral signatures of ice and water (Dozier, 1989). Day-to-day changes observed by constellation imagery should therefore be approached cautiously, as they may reflect differences between satellites rather than on-the-ground change (Cooley et al., 2017; Poursanidis et al.,

2019). Landsat and Sentinel may have medium spatiotemporal resolution, but they compensate for this with their consistent data quality.

Compared to long-standing satellite sensors such as Landsat and Sentinel, SmallSat constellations offer reduced radiometric resolution, geometric fidelity, and spectral resolution, but the trade-off can be found in the vast volume of data they acquire. Planet Labs were one of the first organisations to mass produce multispectral SmallSats with their Dove satellites, which today provide global daily sub-3 m imagery. Since the first launch of their Doves in 2016, Planet Labs have expanded their market niche to releasing over 300 SmallSats at varying altitudes for improved spatiotemporal resolution. This has obvious benefits for hazard management where events can be sudden in their onset (such as lake outburst events (Miles et al., 2018b), glacier surges (Rashid et al., 2020), or ice avalanches (Shugar et al., 2021)), and where weather windows for successful observations may be short-lived. Studies of short-term (diurnal) variations in ice surface albedo (e.g. Naeimi et al., 2018) will also benefit from more frequent data capture (Altena and Kääb, 2017). Recently launched optical satellites will improve both timeliness and flexibility of imaging – Pléiades Neo (launched in 2021) will revisit the same mid-latitude area up to 15 times per day (Airbus, 2020), while WorldView-Legion (2021) claim to be able to provide data to the user within an hour of the satellite being tasked (Maxar Technologies, 2020). Planet Labs's Pelican satellites will build on both Pléiades Neo and WorldView-Legion by revisiting mid-latitude areas up to 30 times a day and providing data to the user within 5 minutes of acquisition. Other upcoming constellations, such as EarthDaily (planned for launch in 2023), promise to reconcile the long-standing trade-off between data quality and quantity, by producing sensors similar in radiometric resolution and fidelity to Sentinel-2 and capable of delivering daily, 5 m resolution imagery, for better forecasting of glacier hazards (Yan et al., 2017). These satellites are predominantly for-profit commercial missions (as opposed to open-source civilian missions such as Copernicus and Landsat), and the data access to researchers or civilians for studies of the mountain cryosphere is as yet unknown.

Satellite	Launch	Number of satellites	Spatial Resolution	Temporal frequency (equator)	Bit rate	Spectral bands	
Landsat-8	2013	1	15 m (pan); 30 m	16 days	12-bit	Coastal Aerosol: 430 – 450 nm Blue: 450 – 510 nm Green: 530 – 590 nm Red: 640 – 670 nm Near-IR: 850 – 880 nm SWIR1: 1570 – 1650 nm	SWIR2: 2110 – 2290 nm Pan: 500 – 680 nm Cirrus: 1360 – 1380 nm TIRS1: 10.6 – 11.19 µm TIRS2: 11.50 – 12.51 µm
Sentinel-2	2015	2	10 m	5 days	12-bit	Blue: 458 – 523 nm Green: 543 – 578 nm Red: 650 – 680 nm Red Edge: 698 – 713 nm Red Edge: 733 – 748	Red Edge: 773 – 793 Near-IR: 785 – 899 nm Near-IR: 855 – 875 nm SWIR: 1565 – 1655 nm SWIR: 2100 – 2280 nm
Planet SuperDove	2019+	150+	3 m	Daily	12-bit	Blue: 457.5 – 522.5 nm Green: 542 – 577.5 nm Red: 650 – 680 nm	Red Edge: 697.5 – 712.5 nm Near-IR: 855 – 875 nm
Pléiades Neo	2021 (2) + 2022 (2)	4	30 cm	Sub-Daily	12-bit	Deep Blue: 400 – 450 nm Blue: 450 – 520 nm Green: 530 – 590 nm Red: 620 – 690 nm	Red Edge: 700 – 750 nm Near-IR: 770 – 880 nm Pan: 450 – 800 nm
Landsat-9	2021	1	15 m (pan); 30 m	16 days	14-bit	Identical to Landsat-8	
WorldView-Legion	2021	6	0.29 m (pan); 1.16 m	Hourly	?	Pan: 450 - 800 nm Coastal: Blue: 400 - 450 nm Blue: 450 - 510 nm Green: 510 - 580 nm Yellow: 585 - 625 nm	Red: 630 - 690 nm Red Edge1: 695 - 715 nm Red Edge2: 730 - 750 nm Near-IR: 770 - 895 nm
Planet Pelican	2023	32	0.3 m	Hourly	?	Unknown	
EarthDaily	2023	8	5 m	Daily	?	Identical to Sentinel-2	

Table 2.1 – Overview of key specifications of current and future optical satellites that play an important role in monitoring the mountain cryosphere.

Similar advances are being made with multi-sensor missions. Multi-sensor approaches overcome inherent limitations of a single-sensor mission (Markert et al., 2018), providing further insights into surface mass balance (such as using SAR backscatter to monitor snowlines, glacier facies, and firn development) (Winsvold et al., 2018), as well as potential for maintaining coherence between image pairs by reducing their temporal baseline. One such constellation, OptiSAR, aims to launch 8 optical and 8 SAR satellites in tandem orbit pairs, capturing image pairs seconds apart (Fox et al., 2017), though its current development is unknown owing to financial precarity. If launched, on-board intelligence, with communication from the leading SAR satellite, will enable the optical satellite to only acquire over cloud-free areas to improve satellite efficiency (Beckett et al., 2017).

2.3.2. Radar sensors

The weight and power requirements of radar sensors have thus far limited the emergence of small SAR satellites, at least when compared to the rapid evolution of optical sensor constellations (Sandau et al., 2010). Micro-SAR satellites are often forced to compromise on antenna size and power output, resulting in lower overall quality (Seguin and Geudtner, 2018), and aperture widths that are ~10% that of larger single satellites (Rosen et al., 2017). Indeed, small satellites are frequently 'tasked' to preserve power, meaning sudden-onset events such as avalanches, landslides, or GLOFs, may not be captured, and imagery showing conditions immediately preceding the event may need to be filled by alternative freely available data sources (Higman et al., 2018). Nevertheless, the next decade will deliver commercial constellations such as ICEYE, Capella Space, and SAR-XL, which promise to provide imagery at sub-daily repeat time, albeit with a possible compromise on image quality. Table 2.2 outlines upcoming radar sensors, in the context of other (current) satellite missions.

SAR Band	Wavelength (cm)	Frequency (GHz)	Missions	Applications
P	30 – 100	0.3 – 1.0	Biomass*, ICESAR2012†	Tomography
L	15 – 30	1.0 – 2.0	NISAR*, ROSE-L*, SeaSat†, SRTM†, JERS-1†, ALOS†	Tomography, Velocity Mapping, Displacement Mapping, Snow water equivalent
S	7.5 – 15	2.0 – 4.0	NISAR*, NovaSAR-S, Envisat†	Snow hydrology
C	3.75 – 7.5	4.0 – 8.0	Sentinel-1, Sentinel-3, Radarsat, ERS†, Envisat†, SRTM†	Classifying wet/dry snow, firn line mapping, snow line mapping, velocity
X	2.4 – 3.75	8.0 – 12.5	TerraSAR-X, ICEYE, Capella Space, SRTM†	3D capabilities, elevation change, glacier velocity, mass dynamics
Ku	1.67 – 2.4	12.5 – 18.0	CryoSat-2, Sentinel-3, ERS-1/2†, Envisat†	Surface elevation, volume change, mass dynamics
Ka	0.75 – 1.13	26.5 – 40.0	SWOT*, SARAL AltiKa	Surface elevation, continental surface water storage changes

*Table 2.2 – Radar satellites and their applications to monitoring the mountain cryosphere. *denotes confirmed future mission not yet launched as of July 2022. †denotes mission that is no longer in operation.*

Proposed candidate missions to expand the Copernicus mission shows that ESA will continue to focus on the cryosphere, but with dual-frequency missions (e.g. CRISTAL) designed for polar regions rather than mountain glaciers (Kern et al., 2020). In satellite based radar systems, two upcoming L-band missions look to reintroduce subsurface imaging to the forefront of glacier remote sensing. ESA's ROSE-L (Pierdicca et al., 2019) and NASA's NISAR (Rosen et al., 2017) will complement existing radar missions by offering the ability to examine surface velocity and glacier mass balance with reduced temporal decorrelation from deeper penetration into the ice (Strozzi et al., 2008), as well as permafrost displacement and snow-water equivalent. ROSE-L will work in association with other Copernicus missions (e.g. Sentinel-1) to offer new insights into the mountain cryosphere. For example, Sentinel-1 could delineate wet and dry snow, then ROSE-L could quantify the snow-water equivalent of the dry snow (Davidson et al., 2019). The synergy of L-band and S-band sensors onboard NISAR will allow for a more holistic view of glacier dynamics, focussing on glacier velocity and snow hydrology simultaneously. In a

break from convention, these satellite sensors are being designed explicitly with mountain glaciology in mind and, as civilian missions, data will be freely available.

Developments in satellite altimetry have thus far mostly benefitted routine monitoring of ice sheet surface elevations, where large measurement footprints and non-uniform repeat tracks can be compensated for, in contrast to mountain regions where the highly variable surface topography precludes robust interpolation between observations. The upcoming launches of Sentinel-3C and -3D, which will complete the Sentinel-3 constellation, include plans for higher resolution on-board tracking commands to capture meaningful data over mountain glaciers. ICESat-2 offers vastly more data than its predecessor; with six laser beams to reduce the distance between ground tracks and a rapid pulse rate to measure elevation up to every 90 cm on the ground. It will be challenged in mountainous environments with its 91-day repeat time and inability to penetrate clouds; potentially leaving significant data gaps. Initial data from ICESat-2 show that the satellite performs well over mountain glaciers (Figure 2.4), with high precision elevation measurements of the glacier surface. The upcoming Surface Water and Ocean Topography (SWOT) mission (2021) seeks to further innovate radar altimetry, but for the mountain cryosphere its application will likely be limited to low-resolution products (Biancamaria et al., 2016).

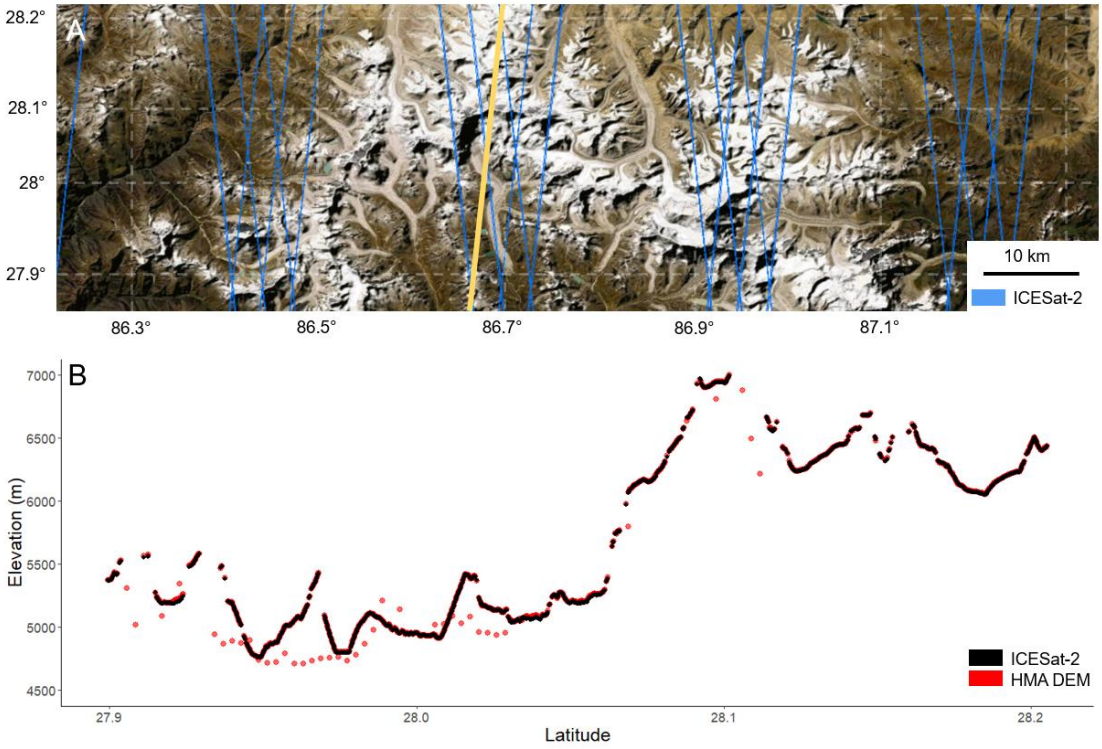

Figure 2.4 - Comparison of elevation retrievals from ICESat-2 with those of the High Mountain Asia (HMA)-2 DEM (Shean et al., 2020) over the Everest region of Nepal. (A) Available ground tracks of ICESat-2 data for the region, with the yellow track indicating data selected in below panel. Image from Google Earth and Maxar Technologies, 2020. (B) Comparison of the ICESat-2 ATL06 product relative to the High Mountain Asia 8 m DEM.

2.3.3. UAVs

The flexible nature of UAVs allows for custom-built mountable sensors to address site-specific research questions. Hyperspectral imaging from UAVs in other geoscience disciplines have shown success in producing SfM 3D models in over 100 spectral bands (Honkavaara et al., 2017). Over mountain glaciers, hyperspectral imagers on UAVs could be used to study contaminants and pollutants at a much higher resolution than has hitherto been possible. For example identifying the components of cryoconite (Di Mauro et al., 2017), the presence of organic matter, or origin and impact of dust on albedo (Di Mauro et al., 2015) in a more efficient way than can be achieved from spot measurements. In landmine detection, ground penetrating SAR instruments have been mounted on UAVs to accelerate clearance (Schartel et al., 2018) which could be applied to measuring snow depth or characterising englacial conditions.

In theory, there are no technical limitations to the deployment of regularly repeating autonomous UAV surveys. UAVs have already been designed to return 'home' to a wireless charging pad when their battery runs low (Junaid et al., 2016; Junaid et al., 2017; Campi et al., 2019), and solar panels could keep a constant energy supply to a battery pad, with autonomous de-icing (Sorensen et al., 2015). With a microcontroller onboard to detect weather patterns, control flight paths, data acquisition, and transmission, UAVs could potentially be designed to conduct surveys completely independent of any pilot or physically present operator. Such an autonomous system would have obvious benefits where change is rapid and early warning of a developing hazard is beneficial, although the legal obstacles to uncrewed flights in this way may become problematic as most countries look to tighten, rather than relax, their UAV regulations (Stöcker et al., 2017).

2.3.4. Other field-based innovations

The principles and main applications of photogrammetry are now well established within the geosciences (Smith et al., 2016), allowing the reconstruction of 3D models from an array of 2D images, and the production of very high-resolution models (cm-scale) from off-the-shelf cameras (James and Robson, 2012; Mallalieu et al., 2017; Giordan et al., 2020). We envisage that the future of this technique is in sensors built with low-cost microprocessors (Figure 2.5), and in its autonomy; from capture to subsequent processing for real-time 3D of the mountain cryosphere.

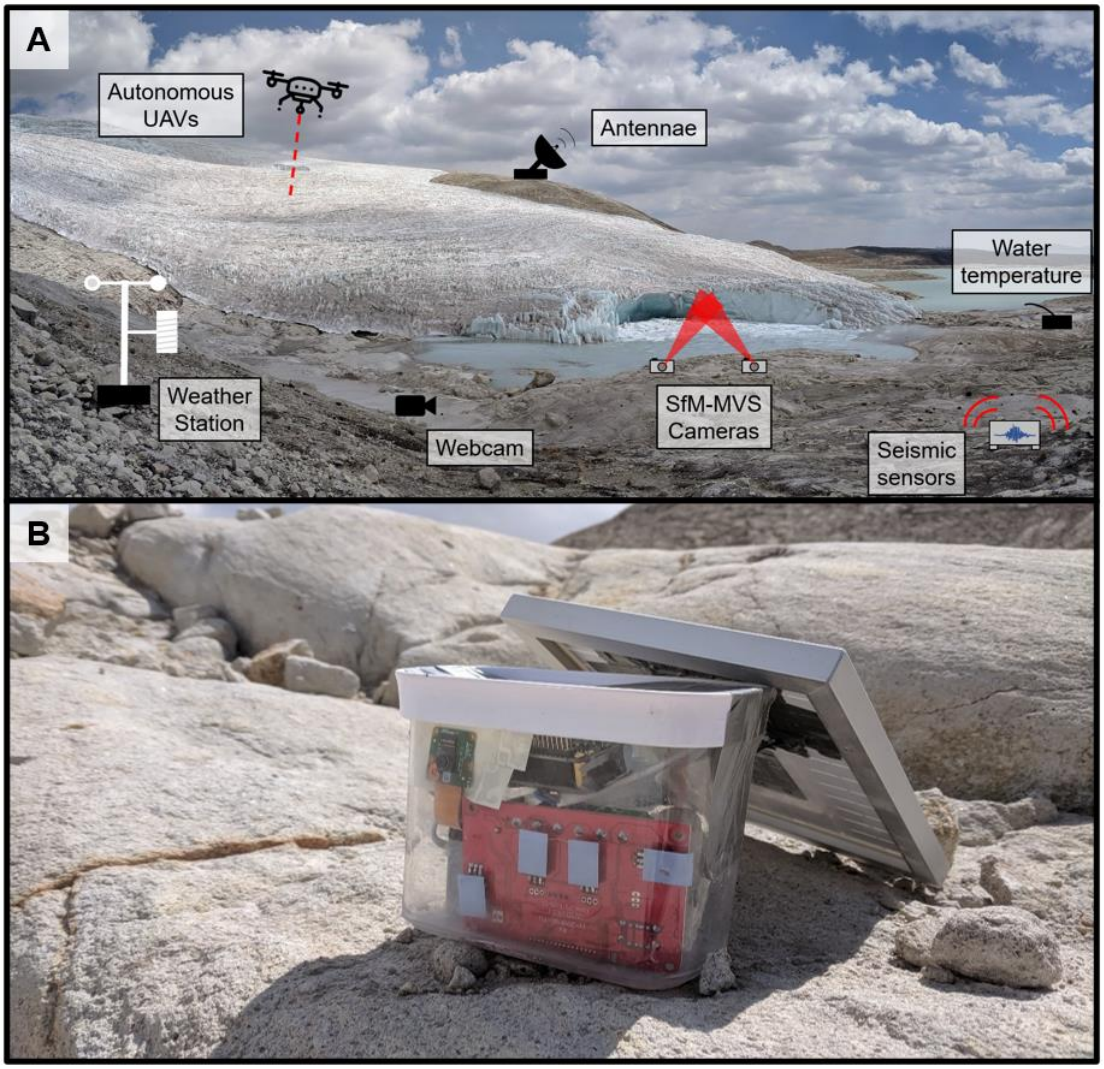

Figure 2.5 - The potential of small low-cost sensors in mountain glaciology. (A) Low-cost in-field remote sensing could be expanded with the use of low-cost sensors to include camera networks, weather stations, seismic stations, acoustic sensors and more communicating in a local network or connected to the internet through 4G/5G networks or satellite internet. (B) Raspberry Pi camera setup costing less than $50 at a glacial margin at the Quelccaya Ice Cap, Peru.

As satellite internet expands coverage and connectivity in remote regions, and decreases in cost through the launch of constellations such as Starlink (SpaceX) and OneWeb, sensors that are left *in situ* will become routinely programmable such that they transmit recorded data autonomously for subsequent cloud storage and/or processing over satellite internet. Such technology already exists over cellular connections, but the lack of a suitable infrastructure in much of the mountain cryosphere currently makes this an unfeasible option. Autonomous SfM

photogrammetry has been proven in studies of soil displacement (Eltner et al., 2017), landslides (Kromer et al., 2017), and rockfalls (Blanch et al., 2019), which indicates it could also be a lucrative line of investigation for glaciology. In a similar vein, webcam images from ski resorts have been used to create snow cover classification maps in the Alps (Portenier et al., 2020), removing the need for physical visits by researchers altogether.

Advances in robotics and robot design may offer insights into mountain glaciers that could open a significant new sub-branch of the discipline. Presently, the englacial system of a glacier remains somewhat of an enigma, with access limited to conduits that are safe and accessible enough for physical exploration (Gulley and Benn, 2007), using ground penetrating radar (Church et al., 2019), or the drilling of boreholes (Miles et al., 2019; Miles et al., 2021b). In the mining industry, robots and automated UAVs have been used to explore and map underground conduits (Mitchell and Marshall, 2017) – similar to the englacial systems of a glacier. Systems that make use of relay and 'sacrifice' robots enable constant communication, regardless of the complexity of the underground system (Cesare et al., 2015). While this technology is still in its primacy (Mitchell and Marshall, 2020), its adaptation for subsurface glacier exploration would make significant steps towards answering questions on the characteristics, dynamics and evolution of the hydrological networks that influence ice flow as well as the timing and magnitude of proglacial discharge (Miles, et al., 2019b). Sensors embedded in the ice via boreholes can also indicate surface melting, ice velocity, water pressure (Hart et al., 2019a), and (when reaching the bed) till deformation and basal icequakes (Hart et al., 2019b). Similarly, sensors deployed around an ice-dammed lake in Canada were used to infer its englacial hydrology (Bigelow et al., 2020).

2.4. Computational innovations to address research gaps

In many cases, knowledge gaps can be addressed using one or more of the data sources currently available to researchers and stakeholders. Here, we argue that computational innovations may create the biggest difference in the next decade of observing the mountain cryosphere (Gomes et al., 2020). We introduce some of the computational innovations that have driven the discipline in the last five years in order to assess their future trajectory. We explore how research gaps could be addressed with techniques such as deep learning and cloud computing, and offer suggestions on future directions.

2.4.1. Cloud Computing and Big Data

Cloud computing platforms, which allow for wide area geospatial analysis, offered a step-change in processing potential for the discipline as processing is moved to the area of data storage. While cloud computing is not 'new', as high performance computing (clustering hardware together to boost computational power) has been used in remote sensing for decades (Lee et al., 2011), the differentiator of cloud computing shifts the financial burden of the hardware for such power. Freely available cloud computing interfaces, such as Google Earth Engine (Gorelick et al., 2017), Climate Engine (Huntington et al., 2017), pipsCloud (Wang et al., 2018), and Sentinel Hub (Sinergise, Ltd.) allow for batch processing and regional scale investigations without compromising on the spatial resolution being studied (Figure 2.6). The platforms allow for spectral investigations, such as NDSI and NDWI (e.g. (Kraaijenbrink et al., 2017; Zhang et al., 2018; Shugar et al., 2020), and tap into freely available archives such as Landsat, Sentinel, and SRTM, as well as user-imported data. Most importantly, the interfaces are designed to be user-friendly to appeal to the growing EO market (Denis et al., 2017) while also providing scope for complex analysis to suit a broad array of applications.

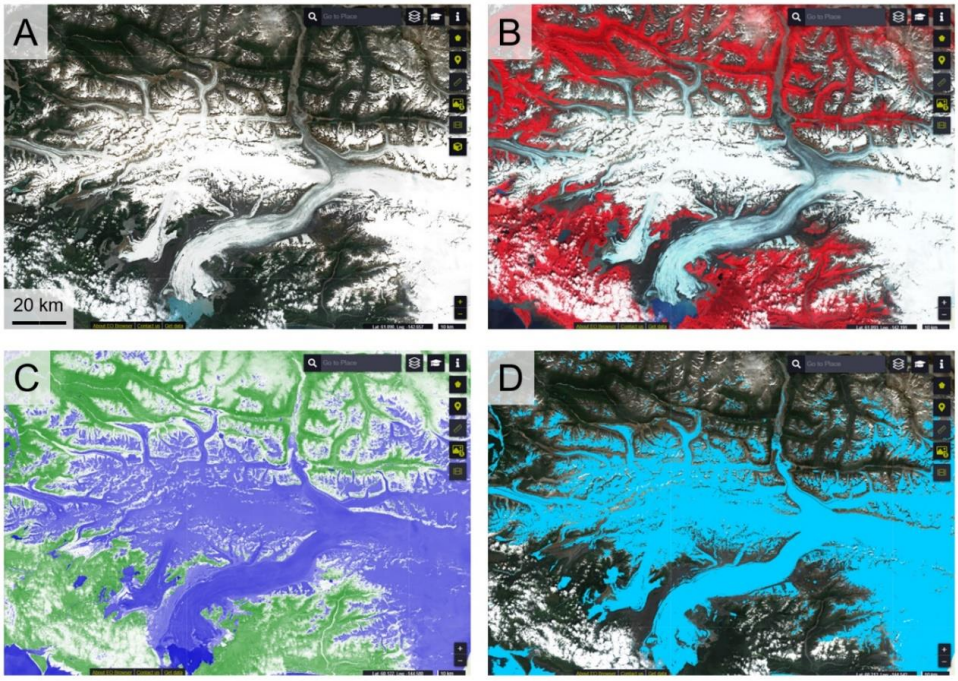

Figure 2.6 - The EO Browser allows analytical cloud computing of Sentinel data in a user-friendly API that can display (A) true colour imagery, (B) false colour composites, (C) NDWI, (D) NDSI, and other analytical analyses. Here, Sentinel-2 data is displayed over Bering Glacier, Alaska. Such platforms open remote sensing of the mountain cryosphere to users with little prior experience.

The applications of cloud computing to accelerate research in the mountain cryosphere are vast. Autonomously, and rapidly, large volumes of near real-time satellite data can be downloaded and processed into a user-friendly output for management, stakeholders and communities to digest. Research can be conducted at a regional scale benefiting from petabytes of data to inform international policy by combining multispectral imagery, elevation data, climate modelling and ice thickness data. For example, in the Himalayas, this approach has been used to predict the future of all glaciers under a 1.5˚C warmer climate (Kraaijenbrink et al., 2017). Conventional computing infrastructure is inefficient at storing, processing, and transferring such large volumes of data. A particular benefit for the mountain cryosphere is that cloud masking and mountain shadowing of optical imagery is easily incorporated into the analysis flow chain for accurate digitisation of glacial lakes (Chen et al., 2017; Shugar et al., 2020) and calving fronts (Lea, 2018) at a global scale. Vast quantities of Sentinel-1 SAR imagery can be ingested for change-over-time studies, for example, to map glacial lakes across the Tibetan Plateau (Zhang et al., 2020) or assess snowmelt across the Alps and Iceland (Nagler et al., 2016) every six days. Furthermore, the advent of freely available cloud computing, together with public data extensive documentation, means processing does not have to be limited to funded scientists or highly-trained specialists.

Increased synchronisation between EO data can benefit mountain glaciology via open source pipelines and packages that can be embedded into coding platforms, and linked to cloud computing for performance. While they may lack a user-friendly interface, they have the potential to answer unique research questions. In particular, the AMES Stereo Pipeline by NASA (Beyer et al., 2018) is now widely used to produce 3D stereo data from thousands of ASTER images for regional glacial mass balance reconstructions since 2000 (Brun et al., 2017; Menounos et al., 2019; Dussaillant et al., 2019; Shean et al., 2020). Over the next few years, similar free packages will provide greater accessibility to satellite data. For example, sPyMicMac (McNabb et al., 2020) will automate the pre-processing of nuances from the Hexagon US reconnaissance mission from the 1970s, providing easier access to these historic data for quantifying regional mass balance over fifty years ago. PyTrx (How et al., 2020) will ingest terrestrial time-lapse data and perform calibration, registration, georectification, feature tracking, and change detection to speed-up monotonous pre-processing of *in situ* camera data. ITS_LIVE (NASA; Gardner et al., 2018) will continue to create glacier velocity products from the 1980s to present day at high temporal frequency by collating measurements from multiple sensors (e.g. data from

the Landsat and Sentinel-1 missions are all used). Each of these freely available packages either performs their analysis using cloud computing, or supports adaptation into a cloud computing environment in order to efficiently process vast volumes of data. Over the mountain cryosphere, cloud computing could therefore lead to near real-time processing of ice surface dynamics, or detection of hazardous events.

2.4.2. Artificial Intelligence and Machine Learning

The broad field of Artificial Intelligence (AI) includes Machine Learning (ML) (whereby systems autonomously learn from themselves without prior programming), which is a powerful tool in solving the various challenges of EO. Deep learning (DL) algorithms are a subset of ML, using multiple layers of neural networks to increase their complexity and accuracy (Zhu et al., 2017; Hoeser and Kuenzer, 2020). For the mountain cryosphere, ML and DL models can be applied to classification, feature spotting, automatic mapping, and visual interpretation tasks as well as time series reconstruction and simulation (Paul et al., 2004; Brenning, 2009; Lary et al., 2016; Zhu et al., 2017; Bolibar et al., 2020). The application of DL algorithms for the cryosphere is still very scarce. Only 2% of studies dealing with DL-based image segmentation and object detection investigated on cryosphere topics (Hoeser et al. 2020). This highlights the unused potential of DL-based applications on the mountain cryosphere (Figure 2.7).

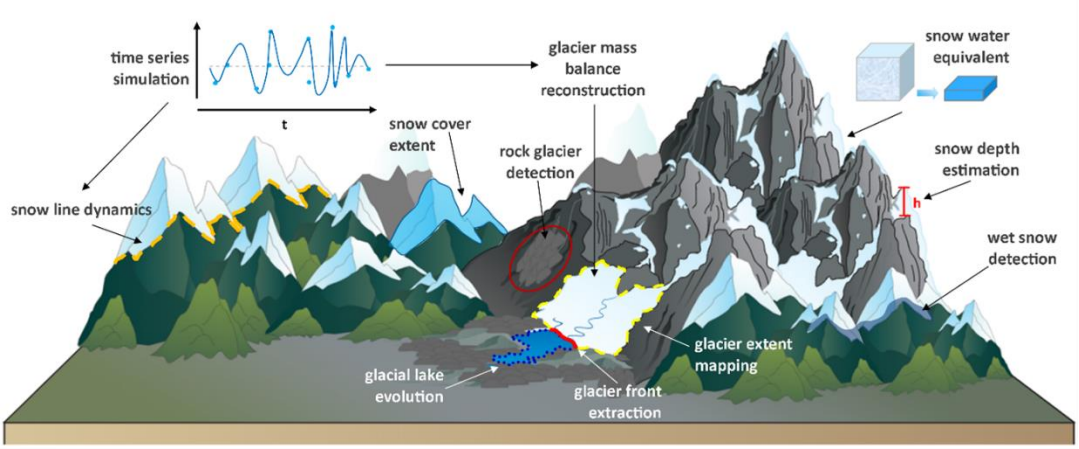

Figure 2.7 – Potential artificial intelligence applications to the mountain cryosphere.

For the first time, ML allowed classifying wet and dry snow in SAR data by applying a random forest classifier. High classification accuracies (F1-score over 90%) in mountainous areas were achieved regardless of underlying land cover (Tsai et al., 2019b). Snow cover mapping was improved by creating a hybrid model including DL (Alex-Net), ML (random forest), and hand-crafted (manually designed) features. Classification accuracies of 98% were reached based on medium-resolution optical and radar Sentinel-1/2 images in addition with a digital elevation model (Nijhawan et al., 2019). Using Sentinel-2 imagery, Google have used DL to generate a real-time land classification product for monitoring dynamic landscapes, such as changing snow cover (Brown et al., 2022). Mapping snow cover extent from high-resolution optical imagery has been performed by Guo et al. (2020) using pre-trained weights of a DeepLabv3+ model for Landsat-8 true-colour imagery to create accurate results with a small dataset of GaoFen-2 imagery. Besides classification tasks, a random forest regressor can be applied to reconstruct incomplete time series. For example, Hu et al. (2020) applied a random forest regression to model regional snowline elevations from optical earth observation data. Current challenges for snow-related AI applications include quantifying the snow-water equivalent and estimating the snow depth (Kopp et al., 2019; Odry et al., 2020).

ML applications on mountain glaciers focus on the determination of the glacier extent by either extracting the calving front (Mohajerani et al., 2019; Baumhoer et al., 2019a; Cheng et al., 2020) or detecting the glacier boundary of debris covered glaciers (Nijhawan et al., 2018; Xie et al., 2020; Khan et al., 2020). Additionally, DL algorithms can be used to simulate time series. For example, Bolibar et al. (2020) modelled glacier evolution by simulating glacier-wide surface mass balance time series by an artificial neutral network. However, even common and simple machine learning algorithms (e.g. random forest) can yield better results than DL-based approaches, emphasising the importance of choosing the right AI model for each specific task. In glaciology, the potential that DL can offer, in automation, efficient processing, and removal of traditionally laborious manual tasks, is slowly being realised and still has unexploited potential.

Intelligent learning does not have to be solely analytical. Embedding AI into sensor design could create powerful tools for in-field glacier monitoring. With data transmission via high-gain antennae (e.g. Carvallo et al., 2017) or satellite internet, we hypothesise that low-cost sensors, embedded within an AI framework, could revolutionise mountain glacier monitoring, as it has done in many other geoscience disciplines (Chan et al., 2020). Such sensors could include Arduinos or Raspberry

Pis (Vujovic and Maksimovic, 2014) that could act as a webcam, capture infra-red images at night, detect thermal signatures, record acoustic events, detect ground displacement or tremors from calving, track velocity with GPS, or communicate with satellites for real-time ground-truthing, for example. Each bespoke sensor can 'talk' intelligently to another, such the network could respond to real-time changes such as calving events, surges, or supraglacial pond drainage. In the wider literature, these intelligent systems have been called the 'Internet of Things' (Gubbi et al., 2013; Khalil et al., 2014; Alzahrani, 2017). There are vastly more complex logistical challenges in the mountain cryosphere, but none of these individual ideas are new. The interconnectedness, intelligent design, and autonomy that can be offered by such an approach marks a step-change in our understanding of the geomorphic processes currently shaping the world's mountain environments.

2.4.3. Open Science

One of the most limiting factors in the use of remote sensing data over mountain glaciers is data availability and, even where data are available, they are not necessarily accessible (Pope et al., 2014). Hazard assessment plans produced for the mountain cryosphere require routine and open information on landslides, slope stability, and future glacial lake expansion (Schaub et al., 2013; Emmer and Vilímek, 2013; Linsbauer et al., 2016; Ambrosi et al., 2018; Kirschbaum et al., 2019). Such data can provide a critical role in informing planning decisions being made by stakeholders in mountain regions. An increasing number of research programmes are committing to making their outputs open access, such as NASA's High Mountain Asia Program, which combines a variety of remotely sensed derivatives (DEMs, glacier thickness, landslide inventories, mass balance) with *in situ* data (wind, precipitation, temperature, irradiance) for free download through an open access portal (https://nsidc.org/data/highmountainasia). This follows a precedent set by civilian programmes (e.g. Landsat and Copernicus) that public funded missions should be open-source at delivery.

Citizen science programmes have great potential to radically transform remote sensing of the mountain cryosphere (Carey et al., 2016). Strengthening local collaborations is vital towards the successful mitigation of hazard risks, and adaptation to the impacts of climate change in mountains (Nussbaumer et al., 2017; Huggel et al., 2020). Knowledges should be co-produced for better understanding concerns and identifying adaptations solutions that work best for each community

(Klenk et al., 2017). This is particularly true of remote sensing work, where it is easy to perform and publish data analysis without ever entering the place we study. There is a dearth of studies that combine remote sensing data over mountain glaciers with local knowledge, and we should learn from where this has proved effective in other disciplines – such as landslide risk management (Holcombe et al., 2021), land degradation analysis (Yiran et al., 2012), and ecology (Eddy et al., 2017).

Remote sensing data require *in situ* calibration and can lead to erroneous results and damaging policy suggestions if relied upon in isolation (such as NASA's infamous false reporting of imminent danger at Lake Palcacoha, Peru; Kaser and Georges, 2003). At the same time, many DL algorithms require a large training set (Zhang et al., 2019a), which is often produced manually. Engaging citizens to classify features works well in disaster management projects such as *Missing Maps* (Scholz et al., 2018). Geotagged photos from social media can also be harvested for damage assessment following flood events (Cervone et al., 2016), identifying tourism and popularity of protected sites (Walden-Schreiner et al., 2018), assessing land cover change (Xing et al., 2017), and reconstructing 3D structures (Themistocleous, 2017), each of which could be applied to the mountain cryosphere. In mountain glaciology, local communities are working alongside researchers in setting up basic equipment such as webcams (Portenier et al., 2020) and mountaineers are increasingly collecting data and observations to report on changes (Watson and King, 2018) as well as to assess the true risk of hazards observed from space (Carey et al., 2016).

Interactive data viewing portals can be an effective way to showcase research outputs, rather than static scientific figures that may alienate non-specialists. Initiatives such as the GLIMS Glacier Viewer (http://www.glims.org/maps/glims), ArcGIS Living Atlas (https://livingatlas.arcgis.com/en/home/), Sentinel Hub (https://apps.sentinel-hub.com/eo-browser/), or the recently launched NASA ITS_LIVE (https://nsidc.org/apps/itslive/; Gardner et al., 2018) are easy to access, understand, and extract information from. When this is the case, data are more readily used (Pope et al., 2014), and offer an effective conduit for engaging stakeholders outside of academia.

2.5. Summary

In this review, we sought to provide an assessment of the current capabilities of remote sensing over the mountain cryosphere, with a view to identifying future avenues of research. Remote sensing has been crucial to understanding and

monitoring the mountain cryosphere. Satellite missions have been used to monitor lakes, quantify ice melt, classify snow, and detect natural hazards. Civilian missions offer science-grade sensors with long archives, while newer commercial constellations offer rapid revisit time at a higher spatial resolution. In the rapidly expanding sector of EO satellites, innovation in sensor design over the next decade will produce higher quality data, expand the offering of complementary sensor technology, and create sub-daily repeat periods. Such vast quantities of data require cloud computing infrastructure to efficiently process, and AI will shape the next decade of processing as monotonous tasks are replaced by automation. DL will further the potential of AI; drawing upon the expanding pool of data available to address outstanding research questions in glaciology. The expanding breadth of sensor options available to UAVs is also now beginning to be realised in mountain glaciology. Furthermore, low-cost sensors could create affordable science for community monitoring systems. It is imperative that data and processing capabilities continue along the road to becoming freely available, so that communities who will be adversely affected by future changes to the mountain cryosphere, can use remote sensing as an effective tool in planning their response.

Chapter 3

Multi-decadal glacier area and mass balance change in the Southern Peruvian Andes

3.1. Introduction

Tropical glaciers are highly sensitive to climatic changes and those in Peru, where the vast majority (~70%) are located, have been rapidly receding for several decades (Chevallier et al., 2011; Salzmann et al., 2013; Schauwecker et al., 2014; Zemp et al., 2019). Consequently, as mountain slopes become destabilised, there has been increased threat from natural hazards, an observed growth in the number and area of glacial lakes, and changes to primary water supply (Drenkhan et al., 2019; Brügger et al., 2021; Veettil and Kamp, 2021; Thompson et al., 2021). Glacier recession is unlikely to be reversed as reductions in precipitation and increases in temperature are projected until at least 2100 (Kronenberg et al., 2016). Studies of future river discharge are unanimous in predicting a reduction in longer-term water supply, particularly during the dry season when glacier melt provides a critical buffer against drought (Vuille et al., 2008).

Compared to other mountain glacier regions around the world, there is a notable dearth of region-wide estimates of mass balance change for those located in Peru (Vuille et al., 2018). Previous studies have focussed on quantifying rates of glacier recession using satellite-based measurements of both area and volume change. At a continental-scale, Dussaillant et al. (2019) assessed mass balance across the Andes, noting that the glaciers of the tropical Andes (-0.42 ± 0.24 m w.e. yr^{-1}) were losing mass at a steady rate between 2000 and 2018. At a national scale, Seehaus et al. (2019) presented areal losses of 28.6% from 2000 to 2016 and a Peru-wide mass balance of -0.457 ± 0.064 m w.e. yr^{-1}. In contrast to Dussaillant et al. (2019), Seehaus et al. (2019) found a recent (2013-2016) increase in the rate of mass loss. The National Inventory of Glaciers in Peru quantified a 48% decline of glacial area from 2,041.85 km^2 in 1962 to 1,058.37 km^2 as of 2021 (ANA, 2021).

Regional studies of glacier recession in Peru disproportionately focus on the largest region; the Cordillera Blanca. Here, glacier loss has accelerated since the 1970s with consequent increases in their terminus elevations (Racoviteanu et al., 2008b), following 20th century retreat from their Little Ice Age maximum extent (Georges, 2004) with a brief glacial advance interruption in the 1920s (Kaser, 1999).

Glaciers in the Cordillera Blanca extend to lower elevations than the second-largest region, the Cordillera Vilcanota, owing to a lower annual freezing line altitude (Sagredo and Lowell, 2012; Schauwecker et al., 2017). Nevertheless, the Cordillera Vilcanota follows similar trends to the Cordillera Blanca, having lost 30% of its glacierised area and 45% of its volume from 1985 to 2006 (Salzmann et al., 2013). The National Inventory of Glaciers shows a decline of 48% of glacierised area in the Cordillera Vilcanota from 1962 to 2017 (INAIGEM, 2017; ANA, 2021). Measurements of mass balance on individual glaciers show that topography is a key control on ice loss; glaciers with a maximum elevation below 5,400 metres above sea level (m a.s.l.) are estimated to be losing mass at a rate (-1.2 m w.e. yr^{-1}) double that of glaciers with an elevation above 5400 m a.s.l. (-0.6 m w.e. yr^{-1}) (Rabatel et al., 2013a).

The controls of glacier recession in the Peruvian Andes appear to be numerous, and are often interlinked. Overall, lower lying and smaller glaciers have been observed to be in rapid retreat (Rabatel et al., 2013a), although there is variability related to aspect, and therefore radiation receipt (Veettil et al., 2018). The surface energy balance of Peruvian glaciers is primarily controlled by precipitation, which impacts albedo and therefore radiation receipt over low-lying glacial termini (Vuille et al., 2008; Fyffe et al., 2021), particularly in the outer tropics (Kaser, 2001). Air temperature controls this precipitation phase, such that warming temperatures increase the proportion of a glacier receiving rainfall rather than snowfall, which subsequently also impacts their albedo and radiation receipt. The pattern is more complex when looking at specific regions of Peruvian glaciers. Some studies have made different links between discrete climatic variables and rates of glacier recession – for example, changes in temperature appear to be most important for glaciers in the Cordillera Huaytapallana (López-Moreno et al., 2014), while precipitation is a more important driver in the Cordillera Blanca (Fyffe et al., 2021). Over longer timescales, specific humidity may also play a key role in mass loss in other areas (Vuille et al., 2008; Salzmann et al., 2013). For tropical glaciers more broadly, Kaser (1999) suggests both air temperature and humidity play a role in causing recent (post-1980s) retreat. There is also some indication that the interannual variability of the El Niño Southern Oscillation (ENSO) impacts glacier mass change in the Peruvian Andes, with heavy snowfall during La Niña phases and stronger ablation during El Niño, though these linkages are weaker (Vuille et al., 2008; Drenkhan et al., 2018).

Given contemporary rates of recession, there is growing concern that many glacierised areas across Peru could be ice-free by the end of the century (Drenkhan et al., 2018). However, robust measurements of glacier change are still sparse, and

future projections are highly uncertain owing to the complexity of climatic and topographic factors driving change between regions (Schauwecker et al., 2017; Hock et al., 2019). The small size of tropical glaciers, and the fact that they are located in steep terrain, presents challenges for satellite-based observations as well as *in-situ* monitoring, meaning gaps in mass balance and ice area loss data persist for some regions, such as the Southern Peruvian Andes (Berthier et al., 2006; Prinz et al., 2018; Taylor et al., 2021). There remains a need for accurate, detailed and comprehensive studies that combine multiple datasets together to fully assess the dynamics of glaciers at high spatial and temporal resolution, the outputs from which can be invaluable for stakeholders and planners working to mitigate ongoing changes in runoff in these locations and guide climate change adaptation (Bury et al., 2011; Carey, Huggel, et al., 2012). A growing archive of satellite observations, along with the increasing availability of cloud-based and high-performance computing, provides an opportunity to fill some of those gaps.

Here, we use the 20-year ASTER (Advanced Spaceborne Thermal Emission and Reflection radiometer) satellite image archive as the basis for our analysis of glacier change in the Peruvian Andes. Previous studies have already defined a framework for producing regional (Dussaillant et al., 2018), continental (Brun et al., 2017; Dussaillant et al., 2019), and global (Hugonnet et al., 2021) measurements of glacier change using these data. Such datasets provide valuable insight into mountain glacier dynamics, their contribution to sea-level rise, and acceleration of melt, but they inevitably focus on the big picture of broad area changes. However, the usefulness of these large-scale datasets has seldom been examined in monitoring small mountain glaciers, particularly at their relatively coarse (100 m+) resolution. The overall aim of this research is, therefore, to provide detailed measurements of glacier area and volume change for the Cordilleras Vilcanota, Vilcabamba, and Urubamba, using the ASTER and Landsat satellite image archives, dating back to the 1970s. We generate medium-resolution (30 m) products of elevation change using the ASTER archive to assess the quality of the global Hugonnet et al. (2021) dataset in measuring mass balance over small mountain glaciers. We explore the key processes driving ice loss across these regions, and discuss likely future changes to these glaciers under various climate scenarios, all of which result in a rise in equilibrium line altitude (ELA) and thus continued, unabated mass loss.

3.2. Study Area

The Cordilleras Vilcanota (246.8 km^2 glacierised area in 2020; from this study), Vilcabamba (100.4 km^2), and Urubamba (24.2 km^2) represent a combined glacierised area of 371.4 km^2 (Figure 3.1). These regions are relatively understudied in comparison to the Cordillera Blanca (which is larger than all three together); yet, they represent a water source for hundreds of thousands of people in the wider Cusco region, many of which are located in the city of Cusco (population 470,000) (Drenkhan et al., 2018; Martínez et al., 2020). Recent glacial lake outburst floods at Salkantaycocha in 2020 (Vilca et al., 2021) and Riticocha in 2010 (Drenkhan et al., 2019) provide stark reminders of the threat that climatic changes pose in this region.

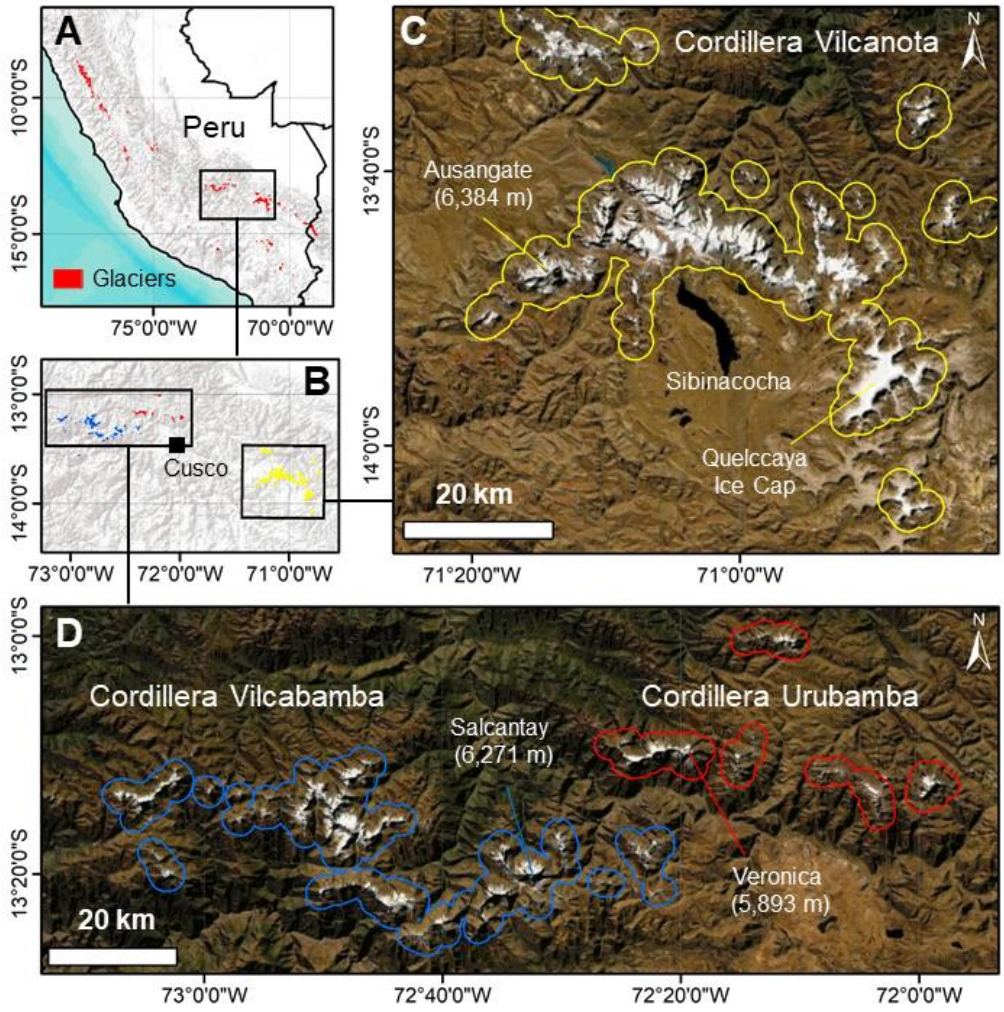

Figure 3.1 – Location of the Southern Peruvian Cordilleras within (A) Peru and (B) the Cusco region. (C) The Cordillera Vilcanota outlined in yellow (with a 2 km buffer around glacierised areas), and (D) The Cordilleras Vilcabamba (blue) and Urubamba (red). Satellite imagery from DigitalGlobe. Glacier outlines from RGI Consortium (2017) (A) and this study (B, C, D).

The Cordillera Vilcanota comprises a central mountain range (ranging from ~4,600 m a.s.l. to the peak of 6,384 m a.s.l at Ausangate) arcing above Sibinacocha – a large (~28 km^2) lake, which began being used for hydroelectricity generation in 1996. The Quelccaya ice cap (ranging from ~5,200 to 5,743 m a.s.l) dominates the east of the Cordillera Vilcanota with a maximum ice thickness of 150 – 170 m (Salzmann et al., 2013). Until recently, Quelccaya was the largest tropical ice cap on Earth, replaced by the Coropuna Ice Cap in the South of Peru (not analysed in this study) (Kochtitzky et al., 2018). In the immediate vicinity of the glaciers of the Cordillera Vilcanota are small indigenous farming communities made up of a few thousand individuals. The largest, the Phinaya community, has witnessed glacier fluctuations for centuries, and is therefore well aware of the causes and consequences of glacier recession and the likely impact it will have on their futures (Orlove, 2009). Recession of glaciers in the Cordillera Vilcanota has previously been documented by Salzmann et al. (2013), but extending only as far back as 2009 for ice area and 2006 for ice volume change, and not benefiting from the availability of more recent and more robust methods of calculating mass balance. The National Inventory of Glaciers provides ice area change from the Cordillera Vilcanota to 2017 (246 km^2) and Cordilleras Vilcabamba and Urubamba to 2016 (96 km^2 and 18 km^2 respectively) (INAIGEM, 2017; ANA, 2021). Detailed assessments of mass balance have been limited to individual glaciers based on field monitoring campaigns (Molina et al., 2015).

The Cordilleras Vilcabamba and Urubamba are smaller in size, and together comprise around half the glacierised area of the Cordillera Vilcanota. They are located to the west and north-west of Cusco and stretch for around 100 km east-west, ranging from ~4600 m a.s.l to peaks of 6,271 m a.s.l at Salcantay in the Vilcabamba and 5,893 m a.s.l at Veronica in the Urubamba. Glaciers in this region have deep spiritual connotations as mountain deities to indigenous communities (Drenkhan et al., 2018). In addition, their demise impacts directly on the agriculture-based economy, which relies on glacial meltwater as a source of irrigation. Measurements of glacier change in this region are extremely limited, restricted to individual watersheds (Drenkhan et al., 2018) or specific glaciers (Veettil et al., 2018).

3.3. Data and Methods

3.3.1. Available datasets

Satellite image archives are increasingly vast, as well as open-access, and computational advances have led to methodological frameworks that allow for robust analyses of glacier change that we employ here in the Cordilleras Vilcanota, Vilcabamba and Urubamba. The Landsat archive provides a record of ice area change almost continuously from 1972 to the present day, interrupted only by periods of heavy cloud and snow and short discontinuities in satellite operation. The small size of some glaciers in this region presents a challenge to delineating ice areas but, for decadal rates of change, the measured rates of recession frequently exceed any uncertainties in the data.

Deriving volumetric changes from these stereoscopic sensors relies on there being sufficient contrast over snow and ice-covered surfaces for feature matching to be successful. Reconnaissance images (e.g. Corona KH-4; Bolch et al., 2008) acquired over the high-elevation accumulation areas of the Cordilleras Vilcanota, Vilcabamba, and Urubamba are largely featureless however, meaning surface elevations cannot be extracted. For this reason, we focussed our mass balance estimations on the ASTER archive, which provides a continuous record from 2000 to the present day of stereoscopic scenes across the world. ASTER acquires images every 16 days through a 14-band nadir sensor and a single band backward looking sensor to acquire stereo images. These data are collected at 15 m and 30 m resolution to produce 30 m-resolution digital elevation models (DEMs). Cloud and snow also interfere with the production of digital elevation models, but the huge data redundancy afforded by the archive means this issue is relatively easy to overcome.

3.3.2. Area change between 1975 and 2020

Orthorectified Landsat-2 scenes (Level L1TP, 60 m spatial resolution; Table 3.1) were used to manually delineate glacier outlines for the 1970s, conducted in ArcMap. All Landsat-2 scenes were acquired between the 25th June – 31st July 1975 to minimise the influence of snow cover. All other glacier outlines were produced from 30 m imagery from the full-archive Landsat-5 Tier 1 Top of Atmosphere (1984 – 2012) and Landsat-8 Tier 1 Top of Atmosphere (2013 – 2020) datasets using a Normalised Difference Snow / Water Index (NDSI, NDWI) in Google Earth Engine. A cloud-free composite was produced for each year by extracting the median pixel value from the driest months (July 1st to September 30th) to minimise snow and cloud cover. Due to

heavy cloud in these regions, there are some years within the time series with no usable imagery. The resulting images were split into their respective boundaries from the Randolph Glacier Inventory 6.0 (RGI) dataset (RGI Consortium, 2017) and manually extended outwards using the ASTER GDEM. On inspection, a small number of RGI outlines in these regions seemed highly improbable, and so we manually delineated flowlines where it was clear the RGI database was merging multiple glaciers together. All shapefiles were clipped to remove polygons smaller than 0.01 km^2 in area and manually inspected to ensure no ice-free area was being incorrectly classified.

Scene ID	**Date acquired**	**Region**
LM02_LT1TP_002070_19750729_20200908_02_T2	29th July 1975	Vilcanota
LM02_LT1TP_003070_19750730_20200908_02_T2	30th July 1975	Vilcanota
LM02_LT1TP_004069_19750731_20200908_02_T2	31st July 1975	Vilcanota
LM02_LT1TP_004069_19750625_20180425_01_T2	25th June 1975	Urubamba
LM02_LT1TP_003069_19750730_20180426_01_T2	30th July 1975	Vilcabamba & Urubamba
LM02_LT1TP_004069_19750731_20180426_01_T2	31st July 1975	Vilcabamba & Urubamba

Table 3.1 – Orthorectified Landsat-2 scenes used in this study.

When determining glacier area, we calculated a conservative estimate of uncertainty for Landsat-2 scenes by assuming all glacier periphery pixels were misclassified, and calculated the total area of these periphery pixels, representing an error of 11%. Studies which have calculated uncertainty in a similar way produce comparable estimates of uncertainty (e.g. 11% for Kochtitzky et al., 2018). Rocky outcrops between glaciers and nunataks were particularly problematic to determine whether they were glacierised or snow-covered. Glacier boundaries from 1984 onwards were calculated via an automated method. Where this method is applied over predominantly clean-ice, associated error is 2 – 5% (Paul et al., 2013), and so we use a conservative estimate of 5% as the uncertainty value for glacier area delineated in this way, as the Southern Peruvian Andes are mostly clean-ice. We

acknowledge that this method excludes any small debris cover patches that exist, but this is consistent with other studies who also exclude these areas due to their scarcity in this region (Salzmann et al., 2013).

3.3.3. Volume change between 2000 and 2020

To calculate glacier volume change, we extracted all L1A ASTER tiles collected over these regions in the 20-year timespan from 1st January 2000 to 31st December 2020. We derived 631 DEMs using the AMES Stereo Pipeline using a 12 m TanDEM-X tile seed with the following parameters:

- --corr-seed-mode = 2
- --disparity-estimation-dem = TanDEM-X tile
- --disparity-estimation-error = 6
- --corr-kernel = 7 7
- --tr = 0.00027 (spatial resolution = 30 m)

To ensure accurate co-registration, they were corrected for planimetric and altimetric shifts against the TanDEM-X tile with a third-order polynomial transformation in stable, off-ice areas using the method of Nuth and Kääb (2011). Using a higher resolution seed DEM (12 m) compared to Hugonnet et al. (2021) (90 m) for co-registration should result in more accurate elevation models. DEMs that passed this correction phase were uploaded to Google Earth Engine using *geeup* (Roy, 2021), and clipped to elevations between 2000 and 6500 m a.s.l. (the approximate range of elevation within these Cordilleras) to exclude grossly erroneous pixels. A single value per pixel per year was extracted from all DEM tiles by collecting the median value (excluding values above and below the median ± 100 m). We trialled using the standard deviation as a filter in this step (i.e. median ± standard deviation), but in some areas the range was too high and this included too many erroneous data points. Using these single values per year, a linear fit through the surface elevation was then calculated over three time periods: 2000 – 2010; 2010 – 2020; and 2000 – 2020 to represent elevation change per year during these intervals. Hugonnet et al. (2021) produce elevation change at 5-year intervals, but the associated error is often far larger than in the decadal intervals, and so we consider only the 10-year products to be usable.

For the conversion of elevation change to mass change, there are three key sources of uncertainty:

1) Error in glacier area (σ_A)
2) Error in the calculated elevation change ($\sigma_{\Delta z}$)
3) Error in ice density calculations $\left(\sigma_{f\Delta V}\right)$

We followed the method presented by Brun et al. (2017) to calculate overall uncertainty for mass balance calculations. We calculate uncertainty for the region-wide mass loss and use this fraction to attribute uncertainty in mass balance. Uncertainty in volume change is calculated using the standard deviation of elevation change on stable ground ($\sigma_{\Delta h}$). We cast a 2 km buffer outwards from the glacier margin into stable ground and used the standard deviation of all pixels in this buffer area as $\sigma_{\Delta h}$. We follow Brun et al. (2017) in using a decorrelation length of 500 m, but use a glacier area uncertainty (σ_A) of 5% as we have greater confidence that this region is predominantly clean-ice. Finally, we use an ice density uncertainty $\left(\sigma_{f\Delta V}\right)$ of 60 kg m^{-3} following Huss (2013).

3.3.4. Calculation of Geodetic Mass Balance, Median Glacier Elevation, and ELA

Geodetic mass balance was calculated by taking into account the elevation change per pixel, pixel size (30 m), and ice density of 850 ± 60 kg m^3 (Huss, 2013). Calculation of surface mass balance, which would include estimates of glacier flow from modelled ice thickness and velocity (Miles et al., 2021a), was not possible in this region owing to lack of available flow data. This precluded a robust estimate of the glacier ELA using our surface elevation data alone. Therefore, in the absence of any *in situ* data, we investigated previously published methods to quantify ELA change through time. These included quantifying changes to the freezing-line altitude (e.g. Schauwecker et al., 2017; Yarleque et al., 2018), the end of summer snowline altitude (Condom et al., 2007; Rabatel et al., 2013b), and the use of the median glacier elevation as an ELA proxy (e.g. Braithwaite and Raper, 2009; King et al., 2017). We adopted this final approach in the absence of higher spatial resolution climate data or reliable cloud-free satellite data to quantify snowlines, though we acknowledge this is likely to underestimate actual ELAs as the glaciers are out of balance with the climate. We calculated median glacier elevation for every glacier, and herein summarise an area-weighted average region-wide median glacier elevation for the Cordilleras

Vilcabamba and Urubamba, and separate the Cordillera Vilcanota into five sub-regions reflecting the differing altitudes and topographies of each (Figure 3.2).

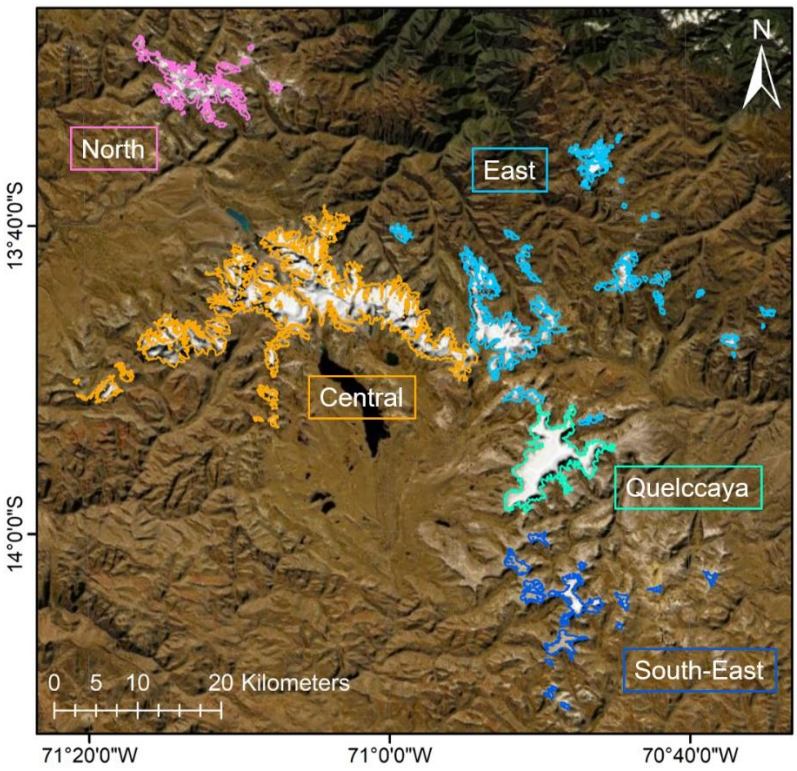

Figure 3.2 – Sub-regions of the Cordillera Vilcanota used in the calculation of median glacier elevation. Glacier outlines shown here from 1984. Basemap from DigitalGlobe.

We also test a new method for calculating glacier ELA shifts using DEM time series data. Hypothetically, we propose that the mean elevation at which glacier surface elevation change is zero could be a proxy for ELA. To our knowledge, this has not before been tested in the literature. For the time periods 2000 – 2010 and 2010 – 2020, we converted the elevation change raster images to points at 30 m resolution. For each glacier, per-pixel volume change was plotted against the elevation of each pixel and a linear regression passed through the points. Where the *y*-intercept of this linear regression equalled zero volume change, the value of elevation was taken to represent the ELA (a visual example of this calculation is given in Figure 3.3). These ELA values are available for each glacier, and for the entire Cordillera Vilcanota. This regional ELA was calculated using the same method, but with all points over glacierised area in the Vilcanota, with a 95% confidence interval. Using all points across the Cordillera Vilcanota yields significant linear regressions (p

< 0.001) with R^2 values for the linear fit models of 0.07 for the first decadal interval, 0.03 for the second decade, and 0.14 for the full 2000 – 2020 dataset.

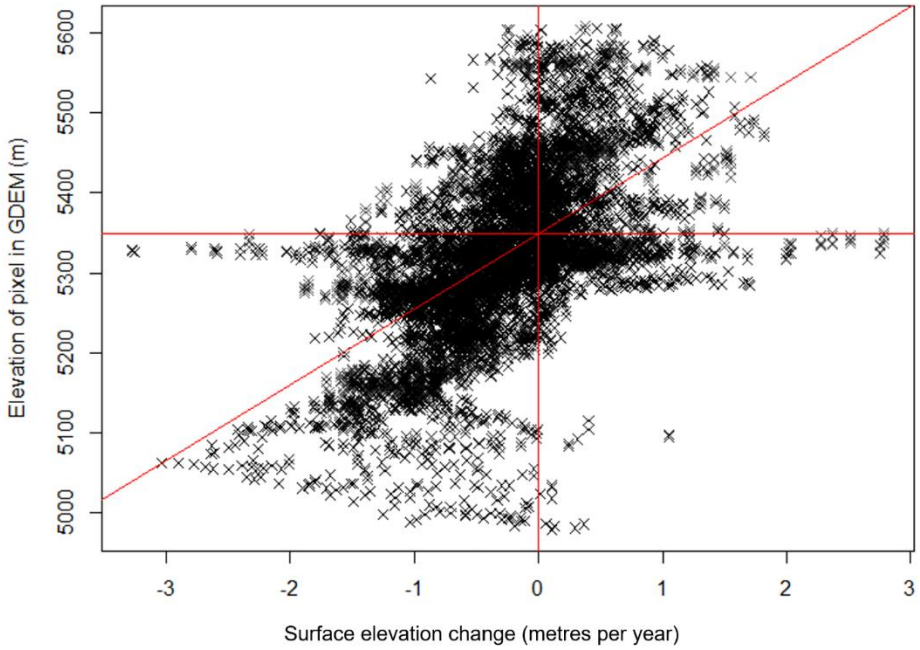

Figure 3.3 – Example, from Chumpe Glacier at the centre of the Cordillera Vilcanota, of a novel approach to calculating ELA. Where the linear regression between elevation and surface elevation change intercepts the zero of surface elevation change, the y*-intercept is the ELA.*

3.3.5. Topography and Climate data

To identify the most significant controls on ice loss in each region, we correlated the variables of change (volume and area loss) against topographic and climate data. Topographic data (aspect, elevation, slope) were derived from the ASTER GDEM and averaged over the shapefiles of each glacier. Climate data were created using the Weather Research and Forecasting (WRF) model and bias-corrected against daily precipitation and maximum and minimum daily temperature data in the region, from 1980 to 2018. Frost days were calculated as the number of days in the year where the minimum daily temperature fell below 0 °C. For full details of the WRF model setup and bias-correction, see (Fyffe et al., 2021).

Climate data were correlated to glacier area change from 1984 (the first year of overlap between the Landsat record and climate dataset) to 2018 (the end of the climate dataset) for every glacier individually. These coefficients were then transformed to z-values using Fisher's Z to ensure a normal distribution of data. A

mean was taken of these Fisher's Z values, which was subsequently back-transformed to achieve an overall region-wide correlation coefficient between ice area and climatic variables. Significance for these values was calculated using the Harmonic mean *p*-value, weighted to the size of the glacier, as a robust measure of significance in large datasets (Wilson, 2019). These steps ensure each glacier is statistically analysed against only the climate data that are of most relevance to that particular glacier.

3.4. Results

3.4.1. Ice area change (1975 – 2020)

Overall, glacierised area of the Southern Peruvian Andes shrunk from 833.6 ± 91.7 km^2 in 1975 to 312.6 ± 15.6 km^2 in 2020 (Figure 3.4). This loss has predominantly occurred at low elevations (Figure 3.5). The Cordillera Vilcanota shrunk from a regional total of 540.6 ± 59.4 km^2 in 1975 to 246.8 ± 12.3 km^2 in 2020. This represents a loss of 54.3% of the glacier ice that was present in 1975 over a 45-year time period. 82 of the 257 glaciers present in 1975 had been lost by 2020 (or shrunk smaller than 0.01 km^2 in size). There has been consistent and steady recession of ice across the region in this time. The Quelccaya ice cap, which is included within the area for the Cordillera Vilcanota, shrunk from 57.4 ± 5.4 km^2 in 1975 to 41.6 ± 2.1 km^2 in 2020, representing a loss (27.5%) that is below the regional average (Figure 3.5). There has, in contrast to the region-wide Cordillera Vilcanota, been an observable slowdown of ice area loss in recent years.

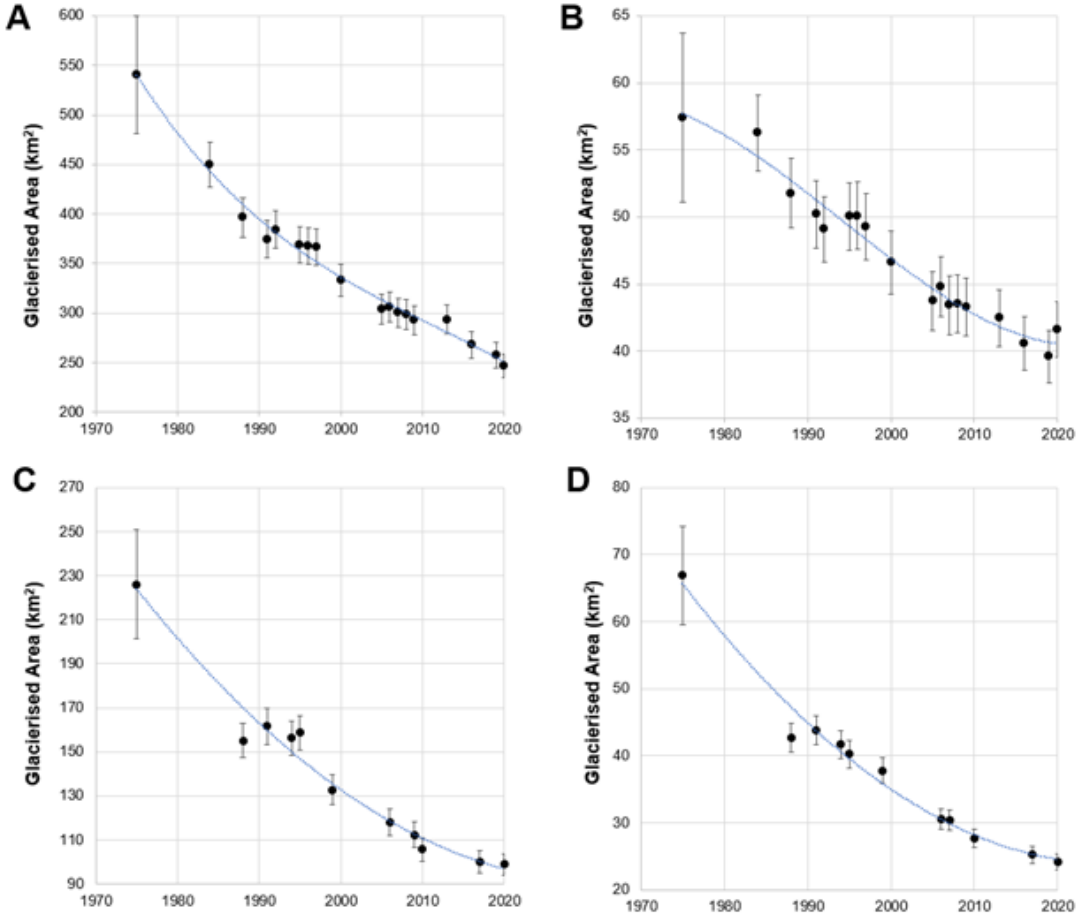

Figure 3.4 – Glacierised Area of (A) Cordillera Vilcanota, (B) Quelccaya ice cap, (C) Cordillera Vilcabamba, and (D) Cordillera Urubamba. Note the varying y*-axis scales. Blue line represents second-order polynomial fit.*

The Cordillera Vilcabamba shrunk from 226.1 ± 24.9 km^2 in 1975 to 98.9 ± 4.9 km^2 in 2020, a loss of 56% of glacierised area. 25 of the 169 glaciers present in 1975 had been lost by 2020. The Cordillera Urubamba shrunk from a glacierised area of 66.9 ± 7.4 km^2 in 1975 to 24.2 ± 1.2 km^2 in 2020; a loss of 64%. This represents the largest relative decline in glacierised area of the regions as this is the lowest-lying of the three Cordilleras (Figure 3.6). Of the 39 glaciers in the Cordillera Urubamba in 1975, seven had been lost by 2020.

These area changes, which predominantly affect lower-lying zones, have driven the glaciers to higher elevations over the 45-year study period (Figure 3.5). It is notable that in all three Cordilleras, glacier ice has all but disappeared from elevations below 4,700 m a.s.l. but is largely preserved above elevations of 5,500 m a.s.l. In each case, the hypsometry is skewed towards lower elevations. In contrast,

the hypsometry of Quelccaya is skewed towards higher elevations, and consequently the bins with greatest area have been largely preserved. For Quelccaya, there is no observed change in glacier area above 5,550 m a.s.l. from 1975 to 2020.

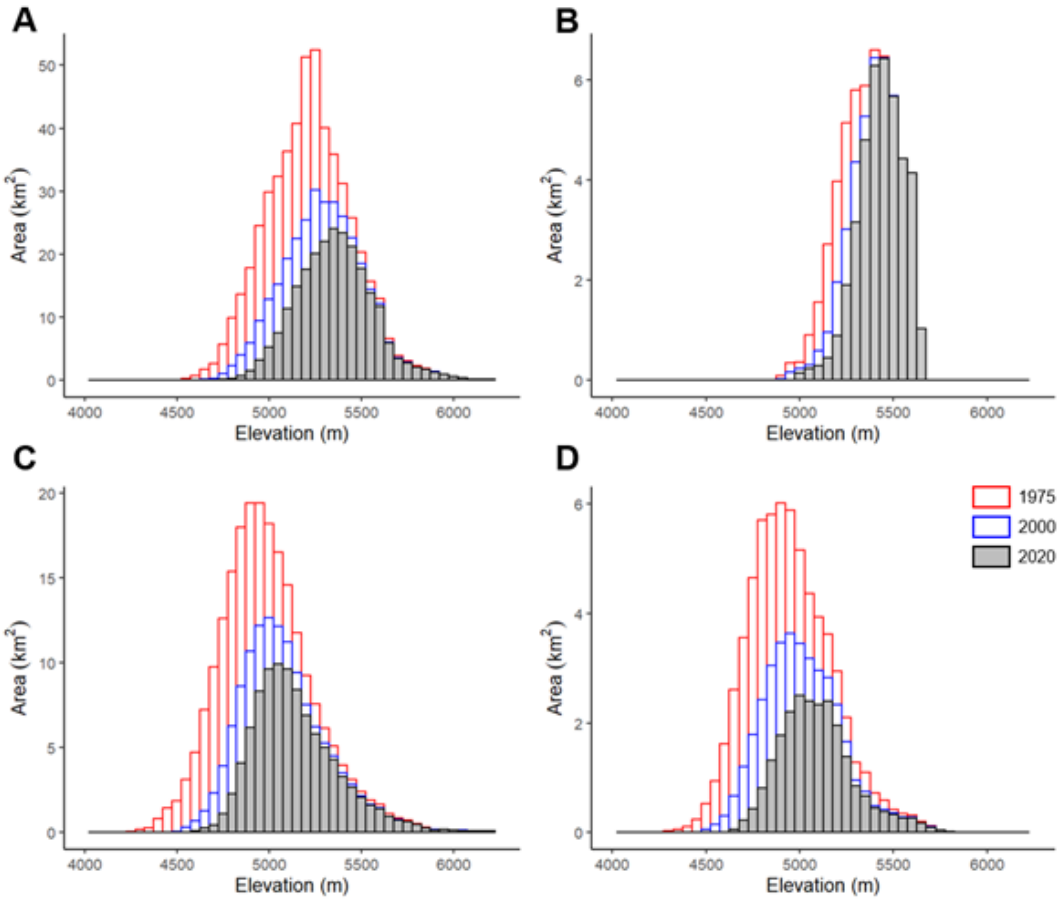

Figure 3.5 – Evolving glacier hypsometry (1975, 2000, and 2020) in 50 m elevation bins for the (A) Cordillera Vilcanota, (B) Quelccaya ice cap, (C) Cordillera Vilcabamba, (D) Cordillera Urubamba. Note varying y*-axis in each graph.*

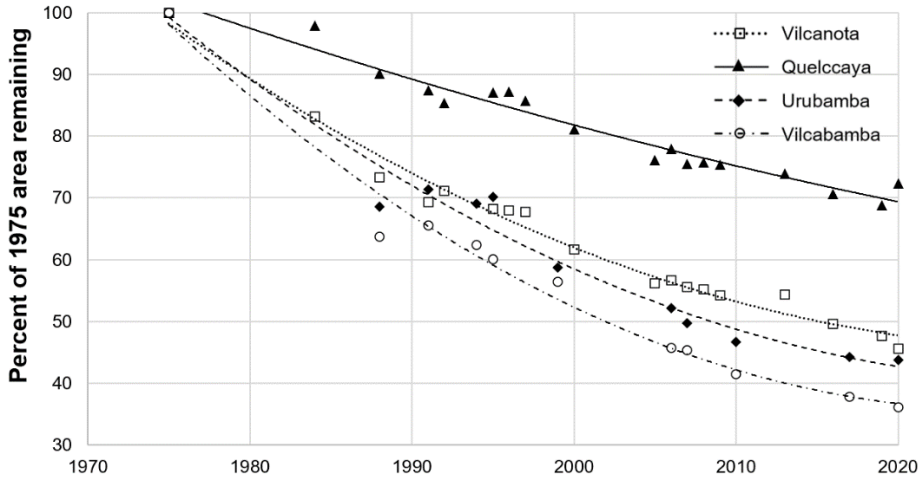

Figure 3.6 – Area change of the Southern Peruvian Cordilleras as a percentage of their original (1975) glacierised area.

Across the Cordillera Vilcanota, there is a moderate correlation between mean annual air temperature (which has risen by ~0.2°C per decade from 1980 to 2020) and rate of ice area change (R = -0.514, p < 0.01), and maximum annual temperature and ice area loss (R = -0.576, p < 0.01) (Table 3.2; Figure 3.7). There is no statistically significant link (at p < 0.01) between ice area change and precipitation, but there is a corresponding correlation between the number of frost days in the year and ice area loss. The key topographic control on rate of ice area change is maximum elevation (R = -0.394, p < 0.01), with a second-order control of slope (R = -0.269, p < 0.01). There is no significant (p < 0.01) co-linearity between maximum elevation and slope. The prevalence of cloud or snow-covered scenes in our record limits our ability to analyse the role that ENSO plays in affecting glacier area change.

Over the Cordilleras Vilcabamba and Urubamba, there is also a moderate correlation between maximum annual temperature and rate of ice area change (R = -0.338, p < 0.01 and R = -0.576, p < 0.01 respectively). There is no statistically significant link between ice area change and precipitation. Similar to the Cordillera Vilcanota, the primary topographic control on ice area change in the Cordilleras Vilcabamba and Urubamba is maximum elevation (R = -0.241, p < 0.01; R = -0.677, p < 0.01 respectively) though this driver is much weaker in the Cordillera Vilcabamba. Slope is not a statistically significant control in the Cordillera Vilcabamba, but is in the Cordillera Urubamba (R = -0.301, p < 0.01), though there is co-linearity between elevation and slope in the Urubamba (R = 0.515, p < 0.01).

Region	Max. annual air temp		Mean annual air temp		Annual precipitation		Number of frost days		Mean elevation	
	R	*p*	*R*	*p*	*R*	*p*	*R*	*p*	*R*	*p*
Vilcanota	-0.576	9.14×10^{-5}	-0.514	0.000962	0.193	0.0331	0.361	0.00891	-0.233	0.000311
Vilcabamba	-0.338	0.00414	-0.277	0.0287	-0.163	0.179	0.305	0.0102	-0.161	0.0449
Urubamba	-0.576	0.000171	-0.446	0.00388	-0.156	0.0816	0.370	0.00285	-0.578	0.000177

Region	Max elevation		Min elevation		Aspect		Slope	
	R	*p*	*R*	*p*	*R*	*p*	*R*	*p*
Vilcanota	-0.394	3.88×10^{-10}	-0.169	0.00937	0.174	0.00762	-0.269	2.83×10^{-5}
Vilcabamba	-0.241	0.00240	0.0803	0.319	-0.0482	0.550	-0.107	0.183
Urubamba	-0.677	4.27×10^{-6}	0.368	0.0252	0.0125	0.942	-0.301	0.0703

Table 3.2. Analysis of correlations exclude the 1975 data point for ice area as this does not overlap with the climate dataset which begins in 1980. Climate data correlated directly against ice area measurements. Topographic data correlated against rate of ice area change as a proportion of 1984 (Vilcanota) or 1988 (Vilcabamba / Urubamba) area.

Figure 3.7 (Next page) - Full statistical tests for drivers of ice area change. Grey areas represent 95% confidence interval for regression.

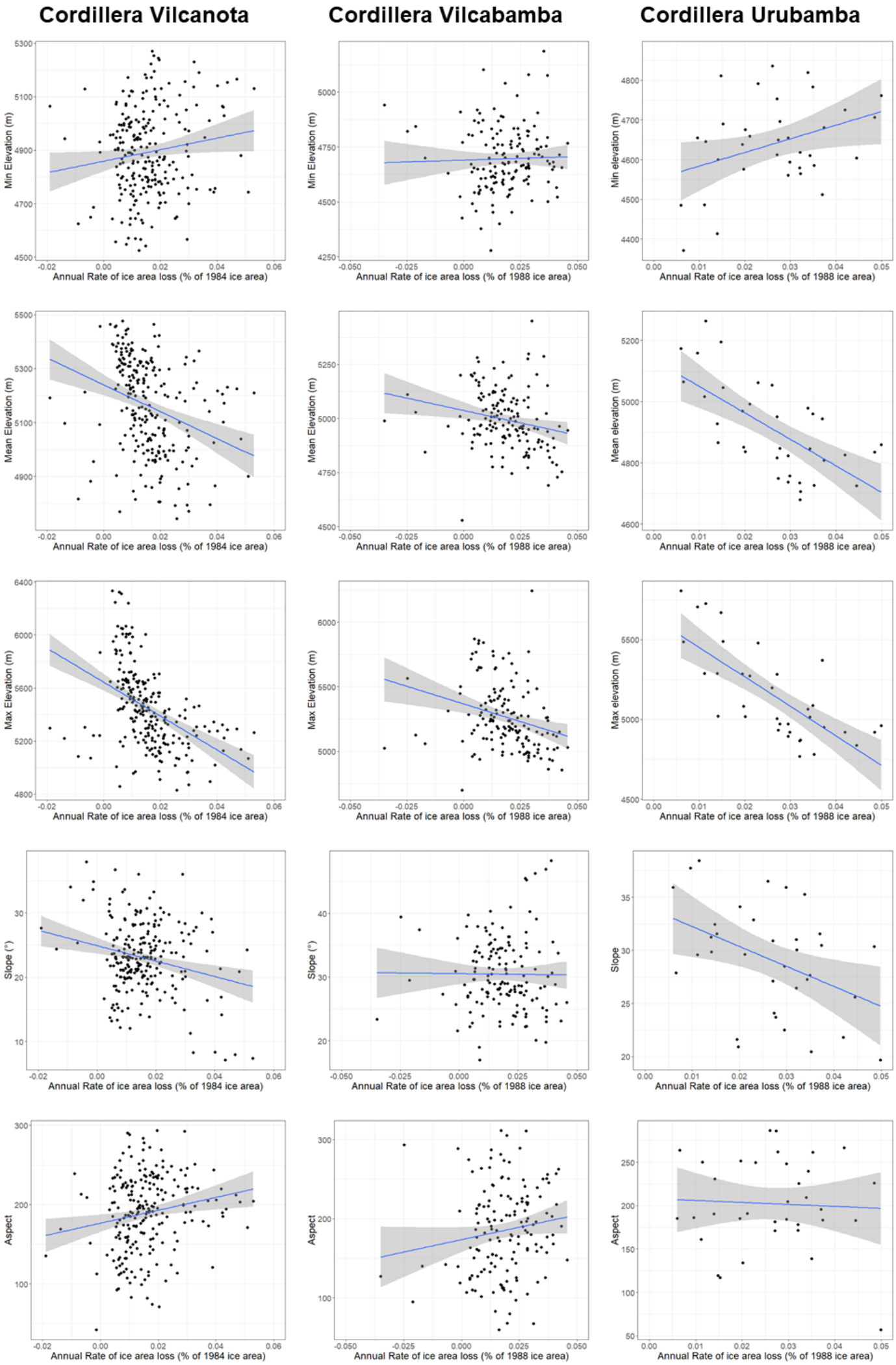
Cordillera Vilcanota
Cordillera Vilcabamba
Cordillera Urubamba
Min Elevation (m)
Min elevation (m)
Mean Elevation (m)
Mean elevation (m)
Max Elevation (m)
Max elevation (m)
Slope (°)
Slope
Aspect
Annual Rate of ice area loss (% of 1984 ice area)
Annual Rate of ice area loss (% of 1988 ice area)

3.4.2. Ice volume and mass balance (2000 – 2020)

Between 2000 and 2020, the Cordillera Vilcanota shrunk at a rate of -0.159 ± 0.022 Gt yr^{-1} (-0.48 ± 0.07 m w.e. yr^{-1}). There was no significant change in the mass balance between the two sub-decadal periods; from -0.49 ± 0.17 m w.e. yr^{-1} between 2000 – 2010 to -0.44 ± 0.16 m w.e. yr^{-1} between 2010 – 2020 (Figure 3.8). Owing to the cloudiness of ASTER data, smaller glaciers, and steeper slopes over the Cordilleras Vilcabamba and Urubamba, the uncertainty in our mass balance calculation was much larger than it was for the Vilcanota. Between 2000 and 2020, the Cordillera Vilcabamba shrunk at a rate of -0.405 ± 0.451 m w.e. yr^{-1}, while the Cordillera Urubamba shrunk at a rate of -0.559 ± 1.575 m w.e. yr^{-1}. We present these figures here for completeness, but do not analyse them further given the extent to which the uncertainty exceeds any signal in the data. Thinning of debris-covered ice, which is not included in the glacier area polygons but only makes up a minimal percentage of ice in the region, can be observed in the surface elevation change dataset (e.g. Figure 3.8B and 3.8C).

There is a moderate correlation between volume change over the full 20-year period and elevation (R = 0.38, p < 0.001), suggesting that low-lying areas are thinning, as well as receding, the most. There is a slight, but significant, correlation between volume change and slope (R = 0.16, p <0.001) and aspect (R = -0.04, p < 0.001). This is particularly noticeable over the Nevado Ausangate cluster of glaciers, where South-facing glaciers are largely shadowed from solar radiation, while North-facing glaciers are experiencing large thinning (Figure 3.8B).

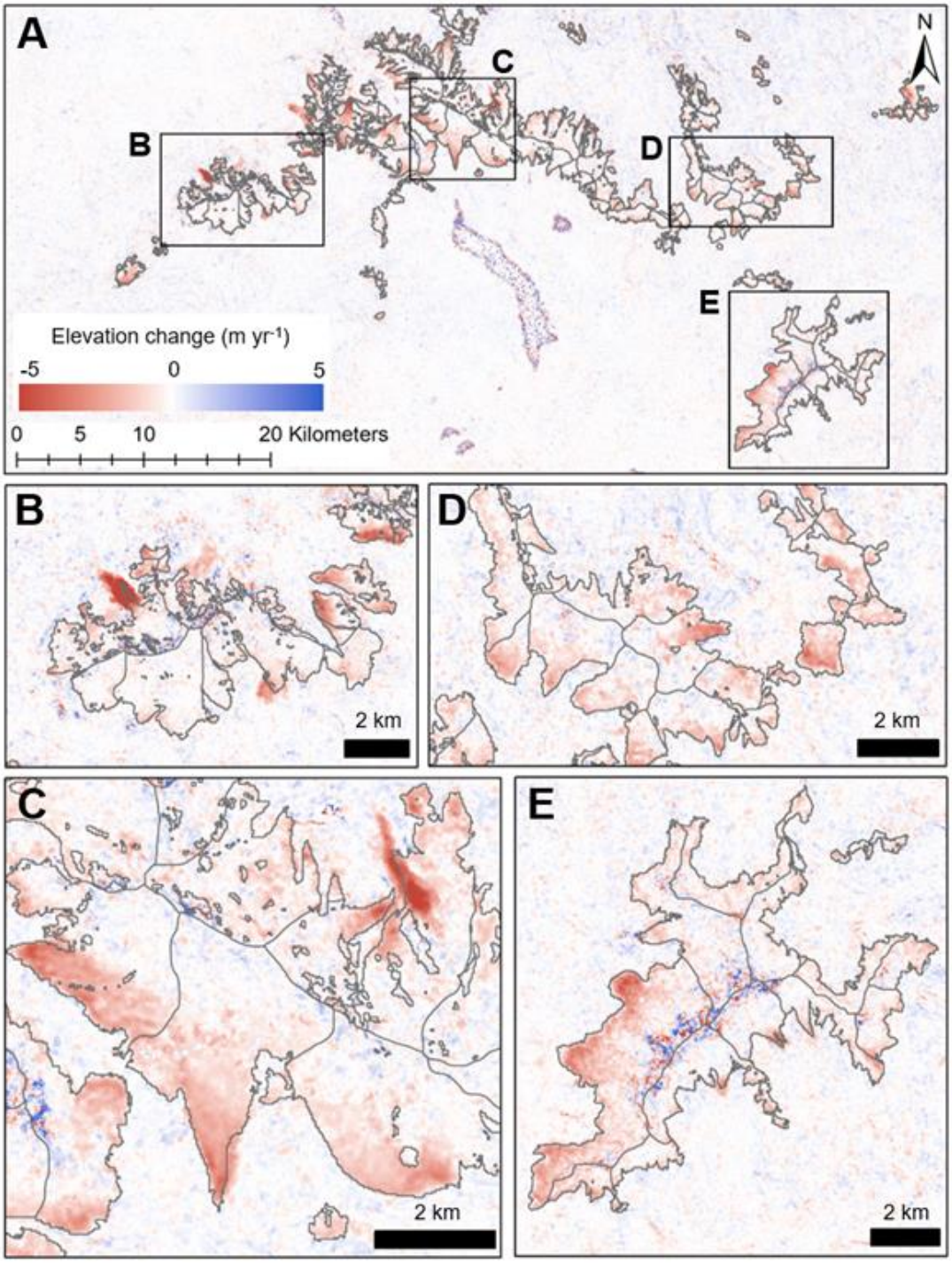

Figure 3.8 – Elevation change from 2000 to 2020 over the central range of the Cordillera Vilcanota. (A) Overview of elevation change in the Cordillera Vilcanota. The large pixelated body in the centre of the figure is Laguna Sibinacocha. (B) Nevado Ausangate. (C) Chumpe Glacier. (D) Cluster of lower-lying Eastern glaciers. (E) Quelccaya ice cap. Glacier outlines from the year 2000 are in light grey. Large surface elevation changes in off-ice areas (most notably in panels B and C) are from debris-covered ice.

The median elevation of the Cordilleras Vilcabamba and Urubamba rose at the fastest rates across the full 1975 – 2020 time series (3.28 m yr^{-1} and 3.27 m yr^{-1} respectively), from 4,966 m a.s.l. to 5,110 m a.s.l. for the Cordillera Vilcabamba and 4,930 m a.s.l. to 5,077 m a.s.l. for the Cordillera Urubamba (Figure 3.9). However, the rate of change between the regions through time varies. The median elevation of the Cordillera Urubamba is accelerating upwards (from 2.88 m yr^{-1} for 2000 – 2010 to 4.59 m yr^{-1} for 2010 – 2020), while the rate of change in the Cordillera Vilcabamba is decelerating (from 3.69 m yr^{-1} for 2000 – 2010 to 3.06 m yr^{-1} for 2010 – 2020) (Figure 3.10).

Figure 3.9 – Change in median glacier elevation between 1975 and 2020 over the Southern Peruvian Andes. The North, East, Central, South-East, and Quelccaya categories are sub-regions of the Cordillera Vilcanota (Figure 3.2). Dotted lines represent linear regressions.

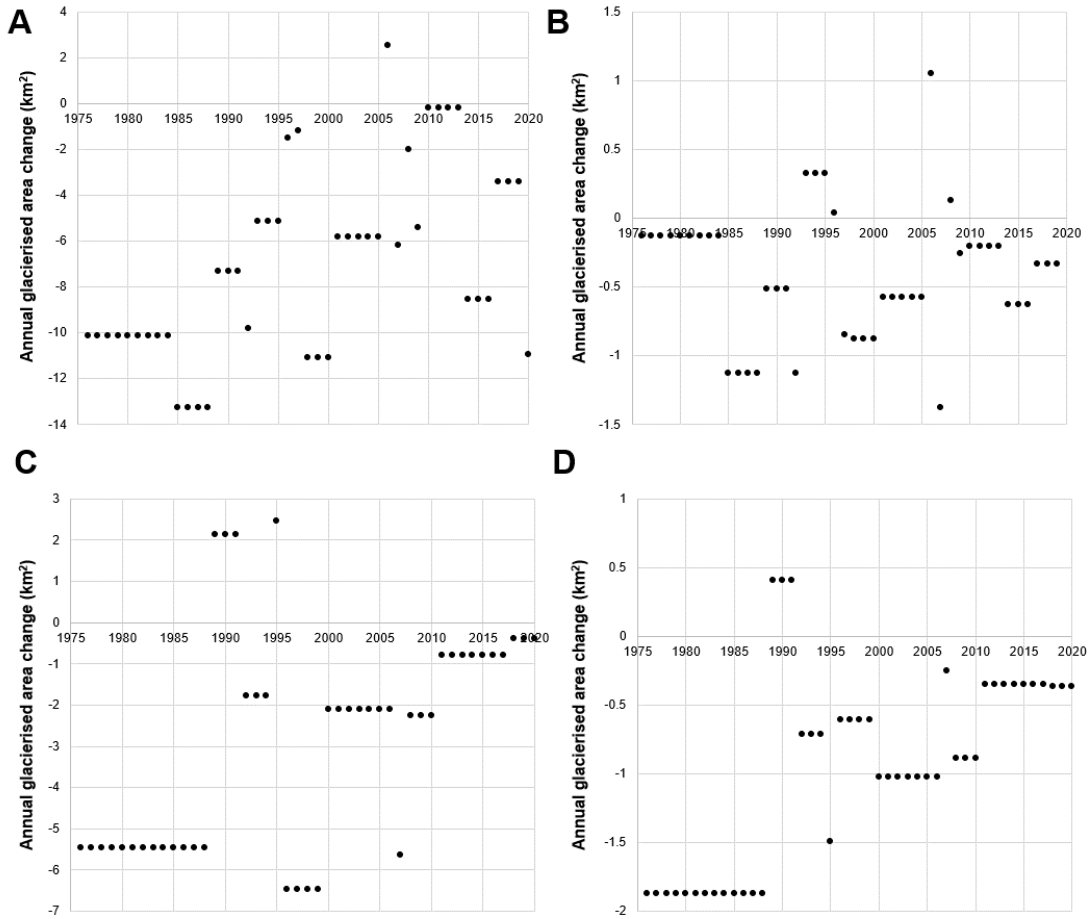

Figure 3.10 – Mean annual rate of ice area change over the (A) Cordillera Vilcanota, (B) Quelccaya ice cap, (C) Cordillera Vilcabamba, and (D) Cordillera Urubamba.

The rate of median elevation change over the Cordillera Vilcanota is lower in all sub-regions than the Cordilleras Vilcabamba and Urubamba. The northernmost region of the Cordillera Vilcanota (Nevado Qolquepunco) has the lowest median elevation of the region (at 5,163 m a.s.l. in 2020; compared to 5,451 m a.s.l. at Quelccaya), but the rate of change has remained steady in recent decades. Quelccaya exhibits the lowest rate of median elevation change of all the regions at 1.59 m yr^{-1} from 1975 to 2020, likely due to its high elevation and flat topography. This rate of change has decelerated to 1.06 m yr^{-1} between 2010 and 2020. The key driver for the rate of median elevation change across the Cordillera Vilcanota is temperature; there is a significant correlation between maximum annual temperature and median elevation (R = 0.603, p < 0.001). The role of precipitation and frost in driving median elevation was not significant at p < 0.01.

Using our hypothetical approach of calculating ELA, where we derive the mean elevation at which surface elevation change is zero, we calculate a mean ELA change across the Cordillera Vilcanota of 1.33 m yr^{-1} between 2000 – 2010 and 2010 – 2020. While absolute ELA corresponds reasonably well with median glacier elevation (R^2 = 0.96; Figure 3.11), high error in the surface elevation change raster over some glaciers renders this approach unusable. For example, in the North sub-region, ELA change is calculated as -1.40 m yr^{-1} through this approach, rather than the 2.54 m yr^{-1} as calculated by the median elevation of each glacier.

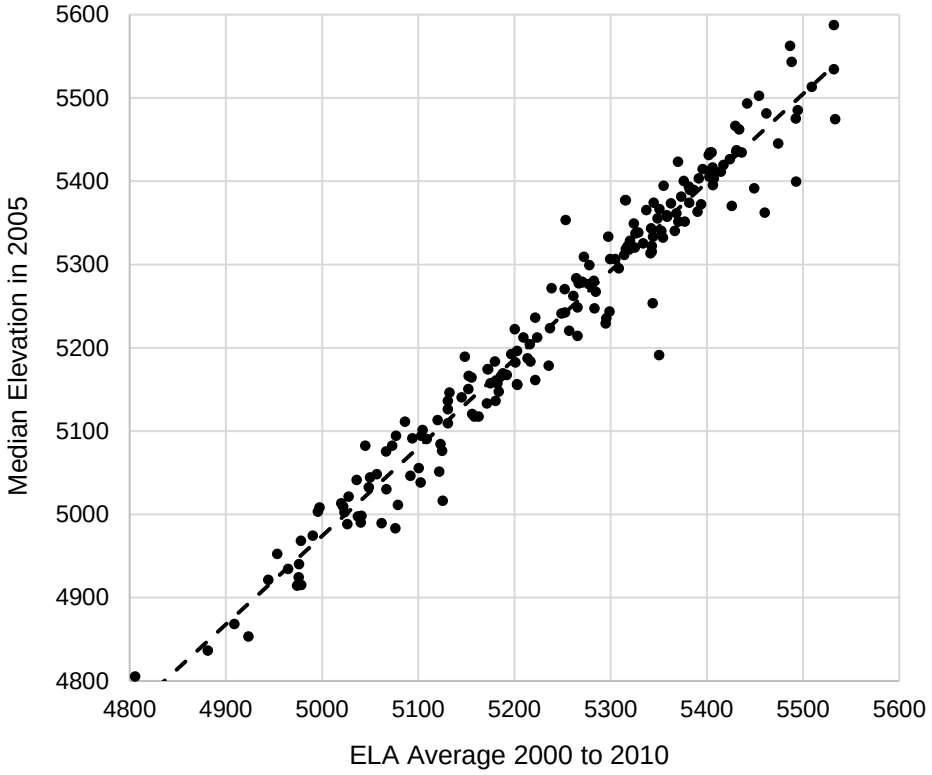

*Figure 3.11 – Comparison of ELA between 2000 and 2010 as calculated by identifying the mean elevation at which surface elevation change is zero (*x*-axis) compared to the median glacier elevation in 2005 (*y*-axis). Each point represents an individual glacier within the Cordillera Vilcanota.*

3.5. Discussion

3.5.1. Comparison to previous works

Published estimates of glacier area in these regions are scarce, and many studies limit their efforts to studying specific watersheds within the wider region (e.g. Veettil and Souza, 2017; Drenkhan et al., 2018). Furthermore, definitions of the boundaries of the Cordilleras are not fixed, with differing assessments of how many smaller periphery glaciers are included in calculations of the glacierised area of the region (Hanshaw and Bookhagen, 2014). Nevertheless, being cognisant of the slight variability in study areas, our estimations of ice recession fit well with the trend presented by other publications (Figure 3.12). To our knowledge, only the National Inventory of Glaciers presents information on glacier area change in the Cordilleras Vilcabamba and Urubamba. Our results for the area of the Cordillera Vilcabamba in 2017 (100.07 ± 5.00 km^2) are comparable to the INAIGEM data (95.54 km^2), but are slightly higher for the Cordillera Urubamba (25.27 ± 1.26 km^2 to the INAIGEM's 24.92 km^2). Note there is a discrepancy between the INAIGEM published estimate for the Cordillera Urubamba of 17.89 km^2 and their dataset of 24.92 km^2, likely due to the way boundaries are drawn between Cordilleras (INAIGEM, 2017; ANA, 2021).

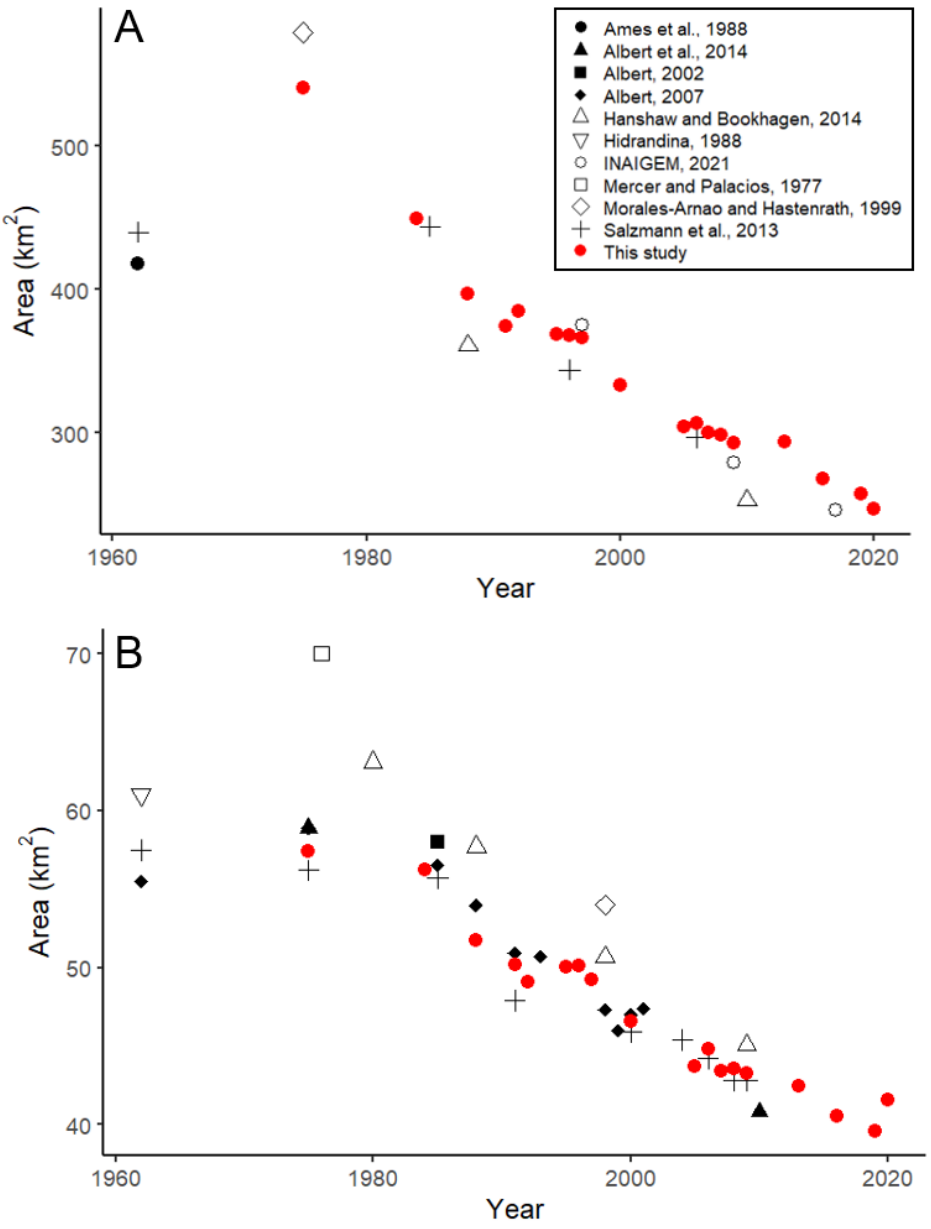

Figure 3.12 – Ice area change comparison to published studies over (A) the Cordillera Vilcanota and (B) the Quelccaya ice cap.

There have been no comparable estimates of mass balance over the Cordillera Vilcanota specifically; however, the global ASTER dataset of glacier change (Hugonnet et al., 2021) provides reasonable context for our findings. The primary difference between the two datasets is their spatial resolution: the current study reports data at 30 m spatial resolution, while Hugonnet et al. (2021) is downsampled to 100 m resolution. Our mass balance estimate over the 20-year time period (-0.477 ± 0.067 m w.e. yr^{-1}) is nearly identical to using their dataset (-0.479 ±

0.048 m w.e. yr^{-1}). We attribute our slightly higher level of uncertainty to our finer spatial resolution which introduces some small artefacts into our dataset. However, the trade-off is that we are able to observe much more closely the changes of individual glaciers (an example comparison is shown over Chumpe glacier, in the Cordillera Vilcanota in Figure 3.13). The problem of very large uncertainty of mass balance change over the Cordilleras Vilcabamba and Urubamba was not unique to our dataset as Hugonnet et al. (2021) had large data gaps over this region, rendering their data unusable. Our high errors were due to cloud rather than steep terrain. Over the Cordilleras Vilcabamba and Urubamba, we produced far fewer DEMs per pixel (~20 DEMs over the 20-year time period) in comparison to the Cordillera Vilcanota (~75 DEMs per pixel).

Our 2020 median glacier elevation estimate of 5,357 m a.s.l. for the central sub-region of the Cordillera Vilcanota is comparable to the 5,399 m a.s.l. (2016 figure) calculated by Drenkhan et al. (2018), with the difference attributed to different spatial areas covered (their study includes only glaciers in the Vilcanota-Urubamba-Vilcabamba basin). Our 1975 – 2020 rate of median elevation increase over the Quelccaya ice cap (15.9 m per decade) is comparable to the 1980 – 2017 estimate of 16.3 m per decade over the Quelccaya ice cap estimated by Yarleque et al. (2018). Our 1975 – 2020 rate of median elevation increase over the Central region of the Cordillera Vilcanota (24.8 m per decade) is slightly higher than the 22.8 m per decade between 1988 and 2010 estimated by Hanshaw and Bookhagen (2014). Our changes in the rate of median glacier elevation change show high variability across regions and decadal intervals (Figure 3.14). This is not inconsistent with the interannual variability of measured ELA change over glaciers in the Cordillera Blanca (Kaser and Georges, 1997; Condom et al., 2007) and Cordillera Ampato (Veettil et al., 2016) which have been attributed to fluctuations in air humidity and the role of ENSO respectively. The interannual variation we exhibit in the Cordillera Vilcanota correlated to maximum air temperature, though this warrants further investigation given the high variability between sub-regions.

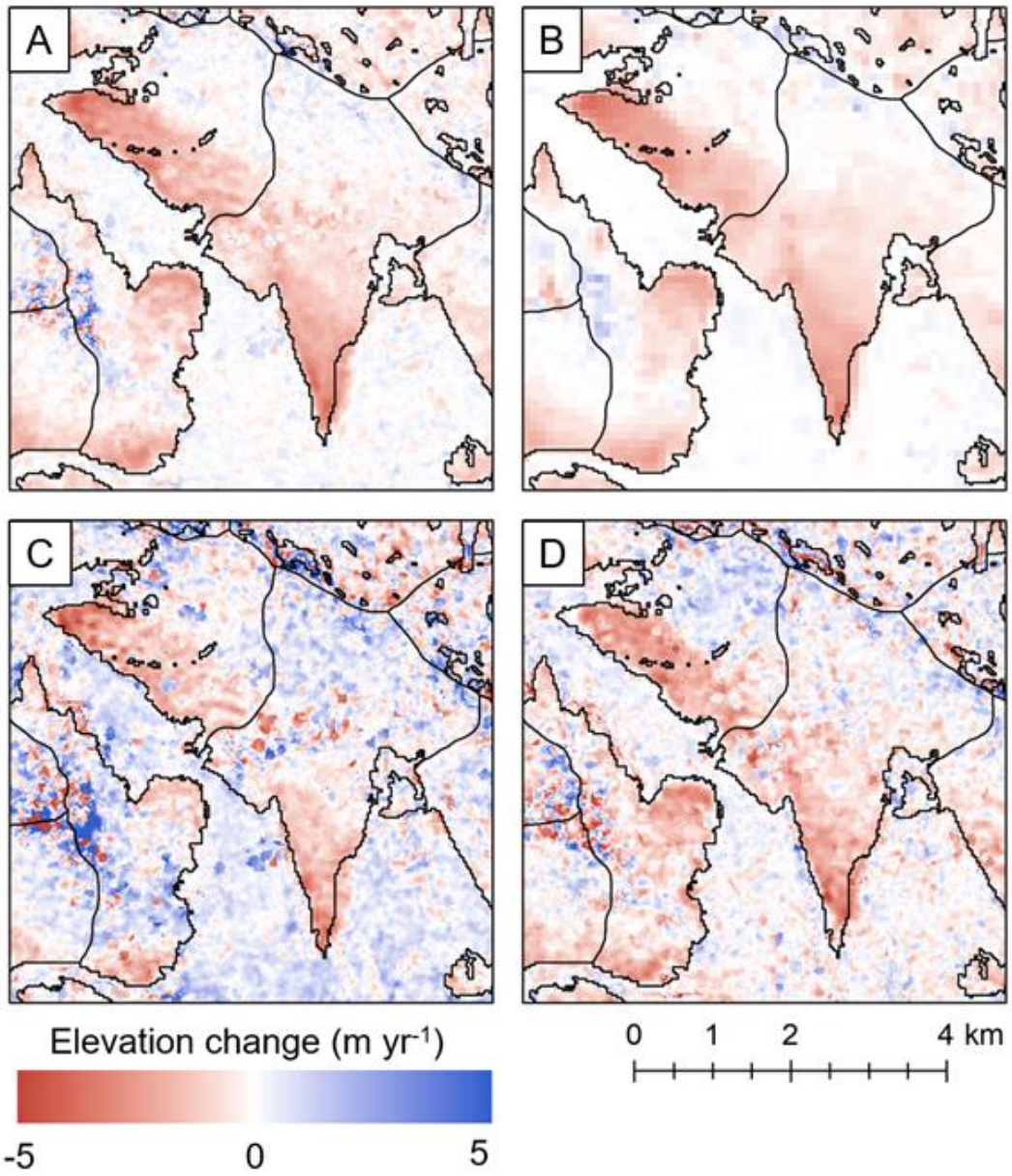

Figure 3.13 – Comparison of datasets over Chumpe Glacier, Cordillera Vilcanota. (A) 2000 to 2020 change in elevation generated by this study, (B) Comparison to Hugonnet et al. (2021) and their 100 m resolution product over the same 20-year time period, (C) 2000 – 2010 change in elevation generated by this study, (D) 2010 – 2020 change in elevation. Black outlines represent the glacier area in 2000 produced by this study.

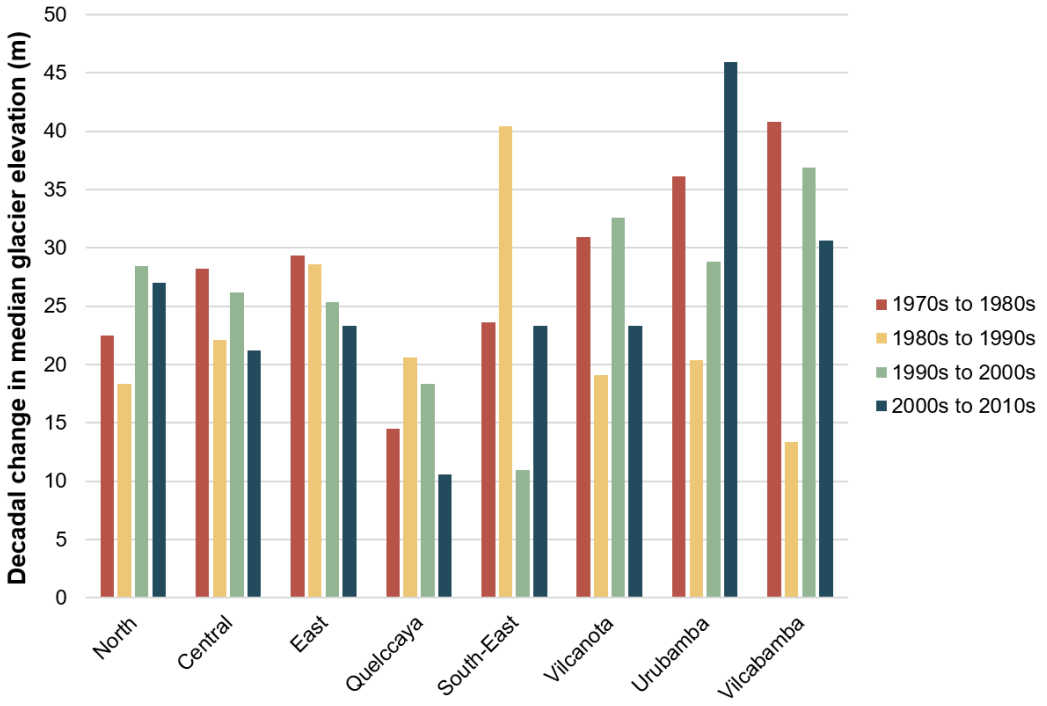

Figure 3.14 – Decadal change in median glacier elevation through time for each region. North, Central, East, Quelccaya, and South-East are sub-regions of the Cordillera Vilcanota (Figure 3.2).

Ice area retreat is prolific across all areas of the Southern Peruvian Cordilleras. In the Cordillera Vilcanota, 82 of 257 glaciers (which represented 11.2% of the 1975 glacierised area) disappeared completely over the study period – most notably a cluster of glaciers to the south-east of the Quelccaya ice cap (Figure 3.15). However, deglaciation is occurring at differing rates between regions. Between 1988 and 2020, the Cordillera Vilcabamba lost 34% of its glacial area, compared to 45% for the Cordillera Vilcanota between 1984 and 2020. This is likely due to the differing morphology of glaciers between the regions – glaciers in the Vilcabamba are generally smaller and at lower elevations (Drenkhan et al., 2018) in comparison to the Vilcanota, which means less relative area is exposed to rapid melt. A differing climate setting between the regions is also likely to affect area change: the Cordilleras Vilcabamba and Urubamba are generally wetter than the Vilcanota (Kaser, 2001; Fyffe et al., 2021) though, unlike Fyffe et al. (2021), we did not observe precipitation to be a statistically significant driver of ice area change. This is likely due to the temporal resolution of our dataset; we examined annual precipitation and often with gaps between years in the dataset. Fyffe et al. (2021) studied the influence of

precipitation at daily to weekly timescales, and found high variability in melt due to these precipitation dynamics. Further work is needed at a higher temporal resolution to better understand the role precipitation plays in regulating ice area change over long time scales.

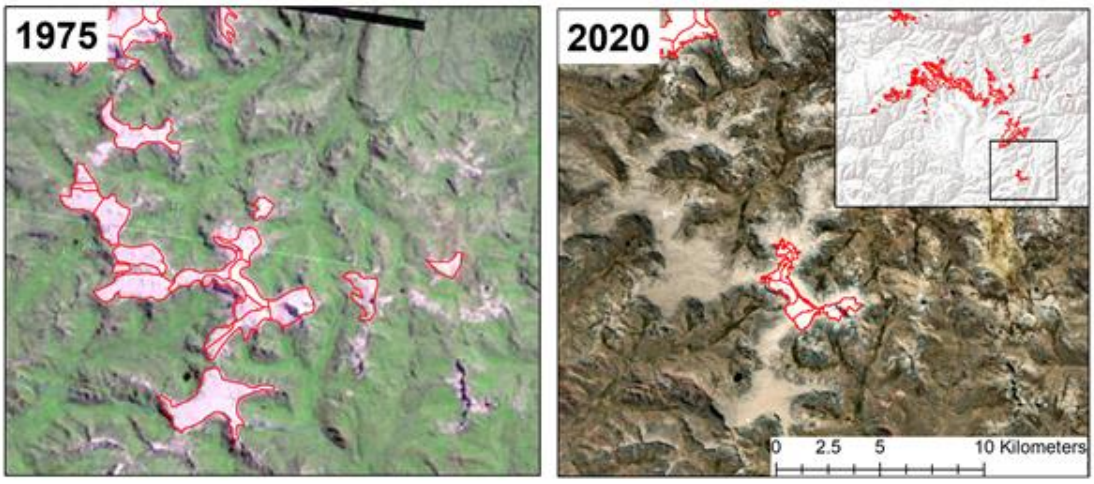

Figure 3.15 – A small cluster of glaciers in the Cordillera Vilcanota to the south-east of the Quelccaya ice cap almost completely melting in the 45-year time span of this series. 1975 background image is from Landsat-2, 2020 image is from DigitalGlobe.

Glacier thinning has been consistent throughout the two decadal intervals studied. It is difficult to make an authentic comparison of our mass balance rate (-0.477 ± 0.067 m w.e. yr^{-1}) to other estimates as differing proportions of the regions are studied. Using thickness-volume scaling, Salzmann et al. (2013) calculated an approximate thinning of -0.39 m a^{-1} from 1985 – 2006 (Seehaus et al., 2019), which would suggest that thinning has accelerated in recent decades when compared to our estimate of -0.563 m a^{-1} from 2000 – 2020. Limited field-based point measurements of mass balance over individual glaciers of the Cordillera Vilcanota have largely focussed on understanding the role micro-topography plays on the spatial differentiation of mass balance; ranging from -4 to 1.4 m w.e. yr^{-1} across the surface of Suyuparina glacier in the Cordillera Vilcanota in 2013 (Molina et al., 2015). While we do not have exact location information on their stakes, our results for the 2010 – 2020 time interval show ranges of -4.79 to 2.28 m w.e. yr^{-1} over the same glacier. Our estimates of mass balance are slightly larger than the -0.42 ± 0.24 m w.e. yr^{-1} calculated by Dussaillant et al. (2019), which suggests this region is also thinning faster than their Andes-wide average. A Peru-wide calculation of glacier thinning from

2000 – 2016 was estimated to be -0.359 ± 0.068 m a^{-1} (Seehaus et al., 2019), which suggests that thinning in the Cordillera Vilcanota is generally faster than the Peru-wide average.

3.5.2. Future Perspectives

In this study, we did not explicitly consider the change in glacial lakes across these regions and how this affects glacier loss. Previous studies (e.g. Drenkhan et al., 2018; Wood et al., 2021), have shown glacial lake expansion across each of these Cordilleras in line with climatic changes. The role of glacial lakes may be important in evaluating future change for tropical mountain glaciers, as lakes have been shown to accelerate ice recession when in direct contact (King et al., 2019). As more lakes develop in overdeepenings left by glacial recession (Colonia et al., 2017), this opens up the opportunity for accelerated ice loss. Similarly, in areas where glacial lakes do currently exist and ice is currently in contact with these lakes (such as the Western face of the Quelccaya ice cap), there may be a slow-down in areal recession in future decades as ice retreats up-slope and out of these lakes. This is particularly important in the Cordillera Vilcanota where 117 new large (> 10,000 m^2) lakes are projected to develop by 2050; the greatest of any Peruvian Cordillera (Guardamino et al., 2019), which is likely to accelerate glacier recession.

Future projections of glacier change in the Andes are stark. Even under a low emissions pathway, Schauwecker et al. (2017) suggest a rise in the freezing line of the Cordillera Vilcanota of 230 ± 190 m by 2100, which would lead to greater committed ice loss. The close relationship between temperature and ELA, projected 2.5 to 4.5°C warming over these glaciers by 2100 (Yarleque et al., 2018; Fyffe et al., 2021), and presence of low-lying glacier tongues across the regions suggest there will be significant melt of the Southern Peruvian Andes this century. Studies projecting future increase in ELA over the Vilcanota and Quelccaya (Schauwecker et al., 2017; Yarleque et al., 2018) also suggest this rate is likely to rise sharply in the coming decades. Low-lying regions within the Cordillera Vilcanota (South-East and North; Figure 3.2) will likely experience the most glacier loss in the near future. Predictions of remaining glacial ice in 2100 for the Cordillera Vilcanota range from a pessimistic 13 km^2 to an optimistic 155 km^2 (5.4 to 63.0% of 2020 ice extent) (Schauwecker et al. 2017).

For people living in close proximity to this glacial ice, this represents a major loss of a freshwater resource. Following the approach of Drenkhan et al. (2018), we

can contextualise this by noting that in our 2000 – 2020 study of volume change, the loss of 3.44 km^3 of water from the Cordillera Vilcanota represents ~84 years of water supply for the city of Cusco. Up to 33% of the population of Cusco rely on glacial meltwater during dry seasons (3% annually) (Martínez et al., 2020). Future ice melt is also unlikely to be even. Key glaciers supplying the Laguna Sibinacocha would lose over 90% of their glacierised area by 2100 (Drenkhan et al., 2018), while the Quelccaya ice cap will likely be below the ELA by mid-century (Yarleque et al., 2018). The low-lying Cordillera Urubamba is particularly at threat of severe ablation over the coming decades owing to the high rate of ELA change, posing an imminent risk of loss of water for irrigation, hydropower, and a drinking source in dry seasons (Chevallier et al., 2011). Ice melt is also unlikely to be even in time. While few studies have examined these specific Cordilleras for the timing of 'peak water' (a maximum river discharge from the glacial melt contribution), indications from other Cordilleras of Peru show that peak water is likely to pass in the near-future (Drenkhan et al., 2014; Mark et al., 2017; Huss and Hock, 2018; Drenkhan et al., 2019).

An immediate concern is also the increased risk of outburst flood events and hazards to communities downstream of these destabilising glaciers (Vilca et al., 2021). Urgent adaptation measures, such as alternative agricultural practices (e.g. sustainable irrigation systems) and GLOF monitoring systems, are needed across the Southern Peruvian Andes to minimise the impact of this loss on communities (Veettil and Kamp, 2019). This must be integrated with a social perspective to recognise the cultural and spiritual loss marked by the recession of these glaciers, and connection of indigenous communities to the ice (Motschmann et al., 2020).

The drivers of ice loss across all three regions are largely due to warming maximum air temperatures (which correlated with ice area loss and ELA changes in all regions) and topographic controls, most notably, elevation. This is as expected; freezing levels are rising in line with temperature rises and low-lying glacier tongues, many of which are low-gradient and thus susceptible to even minor temperature shifts, are now exposed to melt processes (Thompson et al., 2011). However, we did not have the data available to explore all the predicted key climatic drivers of ice loss, such as atmospheric humidity and radiation (Kaser, 1999; Vuille et al., 2008). Furthermore, the role of ENSO as a driver of tropical glacier mass loss is becoming realised over individual glaciers across the Andes (Maussion et al., 2015; Bijeesh Kozhikkodan Veettil et al., 2016), but we could not explore this phenomenon within the available datasets. This signal is thought to be lesser over the Cordilleras Vilcanota, Vilcabamba, and Urubamba as they receive moisture from the Amazon

during La Niña; thereby dampening the ENSO signal (Perry et al., 2014). This highlights the need to complement remote sensing observations with *in situ* data to bridge such gaps.

The optical imagery from Landsat and ASTER used in this study provides useful insights into the dynamics of changes to mountain glaciers, and the long archives of both have been particularly beneficial to generate these results. However, their limitation is highlighted by the lower numbers of usable images we were able to acquire over the Cordilleras Vilcabamba and Urubamba and steep terrain. Mass balance estimates over the Peruvian Andes are few and can be improved using satellite data (Vuille et al., 2018), but the level of uncertainty driven by lack of usable DEM data from ASTER images remains too high. We have demonstrated in this study that the 100 m resolution Hugonnet et al. (2021) dataset provides comparable estimates of mass balance over small mountain glaciers as a higher resolution 30 m product. Radar satellites are able to penetrate cloud, which overcomes the primary limitation, but are challenged by steep topography, which often limits their usefulness to glaciers far larger than those in the Southern Peruvian Andes (Lee et al., 2013). Furthermore, with the steady decay of ASTER as the Terra satellite drifts further out of orbit, and with no current plans for an alternative non-commercially operated stereo satellite, there is an urgent need to find alternative sources to derive regional-level and multi-temporal digital elevation data.

3.6. Conclusions

In this study, we used the Landsat and ASTER archives to quantify glacier area and mass balance change across the Peruvian Cordilleras Vilcanota, Vilcabamba, and Urubamba – three regions typically understudied in the Andes. We identify a decline in both ice area and mass balance across the Southern Peruvian Andes which is most closely linked to the elevation of the individual Cordilleras; low-lying glaciers are most at risk of immediate melt, and those are most prevalent in the Cordillera Vilcanota. Over the period from 1975 to 2020, glaciers in the Southern Peruvian Andes have receded by ~512 km^2 and are now at less than half their original size. These glaciers are also rapidly thinning; losing 3.18 ± 0.44 Gt ice from 2000 – 2020. As the climate continues to warm though, the ELA will shift further upwards, which will consequently expose large flat glaciers (including the Quelccaya ice cap) to net ablation. Optical imagery, and stereo imagery, can provide useful insights into the dynamics of small mountain glaciers, but the heavy presence of cloud and snow

in long archives still limit the usability of these data and future research needs to validate and extend these data with *in situ* measurements. These data provide a closer insight into interdecadal patterns of glacier change in these data sparse regions, and can be used to help inform policymaking to manage the future threat of glacial hazards and ensure water security across the Cusco region.

Chapter 4

Investigating the performance of new satellite altimetry missions over mountain glaciers

4.1. Introduction

Mass loss from mountain glaciers and ice caps is predicted to increase with rapid climate warming (Fox-Kemper et al., 2021), which poses increasing challenges for water resource and hazard management (Keiler et al., 2010; Viviroli et al., 2011). Approximately one-sixth of the world's population rely on mountain glaciers and ice caps as water resources for hydropower, irrigation and drinking (Kundzewicz et al., 2007; Immerzeel et al., 2019). This population is also increasingly threatened by glacial hazards, including severe flood events (Scheffran and Battaglini, 2011). Satellite remote sensing allows the opportunity to monitor glaciers at repeat intervals with high accuracy, for little-to-no cost to the end user. Typical techniques to study the changing dynamics of mountain glaciers for management purposes include DEM differencing (Berthier et al., 2007; Gardelle et al., 2012), optical imagery for area change investigation (Bolch, 2007; Racoviteanu et al., 2008) or Synthetic Aperture Radar (SAR)-based approaches (Rao et al., 2004). It has become increasingly common to include a combination of techniques in such studies to improve confidence in long-term results (Quincey et al., 2007; Shangguan et al., 2015).

Satellite altimeters have been used to improve estimation of mass loss from ice sheets for over three decades, including the European Remote Sensing (ERS-1 and ERS-2) satellites (Shepherd et al., 2012), ICESat (Pritchard et al., 2009) and CryoSat-2 (Helm et al., 2014). While satellite altimetry has been able to quantify increasing mass loss over vast ice sheets (see Slater et al. (2021) for a comprehensive review of these results), the technique has seldom been applied to smaller mountain glaciers or ice caps, despite their importance as water resources. This is largely due to the challenging topography of mountainous regions, with steep slopes decreasing vertical accuracy (Harding et al., 1994). For some altimeters, the footprint (the, typically circular, ground area from which elevation data are captured over) can be too wide (e.g. CryoSat-2 is 1,650 m wide) to accurately acquire data where large topographic variations, such as in a mountain range, are observed. Large cross-track separation means that only a small proportion of mountain glaciers worldwide are intercepted by existing satellite altimetry tracks, leading to region-wide

mass balance estimates being produced based on averaging on-ice elevation change where acquired (Kääb et al., 2012).

The recent launch of two new satellite altimetry missions, Sentinel-3 from the European Space Agency (ESA) and ICESat-2 from the US National Aeronautics and Space Administration (NASA), provides an opportunity to re-evaluate the potential application of satellite altimetry to monitoring glaciers and ice caps. Both satellites acquire data at a high spatial resolution, with new features to improve tracking of complex terrain (Sentinel-3) or the acquisition of large volumes of data across many glaciers in a mountain range (ICESat-2) (Table 4.1). However, while Sentinel-3 is designed as a multi-decadal mission, ICESat-2 is only designed to operate for three years. The launch of CryoSat-2 in 2010 represented a significant advance in spatial resolution and has built up an impressive 12-year archive of altimetry measurements. However, its performance over mountain glaciers has previously been evaluated (e.g. Dehecq et al., 2013; Jakob et al., 2021), and so we limit our analysis to, as yet, unstudied satellites.

	Sentinel-3	**ICESat-2**
Instrument type	Radar	Laser
Altimeter	SRAL	ATLAS
Along-track ground spacing	300 m	70 cm
Repeat orbit	14 days (A+B)	91 days
On-board DEM resolution	5 km	0.05˚
Range window width	60 m	6 km
Distance between tracks at equator	52 – 104 km	3.6 – 10.8 km

Table 4.1 – Comparison of Sentinel-3 and ICESat-2 altimeters

Our aim is to conduct the first detailed examination of the performance of these new altimeters over mountain glaciers and ice caps. In this investigation, we:

i) Compare the elevation data from Sentinel-3 and ICESat-2 to reference DEMs to quantify the accuracy of their measurements;
ii) Where possible, identify potential applications for Sentinel-3 and ICESat-2 as part of monitoring programmes of mountain glacier dynamics;
iii) Explore future satellite altimetry missions and make recommendations for their improvement for acquiring data over mountain glaciers and ice caps.

4.2. Sentinel-3

Sentinel-3 is primarily an ocean monitoring mission, comprised currently of two satellites (Sentinel 3A, launched in February 2016 and Sentinel-3B, launched in April 2018) (Donlon et al., 2012). Two further Sentinel-3 satellites are due to launch in 2024 and 2028 to bring the operation of this mission to the mid-2030s. The potential for Sentinel-3 to monitor glacier change has been evidenced over Antarctica (McMillan et al., 2019) and Greenland (Maddalena et al., 2020), but not yet outside of the ice sheets. Altimetry is performed with the SRAL (Synthetic Aperture Radar Altimeter), which operates in its high-resolution SAR mode. SRAL operates at Ku-band and C-band frequencies, in open-loop (positioning the range window based on an on-board elevation model; Figure 4.1) and closed-loop (range window defined by analysing the waveform returns of previous acquisitions) modes. It is the open-loop tracking mode that provides optimism that Sentinel-3 will outperform predecessor radar altimeters. For example, elevation retrieval from CryoSat-2 was only found to be possible over very large (~800 km^2) individual glaciers (Trantow and Herzfeld, 2016) due to incorrectly tracking underlying terrain and placing the range window at mountain peaks rather than glacier surfaces (Dehecq et al., 2013). The reality may be more nuanced, with CryoSat-2 tracking both peaks and valleys dependent on location, but nevertheless this nuance means that CryoSat-2 remains an unreliable source of information for repeat acquisitions.

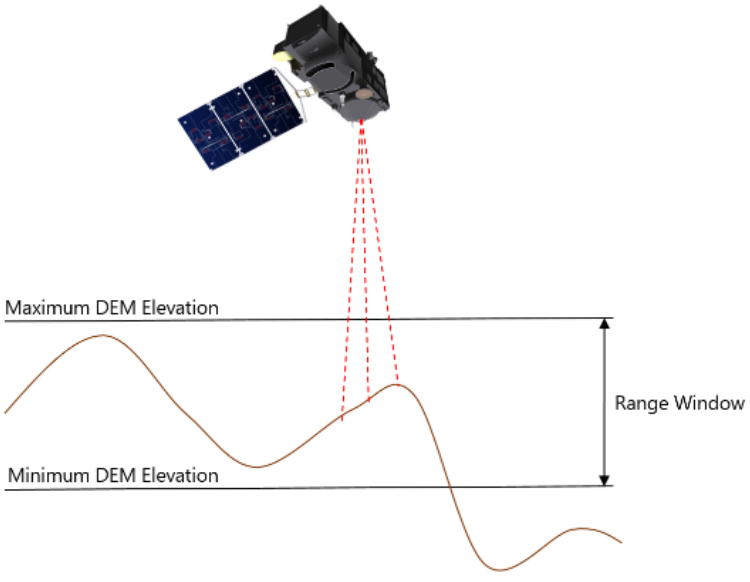

Figure 4.1 – In open-loop tracking mode, Sentinel-3 uses an onboard DEM (the open-loop tracking command; OLTC) to position a 60 m wide 'range window' – a window about the expected surface topography where the satellite 'listens' for an echo return – to capture the surface elevation.

Novel methods of tracking complex terrain are necessary in order to retrieve any usable data from these regions. The Jason-2 satellite (2008 – 2019), with the Poseidon-3 altimeter, was primarily an ocean monitoring mission, but acquired data over land using a pseudo-DEM (limited elevation data over targets of interest) to position a range window; the first open-loop tracking mode (Martin-Puig et al., 2016). This opened the potential for retrieving regular elevation from large (>100 km^2) lakes and wide rivers (Birkett and Beckley, 2010). However, the wide footprint of Poseidon-3 (>1 km) meant that elevation retrieval over mountain glaciers was imprecise (Hwang and Cheng, 2015). Jason-3, the successor mission in this series, used a similarly wide instrument footprint, though with a greater memory capacity for open-loop tracking to be extended to more targets (Biancamaria et al., 2018). Sentinel-3 combines the use of a SAR altimeter from CryoSat-2 for a small (300 m) along-track footprint with open-loop tracking proven by the Jason-2 and Jason-3, thereby theoretically capable of accurate elevation retrieval over mountain glaciers. With its rapid revisit time (27 days), and tandem pair orbit to acquire data over more of Earth's surface, Sentinel-3 represents an opportunity for radar altimeters to acquire repeat, accurate, elevation measurements over mountain glaciers.

4.2.1. Sentinel-3 Methods

We acquired Level-2 enhanced data from Sentinel-3A from a number of ice caps and mountain glaciers across Earth, in both open and closed-loop tracking modes (Table 4.2, Figure 4.2) to explore how differing tracking modes impact data acquisition. Sentinel-3 uses multiple methods to extract elevation, and we explored a number of variables from within the Level-2 enhanced data product. Of particular interest were the elevation, altitude, range, and OCOG (offset centre of gravity) elevation variables. OCOG is a more appropriate re-tracking technique over land-ice as it is better able to process the wider range of waveform shapes that may be expected (Wingham et al., 1986). All analysis was performed using MATLAB R2017a. Most mountain glaciers and ice caps are situated within the open-loop tracking mode, where Sentinel-3 uses the OLTC to position its range window. To compare the performance of Sentinel-3 in both tracking modes, we also studied the Vatnajökull ice cap, where Sentinel-3 operates in closed loop mode. For each region, we compared the performance of Sentinel-3A in retrieving accurate measurements of elevation against reference DEMs, given in Table 4.2.

Fig. 4.2 Ref	Site Name	Type	Relative orbit number	Lat range (°)	Lon range (°)	Elevation range (m)	Open / Closed loop	Reference DEM
A	Vatnajökull	Ice cap	52	64.10 – 64.75	-16.90 – -16.30	366 - 1659	Closed	ArcticDEM & GDEM
B	Peru	Glaciers	60	-13.67 – -13.78	-71.11 – -71.09	4922 - 5772	Open	GDEM
C	Himalaya	Glaciers	33	27.80 – 28.20	86.63 – 86.77	3643 - 7346	Open	High Mountain Asia DEM
D	Patagonia Icefield - North	Ice Cap	338	-49.5 – -48.35	-73.83 – -73.35	0 - 1749	Open	SRTM
E	Patagonia Icefield - South	Ice Cap and Glaciers	32	-50.1 – -48.7	-73.35 – -73.93	114 - 2631	Open	SRTM
F	Patagonia Lakes	Meltwater lakes	89	-50.32 – -49.5	-72.27 – -72.64	179 - 252	Open	SRTM

Table 4.2 – Areas investigated by Sentinel-3.

Ground-based data are essential to validating the accuracy of satellite altimeters. Owing to the logistical challenges associated with visiting all sites, in combination with the COVID-19 pandemic, we have had to use reference DEMs as a comparison. Of global DEMs, the ASTER GDEM shows the lowest RMSE (root mean squared error) to ground-based validation in rugged terrain (Uuemaa et al., 2020) of 11.77 m. For the Himalaya, this is outperformed by the HMA DEM, with a RMSE of 1-2 m (Shean, 2017), though this has not been independently assessed. However, while the ASTER GDEM shows good promise, it has large data gaps and high levels of inaccuracy over bright surfaces such as the accumulation zones of ice caps. For this reason, we use the SRTM DEM over Patagonia, accounting for an approximate 6 m C-band radar penetration (which varies from 3 m over bare ice to 9 m over fresh snow; Rignot et al., 2001). While this variation in penetration is negligible in positioning the 60 m wide range window, it will inevitably result in uncertainty when comparing SRTM to Sentinel-3.

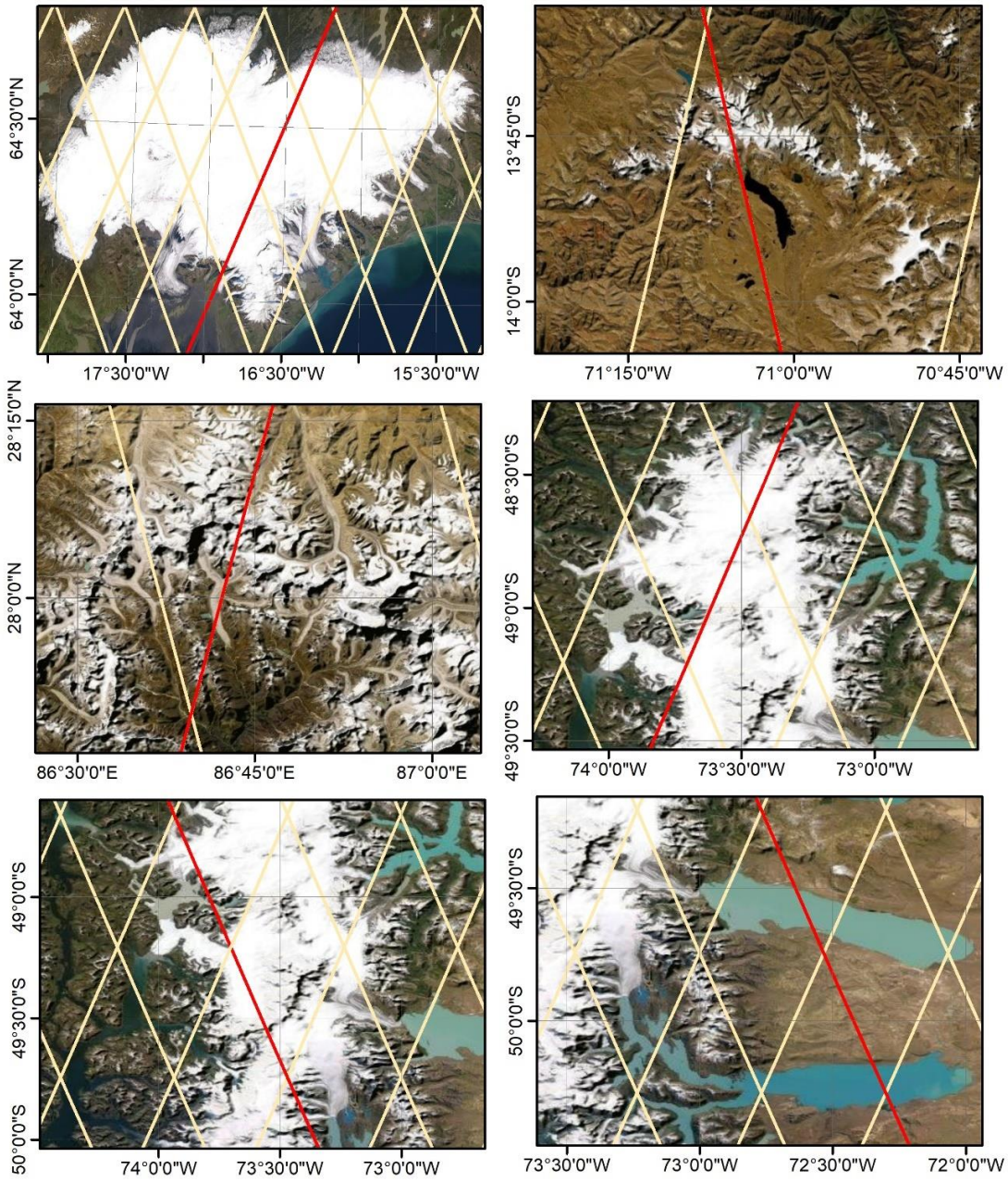

Figure 4.2 – Sentinel-3 track coverage over ice cap and mountain glacier areas studied in this Chapter, in both open (A) and closed-loop (B – F) tracking modes. Full details of each site are given in Table 4.2. Background images from Landsat / DigitalGlobe.

We also assess other, more crude, methods of estimating elevation which avoids retracking algorithms and geophysical corrections and results in a faster end product to the user. In theory, subtracting the range window that Sentinel-3 looks for a pulse return from its altitude should yield this crude estimate of elevation, to allow the user to verify if the retracking algorithms or geophysical corrections are causing

poor elevation returns in the traditional products. This method does not account for poor quality waveforms, or any corrections that are performed on the dataset, but could be a suitable backup in areas of low data availability. For each study area, seven cycles were examined, from cycle 30 (collected between 7th April and 4th May 2018) to cycle 36 (collected between 16th September and 13th October 2018).

In addition to studying glaciers and ice caps themselves, proglacial lake levels can be indicative of glacial dynamics (Pasquini et al., 2008) as their elevation changes seasonally with increasing melt. When such lakes are large enough to have multiple Sentinel-3 returns across them, direct altimetry of the lake surface elevation can be used for water resource management. We therefore also studied the Argentino and Viedma Lakes, which are supplied by glacial melt from the east side of the Southern Patagonian Icefields (Figure 4.2F). Each lake was examined across a full year (Cycle 22 to Cycle 36; September 2017 to September 2018). Multiple returns are recorded across both lakes, so the mean lake surface elevation in each cycle is reported.

4.2.2. Performance of Sentinel-3 over mountain glaciers

4.2.2.1. Open Loop Tracking

In Peru and the Himalaya, where tracking is in open-loop mode, there were zero returns that provided a valid elevation value within the study period on any of the seven cycles analysed (Table 4.3). Subtracting the range window from the altitude in both areas yielded elevation values between 0 and 20 m. In Patagonia Icefield - North, around 1% of returns provided a valid elevation value on any one cycle, with OCOG retracking providing slightly more (3-6%) valid elevation returns. More than 90% of failed returns did not reach the threshold for total power in the waveform, due to incorrect positioning of the range window. We identified significant disparity between the on-board OLTC table and reference DEMs, which may be causing poor elevation retrieval. Patagonia Icefield – South achieved a greater elevation return rate, with around one quarter of returns providing a valid elevation value in any one cycle. However upon further inspection with satellite imagery, these valid returns occured almost exclusively in non-glacierised regions along the track, always returning an elevation value between 170 and 190 m (corresponding to the approximate position of the OLTC). This also occurred with OCOG retracking.

Ref.	Site	Number of returns per cycle	Number of valid elevation returns per cycle	Number of valid OCOG elevation returns per cycle
B	Peru	34-35	0	0
C	Himalaya	76-77	0	0
D	Patagonia Icefield – North	333-334	2-4	9-20
E	Patagonia Icefield - South	442-443	110-111	129-146

Table 4.3 – Valid returns for each area of interest in cycles 30-36. Returns are given as the minimum and maximum number in the seven studied cycles.

The reason for the lack of elevation returns is due to the range window being positioned such that it does not reflect the ice surface, as demonstrated by a lack of power in any radargram. For many inland water sites, such as lakes, reservoirs, and rivers, the OLTC has been updated to accurately represent these targets within the ± 10 m needed for Sentinel-3 to capture altimetry data (Le Gac et al., 2019). Where targets are not specified, the OLTC remains positioned at the elevation of the preceding target until another target repositions it (Jiang et al., 2020). This means that unless *a priori* information is supplied regularly over complex terrain, the OLTC is highly likely to be inaccurate. Cycles 30 to 36, analysed above, were acquired based on version 4.2 of the Sentinel-3A OLTC, which did not include any targets over our sites of interest. Using the ESA crowdsourcing portal (https://www.altimetry-hydro.eu) (Le Gac et al., 2019), we uploaded elevation information covering each of our areas of interest using the DEMs outlined in Table 4.2. The potential for updating the OLTC is, however, extremely limited, because the tracking system is only able to update every ~5 km along-track. Over complex terrain this represents a severe shortfall and so we chose on-ice targets positioned, where possible, in the centre of a glacier. These updates were added to the OLTC version 5.0 which were uploaded to the satellite on 3rd September 2019. The OLTC update moves the range window to within the elevation of glaciers of interest and a greater range of data are available to analyse.

In the Cordillera Vilcanota, Peru, a surface echo is recorded by the satellite for around half of the area of interest, from -13.80° to -13.70° latitude, although the recorded elevation data does not correlate to the underlying DEM (Figure 4.3). As

elevation decreases towards the north end of the track, the coarse spatial resolution of the OLTC means that it cannot track rapid elevation changes, and no signal is recorded in the radargram (Figure 4.3C). Over an unnamed glacier of interest situated to the west of Chumpe glacier, where the OLTC was positioned to record, the difference between GDEM and Sentinel-3A was 27.5 m. In the subsequent orbit, this difference was 214 m. In the Himalaya, where topography is steeper, but the area of interest is wider, Sentinel-3A acquires more data than in Peru (Figure 4.4), with 14 valid elevation returns over the Ngozumpa glacier where the OLTC was positioned. The mean absolute difference to the HMA DEM in this portion of the track is 46.87 m (mean -6.07 m).

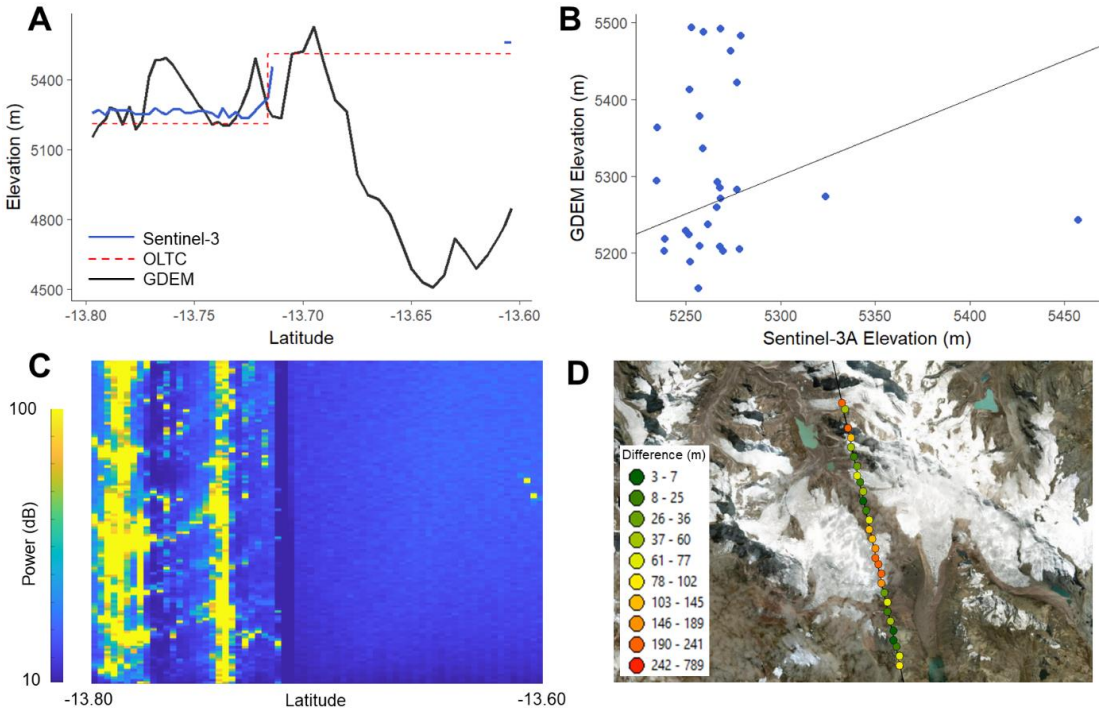

Figure 4.3 – Performance of Sentinel-3A (cycle 42) with updated OLTC over the Cordillera Vilcanota, Peru (orbit 60). (A) Comparison of Sentinel-3 with GDEM along-track, with OLTC positions highlighted. (B) Corresponding radargram showing power returns to the satellite, where blue shows no power. The y-axis represents the 128 bins of the waveform return. (C) GDEM and Sentinel-3A elevation along the Sentinel-3A track. (D) Spatial difference between GDEM and Sentinel-3A elevation.

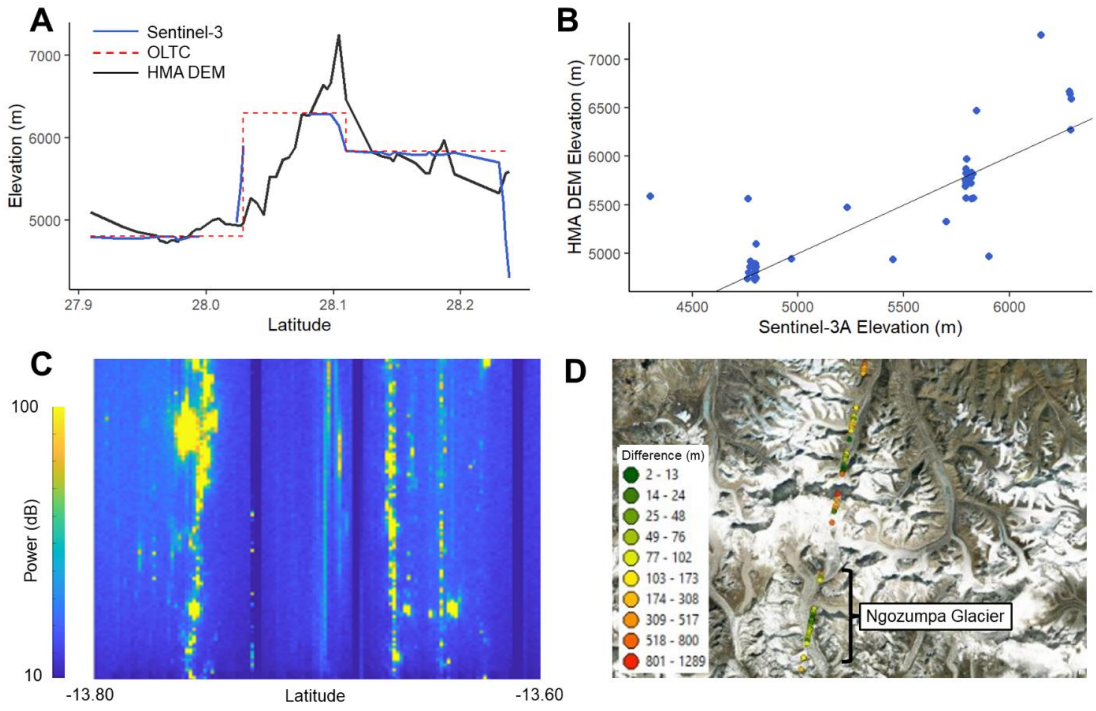

Figure 4.4 – Performance of Sentinel-3A (cycle 42) with updated OLTC over the central Himalaya (orbit 33). (A) Comparison of Sentinel-3 with HMA DEM along-track, with OLTC positions highlighted. (B) Corresponding radargram showing power returns to the satellite, where blue shows no power. The y-axis represents the 128 bins of the waveform return. (C) HMA DEM and Sentinel-3A elevation along the Sentinel-3A track. (D) Spatial difference between HMA DEM and Sentinel-3A elevation. Ngozumpa glacier is positioned to the South of this figure.

Over Patagonia, the updated Sentinel-3A OLTC closely tracks ice surface and acquires data across the ice cap (Figure 4.5). The more gradual topographic changes along these tracks means that the OLTC is able to more closely reflect the underlying elevation and the difference to the GDEM is lower (mean absolute difference of 106.7 m, mean difference of 36.5 m across the track). However, over the margins of the ice cap, where rapid changes in topography do occur, the difference grows, reaching in excess of 500 m. Similar patterns are observed in both orbits 32 and 338. Sentinel-3 performs much better over the Argentino and Viedma proglacial lakes, with consistent and valid elevation returns acquired in each cycle. Over the course of one year, Sentinel-3 monitors the ~2 – 4 m change in water surface height corresponding to glacial melt (Figure 4.6). While lake gauge data were not in place during the course of this investigation, this represents a reasonable seasonal variation of these lakes from 2011-14 (Richter et al., 2015; Carabajal and Boy, 2021).

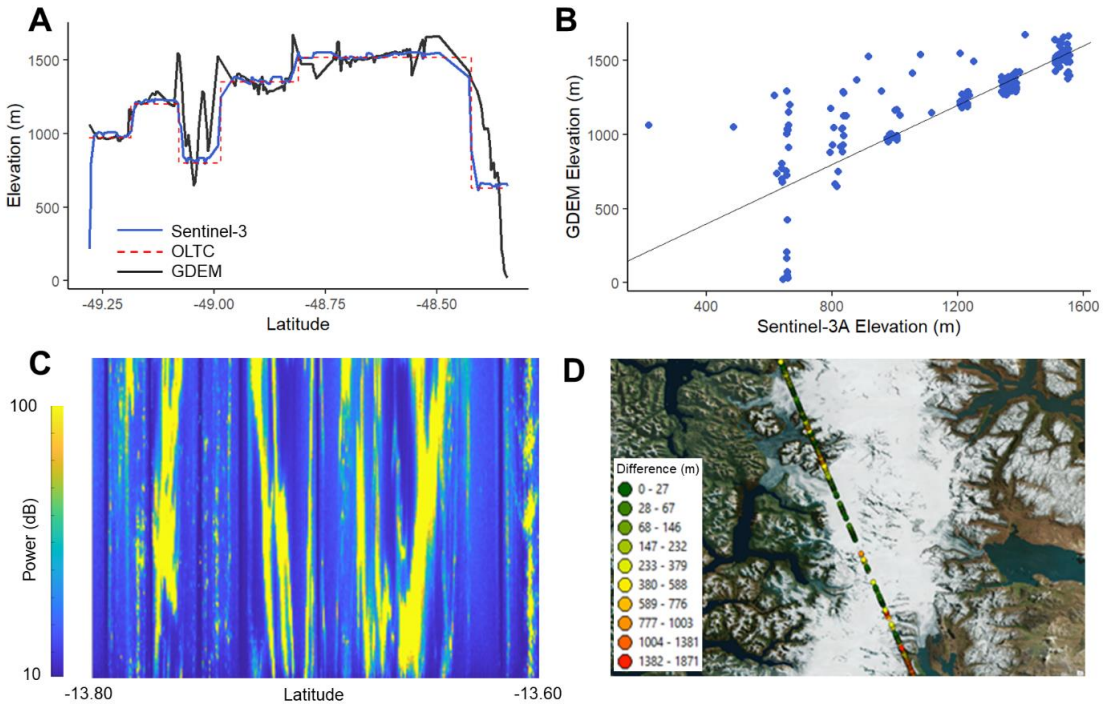

Figure 4.5 – Performance of Sentinel-3A (cycle 42) with updated OLTC over the Patagonia ice cap (orbit 338). (A) Comparison of Sentinel-3 with GDEM along-track, with OLTC positions highlighted. (B) Corresponding radargram showing power returns to the satellite, where blue shows no power. The y-axis represents the 128 bins of the waveform return. (C) GDEM and Sentinel-3A elevation along the Sentinel-3A track. (D) Spatial difference between GDEM and Sentinel-3A elevation.

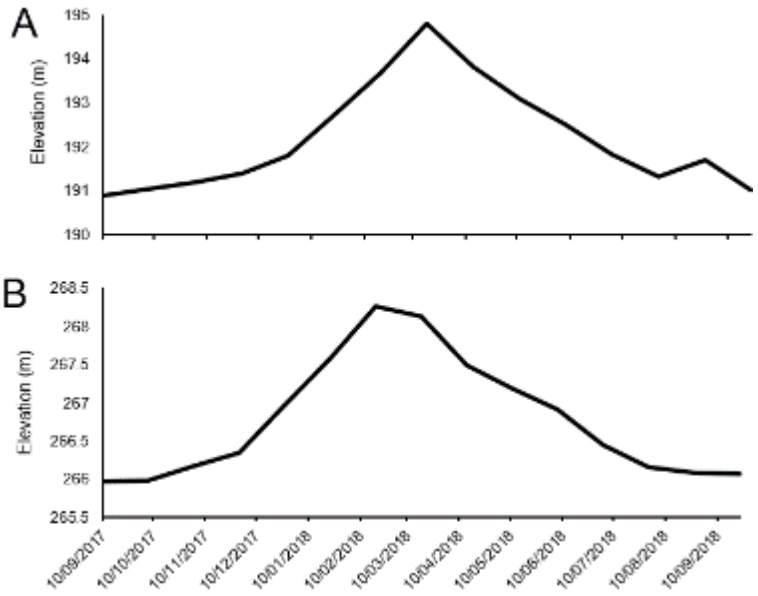

Figure 4.6 – Sentinel-3A elevation (orbit 89) from (A) Viedma and (B) Argentino lakes to the East of the Patagonian ice cap, as recorded over a full year. Location displayed in Figure 4.2.

4.2.2.2. Closed loop tracking

The number of returns across the Vatnajökull ice cap varies greatly between cycles, from a minimum of 127 to a maximum of 222 (mean 176), with the number of valid elevation returns ranging from 23% to 39% of total returns. While there is greater variability in the number of returns between cycles compared to open-loop tracking, there is a higher success rate for valid elevation measurements. Detailed analysis of the quality of waveform returns from cycle 36 (using the waveform_qual_ice_20_ku variable), where 39% of returns record a valid elevation measurement, shows that poor positioning of the range window leads to low power in the waveform, or the leading edge of the peak falling before a given threshold (gate 44) (Figure 4.7). Elevation data across Vatnajökull does not closely match either ArcticDEM or GDEM using any variable (Figure 4.8). The mean difference between Sentinel-3A and ArcticDEM ranged from 100.0 m using the standard elevation variable to 153.3 m by subtracting the altitude of the satellite from the range window.

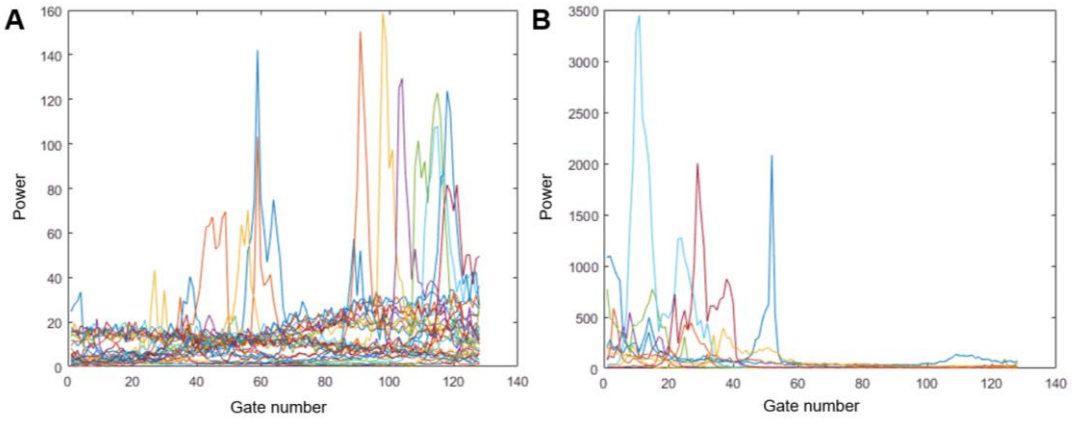

Figure 4.7 – Failed waveforms from the Vatnajökull ice cap, cycle 36, orbit 52, due to (A) lack of power in the waveform or (B) the leading edge not meeting the threshold of gate 44. Note the varying y-axis scales in each.

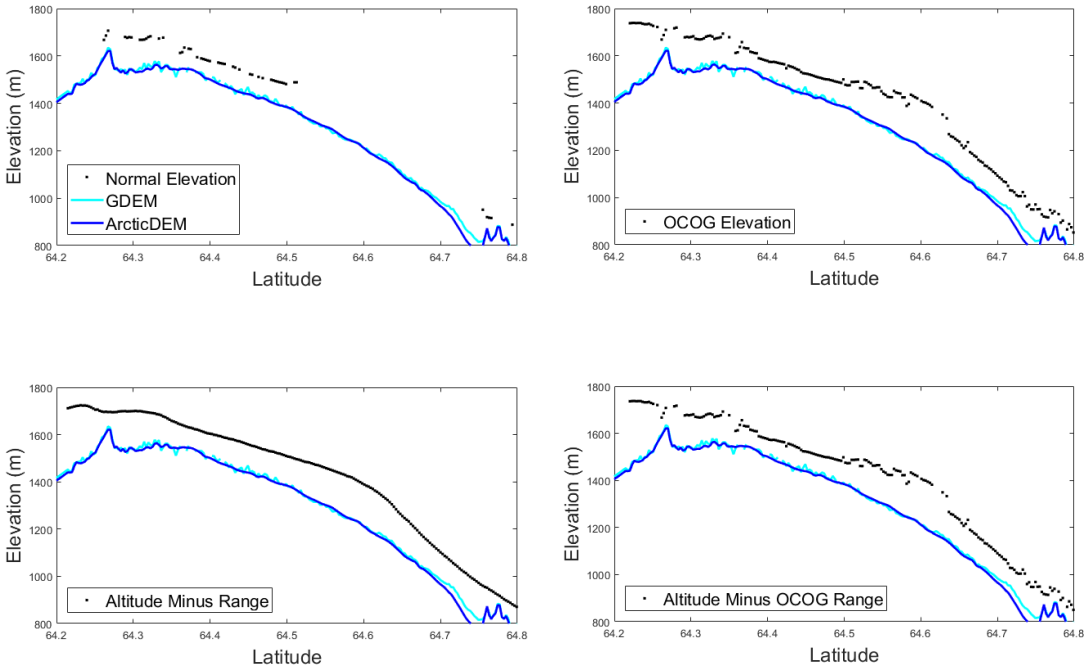

Figure 4.8 – Comparison of four different variables to acquire elevation data from Sentinel-3A using close-loop tracking over the Vatnajökull ice cap (cycle 36, orbit 52).

4.2.3. Use of Sentinel-3 data over mountain glaciers

The lowest difference between Sentinel-3 and a reference DEM is found in open-loop tracking mode, where the OLTC provides *a priori* data of a target. Only once this information is uploaded to the satellite, via regular crowd-sourced OLTC

updates, does Sentinel-3 altimetry become usable. Given the coarse resolution of the OLTC pseudo-DEM, valid elevation retrievals in complex terrain are, in practice, restricted to a single point within a ~5 km portion of track. This may be a usable platform for measuring change on one glacier within a range, but only if the glacier is fortuitously positioned beneath the orbit of Sentinel-3 to acquire data. In the Cordillera Vilcanota, only two Sentinel-3 tracks cover the range, intercepting just nine of the 175 glaciers. Given the narrowness of the mountain range and need to position the OLTC over specific targets, only two glaciers (one per track) of the whole Cordillera Vilcanota could, in practice, be monitored.

Sentinel-3 is first and foremost an ocean monitoring mission. The OLTC allows the SRAL to acquire data over land, which has allowed for highly accurate monitoring of inland water bodies (Le Gac et al., 2019; Taburet et al., 2020). For example, over the Zamebzi river, differences between Sentinel-3-derived elevation and *in situ* water level stations ranged from 2.9 to 31.3 cm at targets of interest (Kittel et al., 2021). Over the Cordillera Vilcanota, differences between the altimeter and the reference DEM spanned several orders of magnitude. Monitoring glacial melt via proglacial lake surface elevation change may be a more promising use of Sentinel-3, as demonstrated over the Argentino and Viedma lakes. This has been demonstrated in the Pyrenees mountain range, where the surface elevation of small (>130 m wide) reservoirs was monitored to 1.39 m accuracy with minimal land influence on the waveforms (Gao et al., 2019). However, the problem of large cross-track separation means that no lakes >100 m wide within the Cordillera Vilcanota are covered by either Sentinel-3A or 3B. A parallel satellite altimeter, also within the ESA Copernicus Programme, Sentinel-6 Michael Freilich, shares this issue with even larger cross-track separation (315 km at the equator).

Retracking methods, whereby the extended range of the waveform is analysed to handle added complexity in waveform shape, may be a useful future avenue for research into satellite radar altimetry over mountainous regions (Gao et al., 2019). In China, acquiring data from mountainous rivers situated between topographic peaks was improved by using the Multiple Waveform Persistent Peak (MWaPP+) retracking algorithm to produce sub-metre error (Jiang et al., 2020). Waveforms from a radar altimeter in complex terrain can become contaminated by off-nadir reflections, resulting in non-conventional waveforms. MWaPP+ assesses adjacent waveforms to calculate the bin at which the underlying water body is best represented by the peak (Villadsen et al., 2016). However, it is noteworthy that data acquisition in mountainous terrain was only possible by first improving the OLTC, in

addition to waveform retracking (Tsai et al., 2020; Jiang et al., 2020). Where the tracking window is inaccurately positioned, even the extended waveform does not capture data.

The novelty of Sentinel-3, in providing high spatial resolution elevation retrieval with a small footprint, is hindered only by its inability to correctly track the underlying surface. Open-loop tracking via the OLTC shifts the range window to a more accurate position, but its narrowness of 60 m means that targets over complex terrain are limited. Narrow range windows are a problem which have affected satellite-based radar altimeters for decades (Ridley and Partington, 1988; Scott et al., 1994) and is typically addressed by retracking algorithms (Deng and Featherstone, 2006), though this relies on the waveform being close to the range window – not over 1000 m apart as we observed prior to altering the OLTC. For Sentinel-3, further development in tracking algorithms and the provision of an OLTC with finer along-track resolution based on accurate DEMs is necessary before this next generation satellite can provide accurate and reliable data over mountain glaciers.

4.3. ICESat-2

ICESat-2, launched in September 2018, is primarily designed to monitor ice sheet mass balance and forest canopy height using a different satellite altimetry approach (Neumann et al., 2019). Whereas Sentinel-3 is a radar altimeter, ICESat-2 uses six laser beams and the Advanced Topographical Laser Altimeter System (ATLAS) to retrieve elevation. Up to 200 quadrillion 532 nm photons leave the satellite each second, providing an along-track spatial resolution of up to 70 cm over a 91-day repeat orbit. Its six laser beams provide up to 3.6 km cross-track separation at the equator, allowing data acquisition from numerous glaciers in a mountain range; contrary to the Sentinel-3A/B spacing of 52 km. ICESat-2 has a 6 km wide range window for elevation retrieval, which means no open-loop tracking mode is necessary. However, ICESat-2 is limited in its scope as the laser beams do not penetrate cloud, unlike Sentinel-3's radar. With a 91-day repeat orbit, this could lead to large data gaps, such that ICESat-2 may only be able to be relied upon for annual monitoring. Nevertheless, its strong performance potential, particularly in mountainous regions, means that ICESat-2 could form part of a suite of techniques used to monitor changing glaciers.

Satellite laser altimetry began with the original ICESat mission, which operated from 2003 to 2010, with the Geoscience Laser Altimeter System (GLAS).

ICESat was designed primarily to monitor ice sheet mass balance (Schutz et al., 2005; Ewert et al., 2012), but also provided accurate elevation retrievals over ice caps and glaciers (Treichler and Kääb, 2016). The most significant limitation with ICESat was that its track positions could vary by a few hundred metres between cycles, rendering repeat observations and regular monitoring of small glaciers difficult (Kropáček et al., 2014). To overcome this, small mountain glaciers could be monitored by comparing elevation retrievals to a reference DEM and using a linear regression to derive elevation trends (Kääb, 2008; Kääb et al., 2012). ICESat-2 looks to overcome this challenge of the original ICESat mission by using six beams to retrieve more tracks than its predecessor; ICESat had an equatorial cross-track spacing of 15 km, compared to ICESat-2's 3.6 km. The distance between retrievals has also decreased from ~170 m to ~70 cm. This means a far greater number of glaciers have regular, accurate, elevation retrievals. Finally, the six beams of ICESat-2 are paired and spaced 90 m apart on the ground, with a fixed reference track running between beam pairs. This means that even if repeat cycles do not accurately overlap each other, the elevation of this reference track can be determined by interpolating the slope between the two beams on both occasions, allowing for accurate and reliable monitoring of elevation change (Markus et al., 2017). Together, these factors suggest that ICESat-2 should be a promising mission for regular observation over small mountain glaciers.

4.3.1. ICESat-2 Methods

Given the vast quantity of data acquired by ICESat-2, we narrowed our study to the Peruvian Cordillera Vilcanota and performed an in-depth analysis on a wider range of potential applications. We used the ATL03 (raw photons) and ATL06 (geolocated, land-ice surface height) products to assess the performance of ICESat-2 over glaciers and lakes of the Cordillera Vilcanota, Peru. The ATL06 product segments ATL03 into 40 m wide windows and passes a linear model through ATL03 photons. The centre point of this linear model per segment is then taken as the elevation of each 40 m window (Smith et al., 2019). This decreases the spatial resolution of the product (40 m compared to a theoretical 70 cm of ATL03), but should increase the accuracy as a result of excluding low confidence photon returns. Early insights from the interior of Antarctica shows that ATL03 has an accuracy <5 cm, while ATL06 has an accuracy <3 cm (Brunt et al., 2019), though this is over a smooth

flat surface and is unlikely to be representative of accuracy over rugged mountainous terrain.

Over oceans and ice sheets, ICESat-2 repeats its ground tracks on a 91-day cycle to acquire overlapping observations. A critical mission objective of ICESat-2 is to capture regular, high spatial resolution information on global carbon stocks by observing the height of vegetation (Abdalati et al., 2010). In order to gain good coverage of global vegetation between tracks, over land, ICESat-2 changes its ground track position every 91 days by adjusting the angle of the ATLAS. Every 2 years, ICESat-2 cycles through eight different off-nadir angles, resulting in low (<2 km) cross-track separation across the time period (Markus et al., 2017). For mountain glaciers, this means that far more glaciers are covered by the tracks than Sentinel-3 (over 90% of glaciers in the Cordillera Vilcanota are intercepted by an ICESat-2 track at one of the eight time periods; Figure 4.9), but most repeat acquisitions are separated by 2 years. For some areas, there is overlap on an annual basis owing to the far left beams overlaying the tracks of the far right beams from a year prior. We analyse all tracks covering the Cordillera Vilcanota from January 2019 to January 2022. Data are acquired from the open-source ICESat-2 viewing interface, Open Altimetry, and analysed in MATLAB and R.

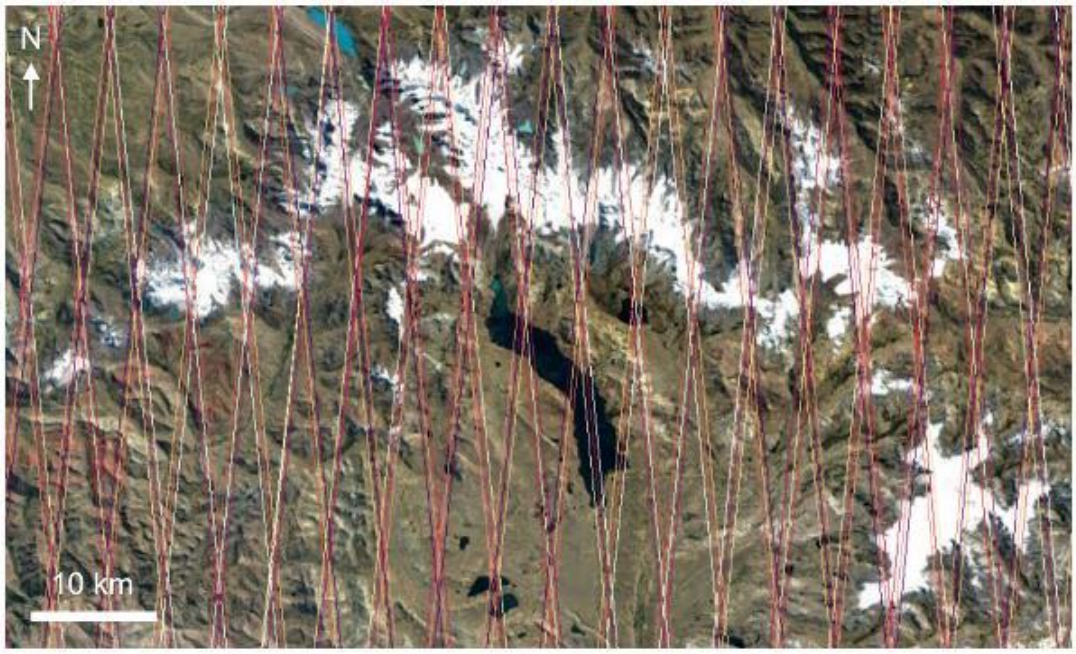

Figure 4.9 – Ground track positions of ICESat-2 over the Cordillera Vilcanota over a 2-year time period. The eight positions are demonstrated in different shading.

4.3.2. Performance of ICESat-2 over mountain glaciers

Analysing the performance of Sentinel-3 involved in-depth analysis into the extremely little data acquired to understand why the satellite was so inaccurate in elevation retrieval. In contrast, it was immediately apparent that ICESat-2 acquires far more promising data and so we used a more sophisticated approach to assess accuracy. To analyse the accuracy of satellite altimeters, they should be compared to ground-based measurements (Vu et al., 2018). Where ground-based comparisons of ICESat-2 have taken place over the flat interior of Antarctica, error is less than 10 cm (Brunt et al., 2019; Brunt et al., 2021). In the absence of comparative studies in mountainous regions, and due to the inability to collect ground-based measurements ourselves owing to the COVID-19 pandemic, we compare ICESat-2 with a 12 m resolution TanDEM-X tile. TanDEM-X has precedence for being the highest accuracy global DEM product in mountainous regions based on a number of ground validated studies in similar terrain, with sub-metre mean error, compared to error greater than 10 m for products such as SRTM and GDEM (Wessel et al., 2018; Guth and Geoffroy, 2021; Chen et al., 2022). However, on steep slopes exceeding 20°, TanDEM-X DEMs rapidly increase in their error (Uuemaa et al., 2020). TanDEM-X DEMs used the original ICESat mission as ground control points, but do not (yet) use ICESat-2 data in their referencing.

We compared all 35,068 points from the ATL06 product acquired in off-ice areas of the Cordillera Vilcanota between January 2020 to January 2022 to a TanDEM-X DEM (Figure 4.10). These points were collected from five of the eight track positions of ICESat-2 as the other three were too clouded to retrieve any data. Owing to differing levels of penetration over water bodies between TanDEM-X and ICESat-2, we removed lakes from this analysis. The mean absolute difference was 2.73 m, with a mean difference (TanDEM-X minus ICESat-2) of -0.85 m (Figure 4.10a). Owing to the increased uncertainty of altimeters over steep terrain (Wang et al., 2019; Zhang et al., 2021), we also compare this difference to slope derived from TanDEM-X and concur with previous estimates that difference rapidly increases beyond slopes of 20° (Figure 4.10b). Using the 21,673 points acquired on slopes less than 20°, mean absolute difference between TanDEM-X and ICESat-2 decreases to 1.25 m, with a mean difference of -0.39 m. However, given the high uncertainty of TanDEM-X itself over steep slopes, it is difficult to comment on whether this difference is derived from inaccuracy from ICESat-2 or TanDEM-X. We can therefore suggest that ICESat-2 is consistent against TanDEM-X, but cannot use TanDEM-X to assess the accuracy of ICESat-2 measurements owing to its own flaws.

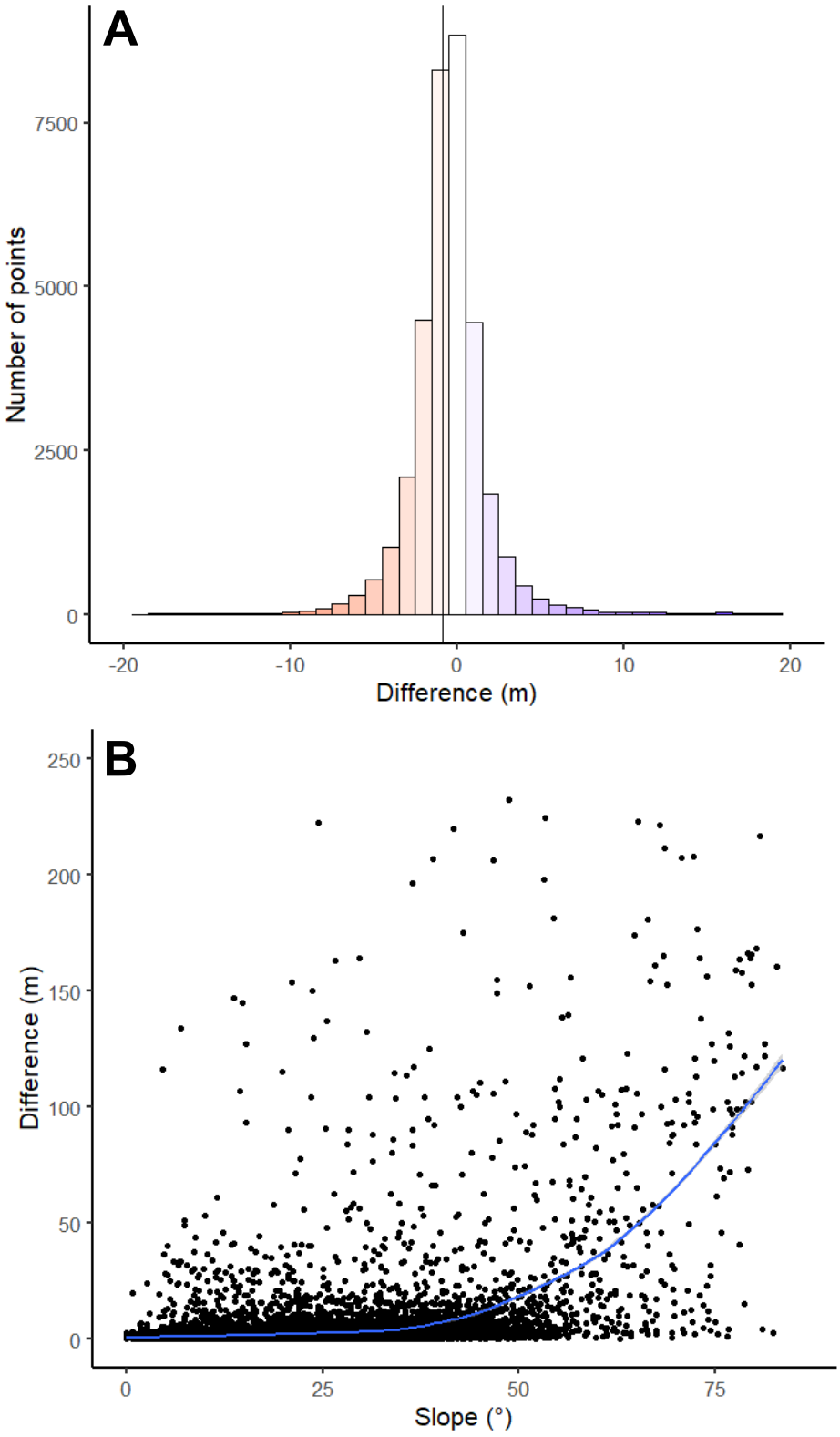

Figure 4.10 – (A) Difference between ICESat-2 and a TanDEM-X DEM from off-ice areas of the Cordillera Vilcanota. (B) Difference between ICESat-2 and TanDEM-X against TanDEM-X-derived slope. Blue line represents a generalized additive model to smooth data.

4.3.3. Applications of ICESat-2 to monitoring glaciers

Given the quality of ICESat-2 in complex off-ice terrain, the next step was to demonstrate a number of potential applications for embedding ICESat-2 into a programme for regular monitoring of mountain glaciers. This included monitoring lakes, glacier mass balance, and seasonal snowfall. The potential of ICESat-2 to provide data for ASTER DEM validation (Chapter 3) is also discussed.

Glacier elevation change

The shifting repeat tracks of ICESat-2 over land (excluding ice sheets) means that monitoring of glacier thinning, and thus mass balance, is only possible every two years when track positions repeat. This is particularly unreliable when considering that cloudy conditions can prevent data acquisitions at all. However, in the fortunate circumstance that two cloud-free acquisitions do occur in succession, glacier surface elevation change can be derived (Figure 4.11). Over a glacier situated to the North of the Cordillera Vilcanota, we use the ATL06 product to observe a mean glacier surface elevation change of -1.49 m yr^{-1} from July 2019 to December 2021, which increases to an average of -2.76 m yr^{-1} over the lowest 1 km of the glacier. These values corroborate closely (around -0.5 m yr^{-1} lower) to the 2000 – 2020 surface elevation change derived by ASTER DEMs in Chapter 3, though acknowledging that these data are gathered at a later time window to ASTER. It is also noteworthy that this glacier was chosen as it was the only suitable site within the Cordillera with data to perform this experiment.

This demonstrates, for the first time over mountain glaciers, the possibility for using ICESat-2 to quantify glacier elevation change, and subsequently glacier mass balance, where data allow. However, the full potential of ICESat-2 in supporting mass balance measurements is likely to be when used in conjunction with a reference DEM, akin to Kääb et al. (2012) used for ICESat. This approach has been adopted over the Himalaya with ICESat and GRACE gravimetry datasets to quantify mass balance change across the region (Wang et al., 2021), and with ASTER DEMs over the Tibetan Plateau (Zhao et al., 2022). Areas where measurements have been made using both ICESat and ICESat-2 also allows for accurate quantification of surface elevation change (Sochor et al., 2021), though the large cross-track separation of ICESat means these areas will be sparse over mountain glaciers. As the ICESat-2 archive grows with time, its usefulness as a tool for quantifying mass balance grows too.

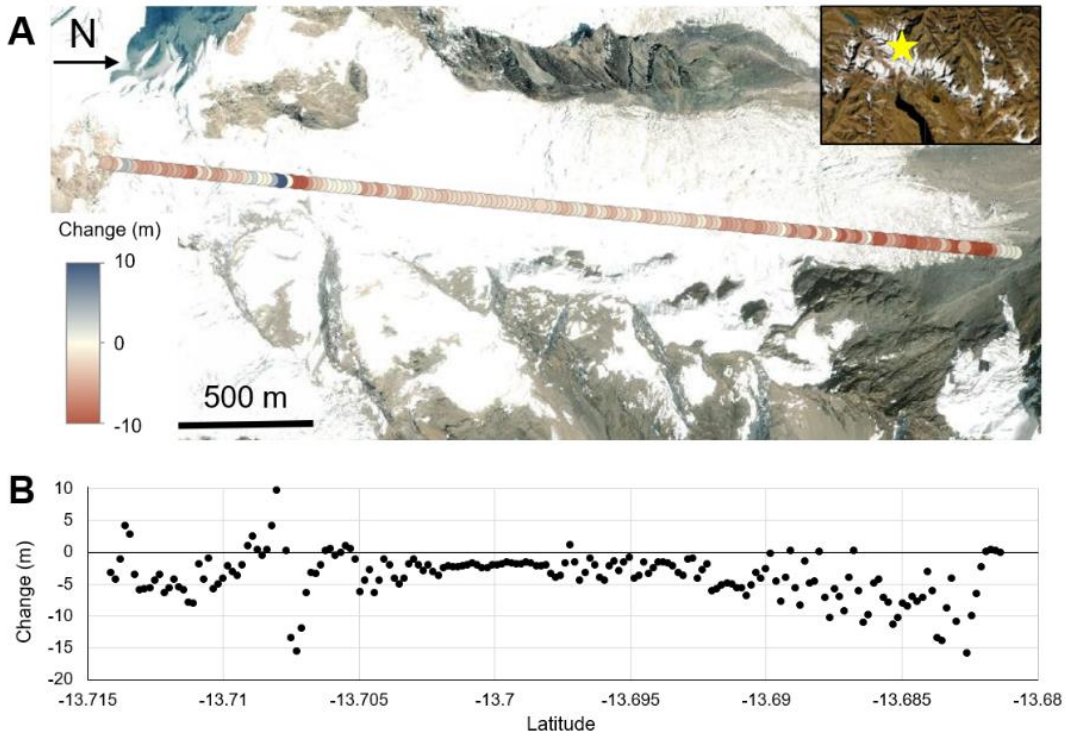

Figure 4.11 – Surface elevation change of a glacier in the Cordillera Vilcanota, as derived by ICESat-2 (A mapped, B graphed). Change is between July 2019 and December 2021, using the ATL06 product over track 133.

Seasonal monitoring of snowfall

In some circumstances, different beams of ICESat-2 crossover between the eight track positions to provide more frequent elevation data. Over the same glacier to the North of the Cordillera Vilcanota, elevation retrievals between July and December 2021 demonstrate seasonal variations in a glacier's surface. We observe a large (>15 m) deposit of snowfall on a south-facing slope of an adjacent glacier, separated by a mountain peak (Figure 4.12). This is difficult to validate as stereo images are inaccurate over bright targets such as fresh snow and field-based measurements are extremely limited. Using the only field-based measurements of accumulation in the Cordillera Vilcanota of 1.2 – 1.4 metres water equivalent in 2013/14 at Suyuparina glacier (Molina et al., 2015), and a density of 100 kg/m^3 for fresh snow (Judson and Doesken, 2000), snowfall of 12 – 14 m is seemingly not unexpected in this region. We hypothesise that ICESat-2 is recording a large deposit of snowfall, and could therefore be used to monitor seasonal changes to glaciers. There is precedence for this in earlier missions as the original ICESat mission was able to quantify snowfall in the interior of Antarctica of 10 – 13 cm in depth

(Bindschadler et al., 2005). To our knowledge, this is the first such quantification of an accumulation event over a mountain glacier using satellite altimetry. The significance of this result in quantifying glacier accumulation is large given the very high degree of uncertainty of elevation change derived by stereo images (Chapter 3).

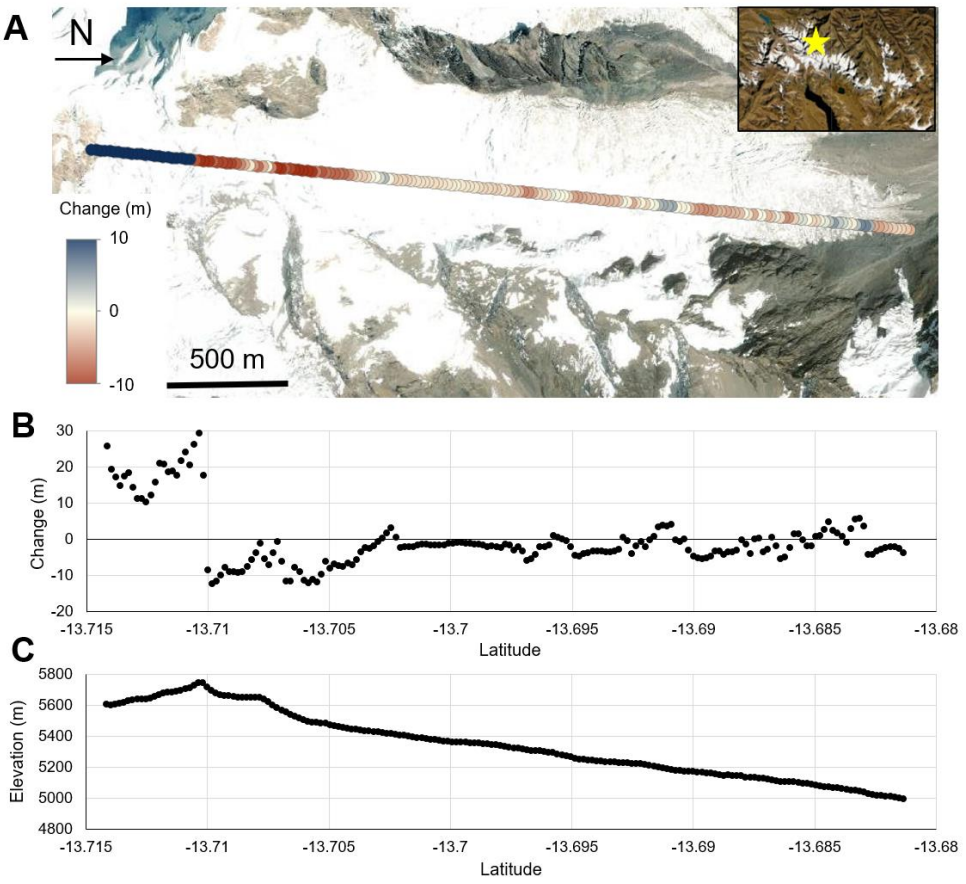

Figure 4.12 – Surface elevation change of a glacier in the Cordillera Vilcanota, as derived by ICESat-2 (A mapped, B graphed). Change is between July 2021 and December 2021, using the ATL06 product over track 133. (C) Elevation of the track from July 2021 to demonstrate the separation of watersheds about the topographic high of ~13.71° latitude.

Validation of optical stereo DEMs

Processing chains for producing DEMs from optical stereo images, such as ASTER, typically require the alignment of the output data to a reference DEM containing stable terrain (Brun et al., 2017; Dussaillant et al., 2019). This can be achieved with as little as 10% of the 20 km x 20 km ASTER tile classified as stable

terrain (Nuth and Kääb, 2011), but does still require its presence. The high accuracy of ICESat-2 opens the opportunity for providing tie points for optical stereo DEMs across unstable terrain when the two datasets are acquired close in time, thereby improving the confidence of this technique. The original ICESat mission was regularly used to provide highly accurate validation for the co-registration of DEMs (Nuth and Kääb, 2011; Korsgaard et al., 2016), but the wide cross-track distance (15 km) limited the spatial coverage of tie points. A more dense mesh of elevation retrievals from ICESat-2 (3.6 km separation) owing to shifting track positions creates thousands of tie points per 20 km x 20 km ASTER tile for co-registering DEMs. For mountain glaciers, this may greatly improve the confidence of optical stereo images and so retrieve regular, accurate, mass balance estimates for every glacier in a mountain range. For large ice caps and ice sheets, ICESat-2 could be used to generate DEMs further into the interior where no stable terrain is present in a scene. A recent global glacier mass balance product using the full ASTER archive (Hugonnet et al., 2021) was limited to quantifying change over the periphery of Greenland due to a lack of stable terrain further inland. ICESat-2 could assist in the derivation of optical stereo DEMs further into the interior of Greenland.

Lake surface elevation change

ICESat-2 acquires high confidence returns of the surface elevation of water bodies (Zhang et al., 2019b). The ATL06 product filters photon returns to only return the surface of water, despite some photons being able to penetrate into the water in ATL03 (Smith et al., 2019). Given the high spatial resolution of ATL06, we observe many small (>40 m width) lakes across the Cordillera Vilcanota with surface elevation data. However, the shifting track patterns of ICESat-2 and cloudiness of this region frequently prevent repeat measurements being made in these small lakes. We analysed the largest lake of the Cordillera Vilcanota, Laguna Sibinacocha, a glacial-fed lake (~28 km^2) which is dammed for hydroelectric power. We extracted all data acquired over Laguna Sibinacocha in the ICESat-2 record and averaged the surface elevation from shore to shore of each pass using only strong beams. ICESat-2 is able to track sub-metre changes in surface water elevation throughout the year (Figure 4.13), as reservoir volume changes due to meltwater variability and control of flow from the dam. While Sentinel-3 acquires no data over Laguna Sibinacocha, so any altimetry measurement is welcomed, the temporal variability of data acquisitions are still a major limitation of ICESat-2. Of the 22 passes of Laguna Sibinacocha performed

from January 2019 to January 2022, the cloudiness of the region means that surface elevation data are only retrieved on seven occasions. The longest data gap in this series is 300 days, suggesting that ICESat-2 would be an unreliable mission for monitoring seasonal changes in surface water elevation.

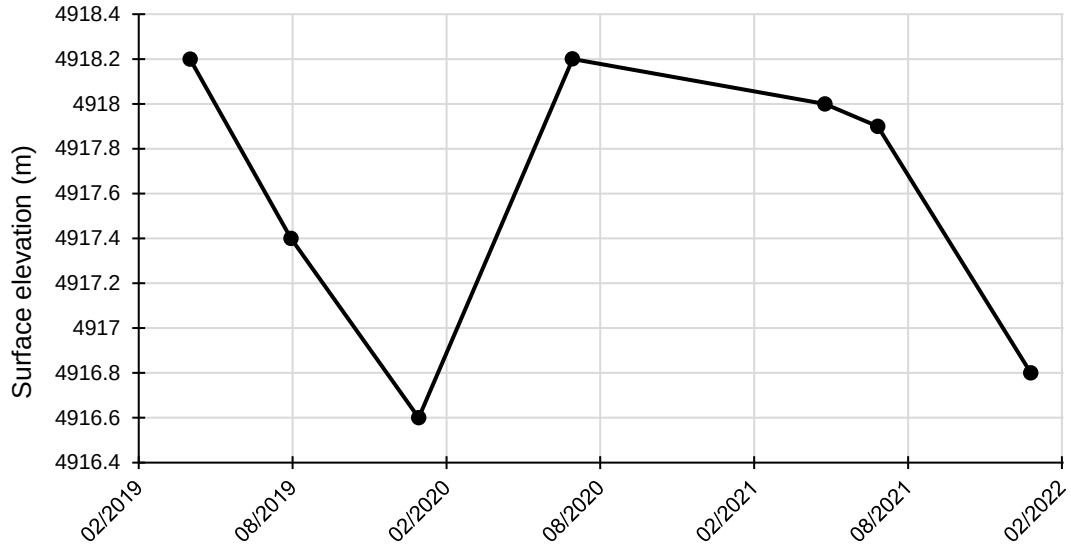

Figure 4.13 – Surface elevation of Laguna Sibinacocha, Cordillera Vilcanota, as measured by ICESat-2. Data are acquired from tracks 125, 133, and 567.

Glacial lake bathymetry

Establishing glacial lake volume is a key parameter in any quantitative glacial hazard assessment. Monitoring the surface elevation indicates how these lakes are changing over time, but not the volume of water that could be released during a GLOF event. A serendipitous result from the ICESat-2 mission has been the ability to accurately derive bathymetry in shallow waters using the ATL03 product (Parrish et al., 2019), which could aid in quantifying the volume of glacial lakes. In clear waters of coral reefs, ICESat-2 photon returns are accurate to depths of ~40 m, though additional processing is needed to account for refraction (Ma et al., 2020; Babbel et al., 2021). Supraglacial lake bathymetry can also be analysed with ICESat-2, to depths of ~10 m, where water is very clear (Datta and Wouters, 2021). Proglacial lake bathymetry is more challenging to derive as these bodies are typically opaque due to sediment influx. However, ICESat-2 data do appear to show some potential for providing limited bathymetric information, albeit at low confidence – such as at Lake

Amayuni, a proglacial lake in the Cordillera Vilcanota, reaching depths of ~9 m (Figure 4.14). With no robust validation depth data available for Lake Amayuni, it is unclear as to whether this is the bed of the lake or simply the maximum depth from which photons are returned. Further analysis over a greater number of lakes is needed, however it is worth noting that Amayuni is the only lake in the Cordillera Vilcanota where bathymetry measurements were apparent; all others which had data from the surface had no bathymetric measurements, likely due to sediment clouding the photon returns. If repeatable, the implications of this could be significant – understanding the volume of lake water in proglacial lakes is paramount to understanding the risk they pose from outburst floods, or the opportunities they pose as a store of drinking water for local residents.

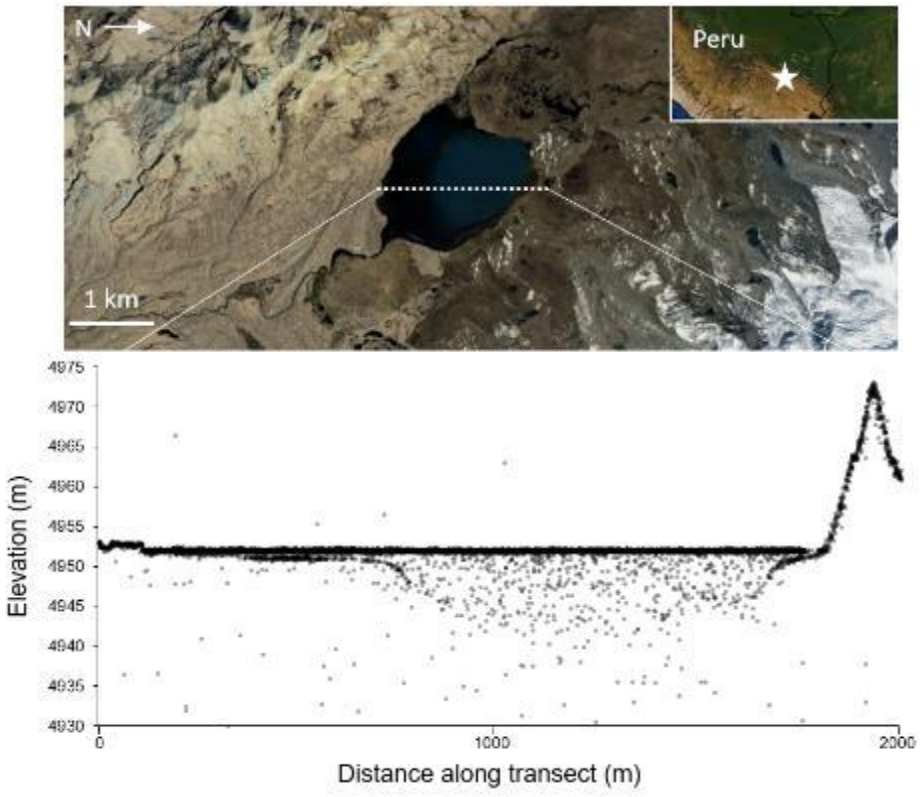

Figure 4.14 – ICESat-2 Track 567 ATL03 product from 4 August 2019 across Laguna Amayuni (−13.81°N, −70.99°E) in the Cordillera Vilcanota. Sediment intrusion in the glacial lake clouds limits the penetration of photons to the bed, which limits its applicability in deriving lake volume to a high confidence in this environment. Top image from Google Earth and CNES/Airbus, 2020.

4.6. Recommendations for future satellite altimetry missions

The future status of satellite altimetry in monitoring the global cryosphere is currently uncertain. With CryoSat-2 towards the end of its operational life (having elapsed 12 years to date), ICESat-2 having already exceeded its expected 3-year mission duration, and Sentinel-3 unable to retrieve data over mountain glaciers or at high latitudes, there may soon be a break in the record of altimetry measurements over ice sheets (International Altimetry Team, 2021). Upcoming radar altimetry missions, if accelerated in their launch, could ensure no data gap occurs. However, given the limitations of radar-based satellite altimetry over mountain glaciers as seen in this chapter, and as observed by the European Union in scoping future satellite missions (Duchossois et al., 2018), this section will evaluate changes to upcoming missions and recommend possible changes that could be made prior to launch in order to acquire elevation over small glaciers in complex terrain.

To ensure continuity of the Sentinel-3 mission, successor missions (Sentinel-3C and 3D) are launching in 2024 and 2028 to directly replace Sentinel-3A and 3B respectively. There will be no differences in instrumentation between 3A/3B and 3C/3D, but small changes could allow for more data acquisition over mountain glaciers. At present, the number of hydrological targets able to be uploaded to Sentinel-3 is ~140,000. The 2021 version 6.1 update to Sentinel-3A (and equivalent version 3.1 update to Sentinel-3B) means that this number has now been reached (Le Gac et al., 2019). An anticipated expansion to the memory allowance for the OLTC (Taburet et al., 2020) will allow more targets to be defined and so more mountain glaciers to be monitored, though still requiring users to upload *a priori* information first. This OLTC upgrade is currently onboard the recently launched Sentinel-6 Michael Freilich mission, which uses an upgraded POSEIDON-4 altimeter based on SRAL. A larger memory and ability to change range window at a resolution of ~1 km along-track (Donlon et al., 2021) means, in theory, that more hydrological targets can be defined, and a greater number of mountain glaciers can be monitored. To further improve the number of glaciers covered by Sentinel-3, changes to its orbit could be made to decrease cross-track separation at the expense of increasing repeat interval. However, should the launches of Sentinel-3C and 3D occur while Sentinel-3A and 3B are still operational, ESA note that they will adopt the same orbit as 3A/B in order to synergise cross-mission instruments (Nordbeck et al., 2021).

In an extension to the Copernicus mission, ESA have designed candidate status to a satellite altimeter with the primary mission objectives of monitoring the

cryosphere. CRISTAL (Copernicus Polar Ice and Snow Topography Altimeter) is currently under development at Airbus with a target launch of 2027. Should CRISTAL launch before CryoSat-2 ends, this will ensure uninterrupted altimetry measurements of ice sheets (International Altimetry Team, 2021). However for mountain glaciers, key changes to the radar altimeter compared to SRAL provide optimism that it will be usable. CRISTAL will have a Ku-band interferometer, akin to CryoSat-2, to improve ground spatial resolution. CRISTAL will operate with a 256 m wide range window with uncompressed open-loop tracking and data acquisition at 100 m along-track resolution (Kern et al., 2020). The wide range window and optimised open-loop tracking could, when provided ground elevation data, derive elevation over complex terrain and be used in monitoring mountain glaciers. In theory, CRISTAL will be twice as accurate and acquire four times the volume of data compared to CryoSat-2 (Kern et al., 2020).

4.5. Conclusions

Innovation in satellite altimeter technology and processing provides, for many mountainous regions, the first usable altimetry data. In this study, we evaluated the performance of Sentinel-3 and ICESat-2 in deriving elevation over mountain glaciers and identified potential avenues for integrating their outputs into regular glacier monitoring schemes. Sentinel-3 poses novelty in its high along-track spatial resolution, combined with an open-loop tracking mode using a pseudo-DEM to position its narrow range window. Without prior elevation information, Sentinel-3 does not capture data over mountainous regions at all. With elevation data uploaded to the OLTC, Sentinel-3 acquires some data but its potential is limited to retrieving accurate data over a single point in a 5 km track where the OLTC is set. Its successor missions, in Sentinel-3C/3D and Sentinel-6, will use an OLTC with the ability to shift the tracking window more regularly (every ~1 km along-track), which should mean more mountain glaciers can be monitored. However, the most severe limitation of Sentinel-3 is its large cross-track separation of 52 km (104 km for each of Sentinel-3A/B respectively). Few mountain glaciers are intercepted by Sentinel-3 and so this mission is not one that could be used in monitoring schemes.

The novelty of ICESat-2 arises from its very high along-track spatial resolution (70 cm), close cross-track separation (3.6 km), and six laser beams to acquire vastly more information than its predecessor, ICESat. These specifications, combined with regularly shifting ground tracks over land, mean that ICESat-2 retrieves data over

vastly more mountain glaciers than Sentinel-3. Additionally, a 6 km wide range window means that ICESat-2 acquires highly accurate data across complex terrain (mean difference to TanDEM-X DEM of -0.85 m). For mountain glaciers, ICESat-2 can derive regular changes to surface lake elevation and, in some circumstances, bathymetry. Where tracks are fortunate to overlap in succession across a glacier, changes to surface elevation can be derived on a seasonal and interannual basis. Here, we quantified (for the first time over a mountain glacier using satellite altimetry), a large snowfall event of ~15 m in the Cordillera Vilcanota. We also provided the first demonstration of quantifying surface elevation change using only ICESat-2 data over a mountain glacier. However, many of these case studies showcase the satellite data in idealised conditions. The cloudiness of mountain glacier regions creates large data gaps, even over large targets (we observed a 300-day data gap over a 28 km^2 target, Laguna Sibinacocha, which is crossed by three ICESat-2 tracks). Furthermore, while the cross-track spacing is the lowest of any satellite altimeter, ICESat-2 still misses many key glaciers and lakes of the Cordillera Vilcanota, including Chumpe glacier, the primary water source of Laguna Sibinacocha. ICESat-2 represents a leap forward in satellite laser altimetry and will no doubt be widely used across the mountain cryosphere, but to be embedded in a comprehensive glacier monitoring programme, will likely be used in tandem with other satellite-derived data sources such as optical stereo DEMs.

Chapter 5

Evaluation of low-cost Raspberry Pi sensors for photogrammetry of glacier calving fronts

5.1. Introduction

Monitoring glacier calving fronts is becoming increasingly important as climate warming changes the stability of the cryosphere. Globally, glacier frontal positions have receded rapidly in recent decades (Marzeion et al., 2014; Zemp et al., 2015), leading to an increased threat of glacial lake outburst floods (GLOFs) from newly formed proglacial lakes at the glacier terminus (Tweed and Carrivick, 2015). Large ice calving events can trigger violent waves and GLOF events (Lüthi and Vieli, 2016), though both the magnitude and frequency of this phenomenon are poorly quantified owing to a lack of appropriate monitoring (Emmer et al., 2015; Veh et al., 2019). Satellites are able to provide near-continuous observations of lake growth (Jawak et al., 2015), hazard development (Quincey et al., 2005; Rounce et al., 2017) and, over large glaciers, calving rate through iceberg detection (Sulak et al., 2017; Shiggins et al., 2021). However, to measure frontal dynamics at a high spatial and temporal resolution, which is particularly necessary over smaller mountain glaciers, monitoring requirements can only be met by *in situ* sensors.

Accurate 3D models of glaciers and their calving fronts are necessary to fully evaluate the hazards they pose (Kääb, 2000; Fugazza et al., 2018) and to better understand frontal dynamics (Ryan et al., 2015). Where *in situ* camera sensors have been used to monitor glacier fronts as part of an early warning system, stationary cameras have previously been used to relay regular images to be analysed externally (Fallourd et al., 2010; Rosenau et al., 2013; Giordan et al., 2016; How et al., 2020). This can be useful for monitoring glacier velocity, snowfall, and calving dynamics, but remains a 2D snapshot of glacier behaviour and offers little in terms of being able to detect the magnitude of an individual event or process. 3D models, on the other hand, permit more detailed analysis, such that the physics involved in glacier calving can even be captured (James et al., 2014; Mallalieu et al., 2020). Unoccupied aerial vehicles (UAVs) have been used regularly to capture high-resolution 3D models of glacier fronts (Ryan et al., 2014; Bhardwaj et al., 2016; Chudley et al., 2019) but, as yet, these systems are not autonomous and are therefore dependent on an operator being present, as well as often being highly expensive (many thousands of dollars).

Arrays of fixed cameras can be positioned around a glacier front to capture images repeatedly over long time periods. The resulting imagery can then be used to photogrammetrically generate 3D models at a high temporal resolution and analyse change over days, months, or years. Off-the-shelf timelapse cameras provide some of the cheapest ways of reliably collecting imagery for repeat photogrammetry and have been deployed at Russell Glacier, Greenland, to monitor seasonal calving dynamics (Mallalieu et al., 2017). Elsewhere in glaciology, timelapse arrays using more expensive DSLR-grade cameras have been used for repeat photogrammetry to quantify ice cliff melt on Langtang glacier at high spatial resolution (Kneib et al., 2022). In other geosciences disciplines, timelapse arrays for photogrammetry have been used to monitor the soil surface during storms (Eltner et al., 2017), the stability of rock slopes (Kromer et al., 2019), and evolution of thaw slumps (Armstrong et al., 2018), for example. The key limitation of these studies, and this setup design, is that a site revisit is necessary to collect data and analysis is therefore far from real-time. Autonomous photogrammetry, whereby 3D models are created with no user input, is still in its infancy but shows great promise, with machine learning used to optimise camera positions (Eastwood et al., 2020), point cloud stacking to enhance timelapse photogrammetry (Blanch et al., 2020), and user-friendly toolsets for monoscopic photogrammetry in glaciology (How et al., 2020). Real-time data transmission is the next step in autonomous timelapse photogrammetry, but trail cameras with cellular connectivity are many hundreds of dollars per unit, rendering this setup unaffordable for most monitoring schemes.

We have designed a system, based on Raspberry Pi computers, to capture science-grade images for structure-from-motion (SfM) photogrammetry in glacial landscapes for ~$120 per unit – less than half the cost of an equivalent off-the-shelf trail camera with connectivity. Raspberry Pi computers are small, low-cost, and were designed with the intention of teaching and learning programming in schools. Their ease of use and affordability means they have also been used extensively as field sensors in the geosciences (Ferdoush and Li, 2014) as the quality of their camera sensors have developed to a science-grade level (Pagnutti et al., 2017). In hazard management, Raspberry Pi cameras have been used as standalone monitoring systems to complement wider internet-of-things (IoT) networks (Aggarwal et al., 2018) and attached to UAVs to produce orthophotographs (Piras et al., 2017). In glacierised environments, the durability, low-cost, and low power requirements of Raspberry Pis means they have been used to complement sensor networks, such as controlling the capture of DSLR-grade time lapse cameras (Carvallo et al., 2017;

Giordan et al., 2020) or as a ground station for UAV-based research (Chakraborty et al., 2019). However, to our knowledge, Raspberry Pis and low-cost camera modules have never been the focus of a glaciology investigation and their potential for SfM in the wider geosciences has yet to be fully realised.

The aim of this study was, therefore, to evaluate the quality of Raspberry Pi imagery for photogrammetric processing, with a view to incorporating low-cost sensors in glacier monitoring systems. Given that the highest accuracy glacier front 3D models gathered from photogrammetry are derived from UAV imagery (typical horizontal uncertainty of 0.12 m (0.14 m vertical), even in the absence of ground control points (Chudley et al., 2019)), we chose to use a UAV-based point cloud as our primary reference dataset. We intensively deployed both sensor systems (ground-based Pis, and aerial UAV) at Fjallsjökull, Iceland over a four-day period. As a secondary objective, we also sought to understand the limitations of Raspberry Pi by deploying Raspberry Pi sensors at a range of distances to the glacier front and removing images in the processing of point clouds to identify the fewest frames necessary for generating accurate 3D models.

5.2. Methods

5.2.1. Study site – Fjallsjökull, Iceland

Fjallsjökull is an outlet glacier of Öræfajökull, an ice-covered volcano to the south of the wider Vatnajökull ice cap, in south-east Iceland (Figure 5.1). Recession and thinning of Fjallsjökull has been underway since the end of the Little Ice Age, but has substantially accelerated in recent decades owing to climate warming (Howarth and Price, 1969; Chandler et al., 2020). Fjallsjökull terminates in a large (~4 km^2) proglacial lake – Fjallsárlón – which is also increasing in size as Fjallsjökull recedes (Schomacker, 2010). Calving of Fjallsjökull is regular and has increased in frequency in recent decades as the glacier has accelerated, driven by the expansion of Fjallsárlón (Dell et al., 2019). As of September 2021, the calving face of Fjallsjökull was approximately 3 km wide, with ~2.4 km of this accessible from a boat (the northernmost 600 m had large, stationary icebergs which were dangerous to navigate; see Figure 5.1). We selected Fjallsjökull as a study site due to its accessibility, ability to conduct surveys from boat and shoreline, and variation in calving margin heights (ranging from ~1 m to ~15 m) to test the performance of our camera system under a diverse range of glaciological settings. This location was also chosen owing to rapidly changing international travel restrictions in place due to the

COVID-19 pandemic, which meant that we could not conduct this analysis in Peru as planned. However, we also present results from a longevity study conducted at the Quelccaya Ice Cap in Peru (-13.917°N, -70.840°E) from September to November 2019, where we positioned a Raspberry Pi camera acquiring data at a proglacial lake for three months.

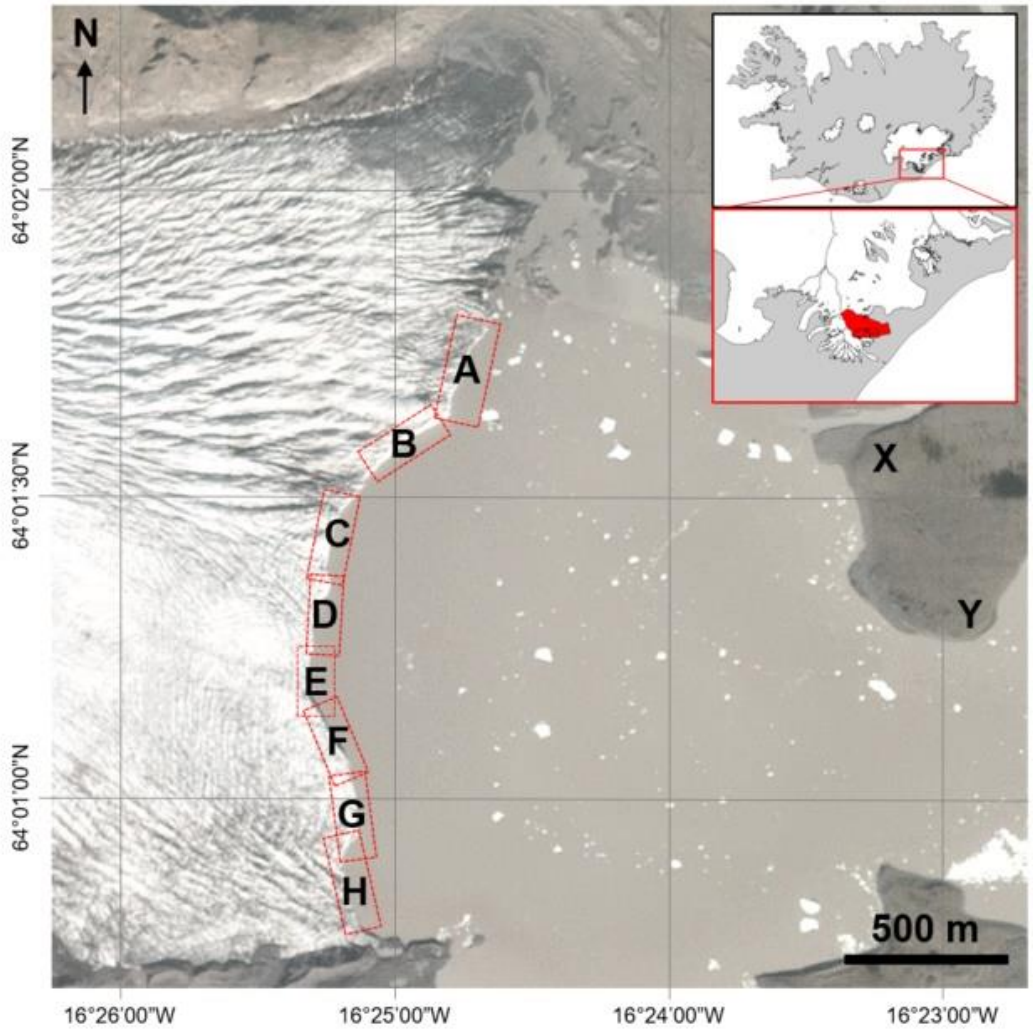

Figure 5.1 – Fjallsjökull (flowing left-to-right), terminating in Fjallsárlón, captured by Planet Imagery on 10th September 2021. A-H denote the eight point cloud sub-sections generated by both the Raspberry Pi and UAV. X-Y denote the start and end of land-based data collection at approximately 25 m intervals along the shoreline, used to generate sub-section B from a distance.

5.2.2. Hardware

Raspberry Pi computers have a variety of commercially available sensors for use in the geosciences (Figure 5.2). SfM photogrammetry has been performed using Raspberry Pi cameras, but only over small spatial scales (<1 m) not relevant to glaciology. For example, medical scientists have used the 'Raspberry Pi Camera Module v2' (8 MP; ~$25) to create 3D body and hand scans (Garsthagen, 2014; Eguiraun et al., 2020). Until May 2020, upon the release of the HD camera module, this 8 MP camera was the only easily compatible, commercial camera sensor for the Raspberry Pi. The Sony IMX219 sensor of the V2 camera offers 'science-grade' radiometric calibration (Pagnutti et al., 2017), and has been deployed in geoscience applications ranging from monitoring coastal environments for flooding (Addona et al., 2022) to rockfall prone cliffs (Blanch et al., 2020). However, its potential as an image source for SfM has not yet been examined in a glacierised environment, nor over the large (~100s metres squared) scale of a calving front.

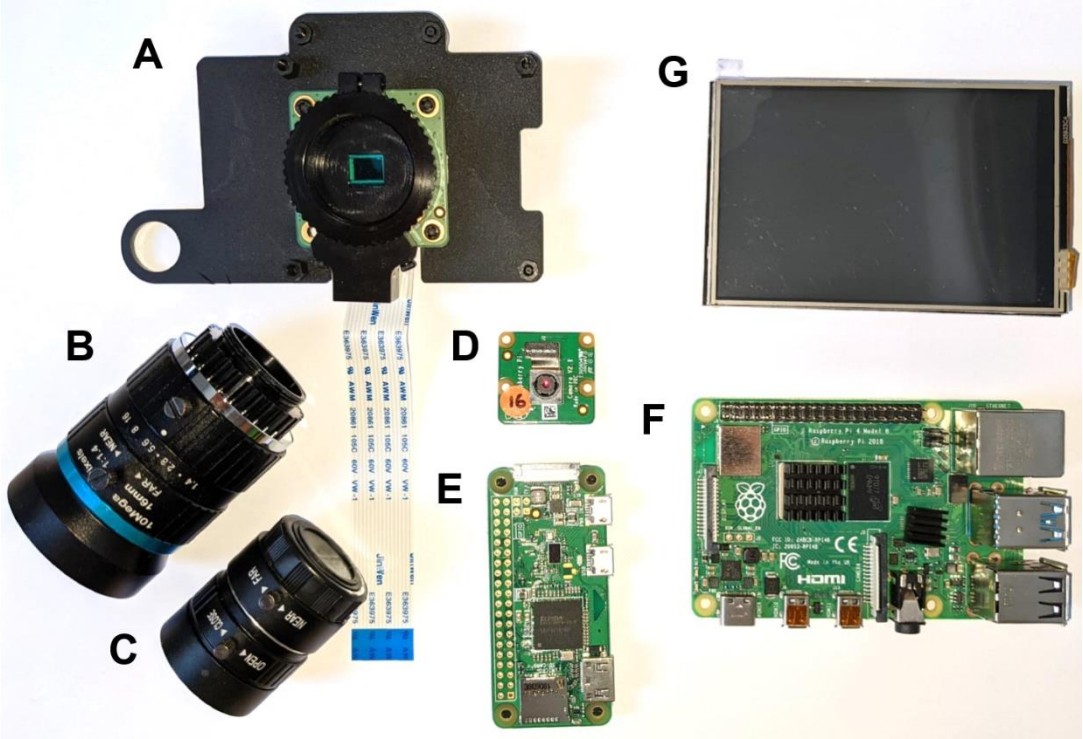

Figure 5.2 – Hardware used in this study. (A) Raspberry Pi HD Camera module. (B) 16 mm telephoto lens. (C) 6 mm wide angle lens. (D) Raspberry Pi Camera Module v2. (E) Raspberry Pi Zero W computer. (F) Raspberry Pi 4 Model B computer. (G) LCD screen, which affixes to Raspberry Pi to view pictures in the field.

We tested the ability of the camera module v2 to generate 3D photogrammetric models during a survey at Quelccaya ice cap, Peru (-13.917°N, -70.840°E) in September 2019. Here, we acquired images from 25 different positions around a small (0.4 km^2) proglacial lake to capture a ~10 m high, ~150 m long calving margin. We found that the image quality was too poor to generate usable 3D models over the ~70 m from the proglacial lake shoreline to the calving margin of the ice cap (Figure 5.3). Point clouds contained large data gaps, required more images than anticipated (34 to generate a ~60 m point cloud), and the cameras were unable to resolve small (centimetre-scale) features. As a result, the camera module v2 was dismissed as a potential sensor moving forward.

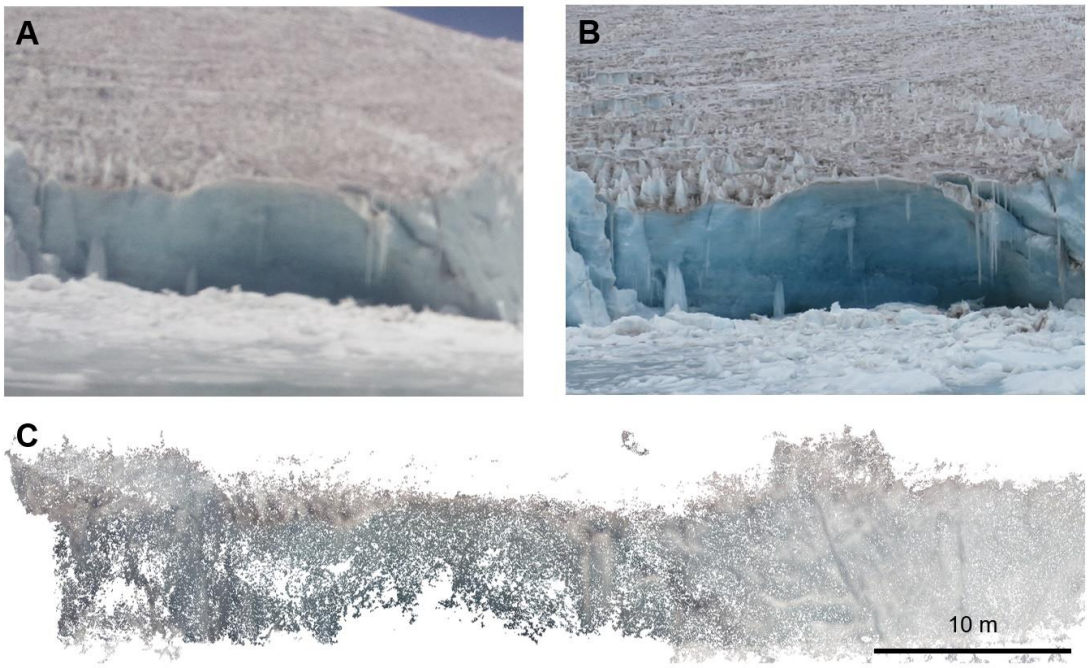

Figure 5.3 – Evaluating the usability of the Raspberry Pi Camera Module v2 in photogrammetry of glaciers. (A) Image acquired from the shoreline of a proglacial lake from a distance of ~70 m with the Raspberry Pi Camera Module v2. (B) Image from the same position as captured by a DSLR camera. (C) Point cloud of glacier calving front generated using 34 images from the Raspberry Pi Camera Module v2.

In May 2020, Raspberry Pi released their high quality camera module ($50 for the sensor board, $25-50 for additional lens; Figure 5.2). This 12.3 MP sensor, with adjustable lenses to create a bespoke approach for each setting, offered promise that low-cost SfM was possible to the standard as set by UAVs and timelapse trail

cameras. Two lenses are produced by Raspberry Pi to work alongside this HD sensor – a 6 mm wide angle lens, and a 16 mm telephoto lens. The 6 mm wide angle lens acquires images with distortion at the sides (Figure 5.4B) in order to capture a greater field of view (63°), which requires correcting before being used in photogrammetry (Hastedt et al., 2016). We therefore opted for the 16 mm telephoto lens in this study to reduce the post-processing required. This was attached to a Raspberry Pi Model 4B and LCD display to visualise images, and adjust focus, as they were captured. Images from the Raspberry Pi were subsequently compared to images taken from a DJI Mavic 2 Pro UAV. Technical comparisons of the setups are given in Table 5.1.

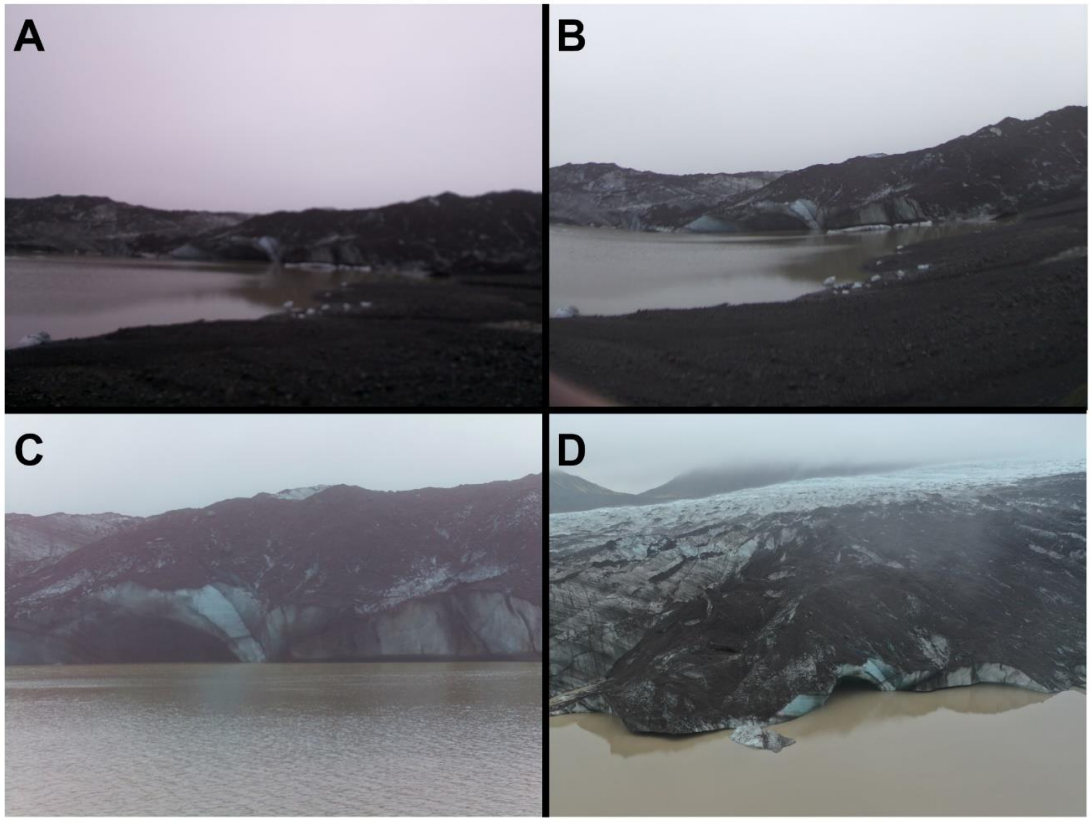

Figure 5.4 – Comparison of sensors at an ice cave feature at Kvíarjökull (~8 km south of Fjallsjökull), acquired over a 2-day period as captured by (A) Camera Module v2 (B) High quality sensor with 6 mm wide angle lens (C) High quality sensor with 16 mm telephoto lens (D) UAV.

The Pi was mounted in a fixed position on a boat which traversed the southernmost ~2.4 km of the ~3 km Fjallsjökull calving face, around 500 m from the glacier, while the UAV flew above this boat (Figure 5.5). The Raspberry Pi was triggered manually approximately once every ten seconds throughout the transect

capturing 315 images in total. While we operated the system manually herein, it is important to note, however, that the system is also designed to trigger autonomously for timelapse purposes. At the same time, the UAV conducted two flights, capturing 729 images, ensuring no calving occurred between collecting data from the two sensors. The UAV flew closer (~250 m) to the glacier terminus than the boat transect to ensure the highest possible accuracy in data collection. In the majority of images, the UAV camera was facing the flat calving face of the glacier. While the UAV has onboard software to autofocus images, we manually checked and altered the focus of the Raspberry Pi camera between images during the boat transect to ensure pictures were not blurry as the boat varied in distance from the glacier.

	Raspberry Pi (HD Camera)	DJI Mavic 2 Pro UAV	Typical time lapse camera package (Canon Rebel T5)
Camera Sensor	Sony IMX477	1” CMOS	CMOS (APS-C)
Image size (px)	4056 x 3040	5472 x 3648	5184 x 3456
Resolution (megapixels)	12.3	20	18
Horizontal field of view	44.6°	77°	63°
Images captured	315	729	N/A
Cost	$120*	$1,500	$2,600

*Table 5.1 – Comparison of technical specifications between Raspberry Pi and UAV sensors. A typical time lapse camera package is provided as a comparison and follows the setup from Kienholz et al. (2019). The Raspberry Pi High Quality camera module is fitted with a 16 mm telephoto lens. *In this study, we used a more expensive Raspberry Pi computer (4B) in order to fit a screen for in-field monitoring of images; however the $120 cost applies to a cheaper model (Zero W).*

In order to test the limits of the Raspberry Pi, we performed additional analysis on sub-section B (Figure 5.1). We collected images of the calving face from a portion of the shoreline of Fjallsárlón, shown as X to Y in Figure 5.1, which ranged from 1.2 to 1.5 km from the calving face. Owing to bad weather, we only collected shoreline data for a limited section (covering sub-section B entirely) before the glacier was obscured from view by fog. This experiment allowed us to assess how the Pi performed at long-range.

We also conducted an additional experiment on sub-section B to determine the performance of the camera under sub-optimal conditions, by removing 21 of the 31 images captured by the boat transect and deriving point clouds from the remaining ten camera positions. This reflects the reality of the trade-off between data quality and practical considerations. In theory, fewer images should result in a lower point density (Micheletti et al., 2015), but the monitoring network would be cheaper as fewer cameras are required.

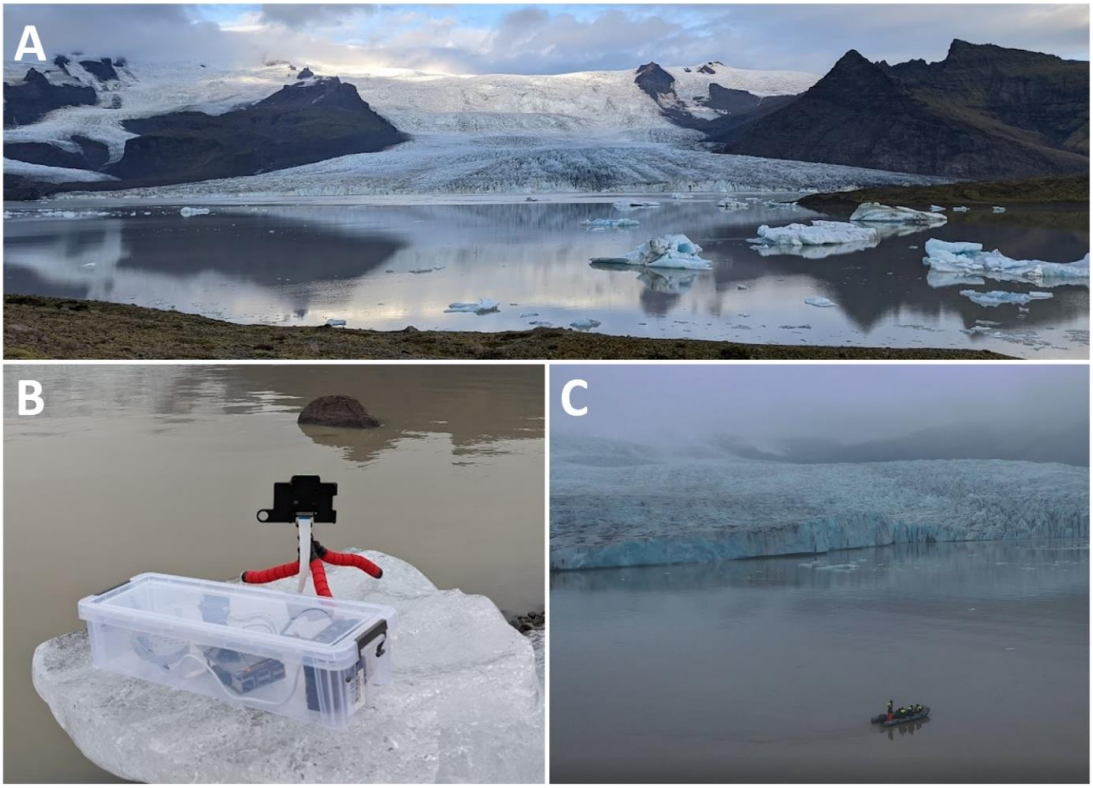

Figure 5.5 – An overview of our data acquisition. (A) Fjallsjökull, leading into Fjallsárlón, as of 17th September 2021. (B) Raspberry Pi on the shoreline survey. The camera was stabilised with a small tripod, with hardware and batteries connected in a weatherproofed receptacle. (C) Boat survey, approximately 500 m from the glacier front, as captured by the UAV.

5.2.3. Photogrammetry and M3C2

For images from both the Raspberry Pi and UAV, far cliffs (rock faces flanking Fjallsjökull; Figure 5.5A) were masked out prior to generating tie points in Agisoft Metashape. Images from the UAV were georeferenced using its onboard GNSS real-

time kinematic positioning (RTK) system. Images from the Raspberry Pi were georeferenced by aligning them to images captured by the UAV and producing a sparse point cloud, before removing UAV images to produce the final dense point clouds. Point clouds from both sensors were therefore referenced to this RTK system only, rather than having a global reference (akin to Luetzenburg et al., 2021). While the Raspberry Pi images could be successfully aligned without UAV images, our workflow was designed to unify the coordinate systems of the point clouds and thereby avoid confounding co-registration errors in the cloud comparison. Eight high quality points clouds were produced from each of the Raspberry Pi and UAV at various stages along the calving face (locations in Figure 5.1) with a mild filter using Agisoft Metashape. Sub-sections were computed at natural break points in the glacier front geometry, at approximately 250 – 350 m intervals, owing to limitations in computer processing. We then cropped point clouds to the calving face, cleaned with a noise filter, and finely aligned the Raspberry Pi clouds to the UAV clouds assuming a 95% overlap in CloudCompare.

Differences between points clouds from the Pi and UAV were compared using the Multiscale Model to Model Cloud Comparison (M3C2) tool in CloudCompare (Lague et al., 2013). M3C2 calculates a series of core points from the Pi cloud and quantifies the distance to the UAV cloud about those points using projection cylinders. This requires users to define key parameters, including the width of normal (D), projection radius (d), and maximum depth of the cylinder (h) (all parameters in metres). We followed approaches developed by Lague et al. (2013), and applied to glacierised environments by Westoby et al. (2016) and Watson et al. (2017), of calculating the normal width to take into consideration surface roughness and the scale of the model. We used a standardised value of 0.6 m across all models as this fell within the range of 20-25 x surface roughness for the vast majority (>98%) of points, following equations presented in Lague et al. (2013). Projection diameter was calculated as a function of point density, so to ensure each projection cylinder had a minimum of five points, we used a value of 1.1 m. Finally, we set the maximum projection depth to 10 m to exclude grossly erroneous values (<0.01% of all values).

5.3. Results

5.3.1. Use of Raspberry Pi cameras to generate point clouds

The Raspberry Pi-based camera captured high-resolution imagery across the full length of Fjallsjökull, at distances of up to 1.5 km. Glacier textures and structures,

such as debris patches and cracks in the ice, were clearly visible within the photos captured by the Raspberry Pi (see example imagery in Figure 5.6) to aid 3D reconstruction. The ground sampling distance (GSD) (the on-ground distance represented by one pixel) of the Raspberry Pi at 500 m range was 3.80 cm and at 1.5 km was 11.41 cm (following calculations by O'Connor et al., 2017). By comparison, trail cameras used by Mallalieu et al. (2017), at a mean distance of 785 m to the glacier, achieved a GSD of 28.05 cm. We successfully generated point clouds along the front face of Fjallsjökull using the 315 Raspberry Pi photos captured from the boat survey. Eight point clouds were generated at high resolution, with survey lengths of ~250 – 350 m each. The full range of calving face heights observed at Fjallsjökull, from ~1 m to ~15 m were examined in this analysis. Point clouds were largely complete, though many were speckled in appearance.

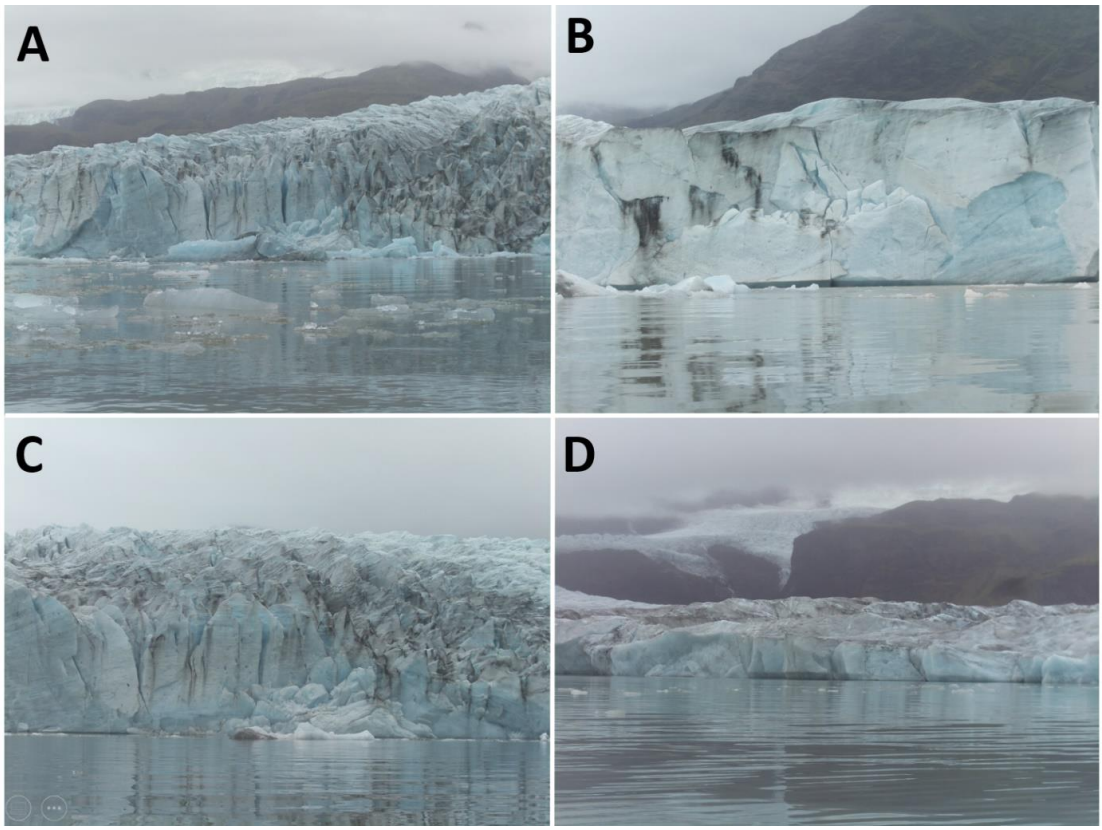

Figure 5.6 – Example images captured by the Raspberry Pi sensor. Images A, B, and C are taken from the boat transect (~500 m from the glacier front) and have an approximate field of vision of ~100 m, while D is captured from the shoreline ~1.2 km from the glacier, with an approximate field of vision of ~400 m.

5.3.2. Comparison between Raspberry Pi and UAV point clouds

Point clouds generated by the Raspberry Pi show a close comparison to those derived from the UAV, with a mean absolute error of M3C2 distance of 0.301 m and a standard deviation of 0.738 m across the Fjallsjökull calving face (Table 5.2, Figure 5.7). Point density of all Raspberry Pi point clouds was high (< 10 cm average spacing between points), allowing small features on the ice surface to be distinguished from ~500 m away. Extremely high M3C2 values (a threshold greater than 1 m difference between the UAV and Raspberry Pi) are found at the far edges of the models where fewer frames are used to produce the point clouds, and at the highest parts of the margin (particularly prominent in panel E of Figure 5.7). These values account for 5.03% of points (3.31% > 1 m; 1.72% < -1 m) and there is a slight positive skew (the Pi is overestimating the range to the glacier) in the error distribution with a mean M3C2 distance of 4.31 cm (Figure 5.8).

Frontal section	Points in Pi Cloud (million)	Points in UAV Cloud (million)	M3C2 mean (m)	M3C2 Standard deviation (m)	M3C2 Mean absolute error (m)
A	2.446	0.634	0.097	1.079	0.445
B	3.289	0.763	0.033	0.461	0.272
C	1.793	0.602	-0.0001	0.563	0.253
D	1.986	1.322	0.030	0.760	0.259
E	2.025	1.346	0.055	1.020	0.363
F	0.891	0.500	-0.012	0.694	0.334
G	2.071	1.472	0.063	0.640	0.298
H	1.276	1.171	0.048	0.530	0.229
ALL	**15.777**	**7.810**	**0.0431**	**0.738**	**0.301**

Table 5.2 – Key statistics and M3C2 comparison between point clouds generated by the Raspberry Pi and UAV. Frontal sub-sections can be seen in Figure 5.1.

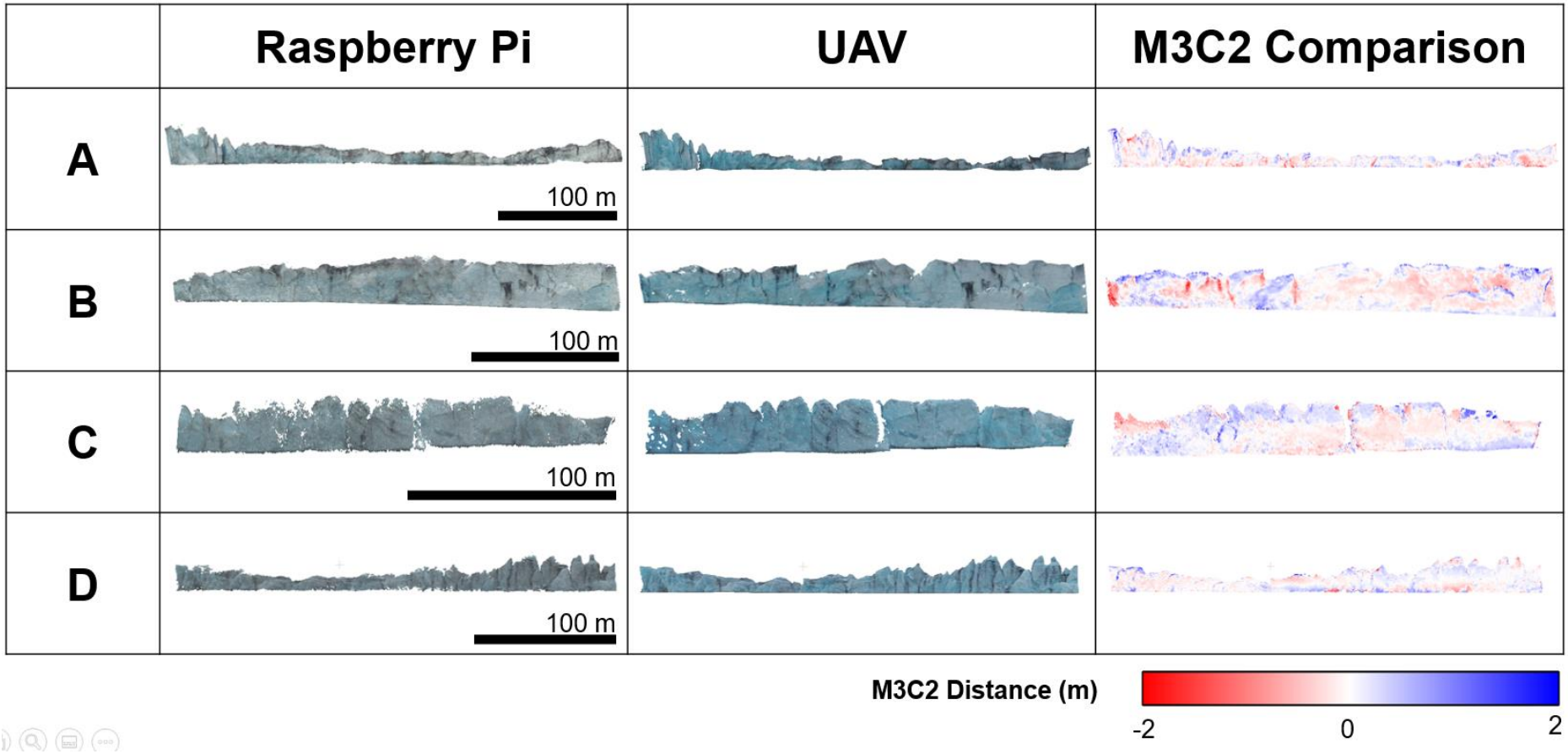

Figure 5.7 (Part 1 of 2) – Fjallsjökull calving face running from northernmost (A) to southernmost (H) sections, as captured by the Raspberry Pi and UAV, and the M3C2 distance between each. Note varying scales between each section are to minimise white space in figure design.

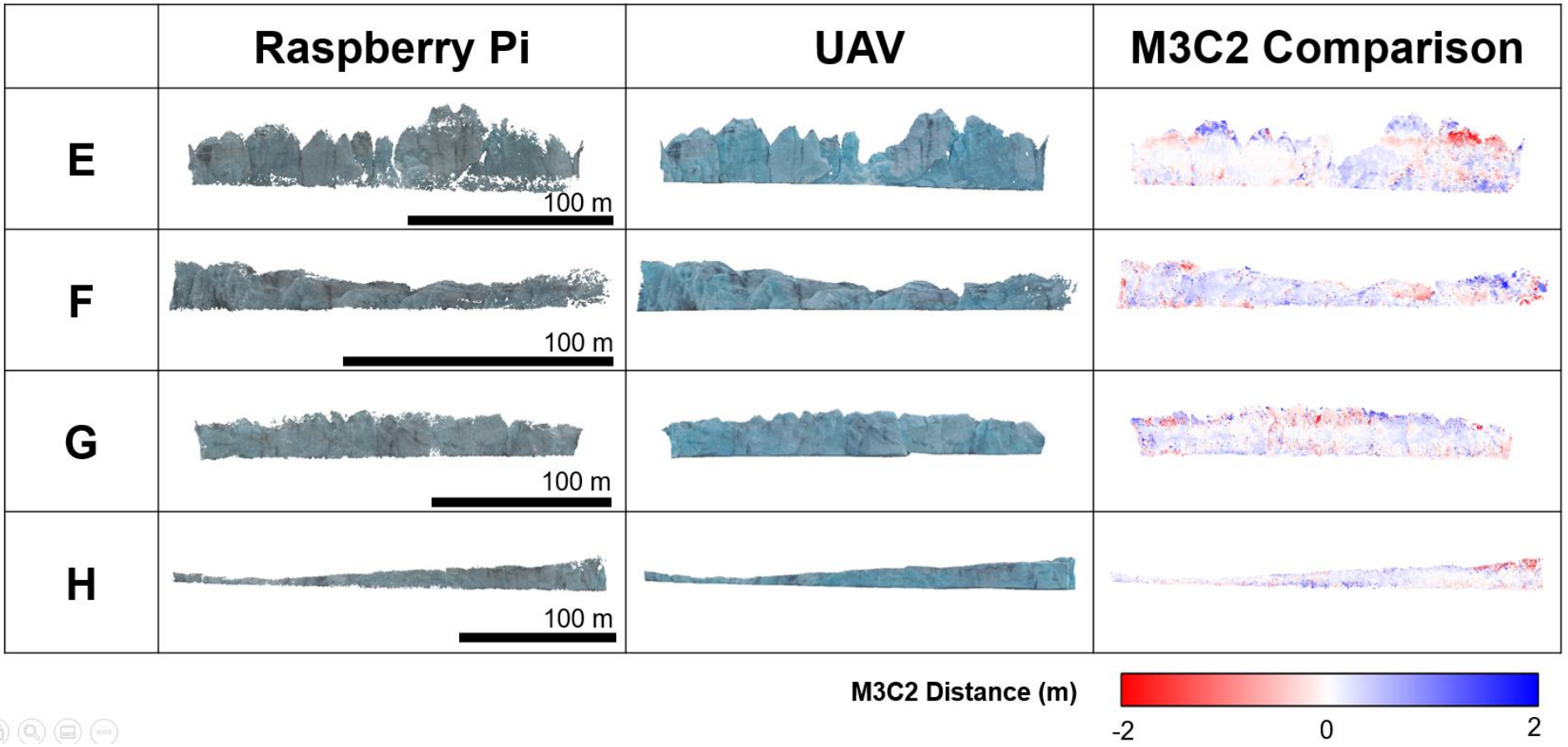

Figure 5.7 (Part 2 of 2) – Fjallsjökull calving face running from northernmost (A) to southernmost (H) sections, as captured by the Raspberry Pi and UAV, and the M3C2 distance between each. Note varying scales between each section are to minimise white space in figure design.

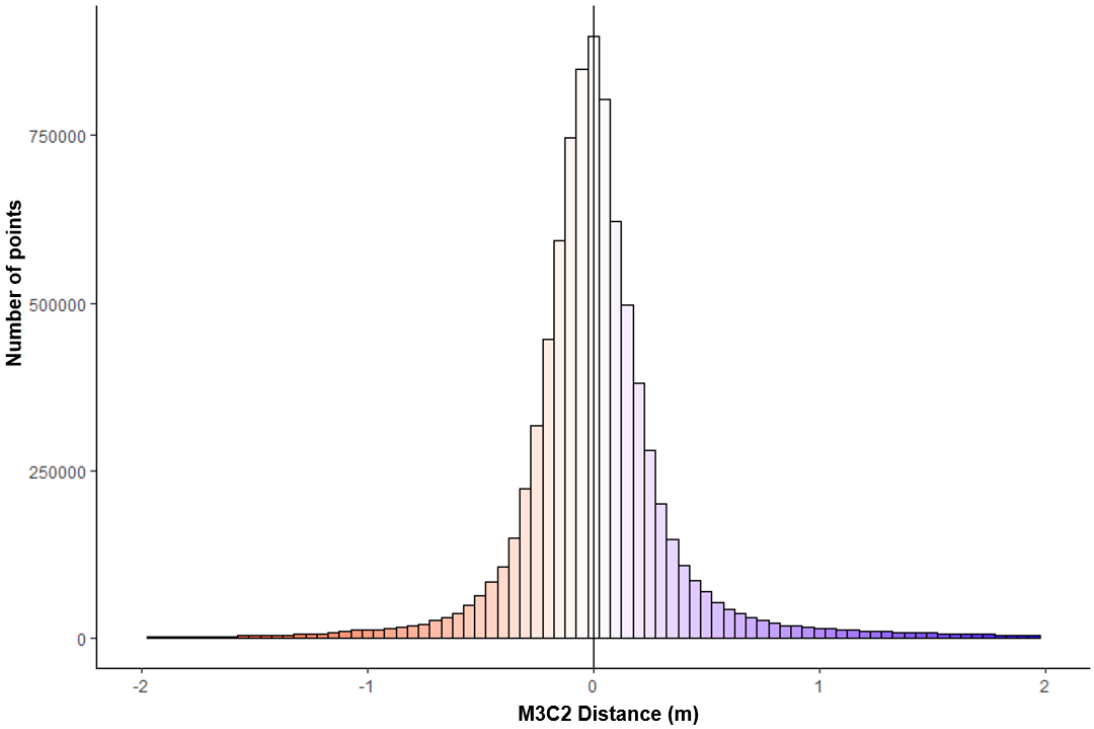

Figure 5.8 – Histogram of M3C2 distance values across the Fjallsjökull calving face, combining all eight sub-sections together. There is a slight positive skew in distribution (mean 4.31 cm). M3C2 distances are cropped here to ±2 m for display purposes, but some values reach ±10 m. Bin widths are 0.05 m.

5.3.3. Exploring the limits of Raspberry Pi cameras in producing 3D models

We analysed sub-section B (~250 m long) under a number of other scenarios to explore the limits of Raspberry Pi cameras in SfM studies. Capturing images from the shoreline of Fjallsárlón, between 1.2 and 1.5 km away from the calving face (denoted by X and Y in Figure 5.1), increased the standard deviation of M3C2 distance (0.742 m compared to 0.461 from the boat transect, a 61% increase) and mean absolute error (0.341 m compared to 0.272 m from the boat transect, a 25% increase). The point cloud itself is largely complete, though visibly more speckled than the point cloud generated from the closer survey (Figure 5.9). We observed similar patterns of error in the point clouds captured from the shoreline as from the boat transect, with the highest errors corresponding to ridges of jagged ice.

Sub-section B was generated using 31 images from the Raspberry Pi in Figure 5.7 and Table 5.2; but timelapse camera arrays are generally limited to 10 – 15 cameras due to cost. We found that using a reduced set of ten images had little impact on mean absolute error (0.263 m compared to 0.272 m using all images, a 3%

decrease), but increased the standard deviation (0.627 m compared to 0.461 m when using all images, a 36% increase). This was most notable towards the periphery of the point cloud (Figure 5.9G), though the point cloud contains more gaps than the original. Sub-section B is approximately 250 m long and an individual image captures ~80 m of the glacier front, which means there was a low level of overlap (2-3 images at the right hand side which is most speckled, Figure 5.9). Given the good quality of images acquired at a greater distance, positioning cameras further away to create more overlap between images would likely address this speckle issue.

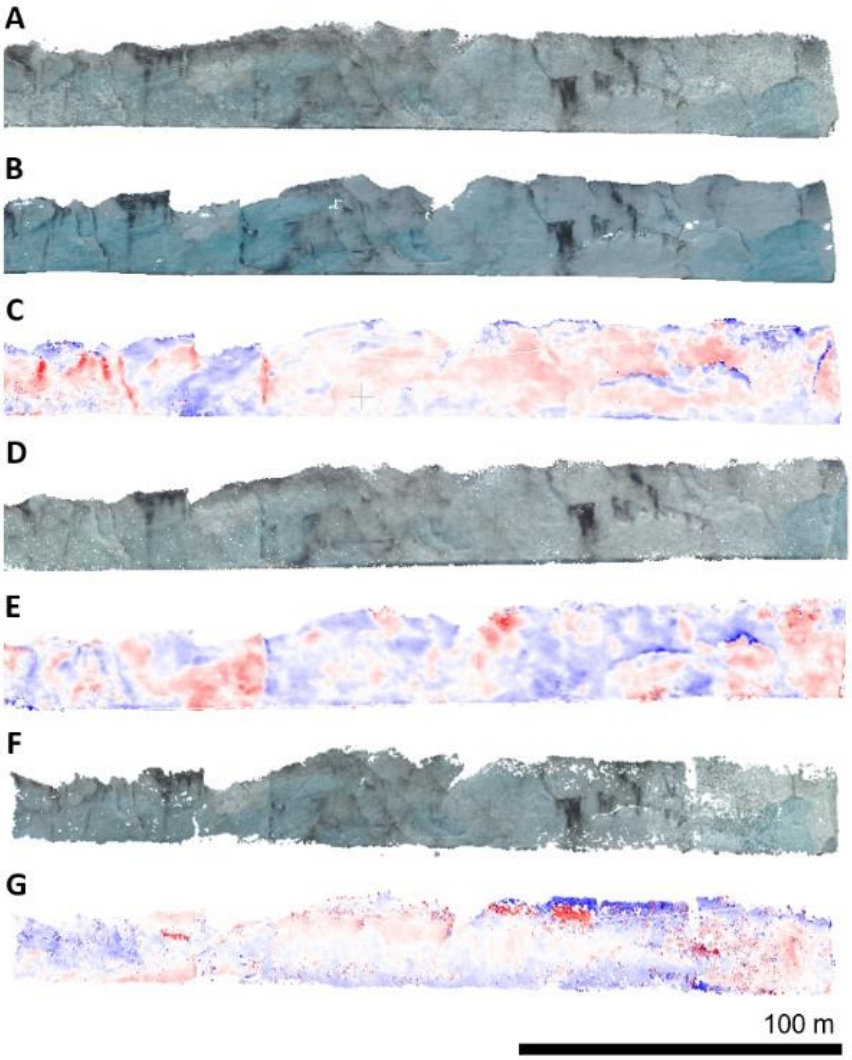

Figure 5.9 – Exploring the limits of the Raspberry Pi sensor in comparison to UAV. (A-C) Sub-section B as generated by (A) Raspberry Pi), (B) UAV, and (C) the corresponding M3C2 comparison. (D) Point cloud generated by Raspberry Pi when positioned from the Fjallsárlón shoreline, at a distance of 1.2 – 1.5 km, and (E) corresponding M3C2 comparison with UAV. (F) Point cloud generated by Raspberry Pi from ten images, and (G) corresponding M3C2 comparison with UAV.

5.3.4. Longevity of Raspberry Pi sensors in glacierised environments

Owing to the impact of the COVID-19 pandemic, a longevity experiment involving Raspberry Pi sensors that we began in September 2019 could not be completed. We report here our lessons learned with this experiment to enable the glaciology community to learn from a wider range of scenarios using Raspberry Pis. In order to examine the robustness and longevity of a Raspberry Pi in a glacierised environment, we situated a Raspberry Pi Zero W with a camera sensor (camera module v2) at a proglacial lake of the Quelccaya Ice Cap, Peru for three months between September and November 2019. The Pi was powered by a 12 V lead-acid battery and 10 W solar panel, regulated to provide a safe voltage to the Pi by a solar charge controller (Figure 5.10). We set the Raspberry Pi sensor approximately 100 m from the glacier calving margin to capture timelapse imagery for three months. During this time, the Pi powered on three times a day to capture an image before powering down. The Pi clock was regulated using a Witty Pi 2 attachment which should have limited clock drift to ~1 second per week (Coca and Popa, 2012), though we were not able to provide an independent assessment of this drift. Images were acquired successfully throughout the three month period; however, their poor quality (owing to the use of a camera module v2) meant that Agisoft Metashape could only produce very low quality point clouds with large data gaps that could not be aligned to a UAV-based point cloud for comparison. Upon retrieval, we observed condensation in the weatherproof box which had affected the quality of some images acquired (a common problem in sub-zero environments; Liu et al., 2021). This could be improved with ventilation (Parajka et al., 2012) or desiccant (Liu et al., 2015). The results of this longevity experiment outline the success of using a Raspberry Pi in a glacierised setting for long time periods, demonstrating their potential as affordable alternatives to timelapse DSLR cameras.

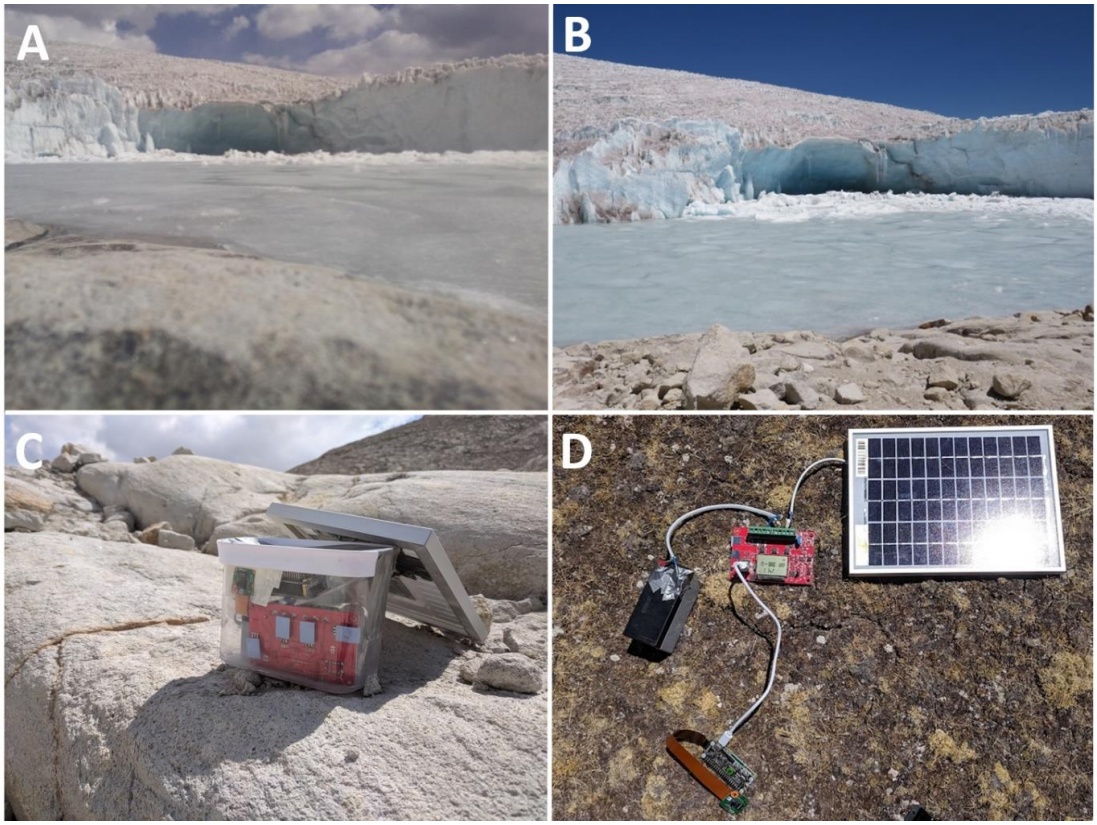

Figure 5.10 – Raspberry Pi setup at the Quelccaya Ice Cap. (A) Example image captured by the Raspberry Pi camera module v2 approximately 100 m from the glacier. (B) Comparison image captured by a DSLR camera. (C) The Raspberry Pi sensor was housed in a transparent, weatherproof box (and later surrounded by rocks to stabilise it). (D) Deconstructed setup, including 12 V lead-acid battery, 10 W solar panel, solar charge controller, and Raspberry Pi Zero with camera module v2 attached.

5.4. Discussion

5.4.1. Raspberry Pis in SfM-based glaciology studies

Raspberry Pi cameras have rarely been tested in a glaciological setting, but our analysis suggests that they could feasibly be deployed for long-term monitoring purposes and, given their comparable quality to a UAV-derived point cloud, have the potential to capture and quantify dynamic events (e.g. calving). Our data show that, from up to 1.5 km away, Raspberry Pi cameras can detect small features within the ice and, when used to generated 3D data, could identify, with confidence, any displacement of ice over ~1 m in size. This also holds true for a camera setup using

a much-reduced array; our experiments using just ten camera positions yielded results that were largely comparable in quality to those comprising the full suite of data (31 camera positions).

Improvements to research design, such as positioning cameras at a more optimal range of heights and angles, are likely to reduce error in the Raspberry Pi point clouds (James and Robson, 2012; Bemis et al., 2014). A key limitation of our research was that images were captured only from a fixed height in the boat. Indeed, it is no coincidence that we observed the lowest errors between the two sensors at approximately the height level of the boat across all point clouds generated. Therefore, using a greater variety of camera angles and positions, for example by positioning cameras above a glacier front using nearby bedrock or moraines, would likely reduce error across the model (Mosbrucker et al., 2017). While our setup and analysis therefore may represent a conservative view of the potential use of Raspberry Pis in photogrammetry, it also reflects the practical considerations of working in field environments which are frequently sub-optimal for deploying fixed cameras.

Our study used relative georeferencing methods, removing the need for absolute positioning of the clouds using surveyed ground control points. Over glacier calving margins, placing ground control points is especially challenging and alternate methods are required (Mallalieu et al., 2017). There is precedent in using the geospatial data from one point cloud to reference another when comparing sensors (Zhang et al., 2019c; Luetzenburg et al., 2021). Alternatively, the positions of the cameras can be used to determine the georeferencing. This ‘direct georeferencing’ can be achieved using GNSS-based aerial triangulation of fixed positions, or an on-board GPS unit that shares the clock of the camera such that a precise time-stamp of location can be associated with each of the acquired images (Chudley et al., 2019).

In this study, we cropped our point clouds to show only the front, flat, calving face of Fjallsjökull. This involved significant trimming of point clouds generated by the UAV (up to 40% of points removed), while the Raspberry Pi only required minor adjustments (~10% of points removed). A key limitation of the Raspberry Pi setup is that it cannot achieve the wide range of viewing angles and heights as a UAV does, and so analysis is limited to the front (i.e. vertical section) of the calving face. While this means the setup can monitor advance/retreat and calving events, the additional ability to generate a 3D model of the top of a glacier surface could potentially provide important information on calving dynamics, such as crevasse formation and

propagation which could be indicative of imminent calving (Benn et al., 2007). In previous work, monitoring the glacier surface in addition to the calving face has enabled the reconstruction of events leading up to major calving events, including the calculation of strain rate and identification of propagation prior to calving (Jouvet et al., 2017). Furthermore, other glacier characteristics, such as surface velocity, can indicate imminent calving but require a more top-down view of the glacier surface (Ryan et al., 2014). Modelling a greater extent of the glacier terminus could be particularly important if such a system was to be integrated into a GLOF early warning system.

For studies making use of a typical DSLR-grade handheld camera, James and Robson (2012) and Smith et al. (2016) suggest a typical relative precision ratio of 1:1000 – an error of 1 m when captured at a distance of 1000 m (though high-quality SfM often far exceeds this (James et al., 2017)). At 500 m distance, we achieved a mean absolute precision of 1:1667 and at 1.2 – 1.5 km distance a mean of 1:978. These values almost match the precision thresholds set for DSLR-grade cameras, and exceed the precision achieved by similarly priced trail cameras used in glacierised environments (Mallalieu et al., 2017). While terrestrial laser scanners can achieve greater levels of precision for monitoring glacier fronts (e.g. Pętlicki et al., 2015), their high weight and cost (tens of thousands of dollars) often precludes their use in glaciology research.

5.4.2. Future applications in glaciology and potential for automation

Glacier dynamics at a calving margin are complex, but a low-cost timelapse camera array can offer insight into many key questions. Ice velocities at the terminus of Fjallsjökull range from ~40 m a^{-1} to ~200 m a^{-1} for lake terminating ice (Dell et al., 2019). Glacier frontal positions and their diurnal variability, can be monitored using this Raspberry Pi approach, as well as calving events that exceed 1 m in depth. Calving dynamics, including characterising different types of calving mechanisms and the impact of seasonality and lake drainage, can also be monitored from timelapse cameras (Mallalieu et al., 2020) to aid in the understanding of how glacier calving contributes to the overall mass balance of a glacier and how this fluctuates over varying timescales (How et al., 2019; Bunce et al., 2021). Using timelapse photogrammetry, it is theoretically possible to detect precursors (rotation, elevation change, creep) to calving events on the order of magnitude of >1 m, such as observed at Sermeq Kujalleq 65 hours prior to calving (Xie et al., 2016).

In addition to calving events, terrestrial-based photogrammetry based on a Raspberry Pi system could monitor other important glacier dynamics at a low-cost. There is a long history of using terrestrial photogrammetry for monitoring glacier thinning to quantify mass balance change of mountain glaciers. While this conventionally involves repeat site visits (Brecher and Thompson, 1993; Piermattei et al., 2015), our approach would not require such regular site visits. Similarly, while glacier velocity measurements can be achieved with a single camera, an SfM approach provides higher spatial accuracy and ability to monitor smaller changes (Lewińska et al., 2021). Where surrounding topography allows, positioning Raspberry Pi cameras to look down on to the glacier surface would allow for the monitoring of supraglacial lake filling and drainage, or ice-cliff recession (Watson et al., 2017). Creep rates of rock glaciers have been successfully monitored through terrestrial photogrammetry (Kaufmann, 2012) and UAV surveys (Vivero and Lambiel, 2019), but again requiring repeated site visits. In each of these additional applications, low-cost Raspberry Pi cameras could produce accurate 3D models at a greater temporal frequency, without the logistical challenges, and financial costs, associated with repeating fieldwork.

We speculate that, given likely sensor innovation and the decreasing cost of technology, the potential of low-cost sensors in glaciology research will only increase (Taylor et al., 2021). We envisage Raspberry Pi computers, or other microprocessors, to play a key role in this expansion. Almost all Raspberry Pi models have built-in WiFi which allows data sharing between individual devices. With a WiFi radio on-site, providing a range of many hundreds of metres, individual cameras could autonomously send their data towards a central, more powerful, Raspberry Pi unit for further analysis. Similar wireless sensor networks in glaciology have been produced to monitor seismicity (Anandakrishnan et al., 2022), ice surface temperatures (Singh et al., 2018), and subglacial hydrology (Prior-Jones et al., 2021). We speculate that an array of Raspberry Pi computers could produce the first near real-time photogrammetry setup for continuous 3D monitoring of glacier calving fronts (Figure 5.11). With the development of autonomous photogrammetry pipelines (Eastwood et al., 2019), this system could, theoretically, run entirely independent of user input. Furthermore, the flexibility of Raspberry Pi computers, particularly their ability to operate multiple sensor types from one unit, opens up the possibility for wide sensor networks across glaciers – creating comprehensive digital monitoring of rapidly changing environments (Hart and Martinez, 2006; Taylor et al., 2021).

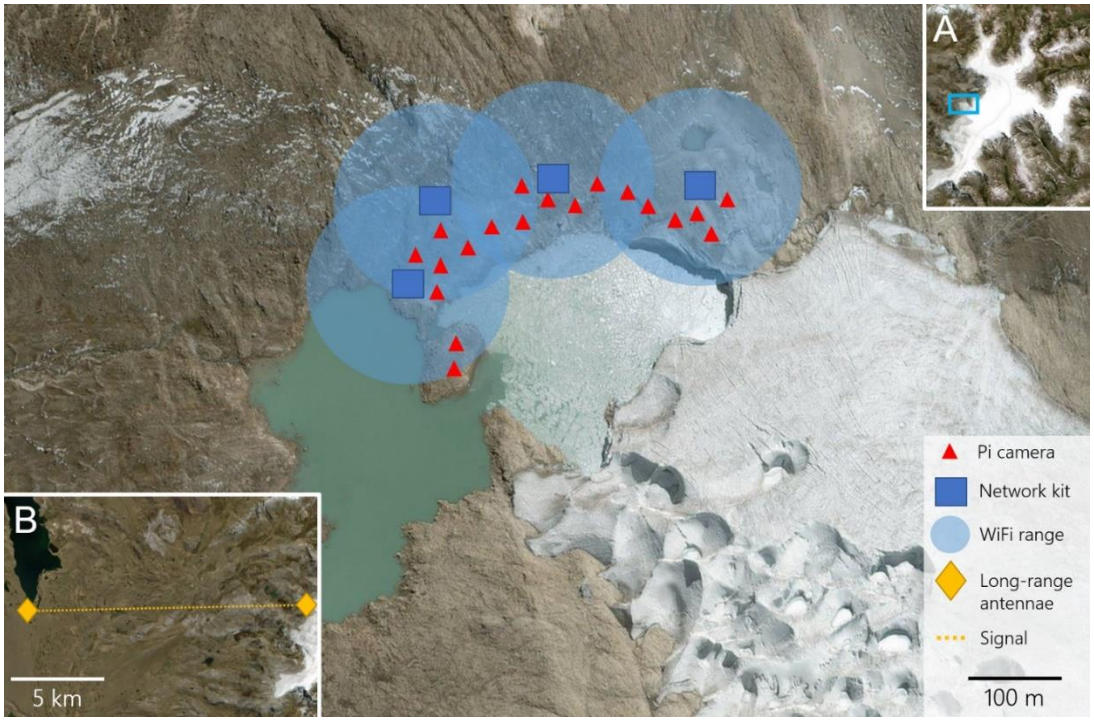

Figure 5.11 – A hypothetical set up for a time-lapse camera array system situated on the Western margin of the Quelccaya ice cap to monitor calving events. The WiFi signal is transmitted to the site via a long-range antennae from a hydroelectric dam ~20 km away, allowing data to be transmitted from the Raspberry Pi computers to a remote location for rapid processing.

There exists considerable potential for low-cost sensors in mountain glacier communities, which are predominantly located in developing countries. Early warning systems situated around glacial lakes in the Himalaya have successfully prevented disaster during a number of GLOF events by allowing time for downstream communities to evacuate (Wang et al., 2022). By reducing the cost of camera-based sensors that are frequently used as part of a monitoring system (for example at Kyagar glacier in the Chinese Karakorum; Haemmig et al., 2014), more cameras can be situated to monitor calving rates, velocity, or stability at higher precision and accuracy in 3D. A low-cost also means that more community-driven initiatives based on this Raspberry Pi system are viable. Such systems must be co-designed, and ultimately owned by, the communities they serve. Simple systems (such as Raspberry Pis), with components that are easily replaceable and with open access documentation, lowers the technical knowledge required to maintain an early warning system and so a greater diversity of stakeholders can engage with its maintenance. Previous work has shown that diversity in engagement, and genuine understanding

of the social structures on which communities are built, is essential for the success of early warning systems like these (Huggel, et al., 2020).

5.4.3. Practical recommendations

While we suggest that Raspberry Pi cameras offer an alternative to expensive, DSLR cameras for timelapse camera arrays, based on our experiences we note a series of recommendations to future researchers and communities looking to use this approach in their own systems:

- Camera setup must be carefully considered and adopt best practice set by others (e.g. Mallalieu et al., 2017) with regards to angle, overlap, and positioning;
- Positioning cameras further away from the target (~1 km) where possible can capture a wider frame of reference while remaining viable for detecting change of magnitude >1 m, so fewer cameras are needed for an array setup;
- There is only a narrow window of focus when using the Raspberry Pi 16 mm telephoto lens, particularly over 1 km from the target, and an in-field screen is essential to ensure correct setup;
- In the absence of an in-field screen, SSH-based access to the Raspberry Pi can allow you to see image acquisitions on a computer screen or smartphone, though leaving wireless connectivity enabled draws more power;
- Raspberry Pi computers draw very little power when commanded to turn on/off between image acquisitions, and can be sustained for many months using a lead-acid battery and small solar panel;
- While Raspberry Pi cameras are robust and usable in sub-zero temperatures, adequate weatherproofing must be used to ensure that the camera lens does not fog over time.

5.5. Conclusions

We conducted a photogrammetric survey along the calving face of Fjallsjökull, Iceland, to compare a SfM point cloud generated using imagery from low-cost Raspberry Pi camera sensor to that derived using imagery captured from a UAV. We successfully produced point clouds along the front of Fjallsjökull, with a mean absolute M3C2 distance between point clouds generated by the two sensors of 30.1

cm, and a standard deviation of 73.8 cm. The Raspberry Pi camera also achieved sub-metre error at distances of 1.2 – 1.5 km from the glacier. This error is comparable to DSLR-grade sensors, and highlights the potential for Raspberry Pi cameras to be used more widely in glaciology research and monitoring systems. For certain applications, we suggest, conservatively, that Raspberry Pi sensors are viable for detecting change of magnitude >1 m, such as calving events and terminus advance/retreat. With WiFi capabilities within the Raspberry Pi computer, real-time data transmission could open an avenue for autonomous photogrammetry to enable this system to be used in warning against geomorphic hazards. More generally, their affordability, flexibility, durability, and ease of use makes them well-positioned to rival more expensive timelapse systems without compromising data accuracy, while also enhancing the potential for autonomy and remote system management.

Chapter 6

Discussion and recommendations on the applicability of these techniques to monitoring Peruvian mountain glaciers

This thesis has demonstrated the applicability of a range of novel remote sensing technologies to monitoring Peru's mountain glaciers, using a variety of sensors, processing techniques, and methodologies. Each technology or technique is novel within the Cordillera Vilcanota, and indeed in its application to mountain glaciers more broadly, showing potential for their integration into management schemes to support policymakers in securing future water resource from glacierised regions. Each chapter within this thesis contains a dedicated discussion section to synthesise findings. This chapter therefore will present a brief summary of findings assessed against the research objectives given in Chapter 1, discuss the implications for this research in the Cordillera Vilcanota and more broadly, and outline future research directions resulting from this work.

6.1. Research summary

Chapter 1 of this thesis began by outlining the importance of mountain glaciers as water resources and the hazards posed to communities living in close proximity to glaciers by climate warming. This thesis sought to show that novel remote sensing technologies could assist in developing adaptation and mitigation interventions to support these communities. Four research objectives were set in Chapter 1 to provide a framework for a holistic assessment of this topic. This section summarises how the results of this thesis have fulfilled the four research objectives.

Objective 1

Explore the current state of remote sensing over the mountain cryosphere, and identify remote sensing techniques and sensors currently in development, or used in other geoscience disciplines, that can be applied to the mountain cryosphere.

Chapter 2 of this thesis presented a comprehensive review of the current capabilities of remote sensing in the mountain cryosphere. Here, key advents in this

discipline were outlined, including cloud computing, artificial intelligence, open source automated pipelines, new satellite missions, and low-cost sensors. Many of these are novel to mountain glacier systems, but have been readily deployed in other geoscience disciplines. Finally, this review outlined upcoming remote sensing technologies, such as planned satellite missions, to highlight future opportunities for research in this discipline.

Objective 2

Quantify the mass balance and area change of glaciers in the Southern Peruvian Andes, concurrently examining the applicability of stereo archives to provide long-term monitoring over small mountain glaciers.

Stereo archives have been exploited, for the first time in this data-scarce region, to quantify the regional glacier mass balance (-0.477 ± 0.067 m w.e. yr^{-1}) of the Cordillera Vilcanota between 2000 and 2020. In addition, open source cloud computing and the Landsat archive were harnessed to quantify a 512 km^2 recession of glacial ice across the Southern Peruvian Andes from 1975 to 2020 – a decline of more than half of their original size. This study identified the key drivers of ice loss as climate warming and the elevation of glaciers. With the median elevation of glaciers rising by 24.8 m per decade in the Cordillera Vilcanota, more glaciers will be pushed into net ablation in the near future.

Objective 3

Explore the applicability for using new satellite altimetry missions (Sentinel-3 and ICESat-2) over small mountain glaciers, concurrently identifying opportunities for integrating altimetry data into glacier monitoring schemes.

Sentinel-3, without the addition of *a priori* elevation information, does not capture elevation data over mountainous regions in open-loop tracking mode. Updating the OLTC to shift the tracking range window allows for some limited data acquisition, but this satellite mission is likely to be useful to only a very small handful of glaciers worldwide. Where Sentinel-3 passes over proglacial lakes, elevation

retrieval is more successful. ICESat-2, with a 6 km range window, acquires elevation data over mountainous areas with a high degree of accuracy (mean difference of -0.85 m to TanDEM-X in off-ice areas). As such, other opportunities for ICESat-2 in glacier monitoring schemes include the ability to quantify glacier surface elevation change after a 2-year repeat, the depth of large accumulation events, interannual lake surface elevation change, and proglacial lake bathymetry.

Objective 4

Create a novel SfM-based system that captures science-grade 3D models of glacier calving fronts at a low-cost, concurrently providing a proof-of-concept for real-time, autonomous SfM for a GLOF hazard warning system.

Using a Raspberry Pi camera sensor, science-grade point clouds (mean difference to a UAV was 0.31 ± 0.74 m) were generated of the calving face of Fjallsjökull, Iceland. The Raspberry Pi also achieved sub-metre difference to the UAV at a distance of 1.2 – 1.5 km from the glacier, comparable to more expensive DSLR cameras. As a hazard warning system, an array of Raspberry Pi sensors situated surrounding a proglacial lake should be able to detect change of magnitude >1 m, such as calving events and terminus advance/retreat. By harnessing the WiFi capabilities of the Raspberry Pi to transmit data upon capture, these sensors could therefore be used to generate real-time point clouds of glacier margins to raise the alarm following a large calving event.

6.2. Applicability of novel remote sensing technologies to the Cordillera Vilcanota

Within the Cordillera Vilcanota, two key stakeholders could benefit from the use of the remote sensing technologies outlined in this thesis: EGEMSA (the energy company operating the hydroelectric dam at Laguna Sibinacocha) alongside other commercial operations relying on meltwater downstream, and residents living in close proximity to the ice.

The hydroelectric plant at Laguna Sibinacocha has been operational since 1996 and, during the dry season, is almost entirely reliant on glacial meltwater to maintain streamflow through the dam (Sarango et al., 2021). However, as the dry

season is projected to increase in duration with climate change, this will lead to an increased reliance on glaciers (up to 83% of water contribution; Martínez et al. (2020)) to maintain reservoir levels (Kronenberg et al., 2016). More broadly across the tropical Andes, glacial meltwater powers up to 732 MW of hydropower production during the dry season (Buytaert et al., 2017). Remote sensing-based modelling has been used to assist in identifying suitable sites for hydropower projects (Kulkarni et al., 2002; Farinotti et al., 2019), but numerical modelling is more typically used to project the impact of climate warming on future meltwater and, subsequently, streamflow (Beniston and Stoffel, 2014; Schaefli, 2015). However, validating these models to understand which trajectory the glacierised environment is following often requires field-based data collection. Once hydropower projects are established, optical satellite data (e.g. Landsat) is often used to quantify ice recession and interannual snow cover (Negi et al., 2009; Ashraf et al., 2012), but such analyses are limited by their lack of elevation-based data.

The original ICESat mission has previously been used to monitor snow depth in Norway, to supply information on seasonal accumulation patterns for hydropower generation downstream (Treichler and Kääb, 2017). As demonstrated in Chapter 4, ICESat-2 is capable of acquiring vastly more data than ICESat over mountain glaciers and, as such, could potentially be used over the Cordillera Vilcanota to monitor accumulation in a similar fashion. ICESat-2 is also able to provide regular elevation acquisitions over these glaciers in order to validate projections of mass loss in the region, to allow for more accurate long-term planning of the longevity of glaciers as water resources. To this end, NASA's open access data portal for ICESat-2, Open Altimetry, allows for easy access to these data with low technical requirements and no cost involved to implement into a regular monitoring programme.

For regional policymakers (such as in CORECC, the regional council of the Cusco region), understanding the spatial variability in rates of glacier recession is a prerequisite for directing adaptation and mitigation programmes, so that interventions can be made in the most appropriate watersheds (Condom et al., 2012). In Chapter 3, low-lying glaciers were identified as at the highest risk of immediate, rapid recession – particularly a cluster of glaciers in the North of the Cordillera Vilcanota (Nevado Qolquepunco). Intervention schemes could include identifying alternative sources of potable water during drought to communities relying on meltwater as their primary water resource (Bury et al., 2013) or modelling the future storage capacity of new lakes (Drenkhan et al., 2019). While the ASTER satellite continues to operate, regular stereo DEMs can still be added to the autonomous pipeline to quantify, across

the region, updating mass balance. Concurrently, with the launch of Landsat-9 and development of Landsat-NeXt, regular updates to ice area change are easily accessible with open access tools such as Google Earth Engine. Integrating these approaches into policymaking at a watershed level means that management have up-to-date data and do not need to await research articles or reports from national government (e.g. INAIGEM, 2017; ANA, 2021).

The expansion in area and volume of lakes at glacier calving margins of the Cordillera Vilcanota has increased in recent decades, and is projected to increase further under all future climate scenarios (Drenkhan et al., 2018). As such, the development of a comprehensive, low-cost SfM-based monitoring system that can be easily handed over to a community to develop to their bespoke needs, could be transformative. Co-designing the system to be targeted to the needs of local residents, and ownership of the final result, is imperative for any such system to be successful (Huggel et al., 2020). Raspberry Pi sensors, and all the components necessary to build these systems, are readily available in nearby towns and, due to the modular build, can be fixed very cheaply. Raspberry Pi computers are designed to be easy to learn and have been successfully deployed in educational schemes in the Global South (Ali et al., 2013). This success could feasibly be replicated within communities of the Cordillera Vilcanota with an appropriate injection of funding.

For early warning and climate adaptation schemes to succeed, communities living in close proximity to the ice must have good knowledge of the threats posed by climate change, clear ownership and understanding of a solution, and capacity to implement this solution (Thompson et al., 2020). Across the Cordillera Vilcanota and wider Vilcanota-Urubamba basin, there is good general public understanding of the cause and risks posed by climate change (Orlove, 2009; Brügger et al., 2021). However, the capacity of local communities to adapt to these risks is low. Where the Peru-wide average HDI (human development index, a United Nations indication of development quantified from 0 to 1) was 0.777 in 2019, communities living beneath Nevado Qolquepunco in Marcapata, Vilcanota had an average HDI of 0.202 (Instituto Peruano de Economía, 2021). As such, the affordability and durability of monitoring schemes is an imperative factor in their success.

Ensuring all stakeholders are involved in decisions relating to management of water resources is also paramount to their success. Where all parties are not considered, this has adverse effects on the ability of monitoring systems to protect the communities they are designed to serve. There is precedence in Peru that urges

such caution – there have been stand-offs between a hydropower company, the national water authority, and local communities at Laguna Parón (Condom et al., 2012). Here, the dam caused lake levels to vary too greatly from their natural expectations, leading to citizens seizing control of the lake to ensure sustainable flows year-round. Technological intervention in climate change adaptation schemes can have unintended, negative consequences on communities by introducing unequal power dynamics which create social tensions (Carey et al., 2012). Such social tensions can spill over and ultimately result in the destruction or removal of glacier monitoring schemes that were designed to help (Huggel et al., 2020). Only when involving all stakeholders and members of communities affected can any of the management schemes discussed in this thesis, from satellite-based monitoring to field-based warning systems, ultimately be a success.

Overall, each of the remote sensing technologies discussed in this research could be integrated within a variety of management opportunities in the Cordillera Vilcanota (Figure 6.1). Key philosophies of open access data, ease of use and deployment, and low-cost, are transparent across all suggested applications.

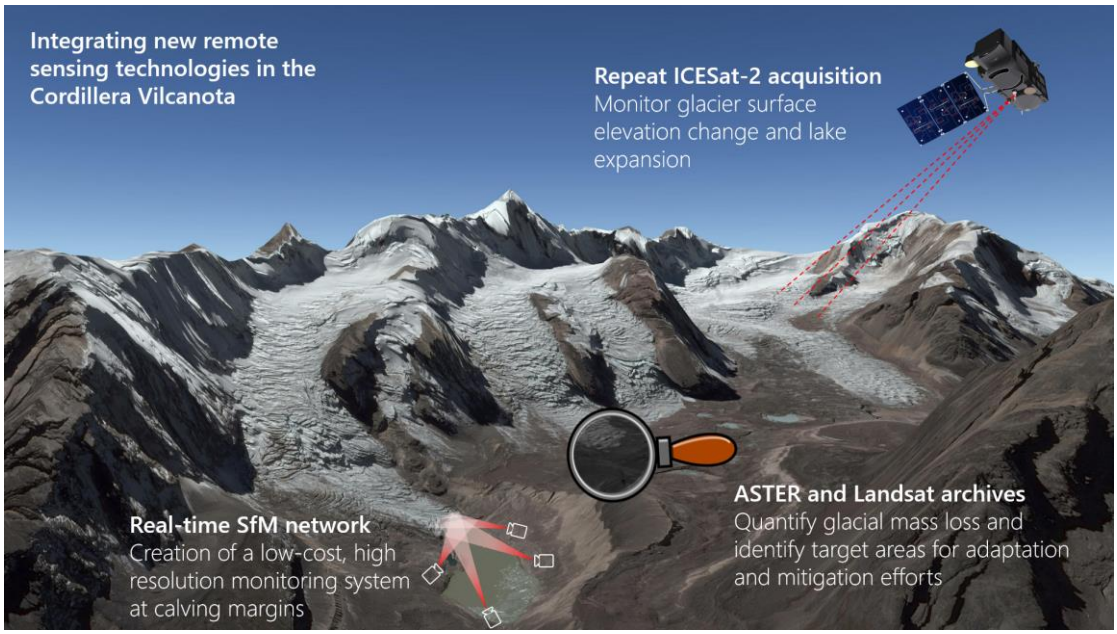

Figure 6.1 – Application of the novel remote sensing technologies presented in this thesis to the Cordillera Vilcanota.

6.3. Wider applications of this research

The primary focus of this thesis has been on the applicability of novel remote sensing techniques to monitor Peruvian glaciers, with a focus on the Cordillera Vilcanota. However, this research can also benefit communities, policymakers, and researchers of other mountain glacier regions worldwide.

In Chapter 3 of this thesis, we compared our estimates of mass balance from an ASTER DEM time series to those of a global dataset generated by Hugonnet et al. (2021). This global dataset is open access, covers all mountain glaciers, and quantifies surface elevation change in 5-year intervals from 2000 to 2020. However, prior to this thesis, its applicability to challenging mountainous terrain had not been explored. Generating mass balance values for the Cordillera Vilcanota using our dataset (-0.477 ± 0.067 m w.e. yr^{-1}) was almost no different to using their dataset (-0.479 ± 0.048 m w.e. yr^{-1}). By comparing their global approach to a bespoke approach with a higher resolution seed DEM and output product, this work provided the first verification for the Hugonnet et al. (2021) global dataset over mountain glaciers. While there remains limitations with the Hugonnet dataset, particularly its coarse spatial resolution and high uncertainty over very small glaciers, generating bespoke ASTER DEMs to assess surface elevation change in small areas (e.g. Minowa et al., 2021; McDonnell et al., 2022) is perhaps no longer necessary. Where these data are needed, this thesis moves the ASTER DEM time-series method to Google Earth Engine, a freely available (for non-commercial use) cloud computing interface, to lower the technical barrier that faces those needing to use this approach.

This thesis has outlined the effectiveness of two key satellite missions in monitoring the mountain cryosphere: ASTER (Chapter 3) and ICESat-2 (Chapter 4), yet both satellites have operated beyond their operational life with no freely available alternatives yet in development. Alternative optical stereo satellites to ASTER, such as WorldView and Pléiades will continue to operate but, as commercial operations, their datasets will not be openly available. Open access satellite data have clear societal and economic benefit, and access to these data have transformed monitoring of the cryosphere (Pope et al., 2014; Wulder and Coops, 2014). Indeed, the public release of the full ASTER catalogue in 2016 immediately led to the creation of the first iteration of the ASTER DEM time-series method to quantifying glacier mass balance (Berthier et al., 2016), which was adapted in this thesis. Similarly, ICESat-2 has the potential to acquire vast volumes of data over mountain glaciers and, while designed as only a three-year mission, has already exceeded its operational life (Markus et al.,

2017). The original ICESat mission remained operational for seven years (planned for five) but, from 2009 to 2018, the IceBridge mission (to ensure no data loss between satellites) only acquired data over ice sheets and Alaskan glaciers. There is a clear need for a new satellite mission to acquire regular elevation data over mountainous terrain in an unbroken record, whether from optical stereo images or altimeters.

The development of a low-cost system to monitoring glacier calving fronts has large benefit outside of Peru. In the Himalaya, the area of glacial lakes have expanded by 14% between 1990 and 2015 (Nie et al., 2017). Although this expansion has not resulted in an increase in GLOF frequency (Veh et al., 2019), disaster risk management is nevertheless vital (Thompson et al., 2020) and can be supported by networks of field-based sensors (Fukui et al., 2008; Kumar et al., 2020). Identification of hazards and the development of early warning systems should be bespoke for each setting they are placed in, and the initiation mechanisms for GLOFs and other hazards may not be the same in different regions. Yet, the timelapse array of Raspberry Pi camera sensors outlined in Chapter 5 could (with the addition of further research) be adapted to monitor the hazard posed by hanging glaciers and avalanches – threats which may be more apparent in the Himalaya than the Peruvian Andes (Lala et al., 2018; Shugar et al., 2021). By identifying ~1 m depth change in a target up to 1.5 km away, the potential for these sensors across mountainous regions is significant.

6.4. Future research directions

In this thesis, the application of new remote sensing technologies and techniques to the mountain cryosphere has been demonstrated. This opens a broad range of future research directions across the discipline of remote sensing of the cryosphere to build upon this work.

To quantify glacier area change in Chapter 3, we used the Landsat archive to delineate annual glacier boundaries. While this required manual intervention, editing was minimal in recent years when using Landsat-8 imagery. Combining this approach with deep learning approaches used to delineate calving fronts of ice sheets (Baumhoer et al., 2019) or enhance the detection of debris covered ice (Xie et al., 2020) could result in an annually updating, self-generated glacier boundary product. Our approach of using NDSI and NDWI to detect glacial ice resulted in some data gaps in years where snow or cloud cover were particularly heavy. A more sophisticated approach, working on a pixel-by-pixel basis to detect cloud and snow,

and harnessing the growing Sentinel-2 archive to increase the number of cloud-free acquisitions, should help minimise these data gaps for subsequent studies. Lastly, when multi-sensor missions become readily available, the combination of SAR and optical data could further strengthen this delineation by building upon historic works (Rott and Mätzler, 1987) to produce transformative, automated products.

The method to produce a time series of ASTER DEMs to monitor surface elevation change has, throughout the evolution of this method, remained open access (Berthier et al., 2016; Brun et al., 2017; Dussaillant et al., 2018; Dussaillant et al., 2019; Hugonnet et al., 2021). However, the technical requirements to replicate this methodology have been high; with a requirement to understand complex pipelines, install computationally intensive software, and adapt long coding scripts. This technical barrier means that this method remained inaccessible outside of academic spheres. In Chapter 3, we lowered these technical barriers by integrating all complex analysis steps into a Google Earth Engine workflow. Additionally, while in this research we generated ASTER DEMs from the Level 1A product, the auto-generated 'AST14' DEM product could also be considered accurate enough for this level of analysis. Users simply need to upload AST14 DEMs of their area of interest to our Google Earth Engine script to replicate the methodology of our study. While the Hugonnet et al. (2021) global dataset covers many applications of this method in glaciology, the option is now available for policymakers to produce their own estimates of mass balance in a way that is bespoke to their region of interest.

Over the coming years, and as the ICESat-2 archive grows, scientific research using altimetry over mountain glaciers will vastly increase. The potential for this satellite are enormous, crossing a broad range of applications to the mountain cryosphere. More accurate estimates of mass balance can be produced to constrain the large uncertainty (in comparison to ice sheets) in global datasets (Slater et al., 2021). Similarly, mass balance of the smallest glaciers (e.g. in the Cordilleras Urubamba and Vilcabamba) can now be quantified, where even the ASTER DEM time series approach failed to produce an accurate measure of mass balance. Over larger ice caps, such as Quelccaya, future research will use ICESat-2 to validate optical stereo DEMs and further reduce the uncertainty of mass balance change in glacier accumulation zones (Pieczonka and Bolch, 2015). To better understand the potential for the ATL03 product of ICESat-2 to derive proglacial lake bathymetry, global datasets of surface water (Pekel et al., 2016) could be combined with the ICESat-2 archive in Google Earth Engine to identify lakes where high confidence photon returns are captured beneath the lake surface.

In order to assess the application of Raspberry Pi camera sensors to operate as part of a timelapse array, each of the components described in Chapter 5 must be brought together in a full proof-of-concept study before the system could be used as a genuine early warning system for GLOFs. Using the lessons learned from this work, the implementation of such a study should be straightforward. Our sensors are designed to autonomously acquire data and, while further work is needed to improve the waterproof casing of these cameras, are ready to be placed into fixed positions at glacial lakes. Future work should look to improve data acquisition via point cloud stacking (Blanch et al., 2020) to ensure robust data can still be generated when weather conditions lead to sub-optimal acquisition. Automating many of the post-processing steps (e.g. following approaches laid out by Eastwood et al., 2019) will be the final research step needed in order to test the ability for Raspberry Pis to be used in an autonomous early warning system. Crucially, moving forward, this work should be co-designed by communities living in close proximity to glaciers to ensure that community knowledge and experience, which may have been overlooked in this thesis, is integrated into the design of any such system.

In light of recent deadly glacier collapse events, such as at Marmolada glacier in the Italian Alps (July 3rd 2022) and a glacier near Chamoli, Uttarakhand, India (7th February 2021), urgent work should be conducted on identifying topographic precursors to warn downstream communities of imminent danger. Potentially precursor seismic signals were detected at Chamoli the day prior to collapse, alongside cracking and wedging of the ice surface (Tiwari et al., 2022). In a ten-year monitoring study of an Italian glacier, where widening crevasses were also identified as a precursor to collapse events, the availability of real-time data was critical in the development of a warning system (Dematteis et al., 2021). The low-cost of Raspberry Pi cameras, their high-quality camera sensors, and their flexibility to adapt to a wide range of physical environments, means that they could become critical in the development of warning systems across mountain glaciers to protect communities from future glacier collapse events.

New remote sensing technologies show clear potential for monitoring mountain glaciers. Over the next decade, petabytes of usable data will be acquired over data-scarce mountain glacier regions to help us gain a deeper understanding of the way they are responding to climatic changes. Ideally, these data will be used by researchers and practitioners to inform water resource management charged with ensuring continued fresh water supply to the millions who rely on glaciers, and saving lives in the face of hazards from an increasingly unstable mountain cryosphere. We

stand at the dawn of this explosion of research potential, and principles of open science and collaboration with communities and stakeholders must be deeply intertwined in order to channel this potential into societal good.

Chapter 7

Conclusions

This thesis sought to identify novel remote sensing technologies and test their performance over mountain glaciers, focused on the Peruvian Cordillera Vilcanota.

Cloud computing and new, automated, pipelines can harness the ASTER and Landsat archives to quantify mass balance and area change over mountain glaciers. For data-scarce regions, these open access tools represent an opportunity to quantify mass balance, identify the key drivers of ice loss, and target action efforts to areas where ice loss is greatest. In the Cordillera Vilcanota, and neighbouring Cordilleras, these innovations in Chapter 3 led to the first region-wide quantification of mass balance, ELA change, and multi-decadal ice area change. As the climate continues to warm, the ELA will continue to rise and expose large, flat glaciers, such as the Quelccaya ice cap, to net ablation. Chapter 3 demonstrates that open access optical stereo datasets, such as ASTER, can play a key role in informing policymaking to manage the future threat of glacial hazards and ensure water security across the Cusco region.

New satellite altimetry missions represent a step-up in capability and can now be used to acquire regular elevation retrievals over mountain glaciers at an unprecedented spatial scale for this technique. While the open-loop tracking mode of Sentinel-3 yielded few elevation data points in rugged terrain, Chapter 4 shows promise that radar altimeters could, with modifications, be useful in studying mountain glaciers. With a higher resolution pseudo-DEM on-board and narrower cross-track separation, satellite radar altimetry could, in future missions, be used to measure interannual surface elevation change of small mountain glaciers worldwide. ICESat-2 acquires vastly more data over mountain glaciers at a finer (sub-metre) accuracy to TanDEM-X DEMs. Chapter 4 demonstrates the breadth of applications of ICESat-2 to monitoring the cryosphere of the Cordillera Vilcanota, from proglacial lake bathymetry and surface elevation change, to high spatial resolution estimates of mass balance where tracks are fortunate to cross over in repeat acquisitions. Chapter 4 demonstrates the opportunities granted by altimeters to monitor select glaciers across small mountain glaciers to assist policymakers in quantifying interannual surface elevation change.

The quality and capability of low-cost sensors means that affordable monitoring and hazard warning schemes can now be developed. Given most mountain glaciers are situated in the Global South, cost is often the biggest barrier towards creating schemes to monitor emerging hazards. Chapter 5 shows that low-cost Raspberry Pi camera sensors are an affordable, and accurate, alternative to more expensive DSLR cameras in glaciology fieldwork. Using an array of Raspberry Pi cameras to generate high resolution point clouds, low-cost SfM could provide regular 3D models of glacier calving margins at an accuracy similar to a UAV. Chapter 5 demonstrates that the affordability, flexibility, and durability of Raspberry Pi sensors makes them well-positioned to rival more expensive time-lapse systems without compromising data accuracy, for remote system management of glacial hazards.

Finally, this thesis demonstrates how the implementation of novel remote sensing technologies can support stakeholders within mountainous regions. Throughout, this thesis highlights the importance of open access datasets and toolkits with low technical barriers to use. Remote sensing technologies, from satellite missions to bespoke in-field sensors, can be integrated into management schemes over small mountain glaciers to support communities living in close proximity to rapidly melting ice.

References

Abdalati, W., Zwally, H.J., Bindschadler, R., Csatho, B., Farrell, S.L., Fricker, H.A., Harding, D., Kwok, R., Lefsky, M., Markus, T., Marshak, A., Neumann, T., Palm, S., Schutz, B., Smith, B., Spinhirne, J. and Webb, C. 2010. The ICESat-2 Laser Altimetry Mission. *Proceedings of the IEEE*. **98**(5), pp.735–751.

Abdel Jaber, W., Floricioiu, D., Rott, H. and Eineder, M. 2012. Dynamics of fast glaciers in the Patagonia Icefields derived from TerraSAR-X and TanDEM-X data *In*: *2012 IEEE International Geoscience and Remote Sensing Symposium*. Munich, Germany: IEEE, pp.3226–3229.

Addona, F., Sistilli, F., Romagnoli, C., Cantelli, L., Liserra, T. and Archetti, R. 2022. Use of a Raspberry-Pi Video Camera for Coastal Flooding Vulnerability Assessment: The Case of Riccione (Italy). *Water*. **14**(7), p.999.

Aggarwal, S., Mishra, P.K., Sumakar, K.V.S. and Chaturvedi, P. 2018. Landslide Monitoring System Implementing IOT Using Video Camera *In*: *2018 3rd International Conference for Convergence in Technology (I2CT)*. Pune, India: IEEE, pp.1–4.

Airbus 2020. Pléiades Neo Trusted Intelligence. *Airbus Intelligence*. [Online]. [Accessed 28 April 2020]. Available from: https://www.intelligence-airbusds.com/en/8671-pleiades-neo-trusted-intelligence.

Ali, M., Alfonsus Vlaskamp, J.H., Eddin, N.N., Falconer, B. and Oram, C. 2013. Technical development and socioeconomic implications of the Raspberry Pi as a learning tool in developing countries *In*: *2013 5th Computer Science and Electronic Engineering Conference (CEEC)*., pp.103–108.

Allison, E.A. 2015. The spiritual significance of glaciers in an age of climate change. *WIREs Climate Change*. **6**(5), pp.493–508.

Altena, B. and Kääb, A. 2017. Glacier ice loss monitored through the Planet cubesat constellation *In*: *2017 9th International Workshop on the Analysis of Multitemporal Remote Sensing Images (MultiTemp)*. Brugge, Belgium: IEEE, pp.1–4.

Alzahrani, S.M. 2017. Sensing for the Internet of Things and Its Applications *In*: *2017 5th International Conference on Future Internet of Things and Cloud Workshops (FiCloudW)*. Prague: IEEE, pp.88–92.

Ambrosi, C., Strozzi, T., Scapozza, C. and Wegmüller, U. 2018. Landslide hazard assessment in the Himalayas (Nepal and Bhutan) based on Earth-Observation data. *Engineering Geology*. **237**, pp.217–228.

ANA 2021. Reserva hídrica en los glaciares del Perú. *Repositorio Institucional - ANA*.

Anandakrishnan, S., Bilén, S.G., Urbina, J.V., Bock, R.G., Burkett, P.G. and Portelli, J.P. 2022. The geoPebble System: Design and Implementation of a Wireless Sensor Network of GPS-Enabled Seismic Sensors for the Study of Glaciers and Ice Sheets. *Geosciences*. **12**(1), p.17.

Armstrong, L., Lacelle, D., Fraser, R.H., Kokelj, S. and Knudby, A. 2018. Thaw slump activity measured using stationary cameras in time-lapse and Structure-from-Motion photogrammetry. *Arctic Science*. **4**(4), pp.827–845.

Arnold, N.S., Rees, W.G., Hodson, A.J. and Kohler, J. 2006. Topographic controls on the surface energy balance of a high Arctic valley glacier. *Journal of Geophysical Research*. **111**(F2), p.F02011.

Ashraf, A., Naz, R. and Roochi, R. 2012. Monitoring and Estimation of Glacial Resource of Azad Jammu and Kashmir Using Remote Sensing and GIS Techniques. *Pakistan Journal of Meteorology*. **8**(16), p.11.

Babbel, B.J., Parrish, C.E. and Magruder, L.A. 2021. ICESat-2 Elevation Retrievals in Support of Satellite-Derived Bathymetry for Global Science Applications. *Geophysical Research Letters*. **48**(5), e2020GL090629.

Bajracharya, S.R. and Mool, P. 2009. Glaciers, glacial lakes and glacial lake outburst floods in the Mount Everest region, Nepal. *Annals of Glaciology*. **50**(53), pp.81–86.

Ballesteros-Cánovas, J.A., Trappmann, D., Madrigal-González, J., Eckert, N. and Stoffel, M. 2018. Climate warming enhances snow avalanche risk in the Western Himalayas. *Proceedings of the National Academy of Sciences*. **115**(13), pp.3410–3415.

Baltsavias, E.P., Favey, E., Bauder, A., Bosch, H. and Pateraki, M. 2001. Digital Surface Modelling by Airborne Laser Scanning and Digital Photogrammetry for Glacier Monitoring. *The Photogrammetric Record*. **17**(98), pp.243–273.

Bamber, J.L. and Rivera, A. 2007. A review of remote sensing methods for glacier mass balance determination. *Global and Planetary Change*. **59**(1–4), pp.138–148.

Baraer, M., Mark, B.G., McKenzie, J.M., Condom, T., Bury, J., Huh, K.-I., Portocarrero, C., Gómez, J. and Rathay, S. 2012. Glacier recession and water resources in Peru's Cordillera Blanca. *Journal of Glaciology*. **58**(207), pp.134–150.

Bash, E., Moorman, B. and Gunther, A. 2018. Detecting Short-Term Surface Melt on an Arctic Glacier Using UAV Surveys. *Remote Sensing*. **10**(10), p.1547.

Bash, E.A. and Moorman, B.J. 2020. Surface melt and the importance of water flow – an analysis based on high-resolution unmanned aerial vehicle (UAV) data for an Arctic glacier. *The Cryosphere*. **14**(2), pp.549–563.

Baumhoer, C.A., Dietz, A.J., Kneisel, C. and Kuenzer, C. 2019a. Automated Extraction of Antarctic Glacier and Ice Shelf Fronts from Sentinel-1 Imagery Using Deep Learning. *Remote Sensing*. **11**(21), p.2529.

Baumhoer, C.A., Dietz, A.J., Kneisel, C. and Kuenzer, C. 2019b. Automated Extraction of Antarctic Glacier and Ice Shelf Fronts from Sentinel-1 Imagery Using Deep Learning. *Remote Sensing*. **11**(21), p.2529.

Beckett, K., Tyc, G. and Fox, P. 2017. Innovative technological advancements in the development and exploitation of a dual-band spaceborne SAR-XL system *In*: *2017 IEEE International Geoscience and Remote Sensing Symposium (IGARSS)*. Fort Worth, TX: IEEE, pp.3858–3861.

Bemis, S.P., Micklethwaite, S., Turner, D., James, M.R., Akciz, S., Thiele, S.T. and Bangash, H.A. 2014. Ground-based and UAV-Based photogrammetry: A multi-scale, high-resolution mapping tool for structural geology and paleoseismology. *Journal of Structural Geology*. **69**, pp.163–178.

Beniston, M. 2012. Impacts of climatic change on water and associated economic activities in the Swiss Alps. *Journal of Hydrology*. **412–413**, pp.291–296.

Beniston, M. and Stoffel, M. 2014. Assessing the impacts of climatic change on mountain water resources. *Science of The Total Environment*. **493**, pp.1129–1137.

Benn, D.I., Warren, C.R. and Mottram, R.H. 2007. Calving processes and the dynamics of calving glaciers. *Earth-Science Reviews*. **82**(3), pp.143–179.

Berthier, E., Arnaud, Y., Kumar, R., Ahmad, S., Wagnon, P. and Chevallier, P. 2007. Remote sensing estimates of glacier mass balances in the Himachal Pradesh (Western Himalaya, India). *Remote Sensing of Environment*. **108**(3), pp.327–338.

Berthier, E., Arnaud, Y., Vincent, C. and Rémy, F. 2006. Biases of SRTM in high-mountain areas: Implications for the monitoring of glacier volume changes. *Geophysical Research Letters*. **33**(8), p.L08502.

Berthier, E., Cabot, V., Vincent, C. and Six, D. 2016. Decadal Region-Wide and Glacier-Wide Mass Balances Derived from Multi-Temporal ASTER Satellite Digital Elevation Models. Validation over the Mont-Blanc Area. *Frontiers in Earth Science*. **4**.

Berthier, E., Vadon, H., Baratoux, D., Arnaud, Y., Vincent, C., Feigl, K.L., Rémy, F. and Legrésy, B. 2005. Surface motion of mountain glaciers derived from satellite optical imagery. *Remote Sensing of Environment*. **95**(1), pp.14–28.

Beyer, R.A., Alexandrov, O. and McMichael, S. 2018. The Ames Stereo Pipeline: NASA's Open Source Software for Deriving and Processing Terrain Data. *Earth and Space Science*. **5**(9), pp.537–548.

Bhardwaj, A., Sam, L., Akanksha, Martín-Torres, F.J. and Kumar, R. 2016. UAVs as remote sensing platform in glaciology: Present applications and future prospects. *Remote Sensing of Environment*. **175**, pp.196–204.

Biancamaria, S., Lettenmaier, D.P. and Pavelsky, T.M. 2016. The SWOT Mission and Its Capabilities for Land Hydrology. *Surveys in Geophysics*. **37**(2), pp.307–337.

Biancamaria, S., Schaedele, T., Blumstein, D., Frappart, F., Boy, F., Desjonquères, J.-D., Pottier, C., Blarel, F. and Niño, F. 2018. Validation of Jason-3 tracking modes over French rivers. *Remote Sensing of Environment*. **209**, pp.77–89.

Bigelow, D.G., Flowers, G.E., Schoof, C.G., Mingo, L.D.B., Young, E.M. and Connal, B.G. 2020. The Role of Englacial Hydrology in the Filling and Drainage of an Ice-Dammed Lake, Kaskawulsh Glacier, Yukon, Canada. *Journal of Geophysical Research: Earth Surface*. **125**(2), e2019JF005110.

Bindschadler, R., Choi, H., Shuman, C. and Markus, T. 2005. Detecting and measuring new snow accumulation on ice sheets by satellite remote sensing. *Remote Sensing of Environment*. **98**(4), pp.388–402.

Birkett, C.M. and Beckley, B. 2010. Investigating the Performance of the Jason-2/OSTM Radar Altimeter over Lakes and Reservoirs. *Marine Geodesy*. **33**(sup1), pp.204–238.

Bisschop, T. 2021. *Detecting Alpine glacier changes from a combination of ICESAT-2 and GEDI data*.[Online] Delft: Delft University of Technology. [Accessed 10 June 2022]. Available from: http://resolver.tudelft.nl/uuid:0f1a8e3e-5df8-484f-8a6d-ba94d8a26a56.

Blanch, X., Abellan, A. and Guinau, M. 2020. Point Cloud Stacking: A Workflow to Enhance 3D Monitoring Capabilities Using Time-Lapse Cameras. *Remote Sensing*. **12**(8), p.1240.

Blanch, X., Abellán, A. and Guinau, M. 2019. Rockfall monitoring at a high-temporal rate using cost-effective photogrammetric systems *In*: *EGU General Assembly Conference Abstracts*. EGU General Assembly Conference Abstracts., p.11591.

Bolch, T. 2007. Climate change and glacier retreat in northern Tien Shan (Kazakhstan/Kyrgyzstan) using remote sensing data. *Global and Planetary Change*. **56**(1), pp.1–12.

Bolch, T., Buchroithner, M., Pieczonka, T. and Kunert, A. 2008. Planimetric and volumetric glacier changes in the Khumbu Himal, Nepal, since 1962 using Corona, Landsat TM and ASTER data. *Journal of Glaciology*. **54**(187), pp.592–600.

Bolch, T., Menounos, B. and Wheate, R. 2010. Landsat-based inventory of glaciers in western Canada, 1985–2005. *Remote Sensing of Environment*. **114**(1), pp.127–137.

Bolibar, J., Rabatel, A., Gouttevin, I., Galiez, C., Condom, T. and Sauquet, E. 2020. Deep learning applied to glacier evolution modelling. *The Cryosphere*. **14**(2), pp.565–584.

Bonekamp, P.N.J., van Heerwaarden, C.C., Steiner, J.F. and Immerzeel, W.W. 2020. Using 3D turbulence-resolving simulations to understand the impact of surface properties on the energy balance of a debris-covered glacier. *The Cryosphere*. **14**(5), pp.1611–1632.

Braithwaite, R.J. and Raper, S.C.B. 2009. Estimating equilibrium-line altitude (ELA) from glacier inventory data. *Annals of Glaciology*. **50**(53), pp.127–132.

Braun, M.H., Malz, P., Sommer, C., Farías-Barahona, D., Sauter, T., Casassa, G., Soruco, A., Skvarca, P. and Seehaus, T.C. 2019. Constraining glacier elevation and mass changes in South America. *Nature Climate Change*. **9**(2), pp.130–136.

Brecher, H.H. and Thompson, L.G. 1993. Measurement of the retreat of Qori Kalis glacier in the tropical Andes of Peru by terrestrial photogrammetry. *Photogrammetric Engineering and Remote Sensing*. **59**(6).

Brenning, A. 2009. Benchmarking classifiers to optimally integrate terrain analysis and multispectral remote sensing in automatic rock glacier detection. *Remote Sensing of Environment*. **113**(1), pp.239–247.

Brown, C.F., Brumby, S.P., Guzder-Williams, B., Birch, T., Hyde, S.B., Mazzariello, J., Czerwinski, W., Pasquarella, V.J., Haertel, R., Ilyushchenko, S., Schwehr, K., Weisse, M., Stolle, F., Hanson, C., Guinan, O., Moore, R. and Tait, A.M. 2022. Dynamic World, Near real-time global 10 m land use land cover mapping. *Scientific Data*. **9**(1), p.251.

Brügger, A., Tobias, R. and Monge-Rodríguez, F.S. 2021. Public Perceptions of Climate Change in the Peruvian Andes. *Sustainability*. **13**(5), p.2677.

Brun, F., Berthier, E., Wagnon, P., Kääb, A. and Treichler, D. 2017. A spatially resolved estimate of High Mountain Asia glacier mass balances from 2000 to 2016. *Nature Geoscience*. **10**(9), pp.668–673.

Brun, F., Buri, P., Miles, E.S., Wagnon, P., Steiner, J., Berthier, E., Ragettli, S., Kraaijenbrink, P., Immerzeel, W.W. and Pellicciotti, F. 2016. Quantifying volume loss from ice cliffs on debris-covered glaciers using high-resolution terrestrial and aerial photogrammetry. *Journal of Glaciology*. **62**(234), pp.684–695.

Brun, F., Wagnon, P., Berthier, E., Shea, J.M., Immerzeel, W.W., Kraaijenbrink, P.D.A., Vincent, C., Reverchon, C., Shrestha, D. and Arnaud, Y. 2018. Ice cliff contribution to the tongue-wide ablation of Changri Nup Glacier, Nepal, central Himalaya. *The Cryosphere*. **12**(11), pp.3439–3457.

Brunt, K.M., Neumann, T.A. and Smith, B.E. 2019. Assessment of ICESat-2 Ice Sheet Surface Heights, Based on Comparisons Over the Interior of the Antarctic Ice Sheet. *Geophysical Research Letters*. **46**(22), pp.13072–13078.

Brunt, K.M., Smith, B.E., Sutterley, T.C., Kurtz, N.T. and Neumann, T.A. 2021. Comparisons of Satellite and Airborne Altimetry With Ground-Based Data From the Interior of the Antarctic Ice Sheet. *Geophysical Research Letters*. **48**(2), e2020GL090572.

Bühler, Y., Adams, M.S., Bösch, R. and Stoffel, A. 2016. Mapping snow depth in alpine terrain with unmanned aerial systems (UASs): potential and limitations. *The Cryosphere*. **10**(3), pp.1075–1088.

Bunce, C., Nienow, P., Sole, A., Cowton, T. and Davison, B. 2021. Influence of glacier runoff and near-terminus subglacial hydrology on frontal ablation at a large Greenlandic tidewater glacier. *Journal of Glaciology*. **67**(262), pp.343–352.

Buri, P., Pellicciotti, F., Steiner, J.F., Miles, E.S. and Immerzeel, W.W. 2016. A grid-based model of backwasting of supraglacial ice cliffs on debris-covered glaciers. *Annals of Glaciology*. **57**(71), pp.199–211.

Burns, P. and Nolin, A. 2014. Using atmospherically-corrected Landsat imagery to measure glacier area change in the Cordillera Blanca, Peru from 1987 to 2010. *Remote Sensing of Environment*. **140**, pp.165–178.

Bury, J., Mark, B.G., Carey, M., Young, K.R., McKenzie, J.M., Baraer, M., French, A. and Polk, M.H. 2013. New Geographies of Water and Climate Change in Peru: Coupled Natural and Social Transformations in the Santa River Watershed. *Annals of the Association of American Geographers*. **103**(2), pp.363–374.

Bury, J.T., Mark, B.G., McKenzie, J.M., French, A., Baraer, M., Huh, K.I., Zapata Luyo, M.A. and Gómez López, R.J. 2011. Glacier recession and human vulnerability in the Yanamarey watershed of the Cordillera Blanca, Peru. *Climatic Change*. **105**(1), pp.179–206.

Buytaert, W., Moulds, S., Acosta, L., Bièvre, B.D., Olmos, C., Villacis, M., Carolina Tovar and Verbist, K.M.J. 2017. Glacial melt content of water use in the tropical Andes. *Environmental Research Letters*. **12**(11), p.114014.

Campi, T., Cruciani, S., Maradei, F. and Feliziani, M. 2019. Innovative Design of Drone Landing Gear Used as a Receiving Coil in Wireless Charging Application. *Energies*. **12**(18), p.3483.

Carabajal, C.C. and Boy, J.-P. 2021. Lake and reservoir volume variations in South America from radar altimetry, ICESat laser altimetry, and GRACE time-variable gravity. *Advances in Space Research*. **68**(2), pp.652–671.

Carey, M. 2005. Living and dying with glaciers: people's historical vulnerability to avalanches and outburst floods in Peru. *Global and Planetary Change*. **47**(2), pp.122–134.

Carey, M., French, A. and O'Brien, E. 2012. Unintended effects of technology on climate change adaptation: an historical analysis of water conflicts below Andean Glaciers. *Journal of Historical Geography*. **38**(2), pp.181–191.

Carey, M., Garrard, R., Cecale, C., Buytaert, W., Huggel, C. and Vuille, M. 2016. Escalando por la Ciencia y el Hielo: De Hans Kinzl y Montañismo- Glaciología a Ciencia Ciudadana en la Cordillera Blanca. *Revista de Glaciares y Ecosistemas de Montaña*. (1).

Carey, M., Huggel, C., Bury, J., Portocarrero, C. and Haeberli, W. 2012. An integrated socio-environmental framework for glacier hazard management and climate change adaptation: lessons from Lake 513, Cordillera Blanca, Peru. *Climatic Change*. **112**(3), pp.733–767.

Carrivick, J.L. and Tweed, F.S. 2016. A global assessment of the societal impacts of glacier outburst floods. *Global and Planetary Change*. **144**, pp.1–16.

Carvallo, R., Llanos, P., Noceti, R. and Casassa, G. 2017. Real-time transmission of time-lapse imagery of glaciers in the southern Andes *In*: *2017 First IEEE International Symposium of Geoscience and Remote Sensing (GRSS-CHILE)*., pp.1–3.

Cervone, G., Sava, E., Huang, Q., Schnebele, E., Harrison, J. and Waters, N. 2016. Using Twitter for tasking remote-sensing data collection and damage assessment: 2013 Boulder flood case study. *International Journal of Remote Sensing*. **37**(1), pp.100–124.

Cesare, K., Skeele, R., Soo-Hyun Yoo, Yawei Zhang and Hollinger, G. 2015. Multi-UAV exploration with limited communication and battery *In*: *2015 IEEE International Conference on Robotics and Automation (ICRA)* [Online]. Seattle, WA, USA: IEEE, pp.2230–2235. [Accessed 11 February 2020]. Available from: http://ieeexplore.ieee.org/document/7139494/.

Chakraborty, S., Das, S., Rai, N., Patra, A., Dhar, A., Sadhu, A., Gautam, B., Verma, P., Singh, A., Sherpa, C. and Karn, L. 2019. Development of UAV Based Glacial Lake Outburst Monitoring System *In*: *IGARSS 2019 - 2019 IEEE International Geoscience and Remote Sensing Symposium*. Yokohama, Japan: IEEE, pp.9372–9375.

Chambers, J.R., Smith, M.W., Quincey, D.J., Carrivick, J.L., Ross, A.N. and James, M.R. 2019. Glacial aerodynamic roughness estimates: uncertainty, sensitivity and precision in field measurements. *Journal of Geophysical Research: Earth Surface*., p.2019JF005167.

Chan, K., Schillereff, D.N., Baas, A.C., Chadwick, M.A., Main, B., Mulligan, M., O'Shea, F.T., Pearce, R., Smith, T.E., van Soesbergen, A., Tebbs, E. and Thompson, J. 2020. Low-cost electronic sensors for environmental research: Pitfalls and opportunities. *Progress in Physical Geography: Earth and Environment*. **45**(3), pp.305–338.

Chandler, B.M.P., Evans, D.J.A., Chandler, S.J.P., Ewertowski, M.W., Lovell, H., Roberts, D.H., Schaefer, M. and Tomczyk, A.M. 2020. The glacial landsystem of Fjallsjökull, Iceland: Spatial and temporal evolution of process-form regimes at an active temperate glacier. *Geomorphology*. **361**, p.107192.

Che, Y., Wang, S., Yi, S., Wei, Y. and Cai, Y. 2020. Summer Mass Balance and Surface Velocity Derived by Unmanned Aerial Vehicle on Debris-Covered Region of Baishui River Glacier No. 1, Yulong Snow Mountain. *Remote Sensing*. **12**(20), p.3280.

Chen, F., Zhang, M., Tian, B. and Li, Z. 2017. Extraction of Glacial Lake Outlines in Tibet Plateau Using Landsat 8 Imagery and Google Earth Engine. *IEEE Journal of Selected Topics in Applied Earth Observations and Remote Sensing*. **10**(9), pp.4002–4009.

Chen, J.L., Wilson, C.R. and Tapley, B.D. 2013. Contribution of ice sheet and mountain glacier melt to recent sea level rise. *Nature Geoscience*. **6**(7), pp.549–552.

Chen, W., Yao, T., Zhang, G., Li, F., Zheng, G., Zhou, Y. and Xu, F. 2022. Towards ice-thickness inversion: an evaluation of global digital elevation models (DEMs) in the glacierized Tibetan Plateau. *The Cryosphere*. **16**(1), pp.197–218.

Cheng, D., Hayes, W., Larour, E., Mohajerani, Y., Wood, M., Velicogna, I. and Rignot, E. 2020. Calving Front Machine (CALFIN): glacial termini dataset and automated deep learning extraction method for Greenland, 1972–2019. *The Cryosphere*. **15**, pp.1663–1675.

Chevallier, P., Pouyaud, B., Suarez, W. and Condom, T. 2011. Climate change threats to environment in the tropical Andes: glaciers and water resources. *Regional Environmental Change*. **11**(1), pp.179–187.

Chudley, T.R., Christoffersen, P., Doyle, S.H., Abellan, A. and Snooke, N. 2019. High-accuracy UAV photogrammetry of ice sheet dynamics with no ground control. *The Cryosphere*. **13**(3), pp.955–968.

Church, G., Bauder, A., Grab, M., Rabenstein, L., Singh, S. and Maurer, H. 2019. Detecting and characterising an englacial conduit network within a temperate Swiss glacier using active seismic, ground penetrating radar and borehole analysis. *Annals of Glaciology*. **60**(79), pp.193–205.

Church, J.A., Clark, P.U., Cazenave, A., Gregory, J.M., Jevrejeva, S., Levermann, A., Merrifield, M.A., Milne, G.A., Nerem, R.S., Nunn, P.D., Payne, A.J., Pfeffer, W.T., Stammer, D. and Unnikrishnan, A.S. 2013. Sea Level Change *In*: T. F. Stocker, D. Qin, G.-K. Plattner, M. Tignor, S. K. Allen, J. Boschung, A. Nauels, Y. Xia, V. Bex and P. M. Midgley, eds. *Climate Change 2013: The Physical Science Basis. Contribution of Working Group I to the Fifth Assessment Report of the Intergovernmental Panel on Climate Change*. Cambridge, United Kingdom and New York, NY, USA: Cambridge University Press, pp.1137–1216.

Clifford, D. 2010. Global estimates of snow water equivalent from passive microwave instruments: history, challenges and future developments. *International Journal of Remote Sensing*. **31**(14), pp.3707–3726.

Coca, E. and Popa, V. 2012. A Practical Solution for Time Synchronization in Wireless Sensor Networks. *Advances in Electrical and Computer Engineering*. **12**(4), pp.57–62.

Colonia, D., Torres, J., Haeberli, W., Schauwecker, S., Braendle, E., Giraldez, C. and Cochachin, A. 2017. Compiling an Inventory of Glacier-Bed Overdeepenings and Potential New Lakes in De-Glaciating Areas of the Peruvian Andes: Approach, First Results, and Perspectives for Adaptation to Climate Change. *Water*. **9**(5), p.336.

Condom, T., Coudrain, A., Sicart, J.E. and Théry, S. 2007. Computation of the space and time evolution of equilibrium-line altitudes on Andean glaciers (10°N–55°S). *Global and Planetary Change*. **59**(1), pp.189–202.

Condom, T., Escobar, M., Purkey, D., Pouget, J.C., Suarez, W., Ramos, C., Apaestegui, J., Tacsi, A. and Gomez, J. 2012. Simulating the implications of glaciers' retreat for water management: a case study in the Rio Santa basin, Peru. *Water International*. **37**(4), pp.442–459.

Cook, S.J. and Quincey, D.J. 2015. Estimating the volume of Alpine glacial lakes. *Earth Surface Dynamics*. **3**(4), pp.559–575.

Cooley, S., Smith, L., Stepan, L. and Mascaro, J. 2017. Tracking Dynamic Northern Surface Water Changes with High-Frequency Planet CubeSat Imagery. *Remote Sensing*. **9**(12), p.1306.

Copland, L., Pope, S., Bishop, M.P., Shroder, J.F., Clendon, P., Bush, A., Kamp, U., Bae Seong, Y. and Owen, L.A. 2009. Glacier velocities across the central Karakoram. *Annals of Glaciology*. **50**(52), pp.41–49.

Covey, R.A. 2006. *How the Incas Built Their Heartland: State Formation and the Innovation of Imperial Strategies in the Sacred Valley, Peru*. University of Michigan Press.

Crétaux, J.-F., Abarca-del-Río, R., Bergé-Nguyen, M., Arsen, A., Drolon, V., Clos, G. and Maisongrande, P. 2016. Lake Volume Monitoring from Space. *Surveys in Geophysics*. **37**(2), pp.269–305.

Dall'Asta, E., Forlani, G., Roncella, R., Santise, M., Diotri, F. and Morra di Cella, U. 2017. Unmanned Aerial Systems and DSM matching for rock glacier monitoring. *ISPRS Journal of Photogrammetry and Remote Sensing*. **127**, pp.102–114.

Datta, R.T. and Wouters, B. 2021. Supraglacial lake bathymetry automatically derived from ICESat-2 constraining lake depth estimates from multi-source satellite imagery. *The Cryosphere*. **15**(11), pp.5115–5132.

Davidson, M., Chini, M., Dierking, W., Djavidnia, S., Haarpaintner, J., Hajduch, G., Laurin, G.V., Lavalle, M., Martinez, C.L., Nagler, T., Pierdicca, N. and Su, B. 2019. *Copernicus L-band SAR Mission Requirements Document*. European Space Agency.

Dehecq, A., Gourmelen, N., Gardner, A.S., Brun, F., Goldberg, D., Nienow, P.W., Berthier, E., Vincent, C., Wagnon, P. and Trouvé, E. 2019. Twenty-first century glacier slowdown driven by mass loss in High Mountain Asia. *Nature Geoscience*. **12**(1), pp.22–27.

Dehecq, A., Gourmelen, N., Shepherd, A. and Trouvé, E. 2013. *Evaluation of CryoSAT-2 for height retrieval over the Himalayan range* [Online]. Dresden, Germany. Available from: https://hal.archives-ouvertes.fr/hal-00973393.

Del Aguila, A. 2015. *Estudio sobre la situación laboral de las mujeres indígenas en el Perú* [Online]. Lima: International Labour Organization. Available from: https://www.ilo.org/wcmsp5/groups/public/---dgreports/---gender/documents/publication/wcms_546285.pdf.

Dell, R., Carr, R., Phillips, E. and Russell, A.J. 2019. Response of glacier flow and structure to proglacial lake development and climate at Fjallsjökull, south-east Iceland. *Journal of Glaciology*. **65**(250), pp.321–336.

Dematteis, N., Giordan, D., Troilo, F., Wrzesniak, A. and Godone, D. 2021. Ten-Year Monitoring of the Grandes Jorasses Glaciers Kinematics. Limits, Potentialities, and Possible Applications of Different Monitoring Systems. *Remote Sensing*. **13**(15), p.3005.

Deng, X. and Featherstone, W.E. 2006. A coastal retracking system for satellite radar altimeter waveforms: Application to ERS-2 around Australia. *Journal of Geophysical Research: Oceans*. **111**(C6).

Denis, G., Claverie, A., Pasco, X., Darnis, J.-P., de Maupeou, B., Lafaye, M. and Morel, E. 2017. Towards disruptions in Earth observation? New Earth Observation systems and markets evolution: Possible scenarios and impacts. *Acta Astronautica*. **137**, pp.415–433.

Deschamps-Berger, C., Gascoin, S., Berthier, E., Deems, J., Gutmann, E., Dehecq, A., Shean, D. and Dumont, M. 2020. Snow depth mapping from stereo satellite imagery in mountainous terrain: evaluation using airborne laser-scanning data. *The Cryosphere*. **14**(9), pp.2925–2940.

Di Mauro, B., Baccolo, G., Garzonio, R., Giardino, C., Massabò, D., Piazzalunga, A., Rossini, M. and Colombo, R. 2017. Impact of impurities and cryoconite on the optical properties of the Morteratsch Glacier (Swiss Alps). *The Cryosphere*. **11**(6), pp.2393–2409.

Di Mauro, B., Fava, F., Ferrero, L., Garzonio, R., Baccolo, G., Delmonte, B. and Colombo, R. 2015. Mineral dust impact on snow radiative properties in the European Alps combining ground, UAV, and satellite observations: Mineral dust on snow in the Alps. *Journal of Geophysical Research: Atmospheres*. **120**(12), pp.6080–6097.

Dietz, A.J., Kuenzer, C. and Dech, S. 2015. Global SnowPack: a new set of snow cover parameters for studying status and dynamics of the planetary snow cover extent. *Remote Sensing Letters*. **6**(11), pp.844–853.

Donlon, C., Berruti, B., Buongiorno, A., Ferreira, M.-H., Féménias, P., Frerick, J., Goryl, P., Klein, U., Laur, H., Mavrocordatos, C., Nieke, J., Rebhan, H., Seitz, B., Stroede, J. and Sciarra, R. 2012. The Global Monitoring for Environment and Security (GMES) Sentinel-3 mission. *Remote Sensing of Environment*. **120**, pp.37–57.

Donlon, C.J., Cullen, R., Giulicchi, L., Vuilleumier, P., Francis, C.R., Kuschnerus, M., Simpson, W., Bouridah, A., Caleno, M., Bertoni, R., Rancaño, J., Pourier, E., Hyslop, A., Mulcahy, J., Knockaert, R., Hunter, C., Webb, A., Fornari, M., Vaze, P., Brown, S., Willis, J., Desai, S., Desjonqueres, J.-D., Scharroo, R., Martin-Puig, C., Leuliette, E., Egido, A., Smith, W.H.F., Bonnefond, P., Le Gac, S., Picot, N. and Tavernier, G. 2021. The Copernicus Sentinel-6 mission: Enhanced continuity of satellite sea level measurements from space. *Remote Sensing of Environment*. **258**, p.112395.

Dozier, J. 1989. Spectral signature of alpine snow cover from the landsat thematic mapper. *Remote Sensing of Environment*. **28**, pp.9–22.

Drenkhan, F., Guardamino, L., Huggel, C. and Frey, H. 2018. Current and future glacier and lake assessment in the deglaciating Vilcanota-Urubamba basin, Peruvian Andes. *Global and Planetary Change*. **169**, pp.105–118.

Drenkhan, F., Huggel, C., Guardamino, L. and Haeberli, W. 2019. Managing risks and future options from new lakes in the deglaciating Andes of Peru: The example of the Vilcanota-Urubamba basin. *Science of The Total Environment*. **665**, pp.465–483.

Drenkhan, F., Huggel, C., Salzmann, N., Giráldez, C., Suarez, W., Rohrer, M., Molina, E., Montoya, N. and Miñan, F. 2014. Present and future water resources supply and demand in the Central Andes of Peru: a comprehensive review with focus on the Cordillera Vilcanota *In*: Vienna, Austria, p.13194. [Accessed 2 March 2022]. Available from: https://ui.adsabs.harvard.edu/abs/2014EGUGA..1613194D.

Duchossois, G., P., Strobl, P., Toumazou, V., Antunes, S., Bartsch, A., Diehl, T., Dinessen, F., Eriksson, P., Garric, G., Houssais, M.-N., Jindrova, M., Munoz-Sabater, J., Nagler, T. and Nordbeck, O. 2018. *User requirements for a Copernicus polar mission. Phase 1 report, User requirements and priorities.* [Online]. Luxembourg: Publications Office of the European Union. [Accessed 19 June 2022]. Available from: https://data.europa.eu/doi/10.2760/22832.

Dussaillant, I., Berthier, E. and Brun, F. 2018. Geodetic Mass Balance of the Northern Patagonian Icefield from 2000 to 2012 Using Two Independent Methods. *Frontiers in Earth Science*. **6**, p.8.

Dussaillant, I., Berthier, E., Brun, F., Masiokas, M., Hugonnet, R., Favier, V., Rabatel, A., Pitte, P. and Ruiz, L. 2019. Two decades of glacier mass loss along the Andes. *Nature Geoscience*. **12**(10), pp.802–808.

Dyurgerov, M.B. and Meier, M.F. 2000. Twentieth century climate change: Evidence from small glaciers. *Proceedings of the National Academy of Sciences*. **97**(4), pp.1406–1411.

Eastwood, J., Sims-Waterhouse, D., Weir, R., Piano, S. and Leach, R.K. 2019. Autonomous close-range photogrammetry using machine learning *In*: *Proc. ISMTII2019*. Niigata, Japan.

Eastwood, J., Zhang, H., Isa, M., Sims-Waterhouse, D., Leach, R. and Piano, S. 2020. Smart photogrammetry for three-dimensional shape measurement *In*: *Optics and Photonics for Advanced Dimensional Metrology*. SPIE, pp.43–52.

Eddy, I.M.S., Gergel, S.E., Coops, N.C., Henebry, G.M., Levine, J., Zerriffi, H. and Shibkov, E. 2017. Integrating remote sensing and local ecological knowledge to monitor rangeland dynamics. *Ecological Indicators*. **82**, pp.106–116.

Egli, L. and Jonas, T. 2009. Hysteretic dynamics of seasonal snow depth distribution in the Swiss Alps. *Geophysical Research Letters*. **36**(2), pp.1–5.

Eguiraun, H., Barrenetxea, L., Amezua, X., Casquero, O., Garcia-Fernandez, R.I. and Tuduri, I. 2020. A Custom-Made Photogrammetry Scanner to Support Paediatric Surgery *In*: F. Cavas-Martínez, F. Sanz-Adan, P. Morer Camo, R. Lostado Lorza and J. Santamaría Peña, eds. *Advances in Design Engineering*. Lecture Notes in Mechanical Engineering. Cham: Springer International Publishing, pp.193–201.

Eltner, A., Kaiser, A., Abellan, A. and Schindewolf, M. 2017. Time lapse structure-from-motion photogrammetry for continuous geomorphic monitoring: Time-lapse photogrammetry for continuous geomorphic monitoring. *Earth Surface Processes and Landforms*. **42**(14), pp.2240–2253.

Emmer, A., Merkl, S. and Mergili, M. 2015. Spatiotemporal patterns of high-mountain lakes and related hazards in western Austria. *Geomorphology*. **246**, pp.602–616.

Emmer, A. and Vilímek, V. 2013. Review Article: Lake and breach hazard assessment for moraine-dammed lakes: an example from the Cordillera Blanca (Peru). *Natural Hazards and Earth System Sciences*. **13**(6), pp.1551–1565.

Ewert, H., Groh, A. and Dietrich, R. 2012. Volume and mass changes of the Greenland ice sheet inferred from ICESat and GRACE. *Journal of Geodynamics*. **59–60**, pp.111–123.

Fahnestock, M., Scambos, T., Moon, T., Gardner, A., Haran, T. and Klinger, M. 2016. Rapid large-area mapping of ice flow using Landsat 8. *Remote Sensing of Environment*. **185**, pp.84–94.

Fair, Z., Flanner, M., Brunt, K.M., Fricker, H.A. and Gardner, A. 2020. Using ICESat-2 and Operation IceBridge altimetry for supraglacial lake depth retrievals. *The Cryosphere*. **14**(11), pp.4253–4263.

Falaschi, D., Lenzano, M.G., Villalba, R., Bolch, T., Rivera, A. and Lo Vecchio, A. 2019. Six Decades (1958–2018) of Geodetic Glacier Mass Balance in Monte San Lorenzo, Patagonian Andes. *Frontiers in Earth Science*. **7**, p.326.

Fallourd, R., Vernier, F., Friedt, J.-M., Martin, G., Trouvé, E., Moreau, L. and Nicolas, J.-M. 2010. Monitoring temperate glacier with high resolution automated digital cameras - Application to the Argentière glacier *In*: *PCV 2010, ISPRS Commission III Symposium*. Paris, France.

Farinotti, D., Round, V., Huss, M., Compagno, L. and Zekollari, H. 2019. Large hydropower and water-storage potential in future glacier-free basins. *Nature*. **575**(7782), pp.341–344.

Ferdoush, S. and Li, X. 2014. Wireless Sensor Network System Design Using Raspberry Pi and Arduino for Environmental Monitoring Applications. *Procedia Computer Science*. **34**, pp.103–110.

Fischer, L., Purves, R.S., Huggel, C., Noetzli, J. and Haeberli, W. 2012. On the influence of topographic, geological and cryospheric factors on rock avalanches and rockfalls in

high-mountain areas. *Natural Hazards and Earth System Sciences*. **12**(1), pp.241–254.

Fitzpatrick, A.A.W., Hubbard, A.L., Box, J.E., Quincey, D.J., van As, D., Mikkelsen, A.P.B., Doyle, S.H., Dow, C.F., Hasholt, B. and Jones, G.A. 2014. A decade (2002-2012) of supraglacial lake volume estimates across Russell Glacier, West Greenland. *The Cryosphere*. **8**(1), pp.107–121.

Fox, P., Tyc, G. and Beckett, K. 2017. The UrtheCast SAR-XL multi-band, multi-aperture spaceborne SAR system *In*: *2017 IEEE Radar Conference (RadarConf)* [Online]. Seattle, WA, USA: IEEE, pp.1761–1764. [Accessed 28 April 2020]. Available from: http://ieeexplore.ieee.org/document/7944492/.

Fox-Kemper, B., Hewitt, H.T., Xiao, C., Aðalgeirsdóttir, G., Drijfhout, S.S., Edwards, T.L., Golledge, N.R., Hemer, M., Kopp, R.E., Krinner, G., Mix, A., Notz, D., Nowicki, S., Nurhati, I.S., Ruiz, L., Sallée, J.-B., Slangen, A.B.A. and Yu, Y. 2021. *Ocean, cryosphere and sea level change*. IPCC.

Fugazza, D., Scaioni, M., Corti, M., D'Agata, C., Azzoni, R.S., Cernuschi, M., Smiraglia, C. and Diolaiuti, G.A. 2018. Combination of UAV and terrestrial photogrammetry to assess rapid glacier evolution and map glacier hazards. *Natural Hazards and Earth System Sciences*. **18**(4), pp.1055–1071.

Fujita, K., Sakai, A., Nuimura, T., Yamaguchi, S. and Sharma, R.R. 2009. Recent changes in Imja Glacial Lake and its damming moraine in the Nepal Himalaya revealed by *in situ* surveys and multi-temporal ASTER imagery. *Environmental Research Letters*. **4**(4), p.045205.

Fukui, H., Limlahapun, P. and Kameoka, T. 2008. Real time monitoring for Imja Glacial Lake in Himalaya — global warming front monitoring system *In*: *2008 SICE Annual Conference*. Chofu, Japan: IEEE, pp.2578–2581.

Fyffe, C.L., Potter, E., Fugger, S., Orr, A., Fatichi, S., Loarte, E., Medina, K., Hellström, R.Å., Bernat, M., Aubry-Wake, C., Gurgiser, W., Baker Perry, L., Suarez, W., Quincey, D.J. and Pellicciotti, F. 2021. The energy and mass balance of Peruvian glaciers. *Journal of Geophysical Research: Atmospheres*.

Gaffey, C. and Bhardwaj, A. 2020. Applications of Unmanned Aerial Vehicles in Cryosphere: Latest Advances and Prospects. *Remote Sensing*. **12**(6), p.948.

Gao, Q., Makhoul, E., Escorihuela, M.J., Zribi, M., Quintana Seguí, P., García, P. and Roca, M. 2019. Analysis of Retrackers' Performances and Water Level Retrieval over the Ebro River Basin Using Sentinel-3. *Remote Sensing*. **11**(6), p.718.

Gardelle, J., Berthier, E. and Arnaud, Y. 2012. Slight mass gain of Karakoram glaciers in the early twenty-first century. *Nature Geoscience*. **5**(5), pp.322–325.

Gardner, A., Lei, Y. and Agram, P.S. 2020. *autoRIFT (autonomous Repeat Image Feature Tracking)* [Online]. Zenodo. [Accessed 22 May 2020]. Available from: https://zenodo.org/record/3756192#.Xse-TjpKhPY.

Gardner, A.S., Fahnestock, M.A., Agram, P.S., Scambos, T., Nilsson, J., Paolo, F.S., Walker, C.C., Meyer, F.J. and Dehecq, A. 2018. ITS_LIVE: A new NASA MEaSUReS initiative to track the movement of the world's ice *In*: *AGU Fall Meeting Abstracts*., pp.C14A-02B.

Garsthagen, R. 2014. An Open Source, Low-Cost, Multi Camera Full-Body 3D Scanner *In*: *Proceedings of the 5th International Conference on 3D Body Scanning Technologies, Lugano, Switzerland, 21-22 October 2014*. Lugano, Switzerland: Hometrica Consulting - Dr. Nicola D'Apuzzo, pp.174–183.

Gascoin, S., Grizonnet, M., Bouchet, M., Salgues, G. and Hagolle, O. 2019. Theia Snow collection: high-resolution operational snow cover maps from Sentinel-2 and Landsat-8 data. *Earth System Science Data*. **11**(2), pp.493–514.

Georges, C. 2004. 20th-Century Glacier Fluctuations in the Tropical Cordillera Blanca, Perú. *Arctic, Antarctic, and Alpine Research*. **36**(1), pp.100–107.

Giordan, D., Allasia, P., Dematteis, N., Dell'Anese, F., Vagliasindi, M. and Motta, E. 2016. A Low-Cost Optical Remote Sensing Application for Glacier Deformation Monitoring in an Alpine Environment. *Sensors (Basel, Switzerland)*. **16**(10), p.1750.

Giordan, D., Dematteis, N., Allasia, P. and Motta, E. 2020. Classification and kinematics of the Planpincieux Glacier break-offs using photographic time-lapse analysis. *Journal of Glaciology*. **66**(256), pp.188–202.

Gomes, V., Queiroz, G. and Ferreira, K. 2020. An Overview of Platforms for Big Earth Observation Data Management and Analysis. *Remote Sensing*. **12**(8), p.1253.

Gonzalez, L., Montes, G., Puig, E., Johnson, S., Mengersen, K. and Gaston, K. 2016. Unmanned Aerial Vehicles (UAVs) and Artificial Intelligence Revolutionizing Wildlife Monitoring and Conservation. *Sensors*. **16**(1), p.97.

Gorelick, N., Hancher, M., Dixon, M., Ilyushchenko, S., Thau, D. and Moore, R. 2017. Google Earth Engine: Planetary-scale geospatial analysis for everyone. *Remote Sensing of Environment*. **202**, pp.18–27.

Guardamino, L. and Drenkhan, F. 2016. Evolución y potencial amenaza de lagunas glaciares en la cordillera de Vilcabamba (Cusco y Apurímac, Perú) entre 1991 y 2014. *Revista de Glaciares y Ecosistemas de Montaña*. (1), pp.16–16.

Guardamino, L., Haeberli, W., Muñoz, R., Drenkhan, F., Tacsi, A. and Cochachin, A. 2019. *Proyección de Lagunas Futuras en las Cordilleras Glaciares del Perú* [Online]. Lima. Available from: https://repositorio.ana.gob.pe/handle/20.500.12543/3597.

Gubbi, J., Buyya, R., Marusic, S. and Palaniswami, M. 2013. Internet of Things (IoT): A vision, architectural elements, and future directions. *Future Generation Computer Systems*. **29**(7), pp.1645–1660.

Guillet, G., King, O., Lv, M., Ghuffar, S., Benn, D., Quincey, D. and Bolch, T. 2022. A regionally resolved inventory of High Mountain Asia surge-type glaciers, derived from a multi-factor remote sensing approach. *The Cryosphere*. **16**(2), pp.603–623.

Gulley, J. and Benn, D.I. 2007. Structural control of englacial drainage systems in Himalayan debris-covered glaciers. *Journal of Glaciology*. **53**(182), pp.399–412.

Guo, X., Chen, Y., Liu, X. and Zhao, Y. 2020. Extraction of snow cover from high-resolution remote sensing imagery using deep learning on a small dataset. *Remote Sensing Letters*. **11**(1), pp.66–75.

Guth, P.L. and Geoffroy, T.M. 2021. LiDAR point cloud and ICESat-2 evaluation of 1 second global digital elevation models: Copernicus wins. *Transactions in GIS*. **25**(5), pp.2245–2261.

Haeberli, W., Buetler, M., Huggel, C., Friedli, T.L., Schaub, Y. and Schleiss, A.J. 2016. New lakes in deglaciating high-mountain regions – opportunities and risks. *Climatic Change*. **139**(2), pp.201–214.

Haemmig, C., Huss, M., Keusen, H., Hess, J., Wegmüller, U., Ao, Z. and Kulubayi, W. 2014. Hazard assessment of glacial lake outburst floods from Kyagar glacier, Karakoram mountains, China. *Annals of Glaciology*. **55**(66), pp.34–44.

Hanshaw, M.N. and Bookhagen, B. 2014. Glacial areas, lake areas, and snow lines from 1975 to 2012: status of the Cordillera Vilcanota, including the Quelccaya Ice Cap, northern central Andes, Peru. *The Cryosphere*. **8**(2), pp.359–376.

Harding, D.J., Bufton, J.L. and Frawley, J.J. 1994. Satellite laser altimetry of terrestrial topography: vertical accuracy as a function of surface slope, roughness, and cloud cover. *IEEE Transactions on Geoscience and Remote Sensing*. **32**(2), pp.329–339.

Harrison, S., Kargel, J.S., Huggel, C., Reynolds, J., Shugar, D.H., Betts, R.A., Emmer, A., Glasser, N., Haritashya, U.K., Klimeš, J., Reinhardt, L., Schaub, Y., Wiltshire, A., Regmi, D. and Vilímek, V. 2018. Climate change and the global pattern of moraine-dammed glacial lake outburst floods. *The Cryosphere*. **12**(4), pp.1195–1209.

Hart, J.K. and Martinez, K. 2006. Environmental Sensor Networks: A revolution in the earth system science? *Earth-Science Reviews*. **78**(3), pp.177–191.

Hart, J.K., Martinez, K., Basford, P.J., Clayton, A.I., Bragg, G.M., Ward, T. and Young, D.S. 2019. Surface melt-driven seasonal behaviour (englacial and subglacial) from a soft-bedded temperate glacier recorded by *in situ* wireless probes. *Earth Surface Processes and Landforms*. **44**(9), pp.1769–1782.

Hart, J.K., Martinez, K., Basford, P.J., Clayton, A.I., Robson, B.A. and Young, D.S. 2019. Surface melt driven summer diurnal and winter multi-day stick-slip motion and till sedimentology. *Nature Communications*. **10**(1), p.1599.

Hastedt, H., Ekkel, T. and Luhmann, T. 2016. Evaluation of the Quality of Action Cameras with Wide-Angle Lenses in Uav Photogrammetry. *ISPRS - International Archives of the Photogrammetry, Remote Sensing and Spatial Information Sciences*. **41B1**, pp.851–859.

Hegglin, E. and Huggel, C. 2008. An Integrated Assessment of Vulnerability to Glacial Hazards. *Mountain Research and Development*. **28**(3), pp.299–310.

Heid, T. and Kääb, A. 2012. Evaluation of existing image matching methods for deriving glacier surface displacements globally from optical satellite imagery. *Remote Sensing of Environment*. **118**, pp.339–355.

Helm, V., Humbert, A. and Miller, H. 2014. Elevation and elevation change of Greenland and Antarctica derived from CryoSat-2. *The Cryosphere*. **8**, pp.1539–1559.

Higman, B., Shugar, D.H., Stark, C.P., Ekström, G., Koppes, M.N., Lynett, P., Dufresne, A., Haeussler, P.J., Geertsema, M., Gulick, S., Mattox, A., Venditti, J.G., Walton, M.A.L., McCall, N., Mckittrick, E., MacInnes, B., Bilderback, E.L., Tang, H., Willis, M.J., Richmond, B., Reece, R.S., Larsen, C., Olson, B., Capra, J., Ayca, A., Bloom, C., Williams, H., Bonno, D., Weiss, R., Keen, A., Skanavis, V. and Loso, M. 2018. The 2015 landslide and tsunami in Taan Fiord, Alaska. *Scientific Reports*. **8**(1), p.12993.

Hock, R., Bliss, A., Marzeion, B., Giesen, R.H., Hirabayashi, Y., Huss, M., Radić, V. and Slangen, A.B.A. 2019. GlacierMIP – A model intercomparison of global-scale glacier mass-balance models and projections. *Journal of Glaciology*. **65**(251), pp.453–467.

Hock, R. and Rasul, G. 2019. High Mountain Areas *In*: *IPCC Special Report on the Ocean and Cryosphere in a Changing Climate*. IPCC, pp.131–202.

Hoeser, T. and Kuenzer, C. 2020. Object Detection and Image Segmentation with Deep Learning on Earth Observation Data: A Review-Part I: Evolution and Recent Trends. *Remote Sensing*. **12**(10), p.1667.

Holcombe, E.A., Hen-Jones, R., Vardanega, P.J., Beesley, M.E.W., Gilder, C.E.L. and Bozzolan, E. 2021. Co-Producing Data and Decision Support Tools to Reduce Landslide Risk in the Humid Tropics *In*: K. Sassa, M. Mikoš, S. Sassa, P. T. Bobrowsky, K. Takara and K. Dang, eds. *Understanding and Reducing Landslide Disaster Risk*. ICL Contribution to Landslide Disaster Risk Reduction. Cham: Springer International Publishing, pp.567–573.

Honkavaara, E., Rosnell, T., Oliveira, R. and Tommaselli, A. 2017. Band registration of tuneable frame format hyperspectral UAV imagers in complex scenes. *ISPRS Journal of Photogrammetry and Remote Sensing*. **134**, pp.96–109.

How, P., Hulton, N.R.J., Buie, L. and Benn, D.I. 2020. PyTrx: A Python-Based Monoscopic Terrestrial Photogrammetry Toolset for Glaciology. *Frontiers in Earth Science*. **8**, p.21.

How, P., Schild, K.M., Benn, D.I., Noormets, R., Kirchner, N., Luckman, A., Vallot, D., Hulton, N.R.J. and Borstad, C. 2019. Calving controlled by melt-under-cutting: detailed calving styles revealed through time-lapse observations. *Annals of Glaciology*. **60**(78), pp.20–31.

Howarth, P.J. and Price, R.J. 1969. The Proglacial Lakes of Breiðamerkurjökull and Fjallsjökull, Iceland. *The Geographical Journal*. **135**(4), p.573.

Huggel, C., Allen, S., Wymann von Dach, S., Dimri, A.P., Mal, S., Linbauer, A., Salzmann, N. and Bolch, T. 2020. An Integrative and Joint Approach to Climate Impacts, Hydrological Risks and Adaptation in the Indian Himalayan Region *In*: A. P. Dimri, B. Bookhagen, M. Stoffel and T. Yasunari, eds. *Himalayan Weather and Climate and their Impact on the Environment*. Cham: Springer International Publishing, pp.553–573.

Huggel, C., Clague, J.J. and Korup, O. 2012. Is climate change responsible for changing landslide activity in high mountains?: Climate change and landslides in high mountains. *Earth Surface Processes and Landforms*. **37**(1), pp.77–91.

Huggel, C., Cochachin, A., Drenkhan, F., Fluixa-Sanmartin, J., Frey, H., Garcia Hernandez, J., Jurt, C., Muñoz Asmat, R., Price, K. and Vicuña, L. 2020. Glacier Lake 513, Peru: Lessons for early warning service development. *WMO Bulletin*. **69**, pp.45–52.

Hugonnet, R., McNabb, R., Berthier, E., Menounos, B., Nuth, C., Girod, L., Farinotti, D., Huss, M., Dussaillant, I., Brun, F. and Kääb, A. 2021. Accelerated global glacier mass loss in the early twenty-first century. *Nature*. **592**(7856), pp.726–731.

Huntington, J.L., Hegewisch, K.C., Daudert, B., Morton, C.G., Abatzoglou, J.T., McEvoy, D.J. and Erickson, T. 2017. Climate Engine: Cloud Computing and Visualization of Climate and Remote Sensing Data for Advanced Natural Resource Monitoring and Process Understanding. *Bulletin of the American Meteorological Society*. **98**(11), pp.2397–2410.

Huss, M. 2013. Density assumptions for converting geodetic glacier volume change to mass change. *The Cryosphere*. **7**(3), pp.877–887.

Huss, M. and Hock, R. 2018. Global-scale hydrological response to future glacier mass loss. *Nature Climate Change*. **8**(2), pp.135–140.

Hwang, C. and Cheng, Y.S. 2015. Detecting elevation changes over mountain glaciers in Tibet and the Himalayas by TOPEX/Poseidon and Jason-2 radar altimeters: comparison with ICESat results *In*: *American Geophysical Union, Fall Meeting 2015* [Online]. San Francisco. [Accessed 18 June 2022]. Available from: https://ui.adsabs.harvard.edu/abs/2015AGUFM.G33B1136H.

Immerzeel, W.W., Kraaijenbrink, P.D.A., Shea, J.M., Shrestha, A.B., Pellicciotti, F., Bierkens, M.F.P. and de Jong, S.M. 2014. High-resolution monitoring of Himalayan glacier dynamics using unmanned aerial vehicles. *Remote Sensing of Environment*. **150**, pp.93–103.

Immerzeel, W.W., Lutz, A.F., Andrade, M., Bahl, A., Biemans, H., Bolch, T., Hyde, S., Brumby, S., Davies, B.J., Elmore, A.C., Emmer, A., Feng, M., Fernández, A., Haritashya, U., Kargel, J.S., Koppes, M., Kraaijenbrink, P.D.A., Kulkarni, A.V., Mayewski, P., Nepal, S., Pacheco, P., Painter, T.H., Pellicciotti, F., Rajaram, H., Rupper, S., Sinisalo, A., Shrestha, A.B., Viviroli, D., Wada, Y., Xiao, C., Yao, T. and Baillie, J.E.M. 2019. Importance and vulnerability of the world's water towers. *Nature*. **577**, pp.364–369.

INAIGEM 2017. *Informe de la Situación de los Glaciares y Ecosistemas de Montaña en el Perú* [Online]. Lima: Instituto Nacional de Investigación en Glaciares y Ecosistemas de Montaña. [Accessed 3 March 2022]. Available from: https://www.inaigem.gob.pe/wp-content/uploads/2019/04/Interiores-Informe-anual-2017.pdf.

Instituto Peruano de Economía 2021. *Índice de Desarrollo Humano - IDH* [Online]. Lima, Peru. [Accessed 29 June 2022]. Available from: https://www.ipe.org.pe/portal/indice-de-desarrollo-humano-idh/.

International Altimetry Team 2021. Altimetry for the future: Building on 25 years of progress. *Advances in Space Research*. **68**(2), pp.319–363.

Jakob, L., Gourmelen, N., Ewart, M. and Plummer, S. 2021. Spatially and temporally resolved ice loss in High Mountain Asia and the Gulf of Alaska observed by CryoSat-2 swath altimetry between 2010 and 2019. *The Cryosphere*. **15**(4), pp.1845–1862.

James, M.R. and Robson, S. 2012. Straightforward reconstruction of 3D surfaces and topography with a camera: Accuracy and geoscience application. *Journal of Geophysical Research: Earth Surface*. **117**(F3).

James, M.R., Robson, S. and Smith, M.W. 2017. 3-D uncertainty-based topographic change detection with structure-from-motion photogrammetry: precision maps for ground control and directly georeferenced surveys. *Earth Surface Processes and Landforms*. **42**(12), pp.1769–1788.

James, T.D., Murray, T., Selmes, N., Scharrer, K. and O'Leary, M. 2014. Buoyant flexure and basal crevassing in dynamic mass loss at Helheim Glacier. *Nature Geoscience*. **7**(8), pp.593–596.

Janke, J.R. 2013. Using airborne LiDAR and USGS DEM data for assessing rock glaciers and glaciers. *Geomorphology*. **195**, pp.118–130.

Janský, B., Engel, Z., Kocum, J., Šefrna, L. and Česák, J. 2011. The Amazon River headstream area in the Cordillera Chila, Peru: hydrographic, hydrological and glaciological conditions. *Hydrological Sciences Journal*. **56**(1), pp.138–151.

Jawak, S.D., Kulkarni, K. and Luis, A.J. 2015. A Review on Extraction of Lakes from Remotely Sensed Optical Satellite Data with a Special Focus on Cryospheric Lakes. *Advances in Remote Sensing*. **04**(03), p.196.

Jiang, L., Nielsen, K., Dinardo, S., Andersen, O.B. and Bauer-Gottwein, P. 2020. Evaluation of Sentinel-3 SRAL SAR altimetry over Chinese rivers. *Remote Sensing of Environment*. **237**, p.111546.

Jorge, D., Barbosa, C., Carvalho, L.D., Affonso, A., Lobo, F. and Novo, E. 2017. SNR (Signal-To-Noise Ratio) Impact on Water Constituent Retrieval from Simulated Images of Optically Complex Amazon Lakes. *Remote Sensing*. **9**(7), p.644.

Joughin, I., Smith, B.E. and Abdalati, W. 2010. Glaciological advances made with interferometric synthetic aperture radar. *Journal of Glaciology*. **56**(200), pp.1026–1042.

Jouvet, G., Weidmann, Y., Seguinot, J., Funk, M., Abe, T., Sakakibara, D., Seddik, H. and Sugiyama, S. 2017. Initiation of a major calving event on the Bowdoin Glacier captured by UAV photogrammetry. *The Cryosphere*. **11**(2), pp.911–921.

Judson, A. and Doesken, N. 2000. Density of Freshly Fallen Snow in the Central Rocky Mountains. *Bulletin of the American Meteorological Society*. **81**(7), pp.1577–1587.

Junaid, A., Konoiko, A., Zweiri, Y., Sahinkaya, M. and Seneviratne, L. 2017. Autonomous Wireless Self-Charging for Multi-Rotor Unmanned Aerial Vehicles. *Energies*. **10**(6), p.803.

Junaid, A.B., Lee, Y. and Kim, Y. 2016. Design and implementation of autonomous wireless charging station for rotary-wing UAVs. *Aerospace Science and Technology*. **54**, pp.253–266.

Kääb, A. 2005. Combination of SRTM3 and repeat ASTER data for deriving alpine glacier flow velocities in the Bhutan Himalaya. *Remote Sensing of Environment*. **94**(4), pp.463–474.

Kääb, A. 2008. Glacier Volume Changes Using ASTER Satellite Stereo and ICESat GLAS Laser Altimetry. A Test Study on EdgeØya, Eastern Svalbard. *IEEE Transactions on Geoscience and Remote Sensing*. **46**(10), pp.2823–2830.

Kaab, A. 2000. Photogrammetry for early recognition of high mountain hazards: New techniques and applications. *Physics and Chemistry of the Earth, Part B: Hydrology, Oceans and Atmosphere*. **25**(9), pp.765–770.

Kääb, A., Berthier, E., Nuth, C., Gardelle, J. and Arnaud, Y. 2012. Contrasting patterns of early twenty-first-century glacier mass change in the Himalayas. *Nature*. **488**(7412), pp.495–498.

Kääb, A., Huggel, C., Fischer, L., Guex, S., Paul, F., Roer, I., Salzmann, N., Schlaefli, S., Schmutz, K., Schneider, D., Strozzi, T. and Weidmann, Y. 2005. Remote sensing of glacier- and permafrost-related hazards in high mountains: an overview. *Natural Hazards and Earth System Science*. **5**(4), pp.527–554.

Kapitsa, V., Shahgedanova, M., Machguth, H., Severskiy, I. and Medeu, A. 2017. Assessment of evolution and risks of glacier lake outbursts in the Djungarskiy Alatau, Central Asia, using Landsat imagery and glacier bed topography modelling. *Natural Hazards and Earth System Sciences*. **17**(10), pp.1837–1856.

Kaser, G. 1999. A review of the modern fluctuations of tropical glaciers. *Global and Planetary Change*. **22**(1), pp.93–103.

Kaser, G. 2001. Glacier-climate interaction at low latitudes. *Journal of Glaciology*. **47**(157), pp.195–204.

Kaser, G. and Georges, C. 2003. *A potential disaster in the icy Andes: a regrettable blunder* [Online]. Austria: University of Innsbruck. [Accessed 1 May 2020]. Available from: https://www.researchgate.net/profile/Georg_Kaser/publication/267236933_A_potential_disaster_in_the_icy_Andes_a_regrettable_blunder/links/555463da08aeaaff3bf1bc7a/A-potential-disaster-in-the-icy-Andes-a-regrettable-blunder.pdf.

Kaser, G. and Georges, C. 1997. Changes of the equilibrium-line altitude in the tropical Cordillera Blanca, Peru, 1930–50, and their spatial variations. *Annals of Glaciology*. **24**, pp.344–349.

Kaufmann, V. 2012. The evolution of rock glacier monitoring using terrestrial photogrammetry: the example of Äußeres Hochebenkar rock glacier (Austria). *Austrian Journal of Earth Sciences*. **105**(2), pp.63–77.

Ke, L., Ding, X. and Song, C. 2015. Heterogeneous changes of glaciers over the western Kunlun Mountains based on ICESat and Landsat-8 derived glacier inventory. *Remote Sensing of Environment*. **168**, pp.13–23.

Keiler, M., Knight, J. and Harrison, S. 2010. Climate change and geomorphological hazards in the eastern European Alps. *Philosophical Transactions of the Royal Society of London A: Mathematical, Physical and Engineering Sciences*. **368**(1919), pp.2461–2479.

Kern, M., Cullen, R., Berruti, B., Bouffard, J., Casal, T., Drinkwater, M.R., Gabriele, A., Lecuyot, A., Ludwig, M., Midthassel, R., Navas Traver, I., Parrinello, T., Ressler, G., Andersson, E., Martin Puig, C., Andersen, O., Bartsch, A., Farrell, S.L., Fleury, S., Gascoin, S., Guillot, A., Humbert, A., Rinne, E., Shepherd, A., Broeke, M.R. van den and Yackel, J. 2020. The Copernicus Polar Ice and Snow Topography Altimeter (CRISTAL) high-priority candidate mission. *The Cryosphere Discussions*. **14**, pp.2235–2251.

Khalil, N., Abid, M.R., Benhaddou, D. and Gerndt, M. 2014. Wireless sensors networks for Internet of Things *In*: *2014 IEEE Ninth International Conference on Intelligent Sensors, Sensor Networks and Information Processing (ISSNIP)*. Singapore: IEEE, pp.1–6.

Khan, A.A., Jamil, A., Hussain, D., Taj, M., Jabeen, G. and Malik, M.K. 2020. Machine-Learning Algorithms for Mapping Debris-Covered Glaciers: The Hunza Basin Case Study. *IEEE Access*. **8**, pp.12725–12734.

Kienholz, C., Amundson, J.M., Motyka, R.J., Jackson, R.H., Mickett, J.B., Sutherland, D.A., Nash, J.D., Winters, D.S., Dryer, W.P. and Truffer, M. 2019. Tracking icebergs with time-lapse photography and sparse optical flow, LeConte Bay, Alaska, 2016–2017. *Journal of Glaciology*. **65**(250), pp.195–211.

King, O., Bhattacharya, A., Bhambri, R. and Bolch, T. 2019. Glacial lakes exacerbate Himalayan glacier mass loss. *Scientific Reports*. **9**(1), p.18145.

King, O., Quincey, D.J., Carrivick, J.L. and Rowan, A.V. 2017. Spatial variability in mass loss of glaciers in the Everest region, central Himalayas, between 2000 and 2015. *The Cryosphere*. **11**(1), pp.407–426.

Kirschbaum, D., Watson, C.S., Rounce, D.R., Shugar, D.H., Kargel, J.S., Haritashya, U.K., Amatya, P., Shean, D., Anderson, E.R. and Jo, M. 2019. The State of Remote Sensing Capabilities of Cascading Hazards Over High Mountain Asia. *Frontiers in Earth Science*. **7**, p.197.

Kittel, C.M.M., Jiang, L., Tøttrup, C. and Bauer-Gottwein, P. 2021. Sentinel-3 radar altimetry for river monitoring – a catchment-scale evaluation of satellite water surface elevation from Sentinel-3A and Sentinel-3B. *Hydrology and Earth System Sciences*. **25**(1), pp.333–357.

Kjeldsen, K.K., Korsgaard, N.J., Bjørk, A.A., Khan, S.A., Box, J.E., Funder, S., Larsen, N.K., Bamber, J.L., Colgan, W., van den Broeke, M., Siggaard-Andersen, M.-L., Nuth, C., Schomacker, A., Andresen, C.S., Willerslev, E. and Kjær, K.H. 2015. Spatial and

temporal distribution of mass loss from the Greenland Ice Sheet since AD 1900. *Nature*. **528**(7582), pp.396–400.

Klenk, N., Fiume, A., Meehan, K. and Gibbes, C. 2017. Local knowledge in climate adaptation research: moving knowledge frameworks from extraction to co-production. *WIREs Climate Change*. **8**(5), p.e475.

Kneib, M., Miles, E.S., Buri, P., Fugger, S., McCarthy, M., Shaw, T.E., Chuanxi, Z., Truffer, M., Westoby, M.J., Yang, W. and Pellicciotti, F. 2022. *Sub-seasonal variability of supraglacial ice cliff melt rates and associated processes from time-lapse photogrammetry* [Online]. Glaciers/Energy Balance Obs/Modelling. [Accessed 10 May 2022]. Available from: https://tc.copernicus.org/preprints/tc-2022-81/.

Kochtitzky, W.H., Edwards, B.R., Enderlin, E.M., Marino, J. and Marinque, N. 2018. Improved estimates of glacier change rates at Nevado Coropuna Ice Cap, Peru. *Journal of Glaciology*. **64**(244), pp.175–184.

Kopp, M., Tuo, Y. and Disse, M. 2019. Fully automated snow depth measurements from time-lapse images applying a convolutional neural network. *Science of The Total Environment*. **697**, p.134213.

Korsgaard, N.J., Nuth, C., Khan, S.A., Kjeldsen, K.K., Bjørk, A.A., Schomacker, A. and Kjær, K.H. 2016. Digital elevation model and orthophotographs of Greenland based on aerial photographs from 1978–1987. *Scientific Data*. **3**(1), p.160032.

Kraaijenbrink, P.D.A., Bierkens, M.F.P., Lutz, A.F. and Immerzeel, W.W. 2017. Impact of a global temperature rise of 1.5 degrees Celsius on Asia's glaciers. *Nature*. **549**(7671), pp.257–260.

Kraaijenbrink, P.D.A., Shea, J.M., Pellicciotti, F., Jong, S.M. de and Immerzeel, W.W. 2016. Object-based analysis of unmanned aerial vehicle imagery to map and characterise surface features on a debris-covered glacier. *Remote Sensing of Environment*. **186**, pp.581–595.

Kromer, R., Walton, G., Gray, B., Lato, M. and Group, R. 2019. Development and Optimization of an Automated Fixed-Location Time Lapse Photogrammetric Rock Slope Monitoring System. *Remote Sensing*. **11**(16), p.1890.

Kromer, R.A., Abellán, A., Hutchinson, D.J., Lato, M., Chanut, M.-A., Dubois, L. and Jaboyedoff, M. 2017. Automated terrestrial laser scanning with near-real-time change detection – monitoring of the Séchilienne landslide. *Earth Surface Dynamics*. **5**(2), pp.293–310.

Kronenberg, M., Schauwecker, S., Huggel, C., Salzmann, N., Drenkhan, F., Frey, H., Giraáldez, C., Gurgiser, W., Kaser, G., Juen, I., Suarez, W., Hernaández, J.G., Sanmarťín, J.F., Ayros, E., Perry, B. and Rohrer, M. 2016. The Projected Precipitation Reduction over the Central Andes may Severely Affect Peruvian Glaciers and Hydropower Production. *Energy Procedia*. **97**, pp.270–277.

Kropáček, J., Neckel, N. and Bauder, A. 2014. Estimation of Mass Balance of the Grosser Aletschgletscher, Swiss Alps, from ICESat Laser Altimetry Data and Digital Elevation Models. *Remote Sensing*. **6**(6), pp.5614–5632.

Kulkarni, A.V., Randhawa, S.S., Rathore, B.P., Bahuguna, I.M. and Sood, R.K. 2002. Snow and glacier melt runoff model to estimate hydropower potential. *Journal of the Indian Society of Remote Sensing*. **30**(4), pp.221–228.

Kumar, B., Sathyan, A., Prabhu, T.S.M. and K, A.K. 2020. Design Architecture of Glacier Lake Outburst Flood (GLOF) Early Warning System Using Ultrasonic Sensors *In*:

2020 IEEE Recent Advances in Intelligent Computational Systems (RAICS)., pp.195–200.

Kundzewicz, Z.W., Mata, L.J., Arnell, N., Döll, P., Kabat, P., Sçen, Z., Shiklomanov, I., Asanuma, J., Betts, R., Cohen, S., Milly, C., Nearing, M., Prudhomme, C., Pulwarty, R., Schulze, R., van Schaik, H., Becker, A. and Bruce, J. 2007. Freshwater resources and their management *In*: *Climate Change 2007: Impacts, Adaptation and Vulnerability. Contribution of Working Group II to the Fourth Assessment Report of the Intergovernmental Panel on Climate Change*. Cambridge, UK: Cambridge University Press, pp.173–210.

Lague, D., Brodu, N. and Leroux, J. 2013. Accurate 3D comparison of complex topography with terrestrial laser scanner: Application to the Rangitikei canyon (N-Z). *ISPRS Journal of Photogrammetry and Remote Sensing*. **82**, pp.10–26.

Lala, J.M., Rounce, D.R. and McKinney, D.C. 2018. Modeling the glacial lake outburst flood process chain in the Nepal Himalaya: reassessing Imja Tsho's hazard. *Hydrology and Earth System Sciences*. **22**(7), pp.3721–3737.

Lary, D.J., Alavi, A.H., Gandomi, A.H. and Walker, A.L. 2016. Machine learning in geosciences and remote sensing. *Geoscience Frontiers*. **7**(1), pp.3–10.

Le Gac, S., Boy, F., Blumstein, D., Lasson, L. and Picot, N. 2019. Benefits of the Open-Loop Tracking Command (OLTC): Extending conventional nadir altimetry to inland waters monitoring. *Advances in Space Research*. **68**(2), pp.843–852.

Lea, J.M. 2018. The Google Earth Engine Digitisation Tool (GEEDiT) and the Margin change Quantification Tool (MaQiT) – simple tools for the rapid mapping and quantification of changing Earth surface margins. *Earth Surface Dynamics*. **6**(3), pp.551–561.

Leach, N., Coops, N.C. and Obrknezev, N. 2019. Normalization method for multi-sensor high spatial and temporal resolution satellite imagery with radiometric inconsistencies. *Computers and Electronics in Agriculture*. **164**, p.104893.

Lee, C.A., Gasster, S.D., Plaza, A., Chang, C.-I. and Huang, B. 2011. Recent Developments in High Performance Computing for Remote Sensing: A Review. *IEEE Journal of Selected Topics in Applied Earth Observations and Remote Sensing*. **4**(3), pp.508–527.

Lee, H., Shum, C.K., Tseng, K.-H., Huang, Z. and Sohn, H.-G. 2013. Elevation changes of Bering Glacier System, Alaska, from 1992 to 2010, observed by satellite radar altimetry. *Remote Sensing of Environment*. **132**, pp.40–48.

Leprince, S., Ayoub, F., Klinger, Y. and Avouac, J.-P. 2007. Co-Registration of Optically Sensed Images and Correlation (COSI-Corr): an operational methodology for ground deformation measurements *In*: *2007 IEEE International Geoscience and Remote Sensing Symposium*. Barcelona, Spain: IEEE, pp.1943–1946.

Lewińska, P., Głowacki, O., Moskalik, M. and Smith, W.A.P. 2021. Evaluation of structure-from-motion for analysis of small-scale glacier dynamics. *Measurement*. **168**, p.108327.

Linsbauer, A., Frey, H., Haeberli, W., Machguth, H., Azam, M.F. and Allen, S. 2016. Modelling glacier-bed overdeepenings and possible future lakes for the glaciers in the Himalaya—Karakoram region. *Annals of Glaciology*. **57**(71), pp.119–130.

Linsbauer, A., Paul, F. and Haeberli, W. 2012. Modeling glacier thickness distribution and bed topography over entire mountain ranges with GlabTop: Application of a fast and robust approach. *Journal of Geophysical Research: Earth Surface*. **117**(F3).

Liu, J., Chen, R., Ding, Y., Han, C. and Ma, S. 2021. Snow process monitoring using time-lapse structure-from-motion photogrammetry with a single camera. *Cold Regions Science and Technology*. **190**, p.103355.

Liu, J., Chen, R. and Wang, G. 2015. Snowline and snow cover monitoring at high spatial resolution in a mountainous river basin based on a time-lapse camera at a daily scale. *Journal of Mountain Science*. **12**(1), pp.60–69.

Liu, K., Song, C., Ke, L., Jiang, L., Pan, Y. and Ma, R. 2019. Global open-access DEM performances in Earth's most rugged region High Mountain Asia: A multi-level assessment. *Geomorphology*. **338**, pp.16–26.

Lopez, P., Sirguey, P., Arnaud, Y., Pouyaud, B. and Chevallier, P. 2008. Snow cover monitoring in the Northern Patagonia Icefield using MODIS satellite images (2000–2006). *Global and Planetary Change*. **61**(3), pp.103–116.

López-Moreno, J.I., Fontaneda, S., Bazo, J., Revuelto, J., Azorin-Molina, C., Valero-Garcés, B., Morán-Tejeda, E., Vicente-Serrano, S.M., Zubieta, R. and Alejo-Cochachín, J. 2014. Recent glacier retreat and climate trends in Cordillera Huaytapallana, Peru. *Global and Planetary Change*. **112**, pp.1–11.

Luckman, A., Quincey, D. and Bevan, S. 2007. The potential of satellite radar interferometry and feature tracking for monitoring flow rates of Himalayan glaciers. *Remote Sensing of Environment*. **111**(2), pp.172–181.

Luetzenburg, G., Kroon, A. and Bjørk, A.A. 2021. Evaluation of the Apple iPhone 12 Pro LiDAR for an Application in Geosciences. *Scientific Reports*. **11**(1), p.22221.

Lüthi, M.P. and Vieli, A. 2016. Multi-method observation and analysis of a tsunami caused by glacier calving. *The Cryosphere*. **10**(3), pp.995–1002.

Ma, Y., Xu, N., Liu, Z., Yang, B., Yang, F., Wang, X.H. and Li, S. 2020. Satellite-derived bathymetry using the ICESat-2 lidar and Sentinel-2 imagery datasets. *Remote Sensing of Environment*. **250**, p.112047.

Maddalena, J., Dawson, G., Chuter, S., Landy, J. and Bamber, J. 2020. Monitoring the Greenland Ice Sheet: A comparison between Sentinel-3 and CryoSat-2 radar altimeters *In*: *EGU General Assembly 2020* [Online]. Virtual: EGU, p.18612. [Accessed 10 June 2022]. Available from: https://ui.adsabs.harvard.edu/abs/2020EGUGA..2218612M.

Mallalieu, J., Carrivick, J.L., Quincey, D.J. and Smith, M.W. 2020. Calving Seasonality Associated With Melt-Undercutting and Lake Ice Cover. *Geophysical Research Letters*. **47**(8).

Mallalieu, J., Carrivick, J.L., Quincey, D.J., Smith, M.W. and James, W.H.M. 2017. An integrated Structure-from-Motion and time-lapse technique for quantifying ice-margin dynamics. *Journal of Glaciology*. **63**(242), pp.937–949.

Mark, B.G., French, A., Baraer, M., Carey, M., Bury, J., Young, K.R., Polk, M.H., Wigmore, O., Lagos, P., Crumley, R., McKenzie, J.M. and Lautz, L. 2017. Glacier loss and hydro-social risks in the Peruvian Andes. *Global and Planetary Change*. **159**, pp.61–76.

Mark, B.G. and Seltzer, G.O. 2003. Tropical glacier meltwater contribution to stream discharge: a case study in the Cordillera Blanca, Peru. *Journal of Glaciology*. **49**(165), pp.271–281.

Markert, K.N., Chishtie, F., Anderson, E.R., Saah, D. and Griffin, R.E. 2018. On the merging of optical and SAR satellite imagery for surface water mapping applications. *Results in Physics*. **9**, pp.275–277.

Markham, B.L., Jenstrom, D., Masek, J.G., Dabney, P., Pedelty, J.A., Barsi, J.A. and Montanaro, M. 2016. Landsat 9: status and plans *In*: J. J. Butler, X. (Jack) Xiong and X. Gu, eds. San Diego, California, United States, p.99720G.

Markus, T., Neumann, T., Martino, A., Abdalati, W., Brunt, K., Csatho, B., Farrell, S., Fricker, H., Gardner, A., Harding, D., Jasinski, M., Kwok, R., Magruder, L., Lubin, D., Luthcke, S., Morison, J., Nelson, R., Neuenschwander, A., Palm, S. and Zwally, H. 2017. The Ice, Cloud, and land Elevation Satellite-2 (ICESat-2): Science requirements, concept, and implementation. *Remote Sensing of Environment*. **190**, pp.260–273.

Marti, R., Gascoin, S., Berthier, E., de Pinel, M., Houet, T. and Laffly, D. 2016. Mapping snow depth in open alpine terrain from stereo satellite imagery. *The Cryosphere*. **10**(4), pp.1361–1380.

Martínez, E., Drenkhan, F., Zogheib, C., Ochoa-Tocachi, B. and Buytaert, W. 2020. Emerging Water Scarcity Risks in Peruvian Glacier-Fed River Basins. *One Earth [preprint]*., pp.1–34.

Martin-Puig, C., Leuliette, E., Lillibridge, J. and Roca, M. 2016. Evaluating the Performance of Jason-2 Open-Loop and Closed-Loop Tracker Modes. *Journal of Atmospheric and Oceanic Technology*. **33**(11), pp.2277–2288.

Marzeion, B., Cogley, J.G., Richter, K. and Parkes, D. 2014. Attribution of global glacier mass loss to anthropogenic and natural causes. *Science*. **345**(6199), pp.919–921.

Maurer, J. and Rupper, S. 2015. Tapping into the Hexagon spy imagery database: A new automated pipeline for geomorphic change detection. *ISPRS Journal of Photogrammetry and Remote Sensing*. **108**, pp.113–127.

Maurer, J.M., Schaefer, J.M., Rupper, S. and Corley, A. 2019. Acceleration of ice loss across the Himalayas over the past 40 years. *Science Advances*. **5**(6), p.eaav7266.

Maussion, F., Gurgiser, W., Großhauser, M., Kaser, G. and Marzeion, B. 2015. ENSO influence on surface energy and mass balance at Shallap Glacier, Cordillera Blanca, Peru. *The Cryosphere*. **9**(4), pp.1663–1683.

Maxar Technologies 2020. WorldView Legion. *WorldView Legion: Our next-generation constellation*. [Online]. [Accessed 28 April 2020]. Available from: https://www.maxar.com/splash/worldview-legion.

McDonnell, M., Rupper, S. and Forster, R. 2022. Quantifying Geodetic Mass Balance of the Northern and Southern Patagonian Icefields Since 1976. *Frontiers in Earth Science*. **10**.

McMillan, M., Muir, A., Shepherd, A., Escolà, R., Roca, M., Aublanc, J., Thibaut, P., Restano, M., Ambrozio, A. and Benveniste, J. 2019. Sentinel-3 Delay-Doppler altimetry over Antarctica. *The Cryosphere*. **13**(2), pp.709–722.

McNabb, R., Girod, L., Nuth, C. and Kääb, A. 2020. An open-source toolset for automated processing of historic spy photos: sPyMicMac *In*: *EGU General Assembly 2020* [Online]. Online: EGU. [Accessed 11 May 2020]. Available from: https://meetingorganizer.copernicus.org/EGU2020/EGU2020-11150.html.

Menounos, B., Hugonnet, R., Shean, D., Gardner, A., Howat, I., Berthier, E., Pelto, B., Tennant, C., Shea, J., Noh, M., Brun, F. and Dehecq, A. 2019. Heterogeneous

Changes in Western North American Glaciers Linked to Decadal Variability in Zonal Wind Strength. *Geophysical Research Letters*. **46**(1), pp.200–209.

Micheletti, N., Chandler, J.H. and Lane, S.N. 2015. Investigating the geomorphological potential of freely available and accessible structure-from-motion photogrammetry using a smartphone. *Earth Surface Processes and Landforms*. **40**(4), pp.473–486.

Miles, E., McCarthy, M., Dehecq, A., Kneib, M., Fugger, S. and Pellicciotti, F. 2021a. Health and sustainability of glaciers in High Mountain Asia. *Nature Communications*. **12**(1), p.2868.

Miles, E.S., Pellicciotti, F., Willis, I.C., Steiner, J.F., Buri, P. and Arnold, N.S. 2016. Refined energy-balance modelling of a supraglacial pond, Langtang Khola, Nepal. *Annals of Glaciology*. **57**(71), pp.29–40.

Miles, E.S., Willis, I., Buri, P., Steiner, J.F., Arnold, N.S. and Pellicciotti, F. 2018a. Surface Pond Energy Absorption Across Four Himalayan Glaciers Accounts for 1/8 of Total Catchment Ice Loss. *Geophysical Research Letters*. **45**(19).

Miles, E.S., Watson, C.S., Brun, F., Berthier, E., Esteves, M., Quincey, D.J., Miles, K.E., Hubbard, B. and Wagnon, P. 2018b. Glacial and geomorphic effects of a supraglacial lake drainage and outburst event, Everest region, Nepal Himalaya. *The Cryosphere*. **12**(12), pp.3891–3905.

Miles, K.E., Hubbard, B., Miles, E.S., Quincey, D.J., Rowan, A.V., Kirkbride, M. and Hornsey, J. 2021b. Continuous borehole optical televiewing reveals variable englacial debris concentrations at Khumbu Glacier, Nepal. *Communications Earth & Environment*. **2**(1), pp.1–9.

Miles, K.E., Miles, E.S., Hubbard, B., Quincey, D.J., Rowan, A.V. and Pallett, M. 2019. Instruments and methods: hot-water borehole drilling at a high-elevation debris-covered glacier. *Journal of Glaciology*. **65**(253), pp.822–832.

Minowa, M., Schaefer, M., Sugiyama, S., Sakakibara, D. and Skvarca, P. 2021. Frontal ablation and mass loss of the Patagonian icefields. *Earth and Planetary Science Letters*. **561**, p.116811.

Mitchell, J. and Marshall, J.A. 2017. Design of a Novel Auto-Rotating UAV Platform for Underground Mine Cavity Surveying *In*: *Proceedings of the 2017 SME Annual Conference & Expo and CMAs*. SME.

Mitchell, J. and Marshall, J.A. 2020. Towards a novel auto-rotating lidar platform for cavity surveying. *Tunnelling and Underground Space Technology*. **97**, p.103260.

Mityók, Z.K., Bolton, D.K., Coops, N.C., Berman, E.E. and Senger, S. 2018. Snow cover mapped daily at 30 meters resolution using a fusion of multi-temporal MODIS NDSI data and Landsat surface reflectance. *Canadian Journal of Remote Sensing*. **44**(5), pp.413–434.

Mohajerani, Y., Wood, M., Velicogna, I. and Rignot, E. 2019. Detection of Glacier Calving Margins with Convolutional Neural Networks: A Case Study. *Remote Sensing*. **11**(74), pp.1–13.

Molina, E., Schauwecker, S., Huggel, C., Haeberli, W., Cochachin, A. and Condom, T. 2015. Iniciación de un monitoreo del balance de masa en el glaciar Suyuparina, Cordillera Vilcanota, Perú. *Climate Change in the Tropical Andes*. **2**(2), pp.1–14.

Mosbrucker, A.R., Major, J.J., Spicer, K.R. and Pitlick, J. 2017. Camera system considerations for geomorphic applications of SfM photogrammetry. *Earth Surface Processes and Landforms*. **42**(6), pp.969–986.

Motschmann, A., Huggel, C., Carey, M., Moulton, H., Walker-Crawford, N. and Muñoz, R. 2020. Losses and damages connected to glacier retreat in the Cordillera Blanca, Peru. *Climatic Change*. **162**(2), pp.837–858.

Murthy, M.S.R., Bajracharya, B., Pradhan, S., Shestra, B., Bajracharya, R., Shakya, K., Wesselmann, S., Ali, M., Bajracharya, S. and Pradhan, S. 2014. Adoption of Geospatial Systems towards evolving Sustainable Himalayan Mountain Development *In*: *ISPRS - International Archives of the Photogrammetry, Remote Sensing and Spatial Information Sciences*. Copernicus GmbH, pp.1319–1324.

Naeimi, A., Sharp, M.J. and Mortimer, C. 2018. The Effect of Black Carbon Deposition on the Albedo Change of the Columbia Icefield, 2000-2016 *In*: *AGU Fall Meeting Abstracts*., pp.C13I-1239.

Nagler, T., Rott, H., Ripper, E., Bippus, G. and Hetzenecker, M. 2016. Advancements for Snowmelt Monitoring by Means of Sentinel-1 SAR. *Remote Sensing*. **8**(4), p.348.

NASA 2021. Landsat NeXt | Landsat Science. [Accessed 10 June 2022]. Available from: https://landsat.gsfc.nasa.gov/satellites/landsat-next/.

Neckel, N., Kropáček, J., Bolch, T. and Hochschild, V. 2014. Glacier mass changes on the Tibetan Plateau 2003–2009 derived from ICESat laser altimetry measurements. *Environmental Research Letters*. **9**(1), p.014009.

Negi, H.S., Thakur, N.K., Kumar, R. and Kumar, M. 2009. Monitoring and evaluation of seasonal snow cover in Kashmir valley using remote sensing, GIS and ancillary data. *Journal of Earth System Science*. **118**(6), pp.711–720.

Neumann, T.A., Martino, A.J., Markus, T., Bae, S., Bock, M.R., Brenner, A.C., Brunt, K.M., Cavanaugh, J., Fernandes, S.T., Hancock, D.W., Harbeck, K., Lee, J., Kurtz, N.T., Luers, P.J., Luthcke, S.B., Magruder, L., Pennington, T.A., Ramos-Izquierdo, L., Rebold, T., Skoog, J. and Thomas, T.C. 2019. The Ice, Cloud, and Land Elevation Satellite – 2 mission: A global geolocated photon product derived from the Advanced Topographic Laser Altimeter System. *Remote Sensing of Environment*. **233**, p.111325.

Nie, Y., Sheng, Y., Liu, Q., Liu, L., Liu, S., Zhang, Y. and Song, C. 2017. A regional-scale assessment of Himalayan glacial lake changes using satellite observations from 1990 to 2015. *Remote Sensing of Environment*. **189**, pp.1–13.

Nijhawan, R., Das, J. and Balasubramanian, R. 2018. A Hybrid CNN + Random Forest Approach to Delineate Debris Covered Glaciers Using Deep Features. *Journal of the Indian Society of Remote Sensing*. **46**(6), pp.981–989.

Nijhawan, R., Das, J. and Raman, B. 2019. A hybrid of deep learning and hand-crafted features based approach for snow cover mapping. *International Journal of Remote Sensing*. **40**(2), pp.759–773.

Nordbeck, O., Duchossois, G., Kohlhammer, G., Andersson, E., Diehl, T., Dinessen, F., Eriksson, P., Flett, D., Garric, G., Gros, J.-C., Jacq, F., Molch, K., Nagler, T., Nicolas, J., Strobl, P., European Commission, and Directorate-General for Defence Industry and Space 2021. *User requirements for a Copernicus polar observing system: phase 3 report : towards operational products and services.* [Online]. [Accessed 20 June 2022]. Available from: https://op.europa.eu/publication/manifestation_identifier/PUB_HVNC29144ENN.

Nussbaumer, S.U., Hoelzle, M., Hüsler, F., Huggel, C., Salzmann, N. and Zemp, M. 2017. Glacier Monitoring and Capacity Building: Important Ingredients for Sustainable Mountain Development. *Mountain Research and Development*. **37**(1), pp.141–152.

Nuth, C. and Kääb, A. 2011. Co-registration and bias corrections of satellite elevation data sets for quantifying glacier thickness change. *The Cryosphere*. **5**(1), pp.271–290.

O'Connor, J., Smith, M. and James, M.R. 2017. Cameras and settings for aerial surveys in the geosciences: optimizing image data. *Progress in Physical Geography*. **41**(3), pp.325–344.

Odry, J., Boucher, M.A., Cantet, P., Lachance-Cloutier, S., Turcotte, R. and St-Louis, P.Y. 2020. Using artificial neural networks to estimate snow water equivalent from snow depth. *Canadian Water Resources Journal / Revue canadienne des ressources hydriques*. **45**(3), pp.252–268.

Orlove, B. 2009. *The Past, the Present and Some Possible Futures of Adaptation*. Rochester, NY: Social Science Research Network.

Pagnutti, M.A., Ryan, R.E., V, G.J.C., Gold, M.J., Harlan, R., Leggett, E. and Pagnutti, J.F. 2017. Laying the foundation to use Raspberry Pi 3 V2 camera module imagery for scientific and engineering purposes. *Journal of Electronic Imaging*. **26**(1), p.013014.

Parajka, J., Haas, P., Kirnbauer, R., Jansa, J. and Blöschl, G. 2012. Potential of time-lapse photography of snow for hydrological purposes at the small catchment scale. *Hydrological Processes*. **26**(22), pp.3327–3337.

Parrish, C.E., Magruder, L.A., Neuenschwander, A.L., Forfinski-Sarkozi, N., Alonzo, M. and Jasinski, M. 2019. Validation of ICESat-2 ATLAS Bathymetry and Analysis of ATLAS's Bathymetric Mapping Performance. *Remote Sensing*. **11**(14), p.1634.

Pasquini, A.I., Lecomte, K.L. and Depetris, P.J. 2008. Climate change and recent water level variability in Patagonian proglacial lakes, Argentina. *Global and Planetary Change*. **63**(4), pp.290–298.

Paul, F., Barrand, N.E., Baumann, S., Berthier, E., Bolch, T., Casey, K., Frey, H., Joshi, S.P., Konovalov, V., Bris, R.L., Mölg, N., Nosenko, G., Nuth, C., Pope, A., Racoviteanu, A., Rastner, P., Raup, B., Scharrer, K., Steffen, S. and Winsvold, S. 2013. On the accuracy of glacier outlines derived from remote-sensing data. *Annals of Glaciology*. **54**(63), pp.171–182.

Paul, F., Huggel, C. and Kääb, A. 2004. Combining satellite multispectral image data and a digital elevation model for mapping debris-covered glaciers. *Remote Sensing of Environment*. **89**(4), pp.510–518.

Pekel, J.-F., Cottam, A., Gorelick, N. and Belward, A.S. 2016. High-resolution mapping of global surface water and its long-term changes. *Nature*. **540**(7633), pp.418–422.

Perov, V., Chernomorets, S., Budarina, O., Savernyuk, E. and Leontyeva, T. 2017. Debris flow hazards for mountain regions of Russia: regional features and key events. *Natural Hazards*. **88**(S1), pp.199–235.

Perry, L.B., Seimon, A. and Kelly, G.M. 2014. Precipitation delivery in the tropical high Andes of southern Peru: new findings and paleoclimatic implications. *International Journal of Climatology*. **34**(1), pp.197–215.

Pętlicki, M., Ciepły, M., Jania, J.A., Promińska, A. and Kinnard, C. 2015. Calving of a tidewater glacier driven by melting at the waterline. *Journal of Glaciology*. **61**(229), pp.851–863.

Pieczonka, T. and Bolch, T. 2015. Region-wide glacier mass budgets and area changes for the Central Tien Shan between ~1975 and 1999 using Hexagon KH-9 imagery. *Global and Planetary Change*. **128**, pp.1–13.

Pieczonka, T., Bolch, T., Junfeng, W. and Shiyin, L. 2013. Heterogeneous mass loss of glaciers in the Aksu-Tarim Catchment (Central Tien Shan) revealed by 1976 KH-9 Hexagon and 2009 SPOT-5 stereo imagery. *Remote Sensing of Environment*. **130**, pp.233–244.

Pierdicca, N., Davidson, M., Chini, M., Dierking, W., Djavidnia, S., Haarpaintner, J., Hajduch, G., Laurin, G.V., Lavalle, M., López-Martínez, C., Nagler, T. and Su, B. 2019. The Copernicus L-band SAR mission ROSE-L (Radar Observing System for Europe) (Conference Presentation) *In*: C. Notarnicola, N. Pierdicca, F. Bovenga and E. Santi, eds. *Active and Passive Microwave Remote Sensing for Environmental Monitoring III*. Strasbourg, France: SPIE, p.13.

Piermattei, L., Carturan, L. and Guarnieri, A. 2015. Use of terrestrial photogrammetry based on structure-from-motion for mass balance estimation of a small glacier in the Italian alps. *Earth Surface Processes and Landforms*. **40**(13), pp.1791–1802.

Piras, M., Grasso, N. and Abdul Jabbar, A. 2017. UAV photogrammetric solution using a Raspberry Pi camera module and smart devices: Test and results. *The International Archives of the Photogrammetry, Remote Sensing and Spatial Information Sciences*. **XLII-2/W6**, pp.289–296.

Pope, A., Rees, W., Fox, A. and Fleming, A. 2014. Open Access Data in Polar and Cryospheric Remote Sensing. *Remote Sensing*. **6**(7), pp.6183–6220.

Portenier, C., Hüsler, F., Härer, S. and Wunderle, S. 2020. Towards a webcam-based snow cover monitoring network: methodology and evaluation. *The Cryosphere*. **14**(4), pp.1409–1423.

Poursanidis, D., Traganos, D., Chrysoulakis, N. and Reinartz, P. 2019. Cubesats Allow High Spatiotemporal Estimates of Satellite-Derived Bathymetry. *Remote Sensing*. **11**(11), p.1299.

Prinz, R., Heller, A., Ladner, M., Nicholson, L. and Kaser, G. 2018. Mapping the Loss of Mt. Kenya's Glaciers: An Example of the Challenges of Satellite Monitoring of Very Small Glaciers. *Geosciences*. **8**(5), p.174.

Prior-Jones, M.R., Bagshaw, E.A., Lees, J., Clare, L., Burrow, S., Werder, M.A., Karlsson, N.B., Dahl-Jensen, D., Chudley, T.R., Christoffersen, P., Wadham, J.L., Doyle, S.H. and Hubbard, B. 2021. Cryoegg: development and field trials of a wireless subglacial probe for deep, fast-moving ice. *Journal of Glaciology*. **67**(264), pp.627–640.

Pritchard, H.D., Arthern, R.J., Vaughan, D.G. and Edwards, L.A. 2009. Extensive dynamic thinning on the margins of the Greenland and Antarctic ice sheets. *Nature*. **461**(7266), pp.971–975.

Prokop, A. 2008. Assessing the applicability of terrestrial laser scanning for spatial snow depth measurements. *Cold Regions Science and Technology*. **54**(3), pp.155–163.

Quincey, D.J., Copland, L., Mayer, C., Bishop, M., Luckman, A. and Belò, M. 2009. Ice velocity and climate variations for Baltoro Glacier, Pakistan. *Journal of Glaciology*. **55**(194), pp.1061–1071.

Quincey, D.J., Lucas, R.M., Richardson, S.D., Glasser, N.F., Hambrey, M.J. and Reynolds, J.M. 2005. Optical remote sensing techniques in high-mountain environments: application to glacial hazards. *Progress in Physical Geography: Earth and Environment*. **29**(4), pp.475–505.

Quincey, D.J., Richardson, S.D., Luckman, A., Lucas, R.M., Reynolds, J.M., Hambrey, M.J. and Glasser, N.F. 2007. Early recognition of glacial lake hazards in the Himalaya using remote sensing datasets. *Global and Planetary Change*. **56**(1), pp.137–152.

Rabatel, A., Bermejo, A., Loarte, E., Soruco, A., Gomez, J., Leonardini, G., Vincent, C. and Sicart, J.E. 2012. Can the snowline be used as an indicator of the equilibrium line and mass balance for glaciers in the outer tropics? *Journal of Glaciology*. **58**(212), pp.1027–1036.

Rabatel, A., Dedieu, J.P. and Vincent, C. 2016. Spatio-temporal changes in glacier-wide mass balance quantified by optical remote sensing on 30 glaciers in the French Alps for the period 1983–2014. *Journal of Glaciology*. **62**(236), pp.1153–1166.

Rabatel, A., Francou, B., Soruco, A., Gomez, J., Cáceres, B., Ceballos, J.L., Basantes, R., Vuille, M., Sicart, J.-E., Huggel, C., Scheel, M., Lejeune, Y., Arnaud, Y., Collet, M., Condom, T., Consoli, G., Favier, V., Jomelli, V., Galarraga, R., Ginot, P., Maisincho, L., Mendoza, J., Ménégoz, M., Ramirez, E., Ribstein, P., Suarez, W., Villacis, M. and Wagnon, P. 2013. Current state of glaciers in the tropical Andes: a multi-century perspective on glacier evolution and climate change. *The Cryosphere*. **7**(1), pp.81–102.

Rabatel, A., Letréguilly, A., Dedieu, J.-P. and Eckert, N. 2013. Changes in glacier equilibrium-line altitude in the western Alps from 1984 to 2010: evaluation by remote sensing and modeling of the morpho-topographic and climate controls. *The Cryosphere*. **7**(5), pp.1455–1471.

Rabus, B.T. and Fatland, D.R. 2000. Comparison of SAR-interferometric and surveyed velocities on a mountain glacier: Black Rapids Glacier, Alaska, U.S.A. *Journal of Glaciology*. **46**(152), pp.119–128.

Racoviteanu, A., Williams, M. and Barry, R. 2008. Optical Remote Sensing of Glacier Characteristics: A Review with Focus on the Himalaya. *Sensors*. **8**(5), pp.3355–3383.

Racoviteanu, A.E., Arnaud, Y., Williams, M.W. and Ordoñez, J. 2008. Decadal changes in glacier parameters in the Cordillera Blanca, Peru, derived from remote sensing. *Journal of Glaciology*. **54**(186), pp.499–510.

Racoviteanu, A.E., Rittger, K. and Armstrong, R. 2019. An Automated Approach for Estimating Snowline Altitudes in the Karakoram and Eastern Himalaya From Remote Sensing. *Frontiers in Earth Science*. **7**, p.220.

Ramirez-Atencia, C., Rodríguez-Fernández, V., Gonzalez-Pardo, A. and Camacho, D. 2017. New Artificial Intelligence approaches for future UAV Ground Control Stations *In*: *2017 IEEE Congress on Evolutionary Computation (CEC)*. Donostia, Spain: IEEE, pp.2775–2782.

Rao, Y.S., Venkataraman, G., Rao, K.S., and Snehmani 2004. SAR interferometry for DEM generation and movemnet of Indian glaciers *In*: *IGARSS 2004. 2004 IEEE International Geoscience and Remote Sensing Symposium*., pp.1128–1131.

Rashid, I., Majeed, U., Jan, A. and Glasser, N.F. 2020. The January 2018 to September 2019 surge of Shisper Glacier, Pakistan, detected from remote sensing observations. *Geomorphology*. **351**, p.106957.

Rastner, P., Bolch, T., Notarnicola, C. and Paul, F. 2014. A Comparison of Pixel- and Object-Based Glacier Classification With Optical Satellite Images. *IEEE Journal of Selected Topics in Applied Earth Observations and Remote Sensing*. **7**(3), pp.853–862.

Rastner, P., Prinz, R., Notarnicola, C., Nicholson, L., Sailer, R., Schwaizer, G. and Paul, F. 2019. On the Automated Mapping of Snow Cover on Glaciers and Calculation of Snow Line Altitudes from Multi-Temporal Landsat Data. *Remote Sensing*. **11**(12), p.1410.

Redpath, T.A.N., Sirguey, P., Fitzsimons, S.J. and Kääb, A. 2013. Accuracy assessment for mapping glacier flow velocity and detecting flow dynamics from ASTER satellite imagery: Tasman Glacier, New Zealand. *Remote Sensing of Environment*. **133**, pp.90–101.

Reid, T.D. and Brock, B.W. 2014. Assessing ice-cliff backwasting and its contribution to total ablation of debris-covered Miage glacier, Mont Blanc massif, Italy. *Journal of Glaciology*. **60**(219), pp.3–13.

RGI Consortium 2017. Randolph Glacier Inventory 6.0. [Accessed 24 November 2021]. Available from: http://www.glims.org/RGI/randolph60.html.

Richter, A., Marderwald, E., Hormaechea, J.L., Mendoza, L., Perdomo, R., Connon, G., Scheinert, M., Horwath, M. and Dietrich, R. 2015. Lake-level variations and tides in Lago Argentino, Patagonia: insights from pressure tide gauge records. *Journal of Limnology*. **75**(1), pp.1–34.

Ridley, J.K. and Partington, K.C. 1988. A model of satellite radar altimeter return from ice sheets. *International Journal of Remote Sensing*. **9**(4), pp.601–624.

Rignot, E., Echelmeyer, K. and Krabill, W. 2001. Penetration depth of interferometric synthetic-aperture radar signals in snow and ice. *Geophysical Research Letters*. **28**(18), pp.3501–3504.

Rizzoli, P., Martone, M., Gonzalez, C., Wecklich, C., Borla Tridon, D., Bräutigam, B., Bachmann, M., Schulze, D., Fritz, T., Huber, M., Wessel, B., Krieger, G., Zink, M. and Moreira, A. 2017. Generation and performance assessment of the global TanDEM-X digital elevation model. *ISPRS Journal of Photogrammetry and Remote Sensing*. **132**, pp.119–139.

Robson, B.A., Nuth, C., Dahl, S.O., Hölbling, D., Strozzi, T. and Nielsen, P.R. 2015. Automated classification of debris-covered glaciers combining optical, SAR and topographic data in an object-based environment. *Remote Sensing of Environment*. **170**, pp.372–387.

Rosen, P.A., Kim, Y., Kumar, R., Misra, T., Bhan, R. and Sagi, V.R. 2017. Global persistent SAR sampling with the NASA-ISRO SAR (NISAR) mission *In*: *2017 IEEE Radar Conference (RadarConf)*. Seattle, WA, USA: IEEE, pp.0410–0414.

Rosenau, R., Schwalbe, E., Maas, H.-G., Baessler, M. and Dietrich, R. 2013. Grounding line migration and high-resolution calving dynamics of Jakobshavn Isbræ, West Greenland. *Journal of Geophysical Research: Earth Surface*. **118**(2), pp.382–395.

Rossini, M., Di Mauro, B., Garzonio, R., Baccolo, G., Cavallini, G., Mattavelli, M., De Amicis, M. and Colombo, R. 2018. Rapid melting dynamics of an alpine glacier with repeated UAV photogrammetry. *Geomorphology*. **304**, pp.159–172.

Rott, H. 1984. The analysis of backscattering properties from SAR data of mountain regions. *IEEE Journal of Oceanic Engineering*. **9**(5), pp.347–355.

Rott, H. and Mätzler, C. 1987. Possibilities and Limits of Synthetic Aperture Radar for Snow and Glacier Surveying. *Annals of Glaciology*. **9**, pp.195–199.

Rounce, D., Watson, C. and McKinney, D. 2017. Identification of Hazard and Risk for Glacial Lakes in the Nepal Himalaya Using Satellite Imagery from 2000–2015. *Remote Sensing*. **9**(7), p.654.

Rounce, D.R., Hock, R. and Shean, D.E. 2020. Glacier Mass Change in High Mountain Asia Through 2100 Using the Open-Source Python Glacier Evolution Model (PyGEM). *Frontiers in Earth Science*. **7**(331).

Roy, D.P., Wulder, M.A., Loveland, T.R., C.E., W., Allen, R.G., Anderson, M.C., Helder, D., Irons, J.R., Johnson, D.M., Kennedy, R., Scambos, T.A., Schaaf, C.B., Schott, J.R., Sheng, Y., Vermote, E.F., Belward, A.S., Bindschadler, R., Cohen, W.B., Gao, F., Hipple, J.D., Hostert, P., Huntington, J., Justice, C.O., Kilic, A., Kovalskyy, V., Lee, Z.P., Lymburner, L., Masek, J.G., McCorkel, J., Shuai, Y., Trezza, R., Vogelmann, J., Wynne, R.H. and Zhu, Z. 2014. Landsat-8: Science and product vision for terrestrial global change research. *Remote Sensing of Environment*. **145**, pp.154–172.

Roy, S. 2021. *samapriya/geeup: geeup: Simple CLI for Earth Engine Uploads* [Online]. Zenodo. [Accessed 12 July 2021]. Available from: https://zenodo.org/record/4852799.

Ryan, J.C., Hubbard, A.L., Box, J.E., Todd, J., Christoffersen, P., Carr, J.R., Holt, T.O. and Snooke, N.A. 2015. UAV photogrammetry and structure from motion to assess calving dynamics at Store Glacier, a large outlet draining the Greenland ice sheet. *The Cryosphere*. **9**, pp.1–11.

Ryan, J.C., Hubbard, A.L., Todd, J., Carr, J.R., Box, J.E., Christoffersen, P., Holt, T.O. and Snooke, N. 2014. *Repeat UAV photogrammetry to assess calving front dynamics at a large outlet glacier draining the Greenland Ice Sheet* [Online]. Glaciers. [Accessed 28 May 2022]. Available from: https://tc.copernicus.org/preprints/8/2243/2014/tcd-8-2243-2014.pdf.

Sagredo, E.A. and Lowell, T.V. 2012. Climatology of Andean glaciers: A framework to understand glacier response to climate change. *Global and Planetary Change*. **86–87**, pp.101–109.

Salomonson, V.V. and Appel, I. 2004. Estimating fractional snow cover from MODIS using the normalized difference snow index. *Remote Sensing of Environment*. **89**(3), pp.351–360.

Salzmann, N., Huggel, C., Rohrer, M., Silverio, W., Mark, B.G., Burns, P. and Portocarrero, C. 2013. Glacier changes and climate trends derived from multiple sources in the data scarce Cordillera Vilcanota region, southern Peruvian Andes. *The Cryosphere*. **7**(1), pp.103–118.

Sandau, R., Brieß, K. and D'Errico, M. 2010. Small satellites for global coverage: Potential and limits. *ISPRS Journal of Photogrammetry and Remote Sensing*. **65**(6), pp.492–504.

Sarango, D., Velasquez, T., Rozas, G. and Gastelo, J. 2021. Influencia de los volúmenes hídricos almacenados en la laguna Sibinacocha en la 2da etapa de rehabilitación de la central hidroeléctrica Machupicchu. *Revista de Investigación de Física*. **21**(2), pp.39–48.

Scaioni, M., Barazzetti, L., Yordanov, V., Azzoni, R.S., Fugazza, D., Cernuschi, M. and Diolaiuti, G.A. 2019. Structure-From-Motion Photogrammetry to Support the Assessment of Collapse Risk in Alpine Glaciers *In*: O. Altan, M. Chandra, F. Sunar and T. J. Tanzi, eds. *Intelligent Systems for Crisis Management*. Lecture Notes in Geoinformation and Cartography. Cham: Springer International Publishing, pp.239–263.

Scambos, T.A., Dutkiewicz, M.J., Wilson, J.C. and Bindschadler, R.A. 1992. Application of image cross-correlation to the measurement of glacier velocity using satellite image data. *Remote Sensing of Environment*. **42**(3), pp.177–186.

Schaefli, B. 2015. Projecting hydropower production under future climates: a guide for decision-makers and modelers to interpret and design climate change impact assessments. *WIREs Water*. **2**(4), pp.271–289.

Schartel, M., Burr, R., Mayer, W., Docci, N. and Waldschmidt, C. 2018. UAV-Based Ground Penetrating Synthetic Aperture Radar *In*: *2018 IEEE MTT-S International Conference on Microwaves for Intelligent Mobility (ICMIM)*. Munich: IEEE, pp.1–4.

Schaub, Y., Haeberli, W., Huggel, C., Künzler, M. and Bründl, M. 2013. Landslides and New Lakes in Deglaciating Areas: A Risk Management Framework *In*: C. Margottini, P. Canuti and K. Sassa, eds. *Landslide Science and Practice*. Berlin, Heidelberg: Springer Berlin Heidelberg, pp.31–38.

Schauwecker, S., Rohrer, M., Acuña, D., Cochachin, A., Dávila, L., Frey, H., Giráldez, C., Gómez, J., Huggel, C., Jacques-Coper, M., Loarte, E., Salzmann, N. and Vuille, M. 2014. Climate trends and glacier retreat in the Cordillera Blanca, Peru, revisited. *Global and Planetary Change*. **119**, pp.85–97.

Schauwecker, S., Rohrer, M., Huggel, C., Endries, J., Montoya, N., Neukom, R., Perry, B., Salzmann, N., Schwarb, M. and Suarez, W. 2017. The freezing level in the tropical Andes, Peru: An indicator for present and future glacier extents. *Journal of Geophysical Research: Atmospheres*. **122**(10), pp.5172–5189.

Scheffran, J. and Battaglini, A. 2011. Climate and conflicts: the security risks of global warming. *Regional Environmental Change*. **11**(1), pp.27–39.

Scherler, D., Leprince, S. and Strecker, M. 2008. Glacier-surface velocities in alpine terrain from optical satellite imagery—Accuracy improvement and quality assessment. *Remote Sensing of Environment*. **112**(10), pp.3806–3819.

Schneider, D., Huggel, C., Cochachin, A., Guillén, S. and García, J. 2014. Mapping hazards from glacier lake outburst floods based on modelling of process cascades at Lake 513, Carhuaz, Peru. *Advances in Geosciences*. **35**, pp.145–155.

Scholz, S., Knight, P., Eckle, M., Marx, S. and Zipf, A. 2018. Volunteered Geographic Information for Disaster Risk Reduction—The Missing Maps Approach and Its Potential within the Red Cross and Red Crescent Movement. *Remote Sensing*. **10**(8), p.1239.

Schomacker, A. 2010. Expansion of ice-marginal lakes at the Vatnajökull ice cap, Iceland, from 1999 to 2009. *Geomorphology*. **119**(3), pp.232–236.

Schutz, B.E., Zwally, H.J., Shuman, C.A., Hancock, D. and DiMarzio, J.P. 2005. Overview of the ICESat Mission. *Geophysical Research Letters*. **32**(21).

Scott, R.F., Baker, S.G., Birkett, C.M., Cudlip, W., Laxon, S.W., Mantripp, D.R., Mansley, J.A., Morley, J.G., Rapley, C.G., Ridley, J.K., Strawbridge, F. and Wingham, D.J. 1994. A comparison of the performance of the ice and ocean tracking modes of the ERS-1 radar altimeter over non-ocean surfaces. *Geophysical Research Letters*. **21**(7), pp.553–556.

Seehaus, T., Malz, P., Sommer, C., Lippl, S., Cochachin, A. and Braun, M. 2019. Changes of the tropical glaciers throughout Peru between 2000 and 2016 – mass balance and area fluctuations. *The Cryosphere*. **13**(10), pp.2537–2556.

Seguin, G. and Geudtner, D. 2018. Challenges for Next Generation SAR *In*: *EUSAR 2018; 12th European Conference on Synthetic Aperture Radar*., pp.1–4.

Shangguan, D.H., Bolch, T., Ding, Y.J., Kröhnert, M., Pieczonka, T., Wetzel, H.U. and Liu, S.Y. 2015. Mass changes of Southern and Northern Inylchek Glacier, Central Tian Shan, Kyrgyzstan, during ~1975 and 2007 derived from remote sensing data. *The Cryosphere*. **9**(2), pp.703–717.

Shean, D. 2017. High Mountain Asia 8-meter DEM Mosaics Derived from Optical Imagery, Version 1. [Accessed 26 June 2022]. Available from: https://nsidc.org/data/HMA_DEM8m_MOS/versions/1.

Shean, D.E., Bhushan, S., Montesano, P., Rounce, D.R., Arendt, A. and Osmanoglu, B. 2020. A Systematic, Regional Assessment of High Mountain Asia Glacier Mass Balance. *Frontiers in Earth Science*. **7**, p.363.

Shepherd, A., Ivins, E., Rignot, E., Smith, B., van den Broeke, M., Velicogna, I., Whitehouse, P., Briggs, K., Joughin, I., Krinner, G., Nowicki, S., Payne, T., Scambos, T., Schlegel, N., A, G., Agosta, C., Ahlstrøm, A., Babonis, G., Barletta, V., Blazquez, A., Bonin, J., Csatho, B., Cullather, R., Felikson, D., Fettweis, X., Forsberg, R., Gallee, H., Gardner, A., Gilbert, L., Groh, A., Gunter, B., Hanna, E., Harig, C., Helm, V., Horvath, A., Horwath, M., Khan, S., Kjeldsen, K.K., Konrad, H., Langen, P., Lecavalier, B., Loomis, B., Luthcke, S., McMillan, M., Melini, D., Mernild, S., Mohajerani, Y., Moore, P., Mouginot, J., Moyano, G., Muir, A., Nagler, T., Nield, G., Nilsson, J., Noel, B., Otosaka, I., Pattle, M.E., Peltier, W.R., Pie, N., Rietbroek, R., Rott, H., Sandberg-Sørensen, L., Sasgen, I., Save, H., Scheuchl, B., Schrama, E., Schröder, L., Seo, K.-W., Simonsen, S., Slater, T., Spada, G., Sutterley, T., Talpe, M., Tarasov, L., van de Berg, W.J., van der Wal, W., van Wessem, M., Vishwakarma, B.D., Wiese, D., Wouters, B., and The IMBIE team 2018. Mass balance of the Antarctic Ice Sheet from 1992 to 2017. *Nature*. **558**(7709), pp.219–222.

Shepherd, A., Ivins, E.R., A, G., Barletta, V.R., Bentley, M.J., Bettadpur, S., Briggs, K.H., Bromwich, D.H., Forsberg, R., Galin, N., Horwath, M., Jacobs, S., Joughin, I., King, M.A., Lenaerts, J.T.M., Li, J., Ligtenberg, S.R.M., Luckman, A., Luthcke, S.B., McMillan, M., Meister, R., Milne, G., Mouginot, J., Muir, A., Nicolas, J.P., Paden, J., Payne, A.J., Pritchard, H., Rignot, E., Rott, H., Sørensen, L.S., Scambos, T.A., Scheuchl, B., Schrama, E.J.O., Smith, B., Sundal, A.V., Angelen, J.H. van, Berg, W.J. van de, Broeke, M.R. van den, Vaughan, D.G., Velicogna, I., Wahr, J., Whitehouse, P.L., Wingham, D.J., Yi, D., Young, D. and Zwally, H.J. 2012. A Reconciled Estimate of Ice-Sheet Mass Balance. *Science*. **338**(6111), pp.1183–1189.

Shiggins, C., Lea, J.M., Fahrner, D. and Brough, S. 2021. Automatically detecting icebergs using Google Earth Engine and ArcticDEM *In*: *EGU General Assembly 2021* [Online]. Online: EGU. [Accessed 28 May 2022]. Available from: http://rgdoi.net/10.13140/RG.2.2.21053.18402.

Shugar, D.H., Burr, A., Haritashya, U.K., Kargel, J.S., Watson, C.S., Kennedy, M.C., Bevington, A.R., Betts, R.A., Harrison, S. and Strattman, K. 2020. Rapid worldwide growth of glacial lakes since 1990. *Nature Climate Change*. **10**(10), pp.939–945.

Shugar, D.H., Jacquemart, M., Shean, D., Bhushan, S., Upadhyay, K., Sattar, A., Schwanghart, W., McBride, S., Vries, M.V.W. de, Mergili, M., Emmer, A., Deschamps-Berger, C., McDonnell, M., Bhambri, R., Allen, S., Berthier, E., Carrivick, J.L., Clague, J.J., Dokukin, M., Dunning, S.A., Frey, H., Gascoin, S., Haritashya, U.K., Huggel, C., Kääb, A., Kargel, J.S., Kavanaugh, J.L., Lacroix, P., Petley, D., Rupper, S., Azam, M.F., Cook, S.J., Dimri, A.P., Eriksson, M., Farinotti, D., Fiddes, J., Gnyawali, K.R., Harrison, S., Jha, M., Koppes, M., Kumar, A., Leinss, S., Majeed, U., Mal, S., Muhuri, A., Noetzli, J., Paul, F., Rashid, I., Sain, K., Steiner,

J., Ugalde, F., Watson, C.S. and Westoby, M.J. 2021. A massive rock and ice avalanche caused the 2021 disaster at Chamoli, Indian Himalaya. *Science*. **373**(6552), pp.300–306.

Singh, D.K., Gusain, H.S., Mishra, V., Gupta, N. and Das, R.K. 2018. Automated mapping of snow/ice surface temperature using Landsat-8 data in Beas River basin, India, and validation with wireless sensor network data. *Arabian Journal of Geosciences*. **11**(6), p.136.

Slater, T., Lawrence, I.R., Otosaka, I.N., Shepherd, A., Gourmelen, N., Jakob, L., Tepes, P., Gilbert, L. and Nienow, P. 2021. Review article: Earth's ice imbalance. *The Cryosphere*. **15**(1), pp.233–246.

Smith, B., Fricker, H.A., Holschuh, N., Gardner, A.S., Adusumilli, S., Brunt, K.M., Csatho, B., Harbeck, K., Huth, A., Neumann, T., Nilsson, J. and Siegfried, M.R. 2019. Land ice height-retrieval algorithm for NASA's ICESat-2 photon-counting laser altimeter. *Remote Sensing of Environment*. **233**, p.111352.

Smith, M.W., Carrivick, J.L. and Quincey, D.J. 2016. Structure from motion photogrammetry in physical geography. *Progress in Physical Geography: Earth and Environment*. **40**(2), pp.247–275.

Smith, T. and Bookhagen, B. 2018. Changes in seasonal snow water equivalent distribution in High Mountain Asia (1987 to 2009). *Science Advances*. **4**(1), p.e1701550.

Sochor, L., Seehaus, T. and Braun, M.H. 2021. Increased Ice Thinning over Svalbard Measured by ICESat/ICESat-2 Laser Altimetry. *Remote Sensing*. **13**(11), p.2089.

Song, C., Ke, L., Huang, B. and Richards, K.S. 2015. Can mountain glacier melting explains the GRACE-observed mass loss in the southeast Tibetan Plateau: From a climate perspective? *Global and Planetary Change*. **124**, pp.1–9.

Sorensen, K.L., Helland, A.S. and Johansen, T.A. 2015. Carbon nanomaterial-based wing temperature control system for in-flight anti-icing and de-icing of unmanned aerial vehicles *In*: *2015 IEEE Aerospace Conference*. Big Sky, MT: IEEE, pp.1–6.

Stöcker, C., Bennett, R., Nex, F., Gerke, M. and Zevenbergen, J. 2017. Review of the Current State of UAV Regulations. *Remote Sensing*. **9**(5), p.459.

Strozzi, T., Kouraev, A., Wiesmann, A., Wegmüller, U., Sharov, A. and Werner, C. 2008. Estimation of Arctic glacier motion with satellite L-band SAR data. *Remote Sensing of Environment*. **112**(3), pp.636–645.

Strozzi, T., Wiesmann, A., Kääb, A., Joshi, S. and Mool, P. 2012. Glacial lake mapping with very high resolution satellite SAR data. *Natural Hazards and Earth System Sciences*. **12**(8), pp.2487–2498.

Sulak, D.J., Sutherland, D.A., Enderlin, E.M., Stearns, L.A. and Hamilton, G.S. 2017. Iceberg properties and distributions in three Greenlandic fjords using satellite imagery. *Annals of Glaciology*. **58**(74), pp.92–106.

Surazakov, A.B., Aizen, V.B., Aizen, E.M. and Nikitin, S.A. 2007. Glacier changes in the Siberian Altai Mountains, Ob river basin, (1952–2006) estimated with high resolution imagery. *Environmental Research Letters*. **2**(4), p.045017.

Taburet, N., Zawadzki, L., Vayre, M., Blumstein, D., Le Gac, S., Boy, F., Raynal, M., Labroue, S., Crétaux, J.-F. and Femenias, P. 2020. S3MPC: Improvement on Inland Water Tracking and Water Level Monitoring from the OLTC Onboard Sentinel-3 Altimeters. *Remote Sensing*. **12**(18), p.3055.

Taylor, L.S., Quincey, D.J., Smith, M.W., Baumhoer, C.A., McMillan, M. and Mansell, D.T. 2021. Remote sensing of the mountain cryosphere: Current capabilities and future opportunities for research. *Progress in Physical Geography: Earth and Environment*. **45**(6), pp.931–964.

Themistocleous, K. 2017. Model reconstruction for 3d vizualization of cultural heritage sites using open data from social media: The case study of Soli, Cyprus. *Journal of Archaeological Science: Reports*. **14**, pp.774–781.

Thompson, I., Shrestha, M., Chhetri, N. and Agusdinata, D.B. 2020. An institutional analysis of glacial floods and disaster risk management in the Nepal Himalaya. *International Journal of Disaster Risk Reduction*. **47**, p.101567.

Thompson, L.G., Davis, M.E., Mosley-Thompson, E., Porter, S.E., Corrales, G.V., Shuman, C.A. and Tucker, C.J. 2021. The impacts of warming on rapidly retreating high-altitude, low-latitude glaciers and ice core-derived climate records. *Global and Planetary Change*. **203**, p.103538.

Thompson, L.G., Mosley-Thompson, E., Davis, M.E. and Brecher, H.H. 2011. Tropical glaciers, recorders and indicators of climate change, are disappearing globally. *Annals of Glaciology*. **52**(59), pp.23–34.

Tiwari, A., Sain, K., Kumar, A., Tiwari, J., Paul, A., Kumar, N., Haldar, C., Kumar, S. and Pandey, C.P. 2022. Potential seismic precursors and surficial dynamics of a deadly Himalayan disaster: an early warning approach. *Scientific Reports*. **12**(1), p.3733.

Trantow, T. and Herzfeld, U.C. 2016. Spatiotemporal mapping of a large mountain glacier from CryoSat-2 altimeter data: surface elevation and elevation change of Bering Glacier during surge (2011–2014). *International Journal of Remote Sensing*. **37**(13), pp.2962–2989.

Treichler, D. and Kääb, A. 2016. ICESat laser altimetry over small mountain glaciers. *The Cryosphere*. **10**(5), pp.2129–2146.

Treichler, D. and Kääb, A. 2017. Snow depth from ICESat laser altimetry — A test study in southern Norway. *Remote Sensing of Environment*. **191**, pp.389–401.

Tsai, Dietz, Oppelt, and Kuenzer 2019. Wet and Dry Snow Detection Using Sentinel-1 SAR Data for Mountainous Areas with a Machine Learning Technique. *Remote Sensing*. **11**(8), p.895.

Tsai, Y.-L.S., Dietz, A., Oppelt, N. and Kuenzer, C. 2019. Remote Sensing of Snow Cover Using Spaceborne SAR: A Review. *Remote Sensing*. **11**(12), p.1456.

Tsai, Y.-L.S., Klein, I., Dietz, A. and Oppelt, N. 2020. Monitoring Large-Scale Inland Water Dynamics by Fusing Sentinel-1 SAR and Sentinel-3 Altimetry Data and by Analyzing Causal Effects of Snowmelt. *Remote Sensing*. **12**(23), p.3896.

Tweed, F.S. and Carrivick, J.L. 2015. Deglaciation and proglacial lakes. *Geology Today*. **31**(3), pp.96–102.

Ukita, J., Narama, C., Tadono, T., Yamanokuchi, T., Tomiyama, N., Kawamoto, S., Abe, C., Uda, T., Yabuki, H., Fujita, K. and Nishimura, K. 2011. Glacial lake inventory of Bhutan using ALOS data: methods and preliminary results. *Annals of Glaciology*. **52**(58), pp.65–71.

Uuemaa, E., Ahi, S., Montibeller, B., Muru, M. and Kmoch, A. 2020. Vertical Accuracy of Freely Available Global Digital Elevation Models (ASTER, AW3D30, MERIT, TanDEM-X, SRTM, and NASADEM). *Remote Sensing*. **12**(21), p.3482.

Vanhellemont, Q. and Ruddick, K. 2018. Atmospheric correction of metre-scale optical satellite data for inland and coastal water applications. *Remote Sensing of Environment*. **216**, pp.586–597.

Vasuki, Y., Holden, E.-J., Kovesi, P. and Micklethwaite, S. 2014. Semi-automatic mapping of geological Structures using UAV-based photogrammetric data: An image analysis approach. *Computers & Geosciences*. **69**, pp.22–32.

Veettil, B.K. 2018. Glacier mapping in the Cordillera Blanca, Peru, tropical Andes, using Sentinel-2 and Landsat data. *Singapore Journal of Tropical Geography*. **39**(3), pp.351–363.

Veettil, Bijeesh Kozhikkodan, Bremer, U.F., de Souza, S.F., Maier, É.L.B. and Simões, J.C. 2016. Influence of ENSO and PDO on mountain glaciers in the outer tropics: case studies in Bolivia. *Theoretical and Applied Climatology*. **125**(3), pp.757–768.

Veettil, Bijeesh K., Bremer, U.F., de Souza, S.F., Maier, É.L.B. and Simões, J.C. 2016. Variations in annual snowline and area of an ice-covered stratovolcano in the Cordillera Ampato, Peru, using remote sensing data (1986–2014). *Geocarto International*. **31**(5), pp.544–556.

Veettil, B.K. and Kamp, U. 2021. Glacial Lakes in the Andes under a Changing Climate: A Review. *Journal of Earth Science*. **32**, pp.1575–1593.

Veettil, B.K. and Kamp, U. 2019. Global Disappearance of Tropical Mountain Glaciers: Observations, Causes, and Challenges. *Geosciences*. **9**(5), p.196.

Veettil, B.K. and Souza, S.F. de 2017. Study of 40-year glacier retreat in the northern region of the Cordillera Vilcanota, Peru, using satellite images: preliminary results. *Remote Sensing Letters*. **8**(1), pp.78–85.

Veettil, B.K., Wang, S., Simões, J.C., Ruiz Pereira, S.F. and de Souza, S.F. 2018. Regional climate forcing and topographic influence on glacier shrinkage: eastern cordilleras of Peru. *International Journal of Climatology*. **38**(2), pp.979–995.

Veh, G., Korup, O., von Specht, S., Roessner, S. and Walz, A. 2019. Unchanged frequency of moraine-dammed glacial lake outburst floods in the Himalaya. *Nature Climate Change*. **9**(5), pp.379–383.

Viani, C., Machguth, H., Huggel, C., Godio, A., Franco, D., Perotti, L. and Giardino, M. 2020. Potential future lakes from continued glacier shrinkage in the Aosta Valley Region (Western Alps, Italy). *Geomorphology*. **355**, p.107068.

Vilca, O., Mergili, M., Emmer, A., Frey, H. and Huggel, C. 2021. The 2020 glacial lake outburst flood process chain at Lake Salkantaycocha (Cordillera Vilcabamba, Peru). *Landslides*. **18**(6), pp.2211–2223.

Vilímek, V., Zapata, M.L., Klimeš, J., Patzelt, Z. and Santillán, N. 2005. Influence of glacial retreat on natural hazards of the Palcacocha Lake area, Peru. *Landslides*. **2**(2), pp.107–115.

Villadsen, H., Deng, X., Andersen, O.B., Stenseng, L., Nielsen, K. and Knudsen, P. 2016. Improved inland water levels from SAR altimetry using novel empirical and physical retrackers. *Journal of Hydrology*. **537**, pp.234–247.

Vivero, S. and Lambiel, C. 2019. Monitoring the crisis of a rock glacier with repeated UAV surveys. *Geographica Helvetica*. **74**(1), pp.59–69.

Viviroli, D., Archer, D.R., Buytaert, W., Fowler, H.J., Greenwood, G.B., Hamlet, A.F., Huang, Y., Koboltschnig, G., Litaor, M.I., López-Moreno, J.I., Lorentz, S., Schädler, B.,

Schreier, H., Schwaiger, K., Vuille, M. and Woods, R. 2011. Climate change and mountain water resources: overview and recommendations for research, management and policy. *Hydrology and Earth System Sciences*. **15**(2), pp.471–504.

Vu, P.L., Frappart, F., Darrozes, J., Marieu, V., Blarel, F., Ramillien, G., Bonnefond, P. and Birol, F. 2018. Multi-Satellite Altimeter Validation along the French Atlantic Coast in the Southern Bay of Biscay from ERS-2 to SARAL. *Remote Sensing*. **10**(1), p.93.

Vuille, M., Carey, M., Huggel, C., Buytaert, W., Rabatel, A., Jacobsen, D., Soruco, A., Villacis, M., Yarleque, C., Elison Timm, O., Condom, T., Salzmann, N. and Sicart, J.-E. 2018. Rapid decline of snow and ice in the tropical Andes – Impacts, uncertainties and challenges ahead. *Earth-Science Reviews*. **176**, pp.195–213.

Vuille, M., Kaser, G. and Juen, I. 2008. Glacier mass balance variability in the Cordillera Blanca, Peru and its relationship with climate and the large-scale circulation. *Global and Planetary Change*. **62**(1), pp.14–28.

Vujovic, V. and Maksimovic, M. 2014. Raspberry Pi as a Wireless Sensor node: Performances and constraints *In*: *2014 37th International Convention on Information and Communication Technology, Electronics and Microelectronics (MIPRO)*. Opatija, Croatia: IEEE, pp.1013–1018.

Waechter, A., Copland, L. and Herdes, E. 2015. Modern glacier velocities across the Icefield Ranges, St Elias Mountains, and variability at selected glaciers from 1959 to 2012. *Journal of Glaciology*. **61**(228), pp.624–634.

Walden-Schreiner, C., Rossi, S.D., Barros, A., Pickering, C. and Leung, Y.-F. 2018. Using crowd-sourced photos to assess seasonal patterns of visitor use in mountain-protected areas. *Ambio*. **47**(7), pp.781–793.

Wang, C., Wang, C., Wang, C., Zhu, X., Zhu, X., Zhu, X., Nie, S., Nie, S., Nie, S., Xi, X., Li, D., Zheng, W. and Chen, S. 2019. Ground elevation accuracy verification of ICESat-2 data: a case study in Alaska, USA. *Optics Express*. **27**(26), pp.38168–38179.

Wang, L., Ma, Y., Yan, J., Chang, V. and Zomaya, A.Y. 2018. pipsCloud: High performance cloud computing for remote sensing big data management and processing. *Future Generation Computer Systems*. **78**, pp.353–368.

Wang, Q., Yi, S. and Sun, W. 2021. Continuous Estimates of Glacier Mass Balance in High Mountain Asia Based on ICESat-1,2 and GRACE/GRACE Follow-On Data. *Geophysical Research Letters*. **48**(2), e2020GL090954.

Wang, W., Zhang, T., Yao, T. and An, B. 2022. Monitoring and early warning system of Cirenmaco glacial lake in the central Himalayas. *International Journal of Disaster Risk Reduction*. **73**, p.102914.

Watson, C.S., Kargel, J.S., Shugar, D.H., Haritashya, U.K., Schiassi, E. and Furfaro, R. 2020. Mass Loss From Calving in Himalayan Proglacial Lakes. *Frontiers in Earth Science*. **7**.

Watson, C.S. and King, O. 2018. Everest's thinning glaciers: implications for tourism and mountaineering. *Geology Today*. **34**(1), pp.18–25.

Watson, C.S., King, O., Miles, E.S. and Quincey, D.J. 2018. Optimising NDWI supraglacial pond classification on Himalayan debris-covered glaciers. *Remote Sensing of Environment*. **217**, pp.414–425.

Watson, C.S., Quincey, D.J., Smith, M.W., Carrivick, J.L., Rowan, A.V. and James, M.R. 2017. Quantifying ice cliff evolution with multi-temporal point clouds on the debris-covered Khumbu Glacier, Nepal. *Journal of Glaciology*. **63**(241), pp.823–837.

Wessel, B., Huber, M., Wohlfart, C., Marschalk, U., Kosmann, D. and Roth, A. 2018. Accuracy assessment of the global TanDEM-X Digital Elevation Model with GPS data. *ISPRS Journal of Photogrammetry and Remote Sensing*. **139**, pp.171–182.

Westoby, M.J., Dunning, S.A., Woodward, J., Hein, A.S., Marrero, S.M., Winter, K. and Sugden, D.E. 2016. Interannual surface evolution of an Antarctic blue-ice moraine using multi-temporal DEMs. *Earth Surface Dynamics*. **4**(2), pp.515–529.

Wilson, D.J. 2019. The harmonic mean p-value for combining dependent tests. *Proceedings of the National Academy of Sciences*. **116**(4), pp.1195–1200.

Wingham, D.J. 1998. Antarctic Elevation Change from 1992 to 1996. *Science*. **282**(5388), pp.456–458.

Wingham, D.J., Rapley, C.G. and Griffiths, H. 1986. New techniques in satellite altimeter tracking systems. *Digest - International Geoscience and Remote Sensing Symposium (IGARSS)*.

Winsvold, S.H., Kääb, A., Nuth, C., Andreassen, L.M., van Pelt, W.J.J. and Schellenberger, T. 2018. Using SAR satellite data time series for regional glacier mapping. *The Cryosphere*. **12**(3), pp.867–890.

Wood, J.L., Harrison, S., Wilson, R., Emmer, A., Yarleque, C., Glasser, N.F., Torres, J.C., Caballero, A., Araujo, J., Bennett, G.L., Diaz-Moreno, A., Garay, D., Jara, H., Poma, C., Reynolds, J.M., Riveros, C.A., Romero, E., Shannon, S., Tinoco, T., Turpo, E. and Villafane, H. 2021. Contemporary glacial lakes in the Peruvian Andes. *Global and Planetary Change*. **204**, p.103574.

Wu, K., Liu, S., Jiang, Z., Xu, J., Wei, J. and Guo, W. 2018. Recent glacier mass balance and area changes in the Kangri Karpo Mountains from DEMs and glacier inventories. *The Cryosphere*. **12**(1), pp.103–121.

Wu, Z., Snyder, G., Vadnais, C., Arora, R., Babcock, M., Stensaas, G., Doucette, P. and Newman, T. 2019. User needs for future Landsat missions. *Remote Sensing of Environment*. **231**, p.111214.

Wulder, M.A. and Coops, N.C. 2014. Satellites: Make Earth observations open access. *Nature*. **513**(7516), pp.30–31.

Wulder, M.A., Loveland, T.R., Roy, D.P., Crawford, C.J., Masek, J.G., Woodcock, C.E., Allen, R.G., Anderson, M.C., Belward, A.S., Cohen, W.B., Dwyer, J., Erb, A., Gao, F., Griffiths, P., Helder, D., Hermosilla, T., Hipple, J.D., Hostert, P., Hughes, M.J., Huntington, J., Johnson, D.M., Kennedy, R., Kilic, A., Li, Z., Lymburner, L., McCorkel, J., Pahlevan, N., Scambos, T.A., Schaaf, C., Schott, J.R., Sheng, Y., Storey, J., Vermote, E., Vogelmann, J., White, J.C., Wynne, R.H. and Zhu, Z. 2019. Current status of Landsat program, science, and applications. *Remote Sensing of Environment*. **225**, pp.127–147.

Xiao, C.-D., Wang, S.-J. and Qin, D.-H. 2015. A preliminary study of cryosphere service function and value evaluation. *Advances in Climate Change Research*. **6**(3–4), pp.181–187.

Xie, S., Dixon, T.H., Voytenko, D., Holland, D.M., Holland, D. and Zheng, T. 2016. Precursor motion to iceberg calving at Jakobshavn Isbræ, Greenland, observed with terrestrial radar interferometry. *Journal of Glaciology*. **62**(236), pp.1134–1142.

Xie, Z., Haritashya, U.K., Asari, V.K., Young, B.W., Bishop, M.P. and Kargel, J.S. 2020. GlacierNet: A Deep-Learning Approach for Debris-Covered Glacier Mapping. *IEEE Access*. **8**, pp.83495–83510.

Xing, H., Meng, Y., Hou, D., Song, J. and Xu, H. 2017. Employing Crowdsourced Geographic Information to Classify Land Cover with Spatial Clustering and Topic Model. *Remote Sensing*. **9**(6), p.602.

Xu, Z., Wu, L. and Zhang, Z. 2018. Use of active learning for earthquake damage mapping from UAV photogrammetric point clouds. *International Journal of Remote Sensing*. **39**(15–16), pp.5568–5595.

Yan, W., Liu, J., Zhang, M., Hu, L. and Chen, J. 2017. Outburst flood forecasting by monitoring glacier-dammed lake using satellite images of Karakoram Mountains, China. *Quaternary International*. **453**, pp.24–36.

Yarleque, C., Vuille, M., Hardy, D.R., Timm, O.E., Cruz, J.D. la, Ramos, H. and Rabatel, A. 2018. Projections of the future disappearance of the Quelccaya Ice Cap in the Central Andes. *Scientific Reports*. **8**(1), p.15564.

Yi, S. and Sun, W. 2014. Evaluation of glacier changes in high-mountain Asia based on 10 year GRACE RL05 models. *Journal of Geophysical Research: Solid Earth*. **119**(3), pp.2504–2517.

Yiran, G.A.B., Kusimi, J.M. and Kufogbe, S.K. 2012. A synthesis of remote sensing and local knowledge approaches in land degradation assessment in the Bawku East District, Ghana. *International Journal of Applied Earth Observation and Geoinformation*. **14**(1), pp.204–213.

Zemp, M., Frey, H., Gärtner-Roer, I., Nussbaumer, S.U., Hoelzle, M., Paul, F., Haeberli, W., Denzinger, F., Ahlstrøm, A.P., Anderson, B., Bajracharya, S., Baroni, C., Braun, L.N., Cáceres, B.E., Casassa, G., Cobos, G., Dávila, L.R., Granados, H.D., Demuth, M.N., Espizua, L., Fischer, A., Fujita, K., Gadek, B., Ghazanfar, A., Hagen, J.O., Holmlund, P., Karimi, N., Li, Z., Pelto, M., Pitte, P., Popovnin, V.V., Portocarrero, C.A., Prinz, R., Sangewar, C.V., Severskiy, I., Sigurđsson, O., Soruco, A., Usubaliev, R. and Vincent, C. 2015. Historically unprecedented global glacier decline in the early 21st century. *Journal of Glaciology*. **61**(228), pp.745–762.

Zemp, M., Huss, M., Thibert, E., Eckert, N., McNabb, R., Huber, J., Barandun, M., Machguth, H., Nussbaumer, S.U., Gärtner-Roer, I., Thomson, L., Paul, F., Maussion, F., Kutuzov, S. and Cogley, J.G. 2019. Global glacier mass changes and their contributions to sea-level rise from 1961 to 2016. *Nature*. **568**(7752), p.382.

Zhang, E., Liu, L., Huang, L. and NG, K.S. 2019. Automatically delineating calving fronts of Greenland glaciers from multi-sensor remote sensing imagery: a general method based on deep learning *In*: *AGU Fall Meeting Abstracts*., pp.C24A-02.

Zhang, G., Chen, W. and Xie, H. 2019. Tibetan Plateau's Lake Level and Volume Changes From NASA's ICESat/ICESat-2 and Landsat Missions. *Geophysical Research Letters*. **46**(22), pp.13107–13118.

Zhang, H., Aldana-Jague, E., Clapuyt, F., Wilken, F., Vanacker, V. and Van Oost, K. 2019. Evaluating the potential of post-processing kinematic (PPK) georeferencing for UAV-based structure- from-motion (SfM) photogrammetry and surface change detection. *Earth Surface Dynamics*. **7**(3), pp.807–827.

Zhang, M., Chen, F. and Tian, B. 2018. An automated method for glacial lake mapping in High Mountain Asia using Landsat 8 imagery. *Journal of Mountain Science*. **15**(1), pp.13–24.

Zhang, M., Chen, F., Tian, B., Liang, D. and Yang, A. 2020. High-Frequency Glacial Lake Mapping Using Time Series of Sentinel-1A/1B SAR Imagery: An Assessment for the Southeastern Tibetan Plateau. *International Journal of Environmental Research and Public Health*. **17**(3), p.1072.

Zhang, Y., Pang, Y., Cui, D., Ma, Y. and Chen, L. 2021. Accuracy Assessment of the ICESat-2/ATL06 Product in the Qilian Mountains Based on CORS and UAV Data. *IEEE Journal of Selected Topics in Applied Earth Observations and Remote Sensing*. **14**, pp.1558–1571.

Zhao, F., Long, D., Li, X., Huang, Q. and Han, P. 2022. Rapid glacier mass loss in the Southeastern Tibetan Plateau since the year 2000 from satellite observations. *Remote Sensing of Environment*. **270**, p.112853.

Zhou, Y., Li, Z. and Li, J. 2017. Slight glacier mass loss in the Karakoram region during the 1970s to 2000 revealed by KH-9 images and SRTM DEM. *Journal of Glaciology*. **63**(238), pp.331–342.

Zhu, X.X., Tuia, D., Mou, L., Xia, G.-S., Zhang, L., Xu, F. and Fraundorfer, F. 2017. Deep Learning in Remote Sensing: A Comprehensive Review and List of Resources. *IEEE Geoscience and Remote Sensing Magazine*. **5**(4), pp.8–36.